

AN ABSTRACT OF THE THESIS OF

Craig Thomas Basta for the degree of Master of Science in Wood Science presented on September 21, 2005.

Title: Characterizing Perpendicular-to-Grain Compression in Wood Construction Applications

Signature redacted for privacy.

Abstract Approved:

Rakesh Gupta

Current compression perpendicular-to-grain (c-perp) design values for wood members are based on mean stress using the ASTM D143 specimen. Base design value, as determined from 0.04-in deformation in the ASTM specimen, is applied to all c-perp applications. While the standard ASTM test was presumably believed to adequately reflect relevant c-perp applications at the time it was developed (likely railroad cross-ties, wall plates and similar cross-sections), the specimen has limited applicability to many of today's c-perp bearing applications.

Previous work has shown that wood-on-wood c-perp bearing is a more severe case as opposed to metal-on-wood bearing. End bearing conditions have been shown to represent a more severe c-perp loading scenario as opposed to load applied over central area. Research has shown that c-perp behavior of wood members is dependant on angle of applied load to annual ring orientation and that the most severe loading case is usually at an angle between 30 and 60 degrees to direction of applied load. Past studies also suggest that depth of member affects c-perp MOE and that higher aspect ratio may lead to instability of the member. As the c-perp behavior observed in the ASTM testing procedure is that of continually increasing stress with increasing deflection and densification, c-perp is generally believed to be serviceability rather than a life safety issue. However, in engineered wood applications, c-perp bearing may occur at areas where structural cohesiveness of a member is necessary to transmit forces through fasteners, such as truss plates. In such scenarios, c-perp has the potential to be a life safety issue.

A study was designed to evaluate c-perp behavior of typical as-constructed assemblies in which members experience c-perp stresses near their longitudinal end through wood-on-

wood contact. The study included both finite element analysis and experimental testing. Two as-constructed assemblies were evaluated in the study. These included assembly of the bottom chord of a truss bearing on the top plate of a wall (BC assembly) and assembly of the compression chord of a shear wall bearing on the bottom plate (BP assembly) of a wall. Finite element analysis modeled wood material as a composite with alternating earlywood and latewood layers with infinite radius of curvature. BC, BP and ASTM configurations were modeled both with load applied perpendicular and parallel to annual rings. Three BC assemblies were tested. These included BC-2X4, BC-2X8, and BC-2X12, which had nominal 2X4, 2X8, and 2X12 members as bottom chord members, respectively. Therefore, within BC test assemblies aspect ratio of the bottom chord members varied greatly. The three BC geometries were each tested with both Douglas-fir and Spruce-Pine-Fir top plate material. BP configuration was also tested with both Douglas-fir and Spruce-Pine-Fir bottom plate material. For each test assembly, paired ASTM tests of the main member (bottom chord member in BC tests, and bottom plate member in BP tests) were conducted. Results were analyzed utilizing a variety of statistical methods.

Finite element analysis revealed that strain was more uniform throughout depth of the bottom chord member when loaded perpendicular to annual rings than when loaded parallel to annual rings. In BC tests majority of deflection was found to occur in the bottom chord member. In BP test, the majority of deflection was found to occur within the bottom plate with only minimal deflection occurring in the longitudinally loaded compression chord.

Due to varying assembly depths, 0.04-in. deflection was found to be a poor criterion for determining c-perp stress values. In order to account for assembly depth, stress values were based on system strain. As 0.04-in. deflection corresponds to two percent strain in the 2-in. deep ASTM specimen, it was determined that stress determination be based on 2-percent system strain. Due to large settlement effects observed in the tested wood-on-wood assemblies, an offset strain was adopted as the method for determining and comparing stress values across differing assemblies and configurations tested.

Within BC tests, the species of top plate material was not found to significantly affect assembly performance. This was due to the overwhelming influence of bottom chord behavior on system behavior. Within BP tests there was suggestive but inconclusive evidence of a significant difference between Douglas-fir and Spruce-Pine-Fir tests. It was

recommended that further BP tests be conducted with larger sample sizes in order to determine the influence of wood species on c-perp behavior of bottom plate members.

Mean stress values of BC and BP assembly tests were found to be significantly lower than that of corresponding ASTM tests of the main member. This finding lends justification to the Canadian 2/3 reduction factor for these scenarios as well as to the design procedures suggested by German researchers. It was determined that the ASTM c-perp test does not adequately represent these bearing scenarios. Adjustment factors are recommended for wood-on-wood bearing and opposite side end bearing.

Aspect ratio was found to affect c-perp failure mode and led to high potential for sudden and catastrophic failure of members. Fifteen percent of 2X12 members tested failed prior to NDS design stresses due to premature failure of the nominal 2X12 bottom chord member. It was estimated that the odds of a 2X12 failing catastrophically are at least 16 times that of a 2X8 failing catastrophically. It was determined that as aspect ratio increases c-perp becomes a life safety as well as a serviceability issue and an adjustment factor for aspect ratio is recommended.

© Copyright by Craig T. Basta

September 21, 2005

All Rights Reserved

Characterizing Perpendicular-to-Grain Compression in Wood Construction Applications

by
Craig Thomas Basta

A THESIS

submitted to

Oregon State University

in partial fulfillment of
the requirements for the
degree of

Master of Science

Presented September 21, 2005

Commencement June 2006

Master of Science thesis of Craig Thomas Basta presented on September 21, 2005

APPROVED:

Signature redacted for privacy.

Major Professor representing Wood Science

Signature redacted for privacy.

Head of the Department of Wood Science and Engineering

Signature redacted for privacy.

Dean of the Graduate School

I understand that my thesis will become part of the permanent collection of Oregon State University libraries. My signature below authorizes release of my thesis to any reader upon request.

Signature redacted for privacy.

Craig Thomas Basta, Author

ACKNOWLEDGMENTS

I would like to thank the following people for their support in helping me complete this project:

- Milo Clauson – For allowing me access to his extremely diverse and extensive knowledge base. For keeping the lab in 147 running and in working order. Without Milo the testing conducted in this study would not have been possible.
- Dr. Rakesh Gupta– For his guidance, support, and providing me the opportunity to take part in this research project at Oregon State University. For assisting me immensely in my education in Timber Engineering and Mechanics.
- Dr. Robert Leichti – For being a highly competent and dedicated wood scientist, and professor. For aiding me immensely with his technical expertise. Oregon State will miss you.
- Kevin White, Lori Elkins, Sarah Bultena, Cameron Carroll, and Erin Anderson – For making me feel like I wasn't the only person on earth trying to write a thesis.
- Dr. Mike Milota – For the use of his lab and in helping me in conditioning test specimens.
- All of my family – For all of there emotional and yes, financial support.
- Action Wood Products in Turner, Oregon – For donating wood material used in testing for this project.
- Don Devisser, WCLIB, – For arranging and helping sort lumber
- Brandt Balgooyen – For statistical consulting

TABLE OF CONTENTS

	<u>Page</u>
CHAPTER 1. INTRODUCTION	1
1.1 BACKGROUND	1
1.2 IMPETUS FOR STUDY	3
1.3 OBJECTIVES	5
CHAPTER 2. LITERATURE REVIEW	7
CHAPTER 3. MATERIALS AND METHODS	19
3.1 TEST ASSEMBLIES	19
3.1.1 Bottom Chord Of Truss On Top Plate Of Wall (BC Assembly)	19
3.1.2 Compression Chord Of Truss On Top Plate Of Wall (BP Assembly)	20
3.2 FINITE ELEMENT ANALYSIS	22
3.2.1 Geometry	22
3.2.2 Boundary Conditions	27
3.2.3 Loading Conditions	27
3.2.4 Material Properties	27
3.3 MATERIAL ACQUISITION AND SPECIMEN MATCHING	28
3.4 SPECIMEN PREPARATION	29
3.5 TEST SETUP AND EQUIPMENT	32
3.6 TESTING AND DATA COLLECTION	35
3.7 DATA ANALYSIS	35
3.8 STATISTICAL ANALYSIS	36
3.8.1 BC Assembly	36
3.8.2 BP Assembly	40
CHAPTER 4. RESULTS AND DISCUSSION	42
4.1 FINITE ELEMENT ANALYSIS	42
4.2 COMPRESSION BEHAVIOR	48
4.2.1 Top Plate Members In BC Assemblies	48
4.2.2 BC-2X4 Assembly	49
4.2.3 BC-2X8 Assembly	51
4.2.4 BC-2X12 Assembly	53
4.2.5 BP Assembly	56
4.2.6 Comparison Of σ_{max} To $\sigma_{2\%-OS}$	58
4.3 $F_{c\perp}$ DETERMINATION	59
4.4 INFLUENCE OF WOOD SPECIES	65

TABLE OF CONTENTS (Continued)

	<u>Page</u>
4.5 COMPARISON OF TESTED ASSEMBLIES TO CORRESPONDING ASTM TESTS OF MAIN MEMBER.....	66
4.6 COMPARISON OF DATA WITH LITERATURE.....	70
4.7 RELATIONSHIP BETWEEN ASPECT RATIO AND C-PERP BEHAVIOR INCLUDING ULTIMATE LIMIT STATE.....	71
4.7.1 STRESS AT 2-PERCENT OFFSET STRAIN ($\sigma_{2\%-OS}$).....	71
4.7.2 MAXIMUM STRESS AND STRAIN AT MAXIMUM STRESS.....	73
4.7.3 PROBABILITY OF CATASTROPHIC FAILURE.....	79
CHAPTER 5. CONCLUSIONS AND RECOMMENDATIONS	82
5.1 CONCLUSIONS	82
5.2 RECOMMENDATIONS FOR FUTURE STUDY.....	85
CHAPTER 6. BIBLIOGRAPHY	86
CHAPTER 7. APPENDICES.....	91
7.1 APPENDIX A: NOTATION	92
7.2 APPENDIX B: STRESS-STRAIN DIAGRAMS.....	94
7.3 APPENDIX C: LOAD –DEFLECTION DIAGRAMS.....	116
7.4 APPENDIX D: RAW DATA.....	138
7.5 APPENDIX E: MEMBER PROPERTIES.....	150
7.6 APPENDIX F: COMPRESSION DAMAGE PICTURES	168
7.7 STATISTICAL CODE	194

LIST OF FIGURES

<u>Figure</u>	<u>Page</u>
1: ASTM C-perp specimen	2
2: Typical load deflection diagram for ASTM specimen depicting offset deflection stress determination	2
3: BC assembly – truss bottom chord on wall top plate	19
4: BP assembly – compression chord bearing on bottom plate of wall	21
5: Finite element model of ASTM specimen with radial loading	24
6: Finite element model of ASTM specimen with tangential loading	24
7: Finite element model of BC-2X12 assembly with radial loading	25
8: Finite element model of BC-2X12 assembly with tangential loading	25
9: Finite element model of BP assembly with radial loading	26
10: Finite element model of BP assembly with tangential loading	26
11: Samples cut from each 2X4 DF board	30
12: Samples cut from each 2X4 SPF board	31
13: Samples cut from each 2X8 DF board	31
14: Samples cut from each 2X12 DF board	32
15: BC-2X4 test setup	33
16: BC-2X8 test setup	33
17: BC-2X12 test setup	34
18: BP test setup	34
19: BC split block model (block #X)	38
20: Block design for BC-2X4 assemblies and. corresponding ASTM tests (block #X)	38
21: Block design for BC-2X8 assemblies and corresponding ASTM tests (block #X)	39
22: Block design for BC-2X12 assemblies and corresponding ASTM tests (block #X)	39

LIST OF FIGURES (Continued)

<u>Figure</u>	<u>Page</u>
23: Block design for BP-DF assemblies and corresponding ASTM tests (block #X)	41
24: Block design for BP-SPF assemblies and corresponding ASTM tests (block #X)	41
25: Finite element analysis strain profile for the ASTM specimen with radial loading	43
26: Finite element analysis strain profile for the ASTM specimen with tangential loading	43
27: Finite element analysis strain profile for the BC-2X12 assembly with radial loading	44
28: Finite element analysis strain profile for the BC-2X12 assembly with tangential loading	44
29: Finite element analysis strain profile for the BP assembly with radial loading	45
30: Finite element analysis strain profile for the BP assembly tangentially loaded	45
31: Characteristic compression damage in 2X4 T.P. members in BC assembly tests	49
32: Characteristic compression damage in BC-2X4 assembly B.C. members	50
33: Characteristic compression damage in BC-2X8 assembly B.C. members	52
34: Characteristic compression damage in BC-2X12 assembly B.C. members	54
35: Characteristic compression damage in 2X4 BP assembly members	57
36: Typical load-deflection diagrams for BC, BP and ASTM tests	60

LIST OF FIGURES (Continued)

<u>Figure</u>	<u>Page</u>
37: Typical stress-strain diagrams for BC, BP and ASTM test	62
38: All assemblies 95-percent C.I. for difference in mean $\sigma_{2\%-OS}$	65
39: All assemblies 95-percent C.I. for mean $\sigma_{2\%-OS}$	67
40: All assemblies vs. corresponding ASTM tests of main member 95- percent C.I. for difference in mean $\sigma_{2\%-OS}$	67
41: All assemblies vs. corresponding ASTM tests of main member 95- percent C.I. for difference in mean $\sigma_{2\%-OS}$ after adjustment for covariate effects	68
42: BC tests all - 95% C.I. for difference in mean $\sigma_{2\%-OS}$ before and after accounting for covariate effect	72
43: BC assemblies σ_{max} before and after adjustment for covariate effects.....	74
44: BC-2X4 assembly σ_{max} as ratio of NDS design value ($F_{c\perp}$).....	75
45: BC-2X8 assembly σ_{max} as ratio of NDS design value ($F_{c\perp}$).....	76
46: BC-2X12 assembly σ_{max} as ratio of NDS design value ($F_{c\perp}$).....	76
47: Histogram of percent strain from offset at σ_{max} for BC-2X4 assemblies	77
48: Histogram of percent strain from offset at σ_{max} for BC-2X8 assemblies	78
49: Histogram of percent strain from offset at σ_{max} for BC-2X12 assemblies	78
50: Calculated Probability of catastrophic failure of 2X8-B.C. member as a function of average ring angle of B.C. member at interface with T.P. member	80
51: Characteristic $RA_{T\&B}$ which lead to catastrophic failure of B.C. member in BC-2X8 assemblies	81

LIST OF TABLES

<u>Table</u>		<u>Page</u>
1:	Test matrix for BC assembly	20
3:	Boards obtained for specimen preparation	29
4:	Comparisons of σ_{\max} to $\sigma_{2\%-\text{OS}}$ for all assemblies	58
5:	BC-2X4 and corresponding ASTM means for all response variables.....	63
6:	BC-2X8 and corresponding ASTM means for all response variables.....	63
7:	BC-2X12 and corresponding ASTM means for all response variables.....	63
8:	BP-DF and corresponding ASTM means for all response variables	64
9:	BP-SPF and corresponding ASTM means for all response variables	64
10:	Ratio of assembly performance to corresponding ASTM test performance with predicted ratios from literature.....	71

CHARACTERIZING PERPENDICULAR-TO-GRAIN COMPRESSION IN WOOD CONSTRUCTION APPLICATIONS

CHAPTER 1. INTRODUCTION

1.1 BACKGROUND

With the exception of shear parallel to grain and compression perpendicular-to-grain (c-perp), current wood design values are based on full-scale specimen testing. C-perp is based on testing of a 2 X 2 X 6-in. specimen using the ASTM D143 standard (ASTM, 2000). To date nearly all allowable stress values have been based on statistical reference to 5-percent parametric tolerance limit on property distribution curves. C-perp as well as modulus of elasticity are the exceptions to this rule and are based on mean property values. C-perp was initially based on proportional limit (PL) stress and is now based on stress at 0.04-in. deflection ($\sigma_{0.04-D}$). This is because no well-defined ultimate strength exists for c-perp using the D143 specimen. Deformation at PL is generally fairly small and some believe this to be a rather arbitrary value (FPL 1999). Since 1982 allowable c-perp value has been based on mean $\sigma_{0.04-D}$, which is an increase of about 60 percent over values based on PL (AFPA 1997).

The American Society for Testing and Materials (ASTM) standard test for c-perp involves load applied to the radial face of the specimen as shown in Figure 1. Load is applied through a metal bearing plate 2-in. in width and placed at right angles to the length of the specimen and equal distance from the ends. Load is applied at a rate of motion of 0.012 in./min. and load-deflection curves are recorded up to 0.1-in. compression which corresponds to 5-percent strain in the 2-in. deep specimen. A typical ASTM load-deflection diagram is shown in Figure 2. Mean stress value, as determined by the ASTM test is divided by 1.67 to reach base design value.

As shown in Figure 2, the linear region in the load-deflection diagram is preceded by a region of nonlinearity and upward curvature. This region, commonly referred to as initial misalignment, is generally attributed to non-parallel surfaces and surface roughness in the ASTM specimen. In an attempt to adjust for these imperfections, stress at 0.04-in. offset deflection ($\sigma_{0.04-OD}$) is often determined.

The offset deflection is calculated by fitting a linear regression to the linear region of the load-deflection diagram. The offset deflection is then calculated as 0.04-in. from the

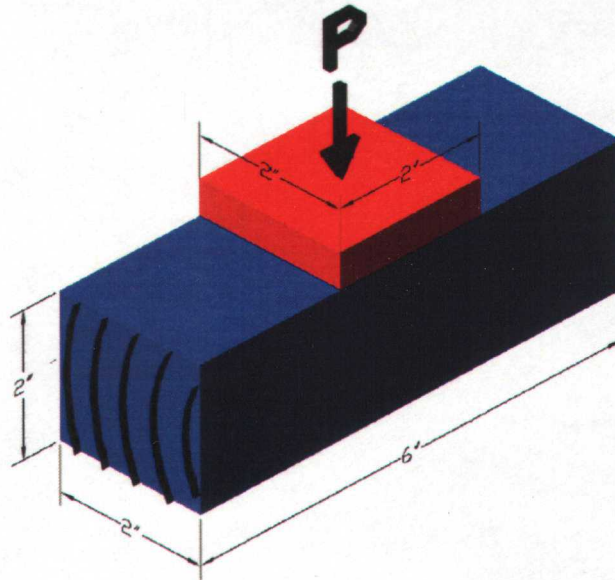


Figure 1: ASTM C-perp specimen

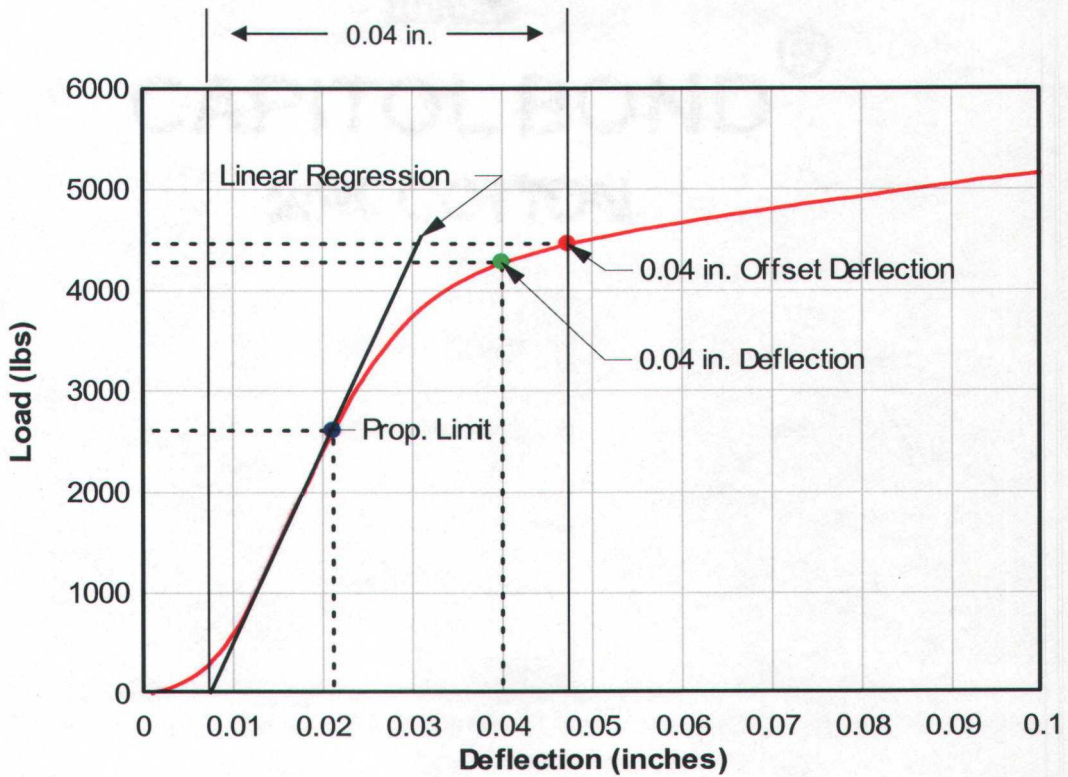


Figure 2: Typical load deflection diagram for ASTM specimen depicting offset deflection stress determination

intersection of the regression line with the deflection-axis (Figure 2). Stress is then calculated at the offset deflection (Ethington et al. 1996). A similar procedure can be applied to the stress-strain diagram.

1.2 IMPETUS FOR STUDY

At the time the ASTM specimen was developed, it was believed to accurately reflect the applicable cases in which wood was subjected to c-perp. Such applications may have included railroad cross-ties, wall plates and applications with aspect ratios (height/width) of 1 or less. However, wood is used in applications in which perpendicular to grain compression is applied to cross sections with aspect ratios much larger than 1. Such applications include lumber as well as engineered wood products used in floor joists, truss applications, I-joists, rim joists, etc. In these applications it has been found that increasing aspect ratios may lead to perpendicular to grain rolling shear failures. In such scenarios, it has been suggested that c-perp be limited by plastic buckling or cross-grain bending while not exceeding design values (Stuart Lewis, Personal Communication, January 17, 2002).

During the period in which the ASTM specimen was developed nails and spikes were typically used at connections subject to transverse compressive stresses. In today's engineered wood structures, compression is often applied at or near fasteners that might be truss plates or other metal plate hardware. These fasteners require the section to maintain cohesiveness for adequate wood to fastener connection. Dimensional instability caused by excessive c-perp stress may cause connection failure leading to sudden and possibly catastrophic failure of the member. Therefore, an ultimate limit state may be reached if such a wood member deforms excessively or structural integrity of the member is compromised. In the 1990s, realization of ultimate transverse compression load stresses with corresponding catastrophic failure (fracture, cross-grain bending, and plate withdrawal) in certain applications, created debate as to whether these increased stress values incorporate enough safety factor (Stuart Lewis, Personal Communication, January 17, 2002). For less critical applications, interest has developed in basing allowable stress in transverse compression on acceptable deformation for particular situations (Bendtsen et al. 1978, Bendtsen and Galligan 1979).

Due to the fact that the metal bearing plate applied to the ASTM specimen surface does not cover the entire area of the specimen, shear stresses as well as compressive stresses

are developed. Shear stresses with corresponding reactions, which develop at the edges of the bearing plate, lead to higher c-perp values than if load is applied over the full area of the specimen (Bodig 1969, Kunesh 1968, Pellican et al. 1994). Therefore the D 143 test has limited applicability to full surface compression as well as end bearing compression scenarios. National Design Specification (NDS) for Wood Construction provides increases in allowable c-perp using bearing areas factors (C_b) (AFPA 2001). However there is no reduction factor provided for the case of c-perp bearing near the longitudinal end of members. A further drawback to the ASTM test specimen is that the metal-on-wood compression produced in this test has been found to inaccurately reflect the typical wood-on-wood compression often present in structural application (Fergus and Suddarth 1981).

Ring orientation has been shown to have a significant effect on c-perp values. However the ASTM test stipulates that load is applied only parallel to growth rings. Whether radial (load applied perpendicular to growth rings) or tangential (load applied parallel to growth rings) compression is more severe seems to be a species dependent phenomenon. It is generally accepted within the wood science community that the most severe ring orientation occurs with ring orientation of about 45 degrees to the radial and tangential faces (Bodig 1965, Kennedy 1968, Ethington et al. 1996, Tabarsa and Chui 2001). Per ASTM D245, average c-perp values for green lumber are multiplied by 1.5 to account for seasoning effects and divided by 1.67 to account for normal duration of load and factor of safety. It is unclear how this 1.67 adjustment factor is related to ring orientation. Ring orientations of around 45 degrees may lead to excessive deformation and/or instability of the wood member with corresponding reduction of fastener performance.

Historically transverse compression stress in wood members has rarely been a design limiting concern. However in recent years increasingly efficient and precise wood design has led to situations in which transverse compression limits design or dictates wood species. This phenomenon has been especially apparent in the truss fabrication industry. In some instances, span length is limited by bearing stress at the interface of the bottom truss chord and the top plate of the supporting wall (Fergus et al. 1981). Design limitations due to transverse compression have provided impetus for studies into design of connections aimed at increasing transverse compression strength (Bulmanis et al. 1983). Further interest in the behavior of wood in transverse compression has been generated in the composite wood products industries (Kunesh 1961, Wanbing 1996).

When shear walls are subjected to shear forces, the end posts serve alternatively as vertical tension and compression chords. For compression chords adequate bearing capacity of the chord on the top and bottom plates of the wall must be provided (Rose 1998). This constitutes wood-on-wood bearing stress that is not directly measured by the ASTM test method. Tests conducted by APA have found that for heavily loaded shear walls with sheathing on both sides, c-perp produced by the bearing of a compression chord against wall plates can be a design limiting concern (Breyer et al. 1999, Rose 1998, Rose and Keith 1996, Tissell 1996). In addition other variables such as cupping of the top and or bottom plate may lead to induced transverse tension forces in the member. This may have the potential to lead to splitting of the top plate and or bottom plate near the center of the wide face.

Recent work in Canada has led to recognition that c-perp loads on opposite sides of a member and near the longitudinal end of a member is a more severe loading case as opposed to single side loading over the central area. This has led to a required one-third reduction in c-perp loads for load applied to opposite sides of a member near the longitudinal end (Lum and Karacabeyli 1994). However, the NDS does not address this issue (NDS 2001). In addition, further design approaches have been suggested by Blass and Gortlacher (2004).

1.3 OBJECTIVES

The objectives of this study are to:

- (1) Evaluate c-perp behavior in the bottom chord of a truss bearing on the top sill plate of a wall and the compression chord of a shear wall bearing against the bottom plate of the wall by
 - (a) estimating relative deformations between contacting wood members in test assemblies using finite element analysis,
 - (b) describing failure modes,
 - (c) determining appropriate criteria for c-perp strength in test assemblies,
 - (c) determining influence of wood species within test assemblies,

(e) comparing c-perp strength of tested assemblies to corresponding ASTM tests, and

(f) comparing results with literature.

(2) Quantify the relationship between aspect ratio and c-perp behavior including ultimate limit state within tested assemblies by

(a) comparing c-perp strength for bottom chord of truss assemblies over a range of aspect ratios,

(b) quantifying maximum stress and strain at maximum stress in high aspect ratio members and

(c) quantifying probability of catastrophic failure within high aspect ratio members.

CHAPTER 2. LITERATURE REVIEW

Several studies conducted in the late 1970(s) suggested that design values for c-perp, based on average proportional limit stresses of small, clear, green, specimens, are unduly conservative. Bendtsen et al. (1978) suggested that allowable c-perp stresses were conservatively developed at a time when ASTM believed that a conservative approach could be tolerated with little consequence. This study made use of load-deflection data stored at the Forest Products Laboratory. The data was based on 33 trees from three counties in Oregon, two counties in Washington, and two counties in Alaska. This information was used to create a specimen composite for the stress-strain curves that was statistically expressive of the variability in the archival data. A statistical procedure to characterize the stress-strain relationship in c-perp was developed. This procedure was demonstrated for western hemlock.

Bendtsen and Galligan (1979) statistically examined and analyzed the c-perp stress-strain relationship as well as the variability of this relationship for several softwood and hardwood species. From this analysis, functions were developed to predict c-perp for other species. The function $Y = A + Bx$, was determined to best describe the stress-strain relationship of wood in transverse compression ($0.730 < r^2 < 0.975$). In this function, x is average proportional limit determined from ASTM D 5555 tables and Y is either the mean of interpolated stresses or the determined tolerance limit for species at a given compression condition. When this model was applied to white Fir, c-perp exceeded currently allowable values at deflection levels greater than about 0.02-in. for dry wood and 0.03-in. for green wood. At the time of publication, procedures were under review that could possibly permit less restrictive design values in c-perp when deformations greater than about 0.02-in. were deemed to be acceptable.

Other researchers studied size and geometry of the test specimen in relation to transverse compressive strength values. Bodig (1963) addressed the issue of increasing modulus of elasticity with increasing thickness of specimens in radial compression. Specimens 0.4-in. in the longitudinal direction, 1.0-in. in the tangential direction and 1.0, 1.5, 2.0, and 3.0-in. high were tested in radial compression. Stresses at proportional limit and maximum load were similar for varying heights of specimens. However, Bodig (1963) found large differences in modulus of elasticity, as well as work to proportional limit per unit volume for differing heights of specimens. Bodig attributed this phenomenon to a weak earlywood

layer which regardless of material above and below it, contributed to the majority of the strain. In this way, the relatively weak layer was always the controlling factor.

Wolcott et al. (1989) conducted compression tests on yellow poplar and poly methyl methacrylate specimens. To eliminate transverse, longitudinal, and shear stresses induced by the bearing condition of the ASTM standard test, load was applied over the full area of the specimens. The effect of test apparatus deformation on the measured test deformation was limited by testing apparatus for strain so that the final results could be adjusted to remove strain attributed to testing equipment. Specimen height was varied between 0.12 and 1.56-in. As found by Bodig (1963), yield strength was unaffected while Young's modulus was found to increase with increasing specimen height. A mechanics of materials solution produced similar results to those achieved in the experiment. Contrary to Bodig (1963), the increase in Young's modulus with increasing specimen height was attributed to the effect of surface roughness and non-parallelism of the specimen.

Leicester et al. (1998) tested both small clear wood specimens as well as structural size timbers in transverse compression. Small clear wood specimens were tested in a configuration consistent with the ASTM c-perp standard test. For structural size timbers, five different configurations were tested. Structural size timbers were 90 x 35 mm and 190 x 35 mm. The data recorded included; load at proportional limit, load at 0.08-in. offset, load at which an audible crack is heard, load at a deformation of 0.2, 0.4, 0.8, and 1.6-in. deformation, and load at failure of the test specimen. A configuration that loads opposite sides of timber members through the longitudinal midpoint was recommended for in-grade testing of structural timbers. It was concluded that both stiffness and 0.08-in. offset stress are useful parameters in determining allowable design values for serviceability limit states. It was further found that at large deformations rigid restraints are required to prevent lateral collapse of the specimen. When local bearing pressure is applied from only one side it was concluded that a deformation limit of 0.2 or 0.4-in. should be used. When bearing pressure is applied from both sides, it was determined that this deformation limit should be doubled.

The standard c-perp test procedure involves a compression force applied by a metal plate over a central portion of the specimen surface. This arrangement has been found to inaccurately reflect applications in which compression force is applied over a wood-on-wood contact area and/or when stress is applied over the full area of the member. Kunesh (1968) investigated the effects of stressed area as well as specimen thickness

and moisture content on strength and elastic properties of wood loaded in radial transverse compression. Samples were prepared from Douglas-fir, *Pseudotsuga menziesii* (Mirb.) Frank, and western hemlock, *Tsuga heterophylla* (Raf.) Sarg. In phase 1, specimens were tested with the load applied over the entire surface of the specimen. In phase 2, specimens were tested with the load concentrated over a central portion of their area as in the standard ASTM method. The phase 1 results showed that almost all strength as well as elastic properties were affected in correspondingly lesser degrees by moisture content, thickness, and stressed area, respectively. Proportional limit, modulus of elasticity, and maximum stress were found to decrease with increasing moisture content. Proportional limit and modulus of elasticity also decreased with increasing stressed area. Proportional limit and maximum stress decreased with increasing thickness. Similar to Bodig (1963) and Wolcott et al. (1989), modulus of elasticity was found to increase with increasing thickness. Proportional limit also was found to be a good indicator of maximum strength. Maximum stress was not affected by the compression area for a given thickness, but strength and elastic properties generally increased with decreasing compression area. In phase 2 the results were similar for elastic properties but not for strength properties. Specimens tested with load applied over a central portion of their area had a significantly higher first inflection load value on the compressive load-deformation curve. For these specimens, maximum strength was increased by an average of 39 percent for western hemlock and by an average of 29 percent for Douglas-fir as compared with phase 1 specimens.

Fergus et al. (1981) conducted studies utilizing three different test configurations including metal-on-wood (in accordance with ASTM 143), wood-on-wood, and wood-on-metal. This study conducted c-perp tests on Pacific silver Fir (*Abies amabilis* (Dougl.) Forbes) and subalpine Fir (*Abies lasiocarpa* (Hook.) Nutt). Specimens were selected randomly without consideration of ring angle orientations to applied load. The testing showed that, stresses attained for wood-on-wood compression reached a maximum of 68 to 85 percent of corresponding ASTM tests. Significant differences were seen between ASTM and wood-on-metal compression tests for subalpine Fir but not for Pacific silver Fir. For subalpine Fir wood-on-metal stress values at given deformations were higher than for ASTM test. Stiffness increases on the order of 2 were noted between moisture contents of 19 and 3-percent but this trend did not significantly affect stress ratios between test orientations. Shearing failure was observed at higher stress levels, but did not generally occur before 0.05-in. of deformation.

Design limiting transverse compression stresses have provided the motivation for studies aimed at improving the transverse load carrying capacity at wood bearing surfaces through use of specialized connections. Bodig (1969) explored the increased bearing capacity that can be obtained by increasing the total edge/area ratio over that of the ASTM test in transverse compression. He showed that increased edge/area ratio leads to increases in stress at proportional limit, stress at 5-percent strain, modulus of elasticity and unit work to proportional limit. The added load-carrying capacity is attributed to shear effect along the edge of compression plates. As the fibers bend along edges of compression plates in contact with the wood material, the resistance to shear increased load carrying capacity to compression capacity of wood. In order to maximize edge to bearing area ratio and this corresponding effect, the bearing plate was divided into smaller sections. Compression plates were prepared in which strips of bearing plate of varying thickness and with varying gaps between them would contact the wood surface. In addition and to further increase edge/area ratio, bearing plates with square teeth of varying size and varying gaps between teeth were prepared. Stress at proportional limit, stress at 5-percent strain, modulus of elasticity and unit work to proportional limit were increased quite dramatically in some instances. It was further demonstrated that for most properties, excluding modulus of elasticity, highest strength was obtained for an arrangement of the edge of bearing areas oriented at 45 degrees from the grain angle. In the case of 1/8-in.² teeth with 1/16-in. gap, measured strength properties were found to be on the order of 2 to 3 times greater than corresponding ASTM values.

Bulmanis et al. (1983) addressed the issue of increasing allowable transverse compression stress at the interface of wood bearing members. The study was specifically focused on the bearing connection of the bottom chord of a truss member on the top plate of the supporting wall. Two methods for reinforcing the interface between the bottom chord of a truss and the top plate of a supporting wall were studied. The objective of the study was to determine if mean compressive stress perpendicular to grain at proportional limit could be increased through use of these reinforcements. Wood connections were constructed with No. 2 & Better Spruce-Pine-Fir. Four series of sample connection were prepared: metal bearing brackets attached to the top plate, truss plates located on the lower edge of the bottom chord of the truss, a combination of these two reinforcements, and the control group consisting of wood-on-wood connections. The bearing bracket alone did not appreciably increase stress at proportional limit. However, locating the truss plate at the lower bottom edge of the bottom chord in such a manner that compression stress is distributed to the vertical faces of the bottom chord led to a 15 percent increase

in compression strength. A symbiotic combination of the two methods was noted to increase compression strength of the connection by 30 percent over the control wood-on-wood connection.

Wolfgang et al. (2003) addressed the issue of using chemical impregnation as a possible means of increasing transverse compression values. This research conducted experiments on the improved transverse compressive strength that spruce wood modified with an aqueous solution of melanine-formaldehyde resin. Impregnation of cell walls with melanine-formaldehyde resin was found to increase tangential compression strength of treated samples by 82-percent and to increase radial compressive strength by 290-percent. Transverse compressive yield was found to transition from plastic yield in control samples to brittle fracture of cell walls in treated samples. While treatment incorporates the need to tolerate more brittle failure modes, the use of melanine-formaldehyde resin impregnation was shown to significantly increase transverse compressive strength of treated wood.

It is known that transverse compression values vary with ring angle. Ring angle is the angle between direction of applied load and annual rings. The relationship between ring angle and transverse compressive behavior is a species dependant phenomenon. Kennedy (1968) studied the effect of varying ring angles on compression strength value. For each of 3 coniferous and 6 hardwood species, at 4 to 5.5-percent moisture content, five specimens were cut at differing ring orientations to loading. Specimens were cut at ring angles with respect to loading of 0, 30, 45, 60, and 90 degrees respectively. Species were tested in transverse compression. Quantitative parameters of specific gravity (green volume), ray volume percentage, latewood percentage, and index of differential density were determined for each wood species tested. Stress at proportional limit and modulus of elasticity were found to be lowest at ring orientations of 30 to 45 degrees to direction of applied load. Inter-species maximum and minimum values of stress at proportional limit as well as modulus of elasticity were found to be highly correlated with specific gravity. Within hardwoods it was concluded that specimens with low latewood percentage or small intra-increment density variation may be expected to be stiffer and stronger in radial compression. Specimens with high percentages of dense latewood may be expected to be stiffer and stronger in tangential compression. Within hardwoods it was concluded that species with high volumes of ray cells and small intra-increment density variation may be expected to be stiffer and stronger under radial compression. Within hardwoods low ray volume as well as high variation in density between latewood and earlywood was found to

minimize the difference between radial and tangential strength properties. The study found that within species, specimens loaded in radial compression tended to exhibit higher strength properties than those loaded in tangential compression.

Ethington et al. (1996) fit a second-order polynomial to the relationship between ring angle and stress at 0.04-in. offset deflection using the data from 232 specimens of dahurian larch tested in transverse compression. No effort was made to select ring orientation of specimens and consequently ring orientation to applied load was random. Ring orientation was measured in 5-degree increments and compared against stress at 0.04-in. offset deflection. Lowest stress was found to occur between 30 to 50 degrees from either tangential or radial loading. Minimum compressive stress occurring at this orientation was found to be 65 to 85 percent of stress perpendicular and parallel to growth rings.

It is generally accepted that wood is weakest in transverse compression at an orientation of load to ring angle of about 45 degrees. While the ASTM test method does not require testing in this orientation, the 1.67 adjustment factor applied to allowable compression values is apparently intended to account for variations in grain orientation, not as a safety factor. The ratio of 60 percent (1/1.67) for allowable transverse compression seems reasonable to account for weakest load orientation.

The reviewed literature emphasized characteristics of wood material on a macro level. Other literature shows the role of cellular properties in determining transverse compression strength characteristics as well as modes of failure on a microscopic level. It appears that Bodig (1965) was one of the first to examine the differences in failure modes between wood specimens loaded in radial and tangential compression. He presented a qualitative rather than a quantitative evaluation of the experiment. Specimens of western red cedar, (*Thuja plicata* Donn), Douglas-fir (*Pseudotsuga menziesii* (Mirb) Franco), Oregon ash (*Fraxinus latifolia* Benth), and red alder (*Alnus rubra* Bong.) were tested in transverse compression in both the radial and tangential directions. Magnified photographs were taken of the specimen behavior at different stages of compression and these stages were identified on stress-strain graphs. Transverse compressive elasticity and strength values were found to be different in the radial and tangential directions. These differences were found to be brought about by anatomical characteristics of the wood. For all specimens except those of Oregon ash in tangential compression, stress versus strain curves for both radial and tangential compression were found to follow irregular patterns. Of special interest is the fact that for all specimens excluding Oregon

ash and red alder in tangential compression, a maximum stress value was observed in both radial and tangential transverse compression. It was observed that in radial compression the initial maximum stress value is determined by the weakest earlywood layer. The strength of other latewood and earlywood layers do not contribute to this value. Failure in the tangential direction was likened to failure of long columns in which the latewood layers serve as columns and the earlywood serve mainly as lateral reinforcement of the latewood layers. It was determined that if the L/d ratios of summerwood layers was in the long-column range, specimens would exhibit a maximum stress in tangential compression. This maximum stress corresponds to buckling of latewood layers. The article proposed that the initial upward curvature of the stress versus strain graph is due to imperfect contact between testing equipment and the irregularities of the specimen surface.

Easterling et al. (1982) characterized the structure of balsa wood by scanning microscopy. Both moduli and crushing strength in the three orthogonal directions were related to the wood structure. Moduli and crushing strength were found to be dependant partially on properties of the cell wall and partially on the geometry and dimensions of the cells themselves. Cell walls were found to bend elastically and plastically collapse through fracture. Relative density was found to be related to the dimensions of cells. When compressed tangentially, a smooth stress-strain curve with a long plateau up to about 0.7 strain was observed. This corresponded to progressive flattening of cells and could be calculated by simple beam theory. When loaded radially, behavior was similar but with a small yield followed by somewhat wavy stress-strain curve up to about 0.7 strain. This corresponded to non-uniform crushing starting at the platen surface and propagating inward. Rays were found to act as reinforcing columns when specimens were loaded radially. Radial modulus could be calculated with a simple weighed average of the rays and cells based on relative moduli and volume fraction. Axial loading was found to produce yield at much higher stress and lower strain followed by highly irregular but generally downward sloping trend in the stress-strain diagram. This corresponded to collapse and fracture of a plane of material in the wood. Increasing density led to higher stress levels and slightly decreasing terminal strain. Unlike tangential and radial modulus, axial modulus was found to vary linearly with density.

Tabarsa and Chui (1999 and 2000) utilized a test system to investigate the influence of the cellular structure of wood on its stress strain relationship under radial compression. The testing included real-time microscopic observation of cellular deformation under radial

applied load. For specimens of white spruce loaded in radial compression, it was found that the initial elastic region of the stress-strain diagram corresponds to deformation of earlywood cells. The slope of this line is related to the MOE of earlywood cells. After reaching the proportional limit, strain increases with little increase in stress. This region was observed to correspond to a period of continuing collapse of earlywood cells. After this plastic deformation, stress increased rapidly with strain. The slope of this region on the stress versus strain graph is directly related to the MOE of the latewood. In manufacturing of composite wood products, perpendicular to grain stresses often compress wood past the proportional limit and cause plastic deformation. This is referred to as densification. This work seems to suggest that densification occurs in part due to collapse of earlywood cells.

Tabarsa and Chui (2001) tested specimens of white spruce, jack pine, white ash, and aspen in radial compression. Specimens of white spruce and jack pine were also tested in tangential compression. Deformation characteristics at different stress levels were photographed using a microscope at differing magnifications. For the specimens of white spruce and jack pine, deformation characteristics were found to be distinctly different when specimens were loaded in radial compression versus tangential compression. Similar to Tabarsa and Chui (2000), radial compression in these species was found to be dominated by deformation of the thin walled earlywood cells and yield was coincident with collapse of these cells. As in Bodig (1965), tangential compression deformation was observed to be caused by bending of latewood layers. Again the phenomenon was likened to buckling of columns. Cell wall deformation contributes to this strain. Failure initiates with buckling of these latewood columns. In the hardwood specimens, largest vessels surrounded by thin-walled paratracheal cells were observed to deform more than fibers. Failure initiated in these vessels.

Lum and Varoglue. (1988) provides insight into design limiting concerns in the truss manufacturing industry regarding perpendicular to grain compression. This paper reports testing of a 40 foot parallel chord roof truss. Full-scale testing results were compared to computer analysis using Structural Analysis of Trusses (SAT) and a standard plane frame structural analysis program (FRAME). In this experiment, the experimental truss failed at 1.94 times design load due to perpendicular-to-grain wood crushing at the right support.

Johnson (1983) compared Hem-Fir and Douglas-fir specimens in c-perp without consideration of ring angle orientation to applied load. Five grades of Douglas-fir and

three grades of hem-Fir were tested. Stress-strain graphs were found to consist of an initial straight line section up to the proportional limit followed by a curved line extending to 0.04 or 0.05-in. of deformation followed by an almost straight line of positive slope extending out to about 0.15-in. of deformation. It was found that average stresses for a given strain could be estimated with a correlation coefficient of 0.94. Specific gravity was found to be a poor indicator of compressive strength due to the overwhelming influence of ring orientation. Douglas-fir specimens were 150-percent as strong in c-perp as hem-Fir specimens of corresponding grade. Dense grain was found to contribute more to transverse compression strength of Douglas-fir than did higher machine grades.

Studies examining the effect of moisture content and temperature on c-perp properties of wood have been conducted both in relation to end use in construction and in relation to the wood composites industry. Such studies provide useful insight into issues of variability in moisture content and drying in service and the corresponding effects on transverse compression and stability. Kunesh (1961) found that when moisture content of specimens of Yellow poplar (*Liriodendron tulipifera* L.) was controlled through all phases of testing, specimens exhibited increasingly elastic behavior with increasing moisture content. Moisture content was found to have the greatest effect on inelastic behavior in both the radial and tangential directions. Wood in green condition was found to be highly elastic so long as this moisture content was maintained. However when the moisture content was lowered after testing, much of the recovered deformation was lost. Unrecoverable strain, stress relaxation, and maximum stress at a given strain level were all found to decrease with increasing temperature as well as moisture content while they increased with increased rates of constant strain. In addition, these properties were found to be mutually dependant. For the specimens of Yellow poplar, the rate of relaxation was independent of unrecovered strain as well as stress relaxation, but was inversely dependent on maximum stress at strain level. Differences in inelastic behavior between tangential and radial direction were attributed to ray cells. Yellow poplar was not found to relax in a linear manner over short relaxation periods.

Wanbing (1996) conducted mecho-sorptive creep tests on samples of California redwood (*Sequoia Sempervirons*), red pine (*Pinus resinosa*) and ponderosa pine (*Pinus ponderosa*). Samples were cycled between 5 and 15-percent moisture content. Mecho-sorptive creep curves obtained for the samples were very similar to those of flexural samples. Larger perpendicular-to-grain compressive stresses as well as higher temperatures were found to produce correspondingly larger mecho-sorptive creep. The

greatest mechano-sorptive creep was seen in drying redwood from green to 15 percent moisture content under 120 psi and at 122 °F. Similar testing at 150 °F resulted in collapse of samples with catastrophic cross-grain bending. As the first desorption/adsorption cycle was found to produce the greatest mechano-sorptive creep, the authors conclude that any wood member subjected to transverse compression stresses in use should be dried to near its equilibrium moisture content before being put into service.

Gibson et al. (1981) characterized the cellular structure of commercial cork and related this to the cork's mechanical properties. Specifically cellular structure was related to its usefulness as friction for shoes and floor covering, energy absorption and packaging, insulation, as well as indentation and bulletin boards. They showed that in the radial section cork cells are roughly hexagonal, and that in tangential and axial section cork cells are brick shaped. Cork cells are roughly closed hexagonal prisms. Stress-strain curves were recorded for cork loaded in tension and compression along the radial, tangential and axial directions. The material was found to be linearly elastic up to about 7-percent strain. Compression across the prism axis bends cell walls and later leads to cell wall buckling. A complete constitutive law describing linear elastic behavior of cork was formulated.

Gibson et al. (1982) analyzed linear and nonlinear elastic and plastic mechanical properties of two-dimensional cellular materials or honeycombs. Honeycomb material was likened to wood material in the axial section. The eight mechanical properties (E_1 , E_2 , ν_1 , ν_2 , shear modulus, elastic collapse stress, stress at proportional limit parallel to X_1 , and stress at proportional limit parallel to X_2) were measured and their dependence on cellular properties investigated. Equations were developed that were determined to adequately describe the before mentioned mechanical properties in terms of bending elastic buckling and plastic collapse of the beams that make up the cell walls.

Pellican et al. (1994a) used a finite element program to analyze stress distribution in wood member subjected to c-perp loading scenarios. Effect of loading geometry, specimen geometry, and material properties were evaluated. Stress distributions in wood members subjected to c-perp loading were found to be complex, even with load applied over the entire surface of wood material. Large shear forces were found to exist close to the edges of loading plates. Similar to Bodig (1969), it was concluded that c-perp load carrying capacity of wood increases with increased edge to surface ratio of loading plates. An empirical formula was developed for computation of maximum stress concentration in

transverse compression as a function of material properties, specimen geometry and loading geometry using multiple regression techniques. The equation had a correlation coefficient of 0.96. It was determined that the equation could be applied to rationally determine true stress state in wood members loaded in transverse compression.

Pellican et al. (1994b) verified the finite element model used in Pellican et al. (1994a) through comparison of numerically determined deformation predictions with experimental data. Twenty-seven specimens were tested and the deformations determined at multiple locations. Results showed the model to be accurate in predicting local deformations to within 5-percent. The model, however, showed a large standard deviation of error equal to 41.5-percent. The large standard deviation in error was attributed to mainly to large errors associated with measurement of very small experimentally obtained deformations.

Stanzl-Tschegg et al. (1995) presented a testing procedure deemed to be appropriate for characterizing fracture of anisotropic complex materials such as wood. This procedure was used to determine fracture energy of spruce in the TL and RL directions. Measured load displacement curves were approximated by finite element analysis and bilinear softening diagrams.

Shiari and Wild (2004) modeled the collapse of individual pulp fibers using nonlinear finite element analysis. Geometry and material properties of fibers were obtained from experimental data on compression tests of individual wood fibers. Cell wall was assumed to be linearly elastic, homogeneous and isotropic. While models were based on gross simplification of geometry and material properties, modeling with square and circular uncollapsed geometry of fibers was able to provide upper and lower bounds on experimentally obtained force-displacement for three fibers modeled.

Lum and Karacabeyli (1994) conducted short term and 2-month constant c-perp tests on two commercial species. Finite element analyses of five typical c-perp scenarios was also performed. Results from this study justified a 15-percent increase in allowable $F_{c\perp}$ for flatwise loading as well as implementation of a 2/3 reduction factor to $F_{c\perp}$ when a member is subject to c-perp loads on opposite faces near it's longitudinal end. The 15-percent allowable increase for flatwise loaded member was based on lower likelihood of such a member having all annual rings oriented at the worst case scenario of 45 degrees to load. Both adjustments are now included in the Canadian code.

Blass and Gorlacher (2004) conducted literature review and a number of test series to derive a mechanical model for partial surface loading c-perp scenarios. A design approach was suggested in which a characteristic value for c-perp is based on full surface compression. This characteristic value is then adjusted upward based on an effective contact length parallel to grain. If the timber member under compression protrudes past the contact area, the effective contact length may be increased and correspondingly the effective area increased. In addition, this design approach proposes to distinguish between ultimate limit and serviceability states.

CHAPTER 3. MATERIALS AND METHODS

3.1 TEST ASSEMBLIES

Two assemblies were tested and evaluated. These assemblies were evaluated because they are very common c-perp construction applications.

3.1.1 Bottom Chord Of Truss On Top Plate Of Wall (BC Assembly)

The truss bottom chord bearing on wall top plate assembly is shown in Figure 3 and is hereafter referred to as BC assembly. The member representative of the bottom chord of truss is hereafter referred to as B.C. member while the members representative of top plate of wall are hereafter referred to as T.P. members. The longitudinal end of the B.C. member is sandwiched between the T.P. members. In BC-DF assemblies all members, both B.C. and T.P., are Douglas-fir. In BC-SPF assemblies, the T.P. members are Spruce-Pine-Fir while the B.C. member is Douglas-fir. The lower T.P. member rests on a rigid metal plate. Load is applied through a metal plate to the surface of T.P. members.

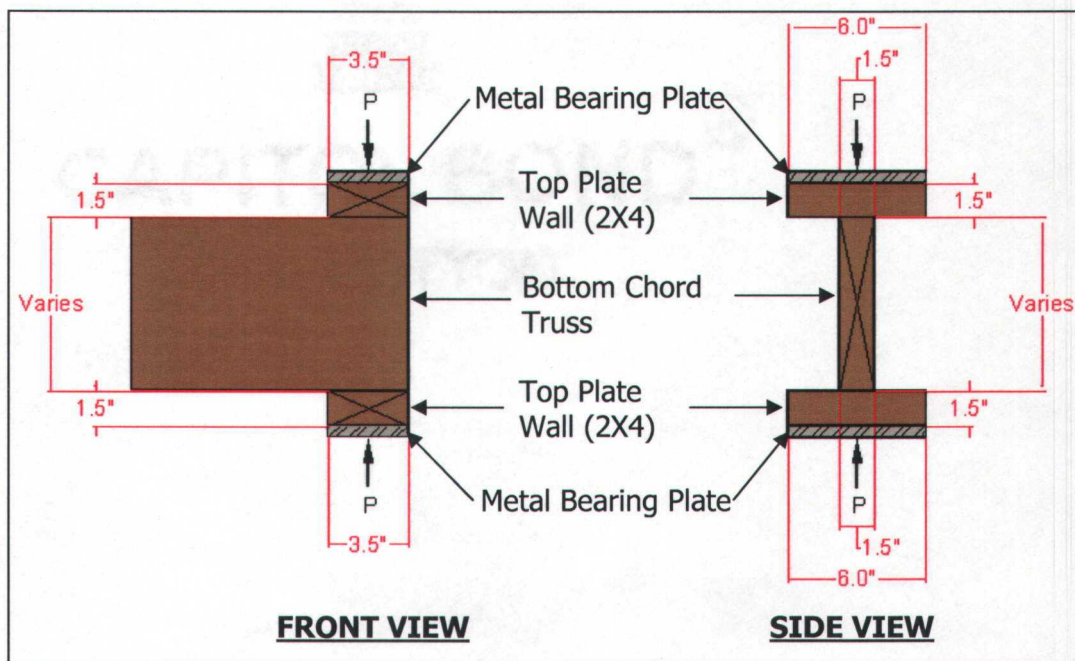


Figure 3: BC assembly – truss bottom chord on wall top plate

The following conditions apply to BC assemblies:

- Load is applied through a metal plate to the full surface on one wide face and wood-on-wood partial surface compression on the other wide face of the T.P. member (Figure 3). This condition is similar to the ASTM test specimen.
- Both narrow faces of the longitudinal end of the B.C. member are loaded (Figure 3). This condition is not represented by the ASTM specimen.
- Bearing is through wood-to-wood contact as apposed to metal-on-wood for the ASTM specimen.
- Aspect ratio of B.C. member varies (2.3 for 2X4, 4.8 for 2X8 and 7.5 for 2X12) as apposed to aspect ratio of 1 for the ASTM specimen.

The test matrix for BC assemblies is shown in Table 1. BC assemblies are labeled according to the nominal dimensions of the B.C. member and the species of T.P. members. For each BC assembly, a corresponding ASTM test was conducted on a sample cut from the same board as the B.C. member. ASTM tests are labeled according to the nominal dimensions and species of the board from which they were cut.

Table 1: Test matrix for BC assembly

Bottom Chord of Truss (DF)	Top Plate of Wall		ASTM Test of B.C. Member
	2X4 DF	2X4 SPF	
2X4	BC-2X4-DF (n=20)	BC-2X4-SPF (n=20)	ASTM-2X4-DF
2X8	BC-2X8-DF (n=17)	BC-2X8-SPF (n=18)	ASTM-2X8-DF (n=20)
2X12	BC-2X12-DF (n=20)	BC-2X12-SPF (n=20)	ASTM-2X12-DF (n=20)

3.1.2 Compression Chord Of Truss On Top Plate Of Wall (BP Assembly)

The compression chord of a shear wall bearing on bottom plate assembly is shown in Figure 4 and is here after referred to as BP assembly. A 3-in. long nominal 2X4 DF member representative of the longitudinally loaded compression chord (C.C.) of a shear wall rests on the wide face of a 6-in. long nominal 2X4 representative of the bottom plate (B.P.) of the wall. The C.C. member bears at the longitudinal end of the B.P. member.

The C.C. member is always DF while the B.P. member is either DF or SPF. The B.P. member's lower surface is fully supported by a rigid metal plate. The longitudinal end of the B.P. member away from the C.C. member bearing is clamped to prevent uplift. This represents the effect of anchor bolts which, in practice, clamp the bottom sill plate to the foundation. Load is applied through a metal plate to the top surface of the C.C. member.

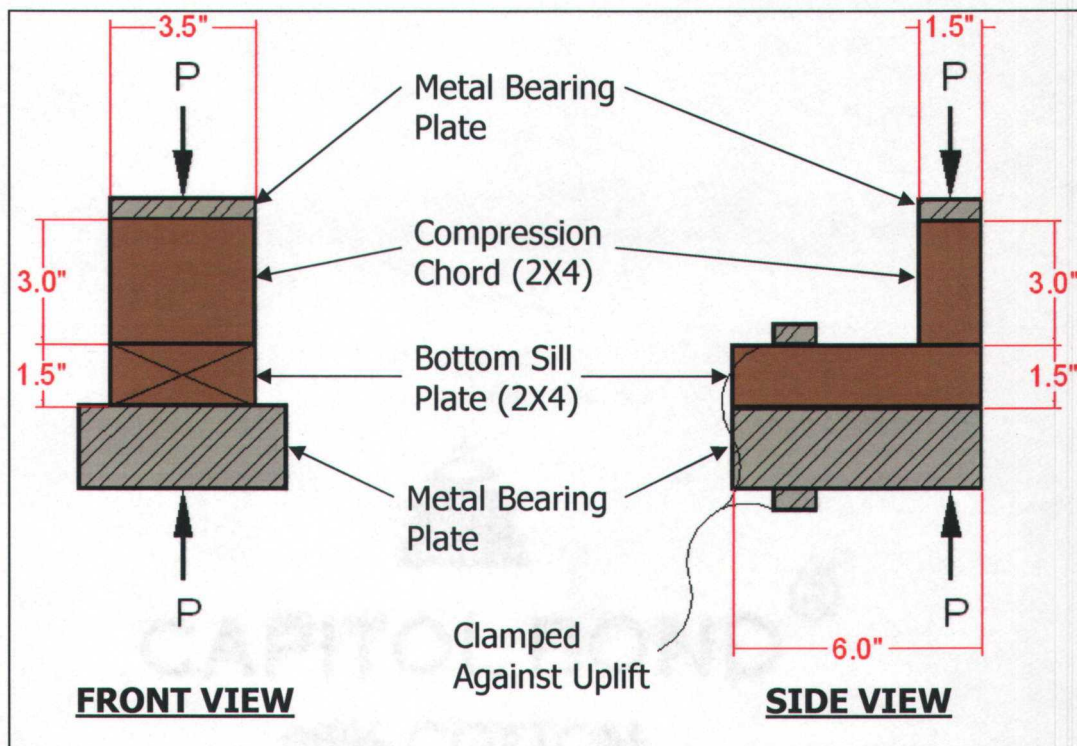


Figure 4: BP assembly – compression chord bearing on bottom plate of wall

The following conditions apply to BP assemblies:

- Load is applied through the longitudinally loaded C.C. member to the top surface of B.P. member through wood to wood bearing as apposed to metal-on-wood bearing for the ASTM specimen.
- Both wide faces of the longitudinal end of the B.P. member are stressed as shown in Figure 4. This condition is not represented by the ASTM specimen.
- The sill plate is fastened to bottom surface to prevent vertical movement/rotation.

The test matrix for BP assemblies is shown in Table 2. BP assemblies are labeled according the species of the B.P. member. For each BP test a corresponding ASTM test was conducted on a sample cut from the same board as the B.P. member. ASTM tests

Table 2: Test matrix for BP assemblies

Bottom Plate of Wall	Compression Chord of Wall	ASTM Test of B.P. Member
	2X4-DF	
2X4-DF	BP-DF (n=20)	ASTM-2X4-DF (n=20)
2X4-SPF	BP-SPF (n=10)	ASTM-2X4-SPF (n=10)

are labeled according to the nominal dimensions and species of the board from which they were cut.

3.2 FINITE ELEMENT ANALYSIS

The objective of finite element analysis was to estimate relative deflection in contacting wood members.

3.2.1 Geometry

Finite element models were constructed using ANSYS 8.1 finite element modeling program. When possible symmetry conditions were utilized in order to allow increased mesh density without exceeding the nodal capacity of the program. Annual rings were constructed as 0.02-in. thick layers in order to model an average ring count of 5 rings/in. Using the SOLID45 element (3-D, 8 nodes), six models were constructed including:

- 1(a) ASTM specimen with radial loading
- 1(b) ASTM specimen with tangential loading
- 2(a) BC assembly with radial loading
- 2(b) BC assembly with tangential loading

3(a) BP assembly with radial loading

3(b) BP assembly with tangential loading

The ASTM specimen geometries (Figure 5 and 6) were constructed as one quarter of the typical ASTM specimen (Figure 1). A metal plate was also constructed as one-quarter of the 4-in.² metal loading plate (Figures 5 and 6). One specimen geometry was constructed with horizontal annual rings i.e. model loaded in radial direction (Figure 5), and one specimen geometry with vertical annual rings, i.e. model loaded in tangential direction.

Two BC assemblies (Figure 7 and 8) were constructed to model a 12-in. long nominal 2X12 compression chord sandwiched between two 6-in. long nominal 2X4 T.P. members (BC-2X12). As near possible model geometry was constructed as one quarter of the configuration depicted in Figure 3, including the metal loading plate. One model was constructed with annual rings running horizontally through the 1.5-in. width of the bottom chord member, i.e. radially loaded model (Figure 7). The second model was constructed with annual rings running vertically through the 11.25-in. depth of the bottom chord member, i.e. tangentially loaded model (Figure 8). In both models, the 2X4 representing the top plate of a wall is loaded radially. Due to ring orientation in tangentially loaded model, it was necessary to construct the model geometry thickness as a multiple of annual ring thickness. This meant that the tangential model was constructed 0.8-in. thick. After applying symmetry boundary conditions the geometry models a 1.6 rather than 1.5-in. thick 2X12 bottom chord member. In each case, annual rings run horizontally through the 3.5-in. dimension of the top plate. Again due to ring orientation of top plate this meant that depth of top plate must be a multiple of annual ring thickness and top plates were constructed 1.6 rather than 1.5-in. deep.

Two BP assemblies (Figure 9 and 10) were constructed as a 6-in. long nominal 2X4 C.C. member resting on a 6-in. long nominal 2X4 B.P. member. As close as possible this model was constructed as one-half of the configuration shown in Figure 4 with the exception that the longitudinally loaded compression chord member measured 6-in. long rather than the 3-in. used in testing and depicted in Figure 3. In addition a metal loading plate was constructed on top of the half geometry of the compression chord. One model was constructed with annual rings running horizontally through the 3.5-in. width of the bottom plate, i.e. radial model (Figure 9). The second model was constructed with annual rings running vertically through the 1.5-in. dimension of the bottom plate (Figure 10). Due

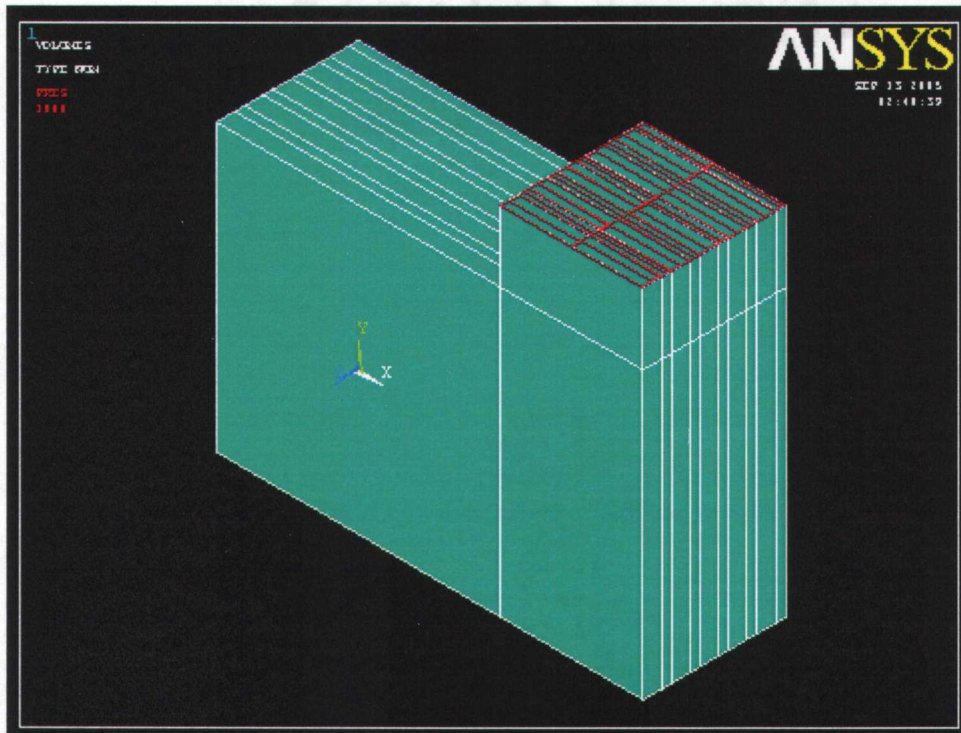


Figure 5: Finite element model of ASTM specimen with radial loading

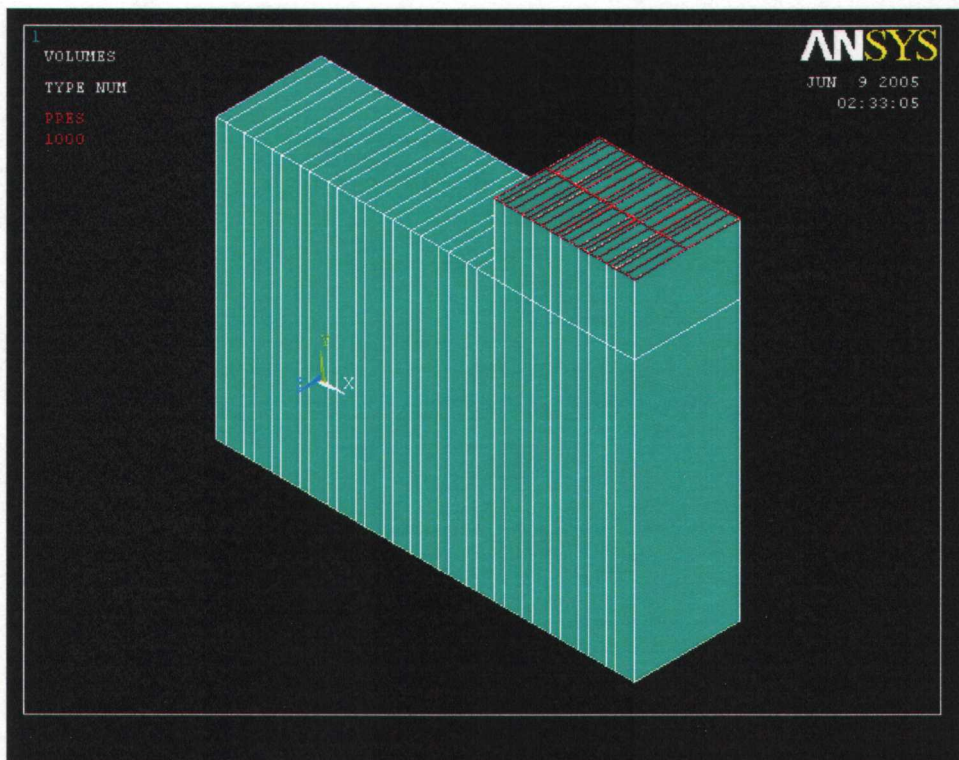


Figure 6: Finite element model of ASTM specimen with tangential loading

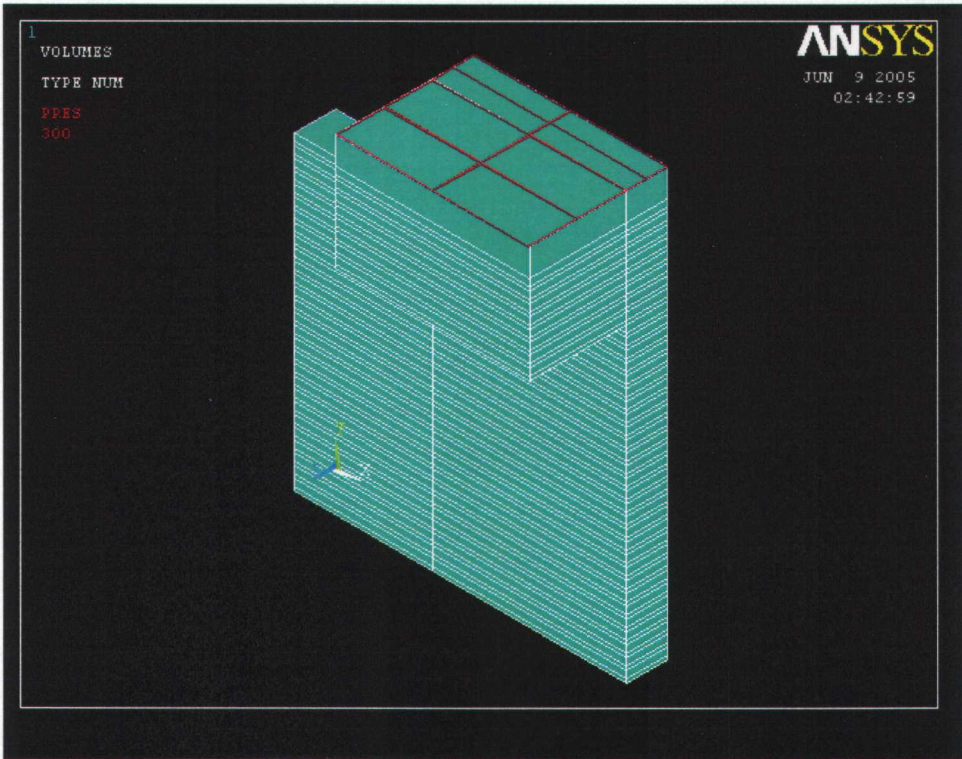


Figure 7: Finite element model of BC-2X12 assembly with radial loading

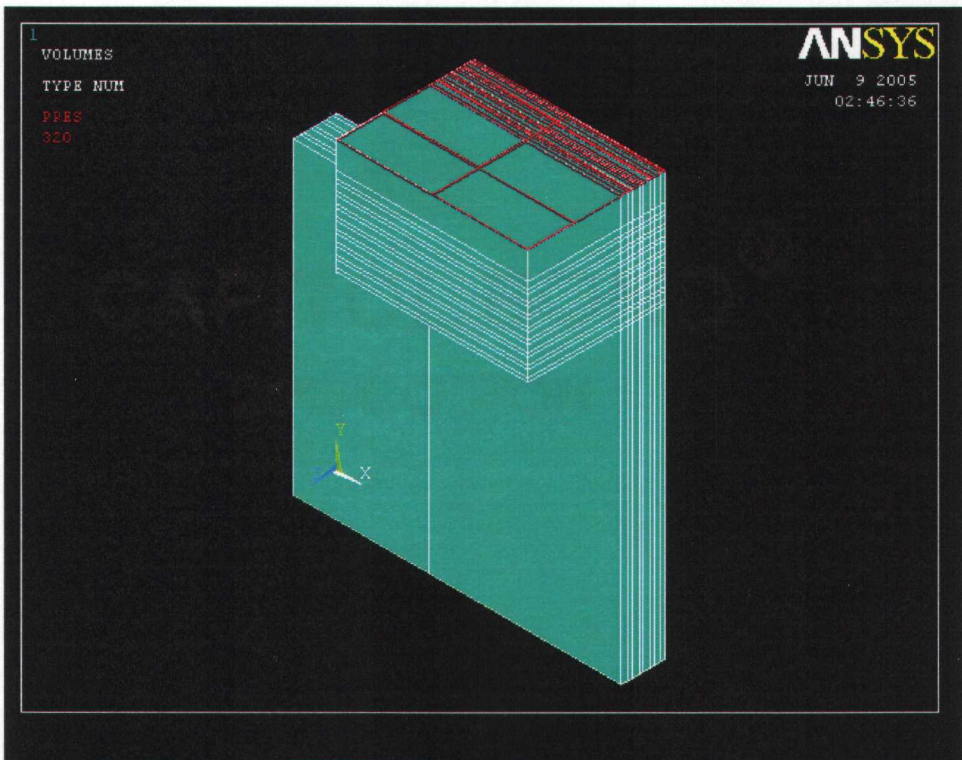


Figure 8: Finite element model of BC-2X12 assembly with tangential loading

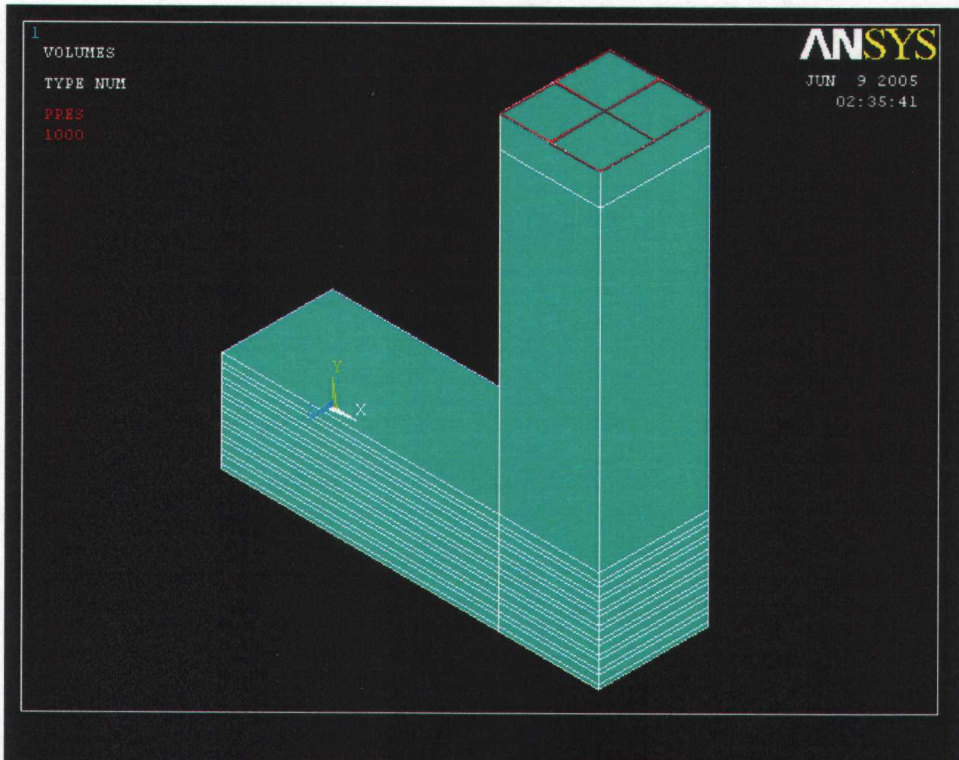


Figure 9: Finite element model of BP assembly with radial loading

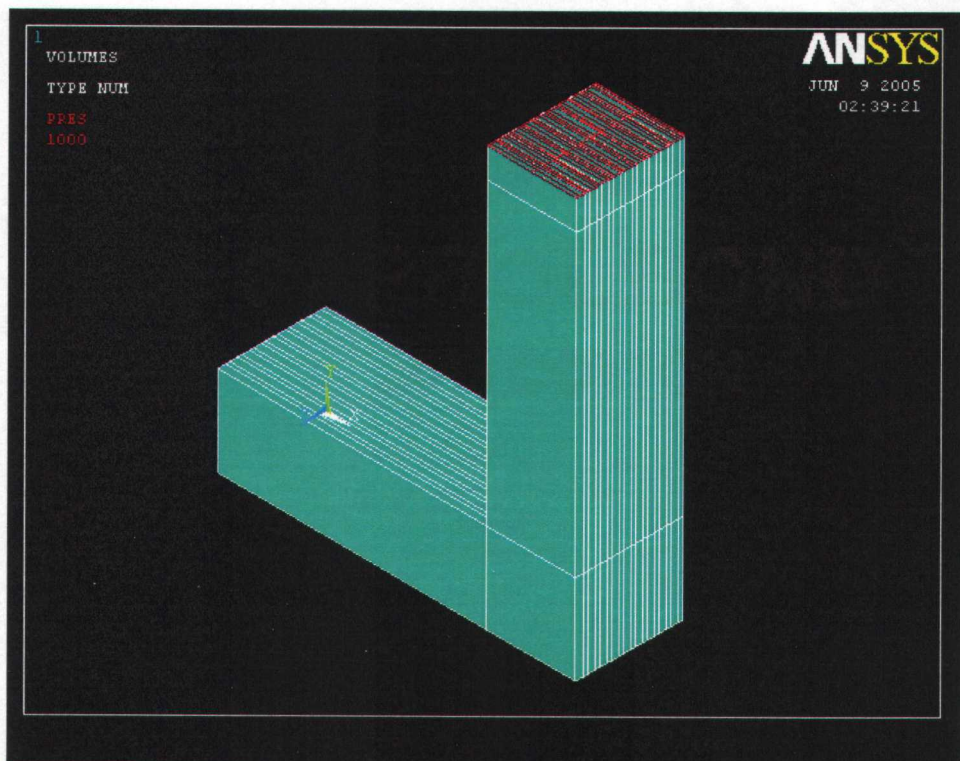


Figure 10: Finite element model of BP assembly with tangential loading

to annual ring orientation in the radial model it was necessary to construct the depth of the bottom plate as a multiple of annual ring thickness, and the bottom plate member was constructed 1.6-in. deep. In the tangential model, it was necessary to construct bottom plate width as a multiple of annual ring thickness and thickness was 1.6-in. When symmetry conditions are applied this means the tangential geometry models a 2X4 bottom plate that is 3.6-in. rather than 3.5-in. wide.

3.2.2 Boundary Conditions

FEM utilized symmetry about x-y and y-z planes for ASTM specimen, symmetry about x-y and x-z planes for BC assembly and symmetry about x-y plane for BP assembly. Due to these symmetry conditions, one-quarter of the ASTM and BC-2X12 assemblies and one half of the BP assembly were modeled.

Nodes on the bottom surface of ASTM and BP models were constrained against vertical movement in order to simulate full support of the lower area of these models. In addition these nodes were constrained in all directions to provide model stability. Coincident nodes were coupled in order to create continuity in the model. This included coincident nodes between metal loading plate and wood members as well as between contacting wood members.

3.2.3 Loading Conditions

In each case, load was applied through the metal loading plate. Red lines indicate where load was applied (Figures 5-10). As explained in the next section, ASTM tangential model was constructed to deflect 0.04-in. at an applied stress of 1000 psi. For consistency, load was applied to produce a bearing stress of 1000 psi at contact between metal loading plate and specimen in ASTM assemblies. In BC and BP assemblies, load was applied to produce a bearing stress of 1000 psi at contact between wood members. Therefore, a bearing stress of 1000 psi was present at the contact surfaces of T.P. and B.C. members in BC assemblies and at contact surface of C.C. and B.P. members in BP assemblies.

3.2.4 Material Properties

With the exception of C.C. (longitudinally loaded 2X4 in BP models), gross wood material was idealized as a composite with alternating layers of earlywood and latewood. Annual

rings were idealized as flat volumes having infinite radius of curvature. This idealization holds more nearly true for flat-sawn lumber away from pith. Both earlywood and latewood were modeled as linear isotropic materials. Based on observation of typical lumber in the lab, latewood layers were constructed 0.07-in. thick. Earlywood layers were 0.13-in thick. This geometry is consistent with a wood material composed of 35-percent latewood, and 65-percent earlywood. This earlywood to latewood ratio is consistent with findings cited in (Haygreen et al. 2003) for fertilized fast grown distinct ring softwoods. The layer geometry is meant to be representative of typical fast grown wood material utilized in many modern construction applications. Transverse compression modulus of elasticity ratio ($E_{\text{latewood}} / E_{\text{earlywood}}$) was constant at 5. The decision to use this ratio was largely based on work by Kretschmann et al. (2003) who found that ratios of latewood to earlywood longitudinal MOE ranged between 0.8 and 6.5. MOE of earlywood and latewood layers were determined so that the tangentially loaded ASTM model would deflect 0.04-in. at an applied stress of 1000 psi. This was done in an attempt to model a typical ASTM c-perp test. Base c-perp design value was determined at 1044 psi (NDS c-perp value for DF multiplied by 1.67). This value was rounded to 1000 psi and the ASTM tangential model was constructed to deflect 0.04-in. (ASTM c-perp deflection value) at this applied stress. Transverse compressive MOE of earlywood was 13,325 psi. Transverse compressive MOE of latewood was 66,625 psi. MOE of steel was 3.00E+07 psi. The B.P. model was run once for each of two different longitudinal E values of compression chord, i.e. case 1 ($E = 1.95E6$ psi) and case 2 ($E = 1E6$ psi)

3.3 MATERIAL ACQUISITION AND SPECIMEN MATCHING

Two by four Douglas-fir (DF) material was obtained from inventory at the Oak Creek Laboratory. Two by four Spruce-Pine-Fir (SPF) material as well as 2X8 and 2X12 DF materials were obtained from Action Wood Products in Turner, Oregon. Twenty boards of each of the before mentioned species and size were obtained for testing. Therefore, a total of 80 boards were obtained for sample preparation (Table 3). Boards were grouped by species and dimension, i.e. 20 DF 2X4s, 20 SPF 2X4s, 20 DF 2X8s, and 20 DF 2X12s (See table 3). Boards in each group were randomly assigned numbers 1 through 20. Members for use in BC, BP, and ASTM testing assemblies were cut from boards and labeled with a test order number corresponding to the board number from which they were cut. Therefore, all test number 1 specimens were cut from board number 1, all test number 2 specimens were cut from board number 2, etc. Board number from which

Table 3: Boards obtained for specimen preparation

Species	Nominal Dimension		
	2X4	2X8	2X12
DF	20	20	20
SPF	20	----	----

specimens were cut therefore corresponded to testing order within their respective test assemblies. When possible, defect free, or close to defect free, samples were cut from wood material, that is an effort was made to cut around knots, wane and other defects in the boards. When defects were present, samples were arranged during testing to minimize their effect.

The lumber materials were sampled as:

From the twenty 2X4 DF boards, 12 test samples were cut from each board (Figure 11).

From the twenty 2X4 SPF boards, 8 test samples were cut from each board (Figure 12).

From the twenty 2X8 DF boards, 3 test samples were cut from each board (Figure 13)

From the twenty 2X12 DF boards, 3 test samples were cut from each board (Figure 14).

3.4 SPECIMEN PREPARATION

Samples were cut in a fashion deemed to be consistent with construction practice. Contact surfaces were rough and members were not always perfectly rectilinear. Prior to testing, all specimens were conditioned at 20 °C and 65 percent humidity until daily weight became stable. Member dimensions (length, width, and thickness) were measured with a digital caliper accurate to within .003-in. and recorded. The data recorded for each sample included rings/in., percent latewood, and average ring angle with respect to load. Additionally top and bottom surface as well as mid depth ring angle with respect to load were recorded for 2X8 and 2X12 samples. Immediately prior to testing, samples were weighed (W_T). After testing, the specimens were photographed and dried at 103 °C for no less than 48 hours. Specimens were then re-weighed and dry weight for each specimen was recorded (W_D). Moisture content at time of testing (M_{CT}) was determined according to ASTM D 4442 Method A. Specific gravity (G_M) was determined according to ASTM D

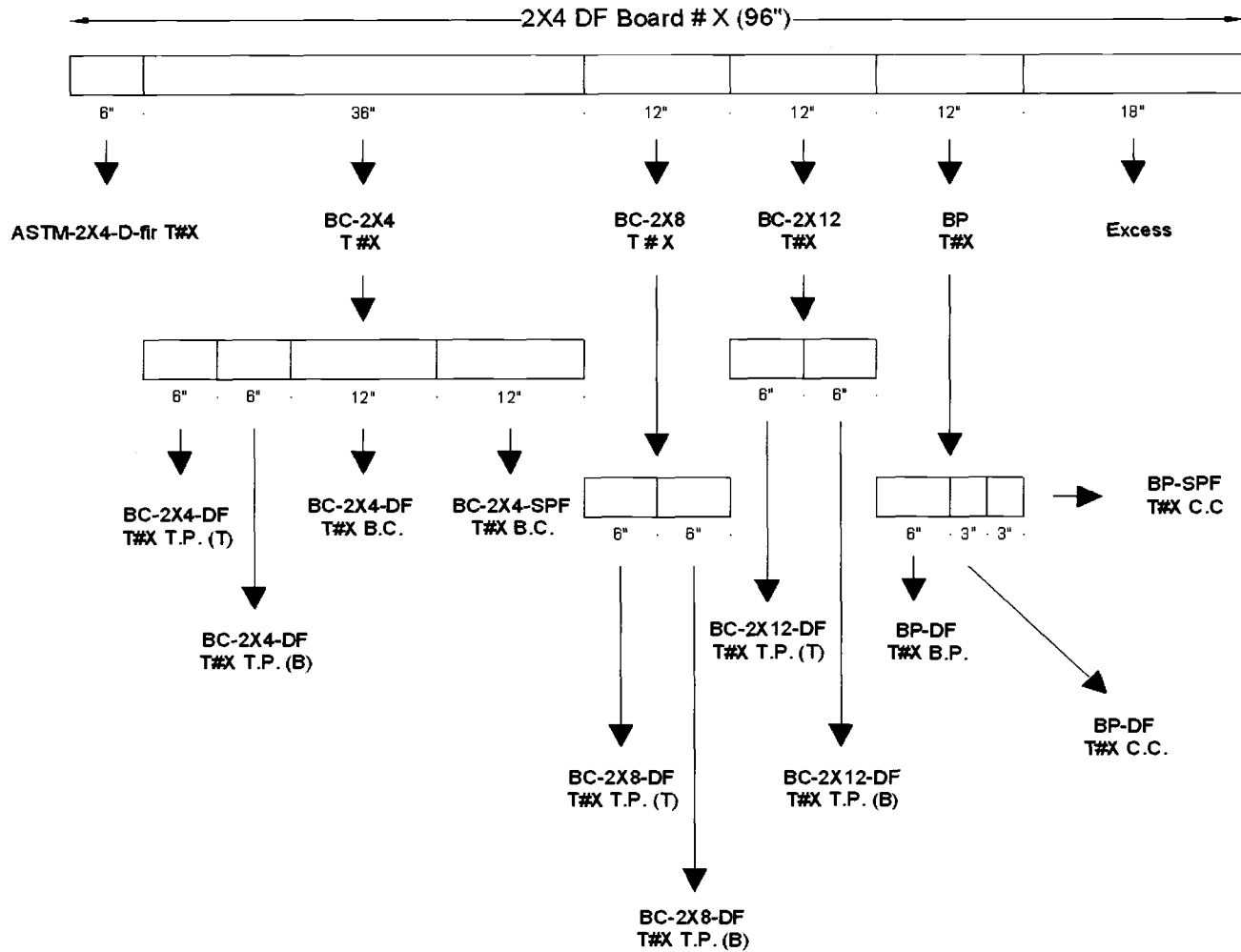


Figure 11: Samples cut from each 2X4 DF board

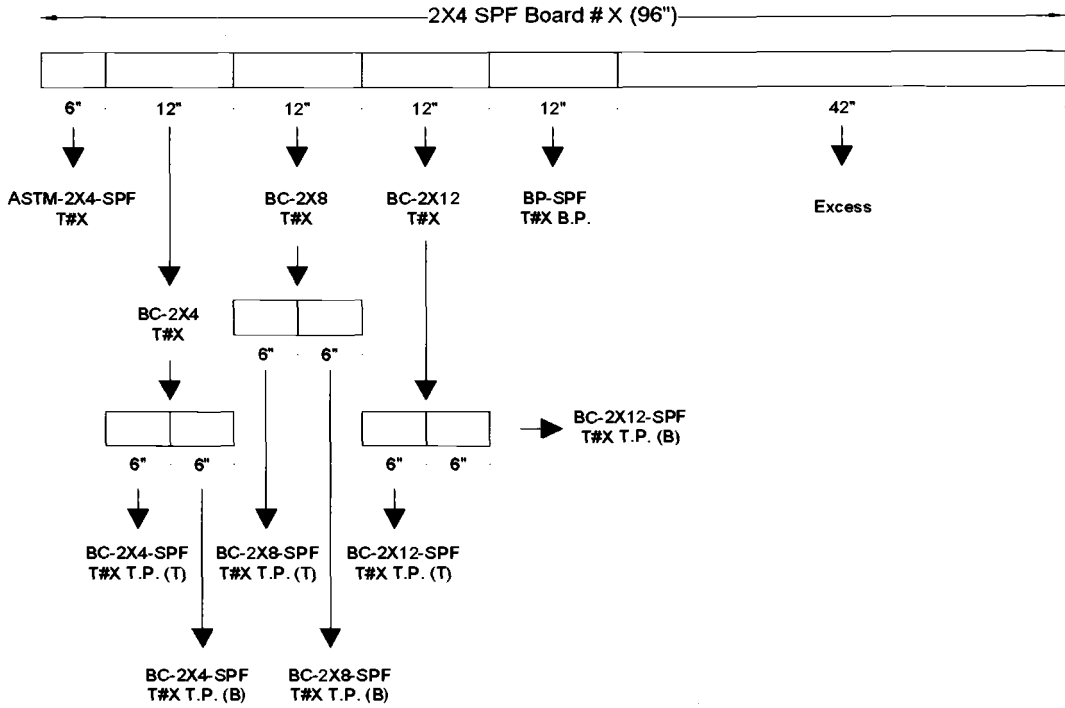


Figure 12: Samples cut from each 2X4 SPF board

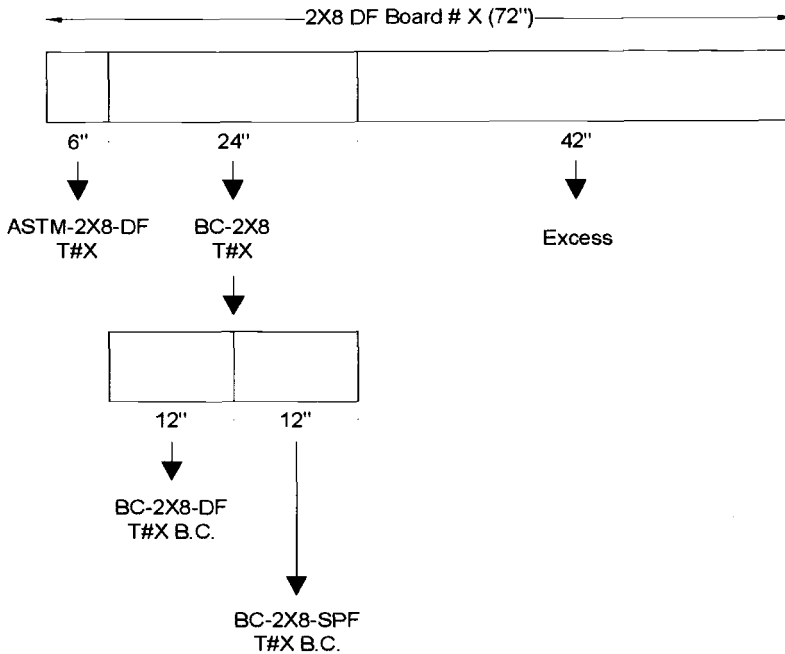


Figure 13: Samples cut from each 2X8 DF board

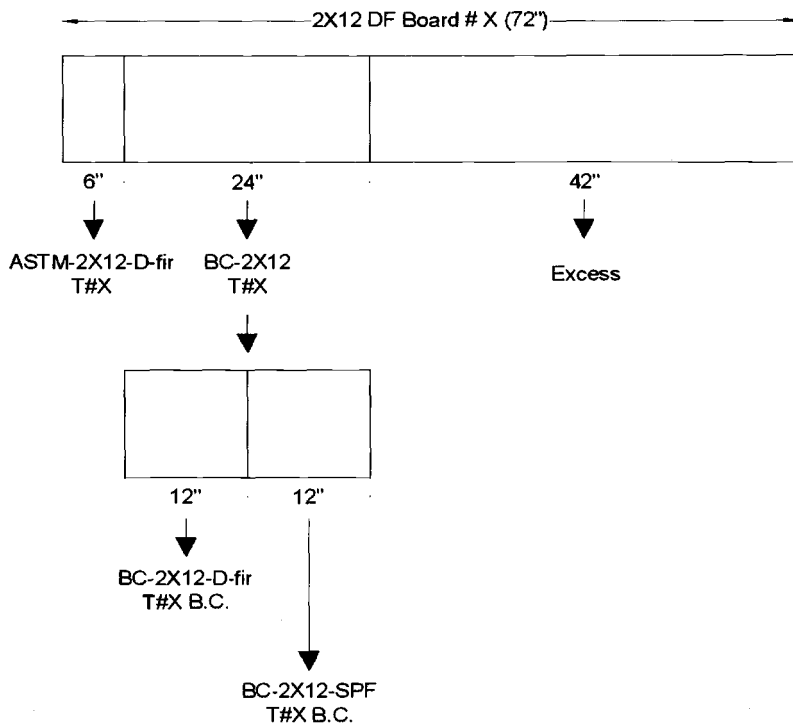


Figure 14: Samples cut from each 2X12 DF board

2395 Method A. G_M was calculated using volume after conditioning (about 12% M_{CT}) and dry weight.

3.5 TEST SETUP AND EQUIPMENT

An MTS hydraulic actuator with a 10-in. stroke was used to apply load. Figures 15 to 17 show the BC assembly test setups during testing. The lower top plate member rests on a metal base plate. Movable magnetic stops were used to hold the lower top plate member in position. The test head was brought flush with the upper top plate member and the truss bottom chord and upper top plate positioned. The test head could translate only vertically but it could not rotate.

Figure 18 shows the BP assembly test setup during testing. The bottom plate member rests on a metal base plate. Movable magnetic stops were used to hold the compression chord and bottom plate member in their respective positions. The compression chord was allowed one degree of freedom and could translate only vertically.

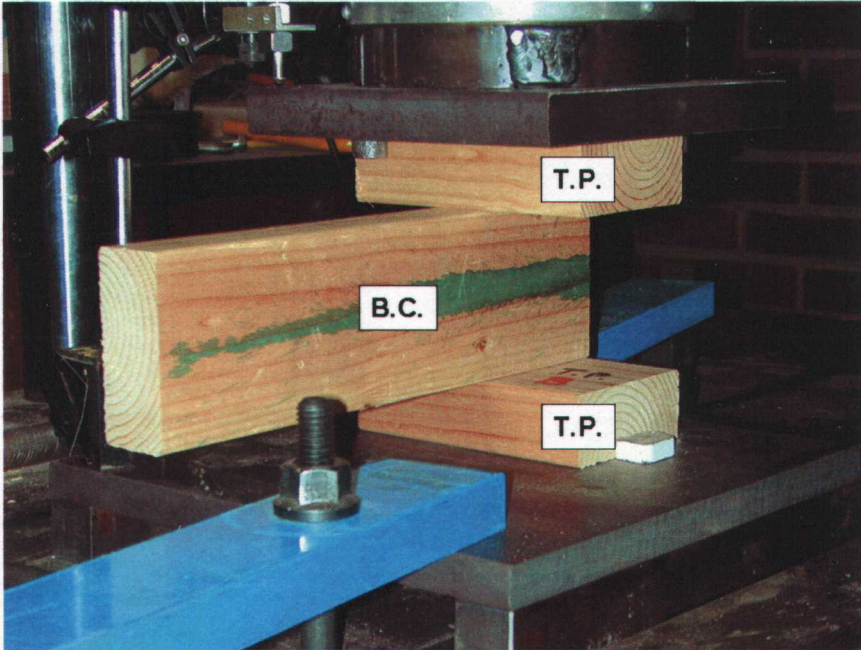


Figure 15: BC-2X4 test setup

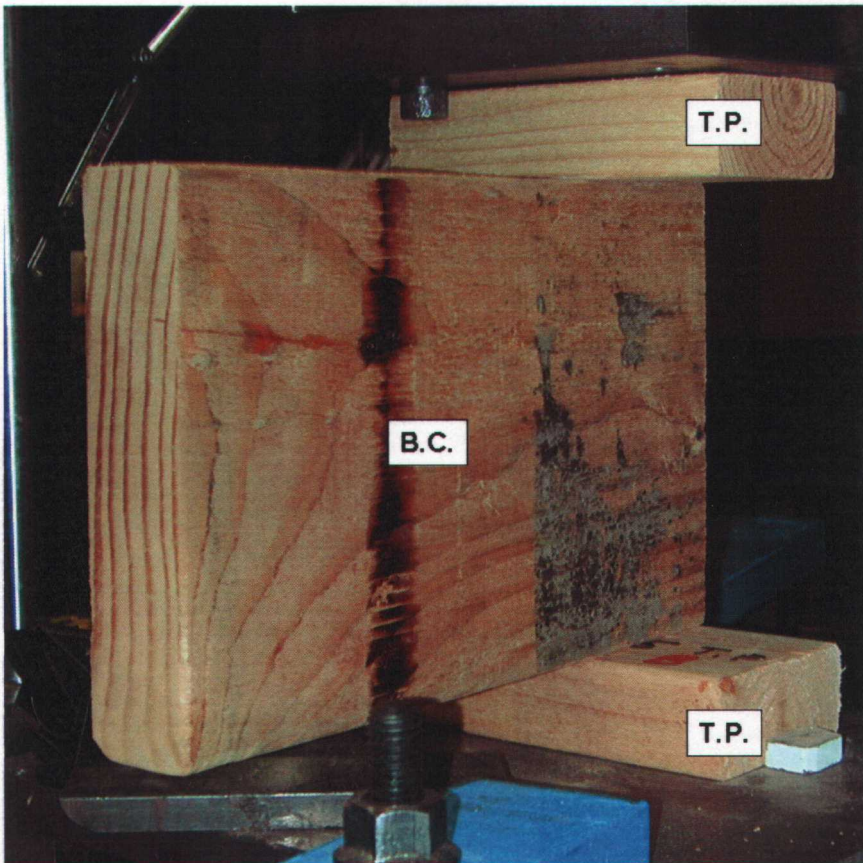


Figure 16: BC-2X8 test setup

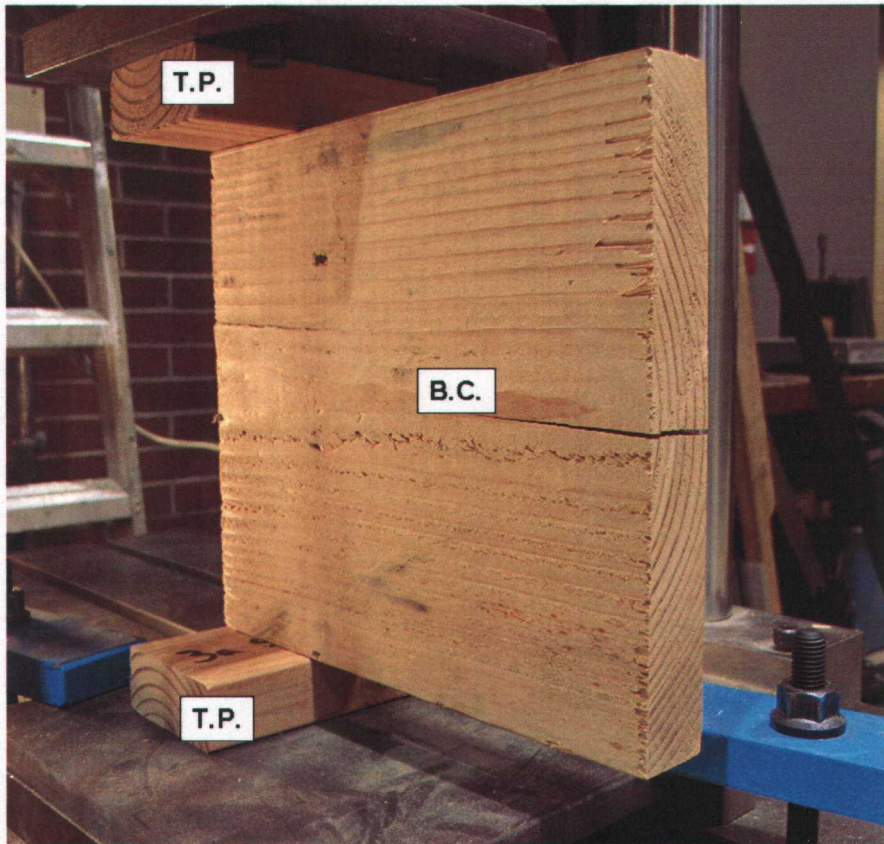


Figure 17: BC-2X12 test setup

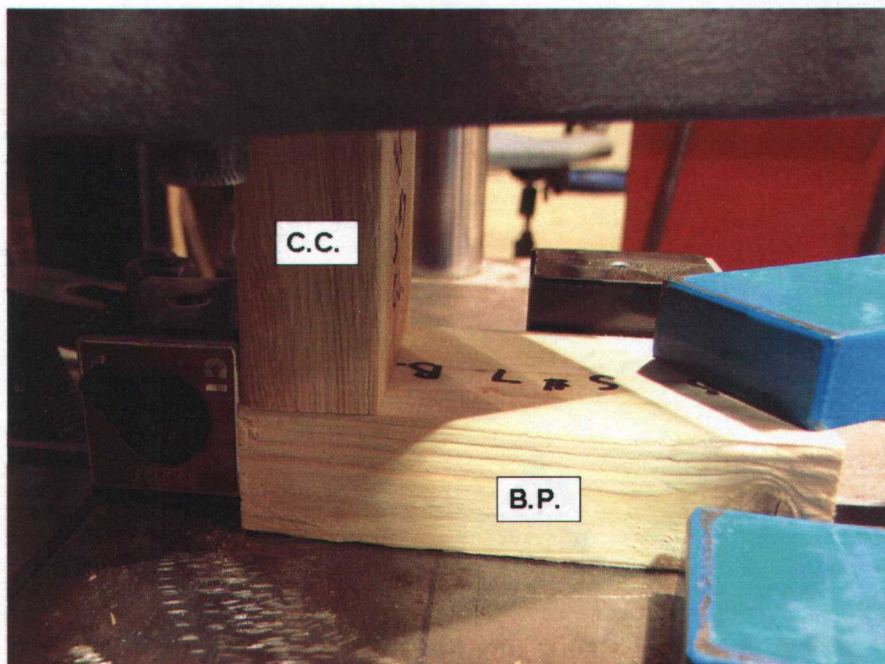


Figure 18: BP test setup

3.6 TESTING AND DATA COLLECTION

The compressive deflection of individual assembly members was not measured. Instead total assembly deflection was measured. A 50,000 lb Strain Sert load cell connected in-line with the hydraulic actuator was used to measure compression forces during testing. Downward displacement was measured by a MTS Temposonics position sensor inline with the hydraulic actuator. Data was routed through a Schaevitz LVDT signal conditioner to a National Instruments AT-MIO/AI 16-50E computer. A labview Vi was utilized to display force and displacement.

BC-2X4 assemblies were tested at a deflection rate of 0.13 in./min. up to 10-percent system strain or 0.65-in. compression. After 0.65-in. compression, head movement was manually increased to 1.3 in./min. and testing continued to beyond 20-percent system strain, or 1.3-in. compression. BC-2X8 assemblies were tested at a deflection rate of 0.2 in./min., and testing continued to beyond 10-percent system strain or 1.025-in. compression. BC-2X12 specimens were tested at a deflection rate of 0.285 in./min., and testing continued to beyond 10-percent system strain or 1.425-in. compression.

BP members were tested at a deflection rate of 0.03 in./min. up to 10-percent strain in the 1.5-in. bottom plate member, or 0.15-in. compression. After 0.15-in. compression, press head movement was manually increased to 0.3 in./min. and testing continued to beyond 25-percent strain in the bottom plate member or .375-in. compression.

ASTM specimens were tested according to the guidelines established in ASTM D-143 for c-perp testing but with the following exceptions; depth measured only 1.5-in. due to availability of standard dimensional lumber, ring angle with respect to applied load was not controlled, and testing was conducted at a constant cross head displacement rate of 0.03 in./min. Load and compressive deflection were recorded throughout testing. Testing was documented with digital photos and videos.

3.7 DATA ANALYSIS

It was necessary to adjust the data to reflect only c-perp deflection. Therefore for BP assembly tests, theoretical deflection occurring in the longitudinal C.C. member was subtracted from the data. Due to the fact that the C.C. member is well within its linear stress-strain relationship at the stresses applied during testing, it was theorized that the

longitudinally loaded member behaves as a spring with constant E value. Theoretical deflection in longitudinally loaded member was assumed to be proportional to load. This assumption was validated by FEM. A constant parallel to grain E value of 1.95E6 psi was assumed for all compression chord members (FPL 1999). Using a mechanics of materials approach theoretical deflection of the longitudinally loaded compression was adjusted out of system deflection to estimate bottom plate compression.

The linear range in the stress-strain diagram was identified by visual inspection. A linear regression was fit to this range of data and used to define stress offsets for assembly tests. Both deflection and offset strain values reported are based on this approach.

For all tests, stress values were recorded at 0.04-in. system deflection ($\sigma_{0.04-D}$), 0.04-in. system offset deflection ($\sigma_{0.04-OD}$), 2-percent system strain ($\sigma_{2\%-S}$) and 2-percent system offset strain ($\sigma_{2\%-OS}$). In addition, maximum stress (σ_{max}) and strain at maximum stress were also calculated. The σ_{max} was defined as maximum stress achieved between 0 and maximum system strain without exceeding 10-percent system strain. All catastrophic failures with corresponding system strains and stresses were recorded.

3.8 STATISTICAL ANALYSIS

All pair-wise statistical tests were accomplished by using a Tukey-Cramer multiple comparison. For all analyses, covariates were tested for correlation to the response variables. The covariate selection process mainly consisted of fitting a rich regression model and implementing backward elimination to determine the final model. In addition, covariate selection was further supported by visual inspection of pair-wise plots of covariates and response, use of scientific knowledge, and testing for multicollinearity. For BC-2X8 and BC-2X12 tests a logistic regression was created to model the likelihood of catastrophic failure of the bottom chord member. Model assumptions were checked for all statistical tests.

3.8.1 BC Assembly

The following covariates were accounted for in ANOVA modeling:

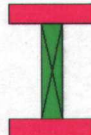
- Average annual rings per in. in top plate material
- Average ring angle with respect to load of top plate material
- Average latewood percentage of top plate material

- Specific gravity of top plate material
- Average annual rings per in. in bottom chord material
- Average ring angle with respect to load in bottom chord material
- Average late wood percentage of bottom chord material
- Specific gravity of bottom chord material

Additional covariates of average ring angle at interface of bottom chord member with top plate members and bottom chord mid depth annual ring angle were included in the logistic regression based on response of catastrophic failure for BC-2X8 and BC-2X12 B.C. members.

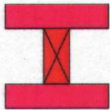
Analysis of BC tests based on responses of $\sigma_{0.04-OD}$ and σ_{max} was conducted utilizing a split-block analysis of variance in which there were 20 blocks, or replications. Figure 19 shows a visual representation of block # X (where X = 1 to 20). BC-2X8-DF assembly had only 17 replications, and as a result the model contained 17 complete blocks and 3 incomplete blocks. Blocks were split by T.P. material (board from which the T.P. members were cut) and B.C. material (board from which the B.C. member was cut). Therefore each block had two factors, i.e. T.P. material and B.C. material. There were 2 levels of the T.P. material factor. These levels corresponded to the board from which T.P. members were cut, i.e. T.P. members cut from DF board (level 1) and T.P. members cut from SPF board (level 2). There were 3 levels of the B.C. material factor. These levels corresponded to the board from which B.C. members were cut, i.e. B.C. cut from 2X4-DF board (level 1), B.C. cut from 2X8-DF board (level 2), and B.C. cut from 2X12-DF board (level 3). The model was run both with and without inclusion of covariate effect on response.

Paired comparisons of BC tests vs. ASTM tests of the main member were conducted utilizing 3 block design models with 20 blocks or replications. Each block had 3 levels of the main factor (test assembly). Figures 20 to 22 show visual representations of block #X (where X = 1-20) for respectively, BC-2X4, BC-2X8 and BC-2X12 assembly comparisons to ASTM main member. For BC-2X4 and BC-2X12 comparisons to ASTM main members, the models included 20 complete blocks. Due to the fact that BC-2X8-DF assembly had only 17 replications, the BC-2X8 model contained 17 complete blocks and 3 incomplete blocks. The main factor was test assembly and levels of test assembly were contingent on the particular comparison being made. Levels of the main factor included BC-2X4-DF,

Factor 2 (B.C. Material)	Factor 1 (T.P. Material)	
	Level 1 (2X4-DF B#X)	Level 2 (2X4-SPF B#X)
Level 1 (2X4-DF B#X)		
Level 2 (2X8-DF B#X)		
Level 3 (2X12-DF B#X)		

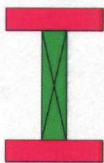
Note: Members of the same color are from the same board

Figure 19: BC split block model (block #X)

Factor 2 (Main Member Material)	Factor 1 (Test Assembly)		
	Level 1 (BC-2X4-DF B#X)	Level 2 (BC-2X4-SPF B#X)	Level 3 (ASTM-2X4-DF B#X)
(2X4-DF B#X)			

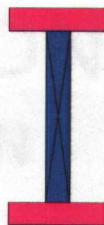
Note: Members of the same color are from the same board

Figure 20: Block design for BC-2X4 assemblies and corresponding ASTM tests (block #X)

Factor 2 (Main Member Material)	Factor 1 (Test Assembly)		
	Level 1 (BC-2X8-DF B#X)	Level 2 (BC-2X8-SPF B#X)	Level 3 (ASTM-2X8-DF B#X)
(2X8-DF B#X)			

Note: Members of the same color are from the same board

Figure 21: Block design for BC-2X8 assemblies and corresponding ASTM tests (block #X)

Factor 2 (Main Member Material)	Factor 1 (Test Assembly)		
	Level 1 (BC-2X12-DF B#X)	Level 2 (BC-2X12-SPF B#X)	Level 3 (ASTM-2X12-DF B#X)
(2X12-DF B#X)			

Note: Members of the same color are from the same board

Figure 22: Block design for BC-2X12 assemblies and corresponding ASTM tests (block #X)

BC-2X8-DF, BC-2X12-DF, BC-2X4-SPF, BC2X8-SPF, BC-2X12-SPF and corresponding ASTM tests of B.C. main members. All responses were compared i.e. $\sigma_{0.04-D}$, $\sigma_{2\%-S}$, $\sigma_{0.04-OD}$ and $\sigma_{2\%-OS}$. Comparisons were conducted both before and after inclusion of covariate effect.

A logistic regression was created to model the likelihood of catastrophic failure of the bottom chord member between 0 and 10 percent system strain in BC-2X8 and BC-2X12 tests. The response in the regression was modeled as fail or no-fail.

3.8.2 BP Assembly

The following covariates were accounted for in ANOVA modeling:

- Average annual rings per in.
- Average ring angle with respect to applied load
- Average late wood percentage
- Specific gravity

Due to differing covariates and configuration in BP assembly as compared with BC assembly, it was not appropriate to include BP assembly in the same model with BC assembly tests. Instead BP assembly was analyzed in 3 block models, each utilizing an ANOVA model with 2 levels of the main factor (test assembly). These ANOVA models were analogous to paired t-tests but allowed for inclusion of covariate effect. In these models the main factor was test assembly. Levels of this factor included BP-DF, BP-SPF, ASTM-DF, and ASTM-SPF depending on the particular comparison being made. In BP-DF assembly comparisons to ASTM main members, the model included 20 complete blocks. Figure 23 shows a visual representations of block #X (where X = 1 to 20) for this comparison. In BP-SPF assembly comparisons to ASTM main members, the model included 10 complete blocks. Figure 24 shows a visual representations of block #X (where X = 1 to 10) for this comparison. In comparison of BP-DF assembly to BP-SPF assembly, member properties specific to wood species were found to have significant covariate effect. It was not deemed appropriate to adjust for these covariates as this would have negated effect of wood species in the comparison. Without inclusion of covariate effect this model was analogous to a 2 independent sample t-test. All responses were compared, i.e. $\sigma_{0.04-D}$, $\sigma_{2\%-S}$, $\sigma_{0.04-OD}$ and $\sigma_{2\%-OS}$. Comparisons included BP-DF vs. paired ASTM tests (both before and after inclusion of covariate effects), BP-SPF vs. paired ASTM tests (both before and after inclusion of covariate effects), and BP-DF vs. BP-SPF (without inclusion of covariate effects).

Factor 2 (Main Member Material)	Factor 1 (Test Assembly)	
	Level 1 (BP-DF B#X)	Level 2 (ASTM-2X4-DF B#X)
(2X4-DF B#X)		

Note: Members of the same color are from the same board

Figure 23: Block design for BP-DF assemblies and corresponding ASTM tests (block #X)

Factor 2 (Main Member Material)	Factor 1 (Test Assembly)	
	Level 1 (BP-SPF B#X)	Level 2 (ASTM-2X4-SPF B#X)
(2X4-SPF B#X)		

Note: Members of the same color are from the same board

Figure 24: Block design for BP-SPF assemblies and corresponding ASTM tests (block #X)

CAPITOL BOND
 100% COTTON

CHAPTER 4. RESULTS AND DISCUSSION

4.1 FINITE ELEMENT ANALYSIS

Figures 25, 27, and 29 show strain profiles for the radially loaded ASTM specimen, the radially loaded BC-2X12 assembly, and the radially loaded BP assembly respectively. Figures 26, 28, and 30 show strain profiles for tangentially loaded ASTM specimen, tangentially loaded BC-2X12 assembly, and tangentially loaded BP assembly respectively. All models exhibit ring orientation specific strain profiles. Radial loading produces regions of high strain in earlywood layers with alternating regions of lower strain in stiffer latewood layers throughout the depth of the member. Similar to findings from Bodig (1965), Kennedy (1968), Easterling et al. (1982), and Tabarsa and Chui (1999, 2000 and 2001), in radially loaded models majority of system deflection occurs within earlywood layers. In tangential loading, the trend is much different. Due to the geometry of these models both earlywood and latewood layers are forced to deflect in unison. Structurally this phenomenon can be likened to latewood layers acting as reinforcing columns which gain lateral support from the softer earlywood layers (Bodig 1965, Kennedy 1968, Tabarsa and Chui 2001). In tangential models the alternating regions of high and low strain observed in radial models are not present.

In finite element modeling (F.E.M.), tangentially loaded members exhibited higher stiffness than did radially loaded members. For example, strain in the radially loaded ASTM model was 3.13-percent as apposed to 2-percent strain in the tangentially loaded ASTM model. As previously discussed, latewood layers tend to reinforce wood material in tangential loading. Bodig (1965), Kennedy (1968) and Tabarsa and Chui (2001) also found that rays tend to reinforce wood material in radial loading. Generally stiffness in radial and tangential loading are near equivalent. Due to the fact that the presence of ray material was not accounted for in modeling, the large differences in stiffness observed between radially and tangentially loaded models are probably unrealistic.

ASTM modeling results show that for the radial loaded model (Figure 25), strain in annual rings directly under the loading plate is fairly constant with depth of the member. The strain profile extends toward the unloaded longitudinal ends of the specimen with increasing depth of the member. In tangential loading (Figure 26), the ASTM model

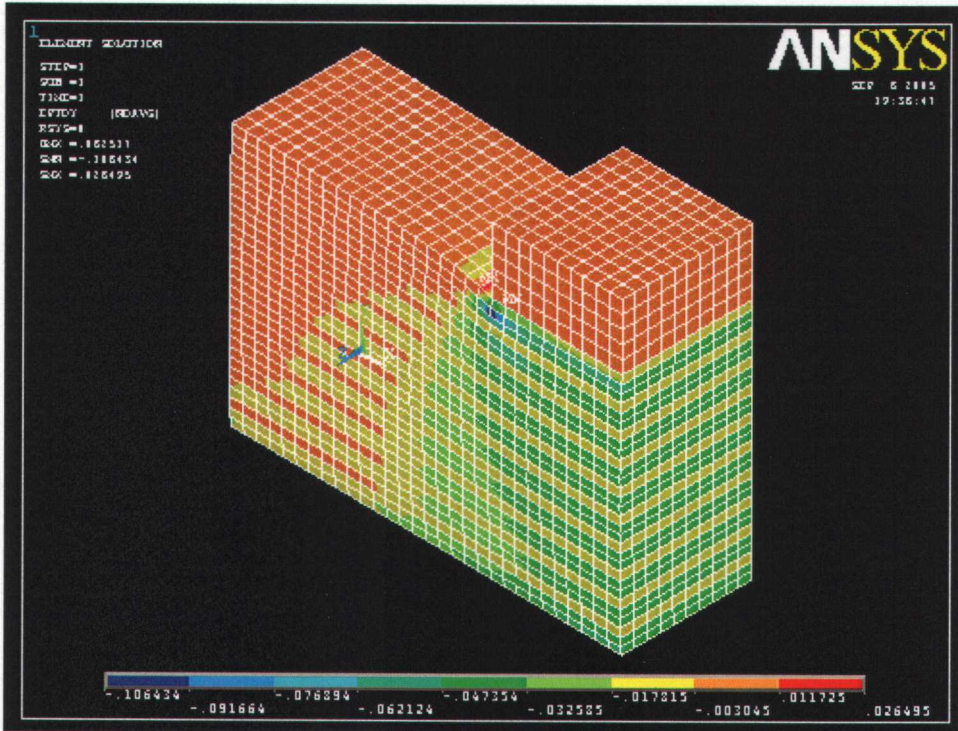


Figure 25: Finite element analysis strain profile for the ASTM specimen with radial loading

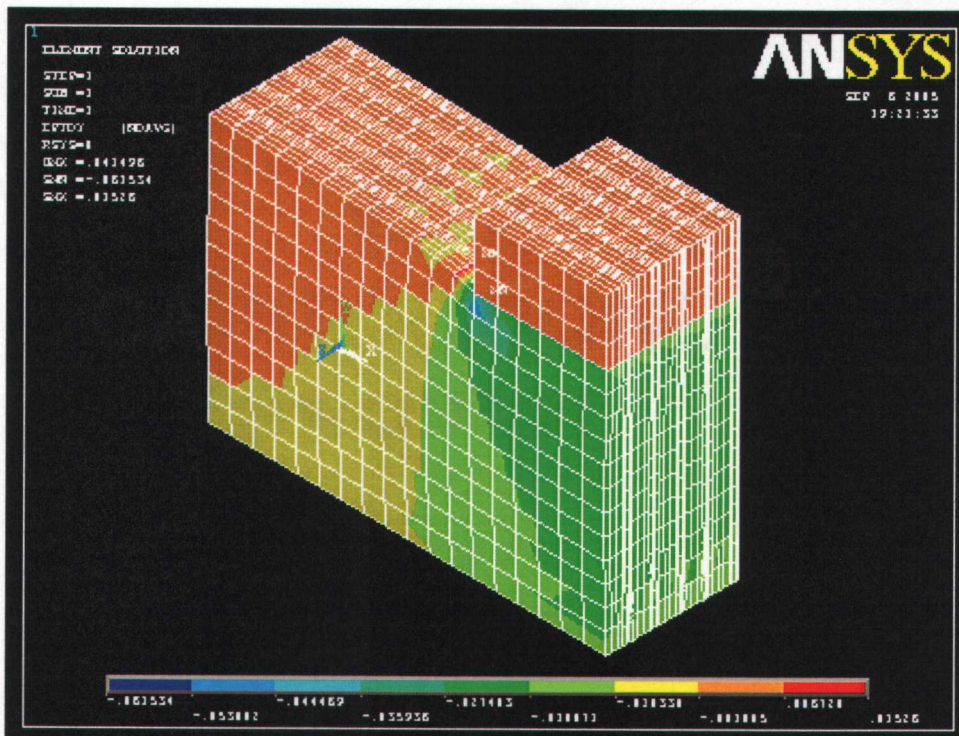


Figure 26: Finite element analysis strain profile for the ASTM specimen with tangential loading

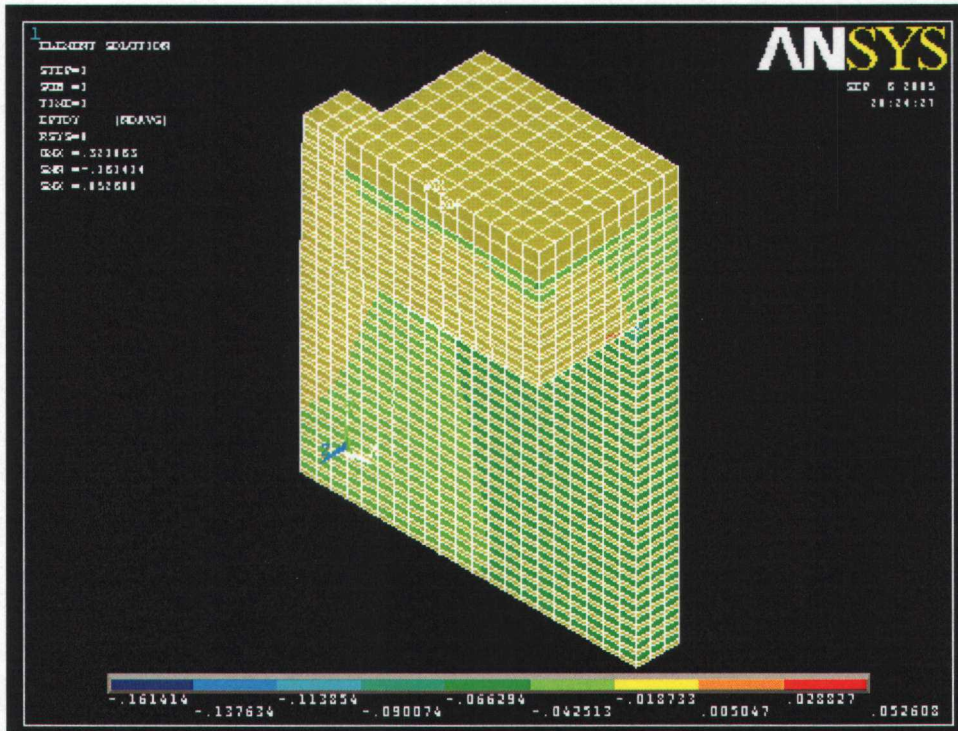


Figure 27: Finite element analysis strain profile for the BC-2X12 assembly with radial loading

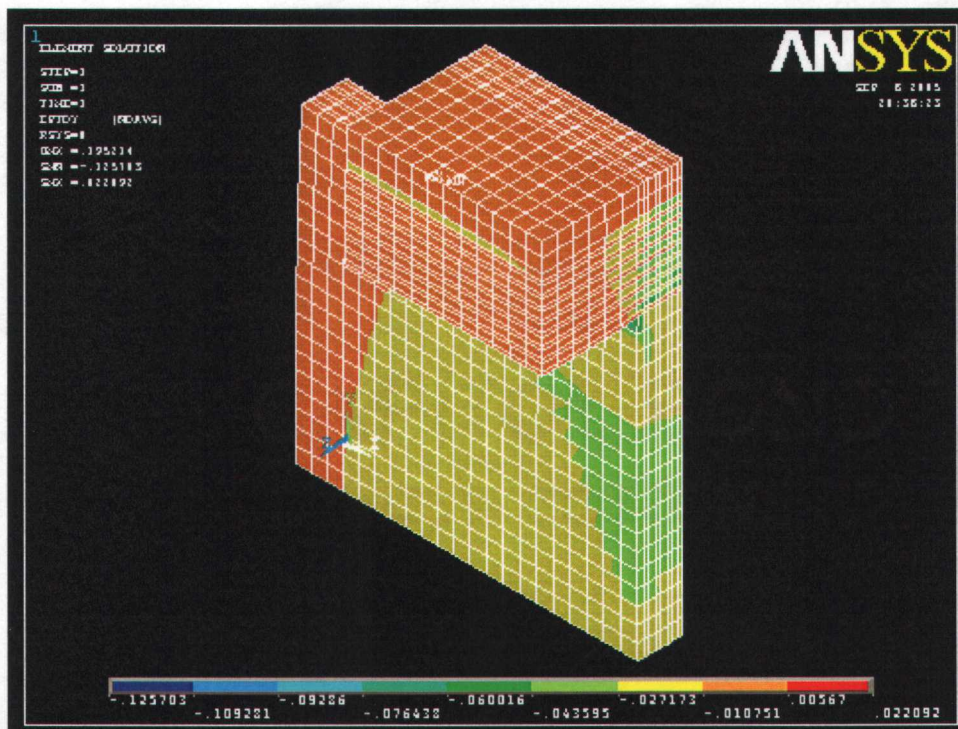


Figure 28: Finite element analysis strain profile for the BC-2X12 assembly with tangential loading

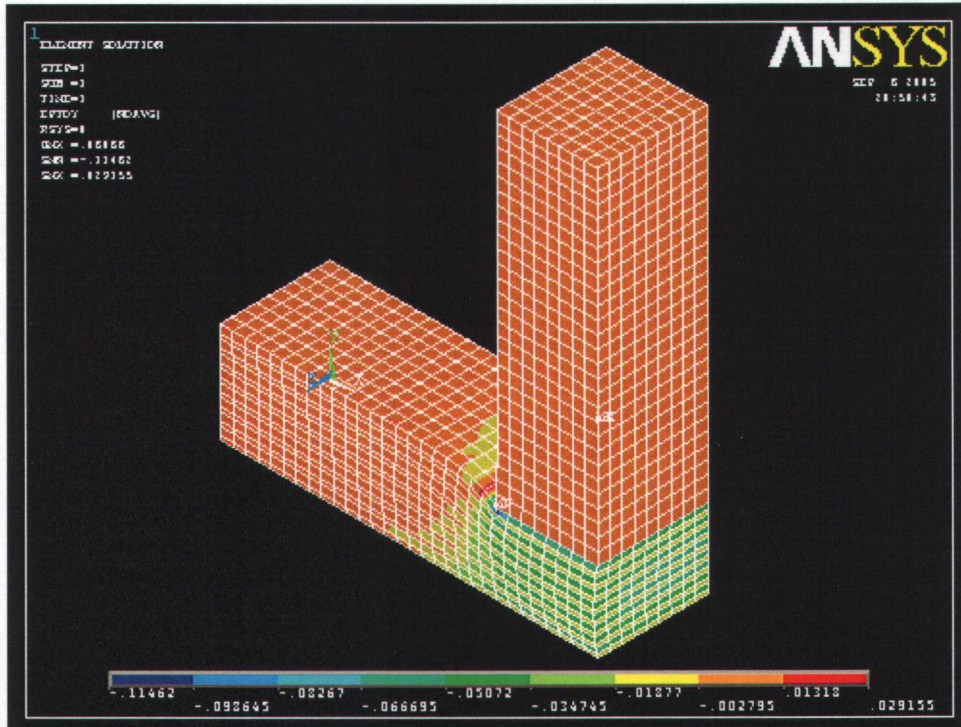


Figure 29: Finite element analysis strain profile for the BP assembly with radial loading

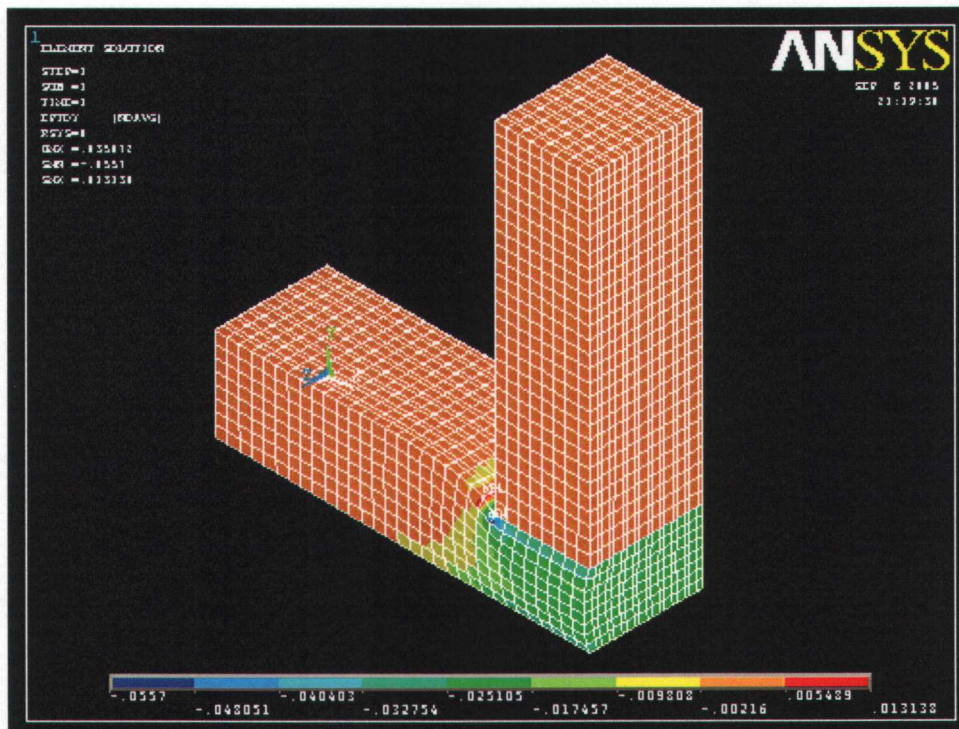


Figure 30: Finite element analysis strain profile for the BP assembly with tangential loading

exhibits higher strain toward the longitudinal middle of the member with strain decreasing with depth and toward the longitudinal ends of the ASTM member. In both radial and tangential loading, ASTM strain profiles reveal that the strained volume is directly under the metal bearing plate and also extends toward the longitudinal ends of the specimen. This is the result of full surface bearing on the bottom surface of the specimen.

Both radially and tangentially loaded ASTM strain profiles reveal a region of high strain at the front edge of the metal bearing plate (blue in strain profile). This is consistent with findings from Kunesh (1968), Bodig (1969) and Pellican et al. (1994). These studies found that high shear stresses (with corresponding strains) develop at the edges of the metal bearing plate and lead to higher compressive stresses than if load is applied over the full area of the specimen. The radially loaded ASTM model exhibited strain of 3.13-percent. The tangentially loaded ASTM model exhibited strain of 2-percent at the same applied load.

Examination of modeling results reveal that for radially loaded B.C. members (Figure 27), strain on a macro level is fairly uniform throughout the depth of the nominal 2X12 member. This is to say that for material directly under the T.P. bearing surface, annual rings near the contact surface with T.P. member experience close to the same strain as do annual rings near mid depth of the B.C. member. In tangential loading (Figure 28) the strain profile reveals that the B.C. member exhibits higher strain toward its loaded longitudinal end with strain decreasing toward mid depth and away from loaded longitudinal end of the B.C. member. In both radial and tangential loading, B.C. strain profiles have strained volume directly under the T.P. bearing surface that also extends away from the loaded longitudinal end of the member. This suggests that wood material not directly under the T.P. bearing surface is attracting load and helping to reinforce the B.C. member away from its loaded longitudinal end. Evidence for this phenomenon is presented in the discussion of compression behavior in T.P. and B.C. members.

In BC model, T.P. member exhibits higher stiffness than the B.C. member in the radially loaded model (strain in the T.P. member was 1.9-percent as apposed to 3.8-percent strain in the B.C.). As shown in figure 3, the T.P. member is loaded over its central area much like the ASTM test specimen. Based on findings from Lum and Karacabeyli (1994), as well as Blass and Gorlacher (2004) this is a less severe loading case than the opposite side end bearing experienced by the B.C. member. It follows that the T.P. member would exhibit higher stiffness than the B.C. member in this loading condition. The T.P. member

does not exhibit higher stiffness than the B.C. member in the tangentially loaded BC model (strain in the T.P. member was 3.4-percent as apposed to 2.5-percent strain in the B.C.) This is because modeled wood material is stiffer when loaded tangentially as compared to the T.P. member which is loaded radially. Based on deflection occurring in T.P. and B.C. members for radially and tangentially loaded BC-2X12 assembly models, the percentage of total system strain occurring in the T.P. members was calculated as 12-percent for the radially loaded model, and 27-percent for the tangentially loaded model. The unrealistically low relative stiffness of the radially loaded material as compared to tangentially loaded material, makes the radially loaded model (in which both T.P. and B.C. are both loaded radially) a better estimator of true total system strain in the T.P. member of a BC assembly test. This is because modeled wood material in the contacting T.P. and B.C. members has similar structural characteristics.

Similar to BC strain profiles, BP strain profiles reveal that the strained volume is directly under the C.C. bearing surface and also extends away from the loaded longitudinal end of the member. This is true in both the radially and tangentially loaded models. This pattern suggests that wood material not directly under the C.C. bearing surface is helping to reinforce the B.P. member away from its loaded longitudinal end. This behavior was not readily observable in the compression behavior of B.P. member. This is due to the high relative stiffness of the longitudinally loaded C.C. as compared with the transversely loaded BP member, i.e. the stiff C.C. member forced near uniform deformation across the surface of BP members.

Results of BP models show the strain in the B.P. member and under the bearing surface of the C.C. with B.P. member is fairly uniform throughout the depth of the B.P member in both radial (Figure 29) and tangential (Figure 30) loading. The results also show that the vast majority of the system strain occurs in the B.C. member. Based on average deflection in C.C. and B.P. members for radially and tangentially loaded BP assembly models, an estimated 3.5-percent of total system strain occurs in the C.C. members (2.4-percent for radially loaded model, and 4.5-percent for tangentially loaded model). However, it is believed that the model overestimates the percentage of total system strain occurring in the longitudinally loaded C.C. member. This is because finite element analysis modeled bulk wood material with a constant E value. The bulk wood material had an E value that was the weighted average of earlywood and latewood layers in the material. Models therefore exhibited a constant relationship between stress and strain or a constant slope in the stress-strain diagram. As shown later, with testing data, B.P.

members were well beyond the linear range in their stress strain diagram at 2-percent offset strain. It is believed that the theoretically calculated deflection in longitudinal loaded member is more representative of actual deflection occurring. Theoretical calculated deflection in C.C. members corresponded to approximately 3-percent of total system strain in BP tests. Modeling indicates that stiffness of the longitudinal member has limited effect on stiffness of bottom plate member, i.e. only about a 1-percent difference between case 1 (longitudinal member $E = 2E6$ psi) and case 2 (longitudinal member $E = 1E6$ psi).

4.2 COMPRESSION BEHAVIOR

4.2.1 Top Plate Members In BC Assemblies

Compression behavior was similar for all T.P. members throughout BC tests. T.P. members exhibited densification in the loaded area that is similar to that seen in the standard ASTM test (Figure 31). The densification in T.P. members was uneven with more densification away from loaded longitudinal end of the B.C. member (Figure 31). This behavior suggests that B.C. members were stiffer (offered more resistance to compression) farther from there loaded longitudinal end. This finding is supported by F.E.M., which showed that material away from the loaded longitudinal end of B.C. members attracted stress and corresponding strain. It is therefore believed that wood material not directly under the compression zone tends to support the compressed wood material at the loaded longitudinal end. No such uncompressed supporting material exists near the longitudinal end. Another way to express this would be to say that shearing forces in the B.C. wood fiber along the edge of the compression zone away from the B.C. longitudinal end help to support and stiffen the compressive resistance of this end. As relative deformation in two contacting compressed members (T.P. and B.C. members) is determined by the relative stiffness of the two contacting materials, the T.P. members show greater compressive deformation farther from the loaded longitudinal end of the B.C. member.

When B.C. members were loaded near tangentially, earlywood and latewood indentations could often be distinguished in the T.P. members (Figure 31(a)). As evidenced by finite element analysis and findings from Bodig (1965), Kennedy (1968), and Tabarsa and Chui (2001), latewood layers act as reinforcing columns within the gross wood material in tangential loading. Therefore, the denser and stiffer latewood material, acting as

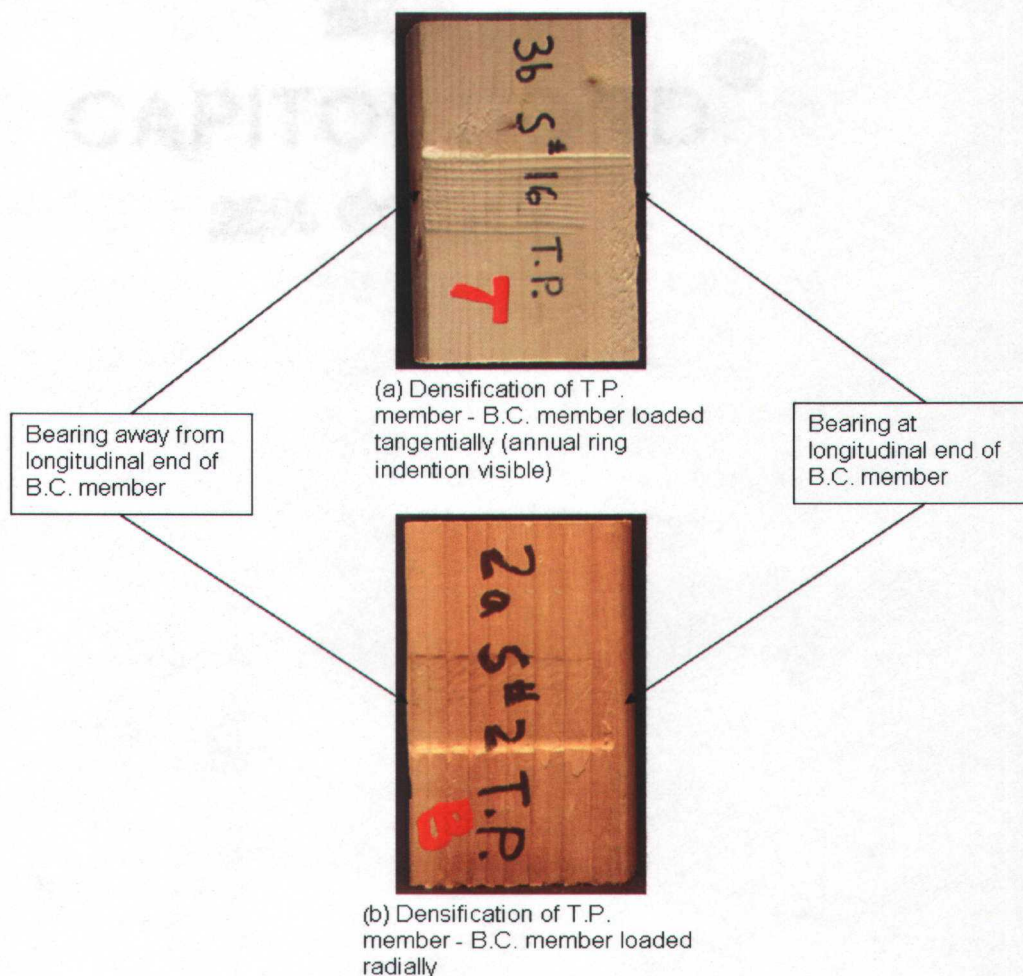


Figure 31: Characteristic compression damage in 2X4 T.P. members in BC assembly tests

reinforcing columns in the compressed B.C., left deeper compression indentations in the T.P. members where these latewood layers interfaced with the T.P. member.

4.2.2 BC-2X4 Assembly

Observed compression behavior in BC-2X4 assemblies varied depending upon ring orientation of the B.C. member. When loaded tangentially, damage to B.C. members was seen as buckling of annual rings with corresponding shear along the earlywood-latewood interface (Figure 32(a and e)). This behavior was attributed to latewood layers acting as reinforcing columns in this orientation which tended to buckle under higher stresses (Bodig (1965), Kennedy (1968), Tabarsa and Chui (2001)). Buckling of annual rings was controlled by ring curvature, i.e. annual rings buckled in the direction of their pre-existing

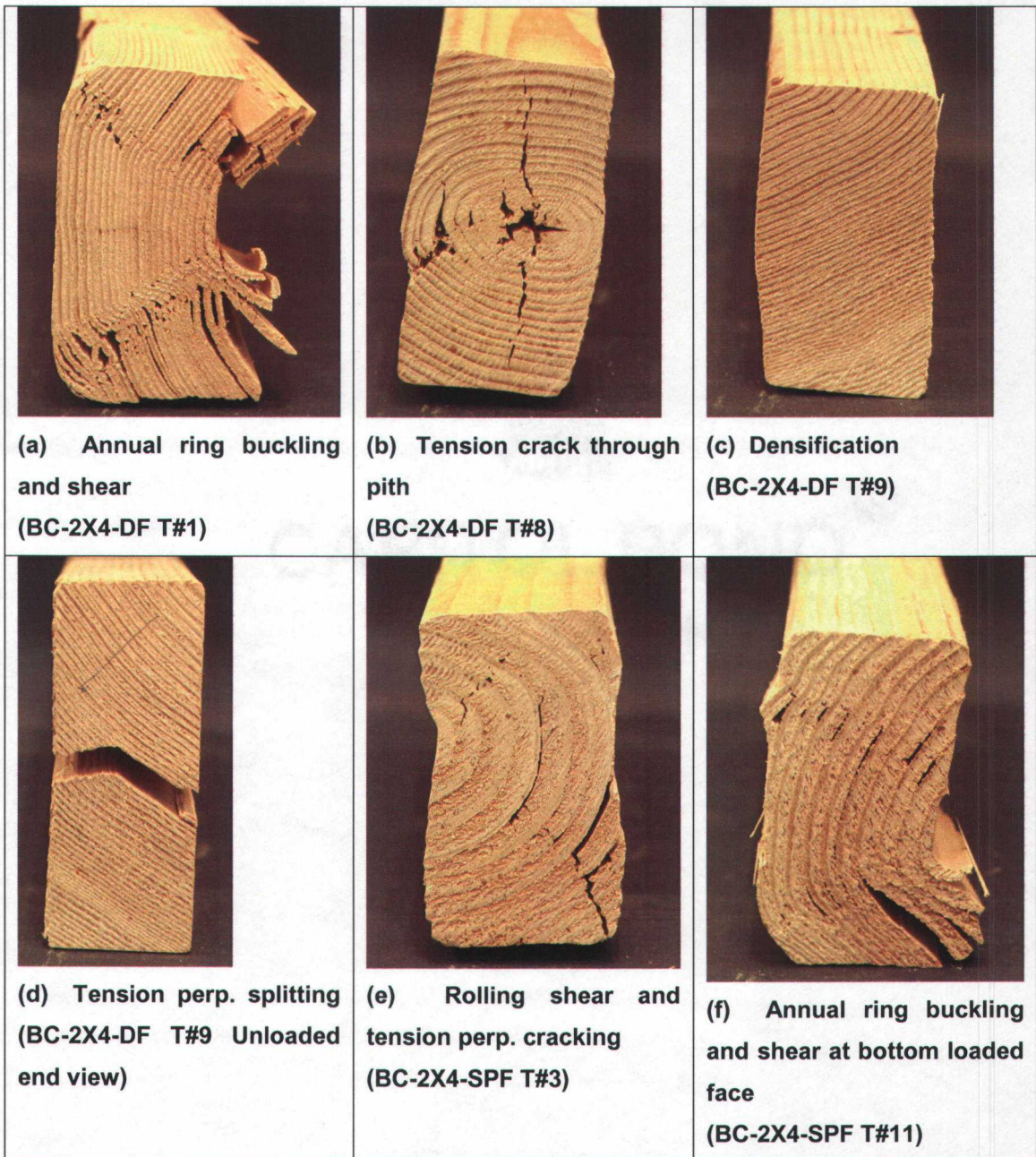


Figure 32: Characteristic compression damage in BC-2X4 assembly B.C. members

curvature. Higher ring curvature led to more severe buckling in the annual rings. B.C. members in which ring orientation deviated further from the plane of loading on either the top or bottom surface tended to buckle more severely near that surface (Figure 32(f)). B.C. members loaded at higher angles to ring orientation exhibited crushing of annual rings with corresponding densification (Figure 32(b and c)). Such specimens had a tendency to crack through the pith when pith was present. This behavior was attributed to Poisson effects leading to tensile stresses in the direction orthogonal to applied load. B.C. members also had a tendency to split at the unloaded end of the member with the split propagating longitudinally along the minor axis but stopping short of the loaded end (Figure 32(d)). This behavior was attributed to transverse tension stresses in the direction of applied load arising from continued densification of the loaded longitudinal end of the member. This splitting was accompanied by a simultaneous drop in load, but the load was quickly recovered and often exceeded the splitting load as testing continued. This splitting effect was similar in both BC-2X4-DF and BC-2X4-SPF B.C. members. Thirty percent of both BC-2X4-DF and BC-2X12-SPF B.C. members split longitudinally in this manner. Compression damage to all BC-2X4 members is shown in appendix F.

BC-2X4 assemblies had a relatively low aspect ratio of 2.33 in the B.C. member and exhibited continual densification without catastrophic failure. Stress carrying capacity often increased, at least initially, with increasing system densification. Well beyond the linear region in the stress-strain diagram, assembly stress increased and decreased as annual rings buckled and or sheared along the earlywood/latewood interface (Appendix B). However, the general trend was that of increasing assembly stress up to a system strain of at least 10-percent. Fifty-percent of BC-2X4-DF and 45-percent of BC-2X12-SPF assemblies continued to densify with increasing assembly stress up to 20-percent system strain which was the conclusion of testing (Appendix F). No catastrophic failures were observed in BC-2X4 assemblies.

4.2.3 BC-2X8 Assembly

Similar to BC-2X4 assemblies, when B.C. members in BC-2X8 tests were loaded near parallel to ring orientation, damage to B.C. members was seen as buckling of annual rings with corresponding rolling shear along the earlywood/latewood interface (Figure 33(b and f)). Again this phenomenon was attributed to latewood layers acting as reinforcing columns that tended to buckle under higher stresses (Bodig 1965, Tabarsa and Chui, 2001). However with the increased aspect ratio (4.8) of BC-2X8 B.C. members this

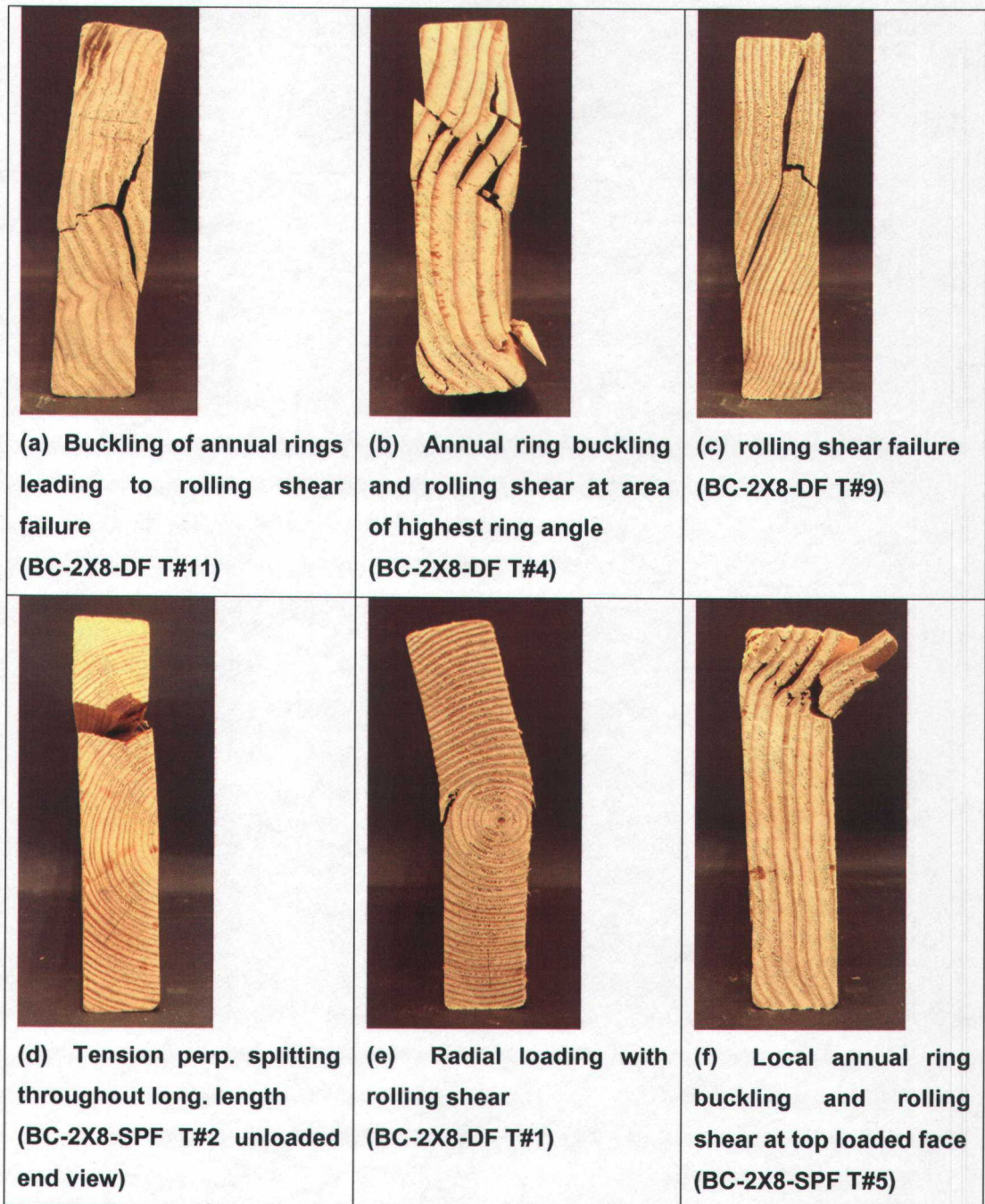


Figure 33: Characteristic compression damage in BC-2X8 assembly B.C. members

annual ring buckling effect was accentuated. In BC-2X8-DF test #11, annual ring buckling led to catastrophic rolling shear failure (Figure 33(a)) of the B.C. member at a system strain of 7.7-percent with σ_{\max} being attained at 5.1-percent system strain. In BC-2X8-DF test #9 (Figure 33(c)), as well as BC-2X8-SPF test #9 (both tests had paired B.C. main member, i.e. from the same board) rolling shear in the B.C. member led to catastrophic failure at system strains of 5.7 and 6.4-percent with σ_{\max} being attained at 3.1 and 3.3-percent, respectively. It should be noted that these two tests exhibited the lowest system strains at σ_{\max} as well as prior to failure while attaining σ_{\max} values that were above average for BC-2X8 assemblies. Test #9 B.C. member had relatively low ring curvature with an average ring angle to applied load of about 15 degrees (Figure 33(c)). As with BC-2X4 assemblies longitudinal splitting in BC-2X8 B.C. members lead to simultaneous drop in load. However this load was usually recovered and exceeded as testing continued. This splitting effect in the B.C. member was similar in both BC-2X8-DF and SPF assemblies. Seventy-percent of both BC-2X8-DF and BC-2X8-SPF B.C. members split longitudinally in this manner. This splitting did not lead to immediate catastrophic failure, although it may have contributed to the global failure.

BC-2X8 assemblies, continued to support load to 10-percent system strain for 32 of the 35 tests conducted. Beyond the linear region in the stress-strain diagram assembly stress increased and decreased as annual rings in the B.C. member buckled and or sheared along the earlywood latewood interface (Appendix B). At 10-percent system strain most B.C. members showed sever cross-grain bending and catastrophic failures appeared imminent. Three Catastrophic failures were observed prior to 10-percent system strain.

4.2.4 BC-2X12 Assembly

When loaded near parallel to annual ring orientation in BC-2X12 assemblies, damage to 2X12 B.C. members was seen in buckling of annual rings with corresponding shear along the earlywood/latewood interface (Figure 34(b and f)). The aspect ratio (7.5) of 2X12-B.C. members accentuated this effect. The aspect ratio also led to cross-grain bending of B.C. members with corresponding rolling shear and high probability of catastrophic failure for all ring orientations. Once again, buckling of annual rings in 2X12-B.C. members was controlled by ring curvature and higher ring curvature led to more severe buckling in the annual rings. As noted in 2X8-B.C. members, specimens loaded near parallel to average ring angle, and with existing cupping opposite the direction of annual ring curvature, would straighten under load and then begin to buckle in the direction of ring curvature. Again,

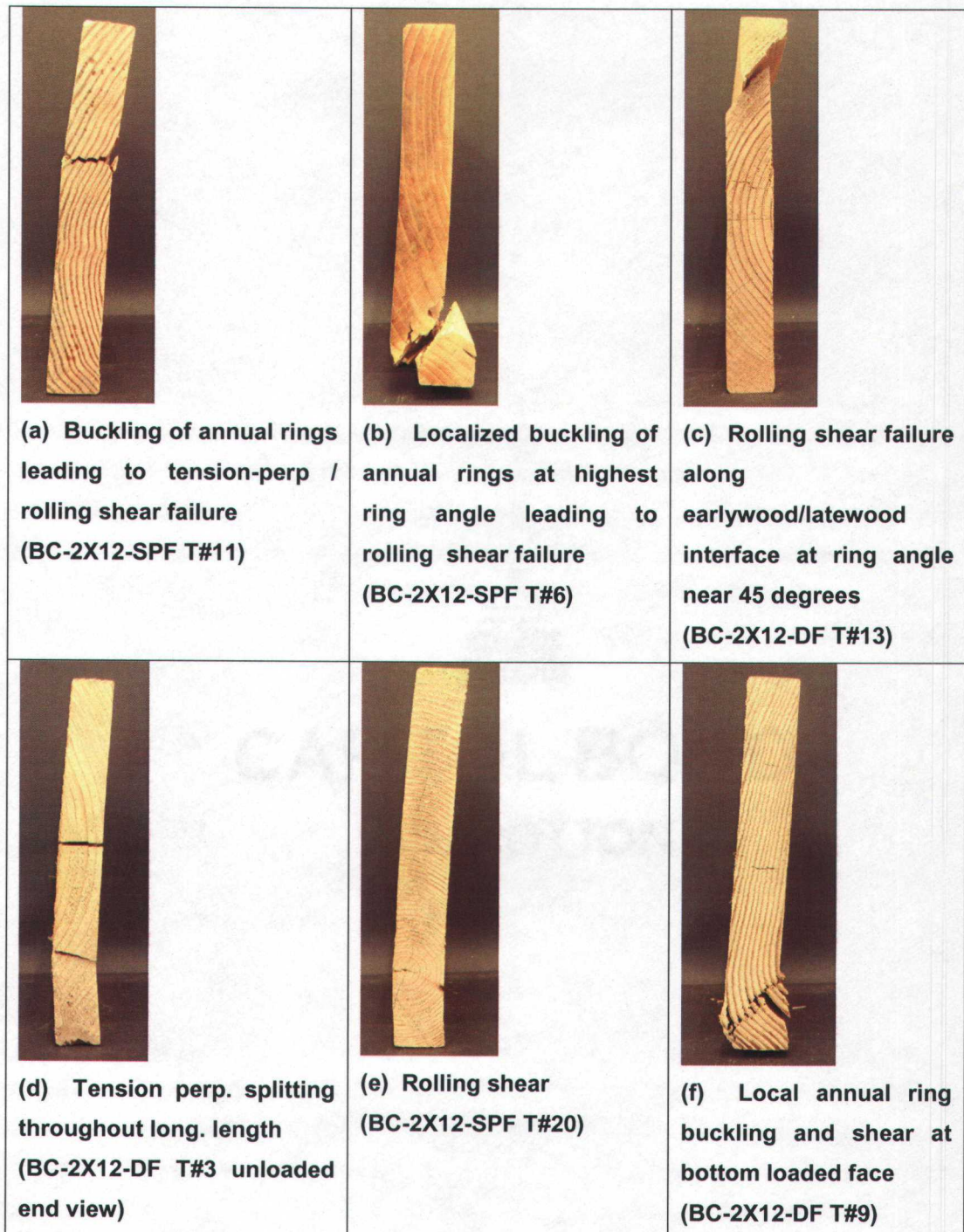


Figure 34: Characteristic compression damage in BC-2X12 assembly B.C. members

localized buckling of annual rings was seen at areas of highest annual ring angle to loading plane (Figure 34(b and f)). This led to rolling shear and cross-grain bending of the B.C. member (Figure 34(a, b, and f)). The tendency of B.C. members to split longitudinally along the major axis was accentuated by high aspect ratio of the B.C. members (Figure 34(d)), with one or more longitudinal splits often developing along the major axis of 2X12 B.C. members. The splitting effect was similar in both BC-2X12-DF and BC-2X12-SPF B.C. members. Eighty-five percent of BC-2X12-DF B.C. members and 90 percent of BC-2X12-SPF B.C. members split longitudinally in this manner. While this splitting phenomenon was coincident with an initial drop in load, generally this load was recovered and exceeded as testing progressed. This splitting effect observed in all BC assemblies may not occur in longer pieces used in construction practice.

B.C. members cut from 2X12 boards number 3, 7, and 13 failed catastrophically before reaching the $F_{c,L}$ design value of 625 psi given in the NDS for Douglas-fir-Larch. This occurred for both DF and SPF BC-2X12 assemblies. Lowest system strain at σ_{max} occurred in test #13 B.C. for both BC-2X12-DF and BC-2X12-SPF assemblies. System strain at σ_{max} was respectively 2.3 and 2.2-percent. These two assemblies also exhibited among the smallest σ_{max} . BC-2X12-DF test #13 (Figure 34(c)) failed catastrophically in the B.C. member immediately after attaining σ_{max} and never attained 2-percent offset strain. Failure of B.C. member in BC-2X12-DF test #13 and BC-2X12-SPF test #13 were similar. Both involved rolling shear failure with separation along the earlywood/latewood interface at a ring angle near 45 degrees.

Five of the 40 BC-2X12 assembly tests supported load to 10-percent system strain. Beyond the linear region in the stress-strain diagram, assembly stress alternately increased and decreased as annual rings in the B.C. member buckled and or sheared along the earlywood-latewood interface (Appendix B). Generally, stress in assemblies varied from increasing to maintaining level to decreasing stress with increasing strain beyond the linear region of the stress-strain curve. Prior to reaching 10-percent system strain, BC-2X12 assemblies reached a maximum stress and either failed catastrophically or were beyond maximum stress levels. Thirty five catastrophic failures were observed prior to reaching 10-percent system strain.

4.2.5 BP Assembly

The observed compression mode in BP members was that of continuous densification with increasing load and eventual shear of the B.P. along the front edge of the C.C. (Figure 35(a, b, d, and f)). This general mode of compression was observed for all B.P. members regardless of ring angle. Also observed was a tendency of B.P. members to split longitudinally along their major axis at higher strains (Figure 35(c and e)). This behavior is attributed to the Poisson effect and/or cross grain bending (resulting from pre-existing cupping in members) which led to tension perpendicular to grain failure. This splitting effect was more prevalent in BP-DF B.P. members than in BP-SPF B.P. members. Forty-five-percent of BP-DF B.P. members split longitudinally while 30-percent of BP-SPF members split longitudinally. It may be that the higher densities of DF B.P. members lead to increased splitting effect. For three BP-DF and one BP-SPF test, longitudinal splitting of the B.P. member lead to longitudinal splitting of the C.C. (Figure 35(e)).

For BP assembly tests, compression behavior was somewhat similar to that observed for typical ASTM specimens, that is the assemblies generally exhibited continual densification without catastrophic failure. B.P. members supported increasing stress even after they split longitudinally. In construction systems, longitudinal splitting of the B.P. could lead to system failure under shear loads because anchor bolts lose bearing capacity. However, B.P. specimens measured only 6-in. long, and it is possible that longer members would not exhibit this longitudinal splitting behavior or the splitting may be localized. Assembly stress invariably increased with increasing B.P. densification well beyond the linear region in the stress-strain diagram. The general trend was that of increasing assembly stress up to a system strain of 25-percent and deliberate test termination. No catastrophic failures were seen in B.P. assemblies.

Bottom plate assemblies tested exhibited large deflections prior to near linearity in the stress strain diagram. These assemblies invariably deflected much more than ASTM specimens for a given stress. For given stresses, deflections in BP assemblies were often two or more times that seen in corresponding ASTM tests.

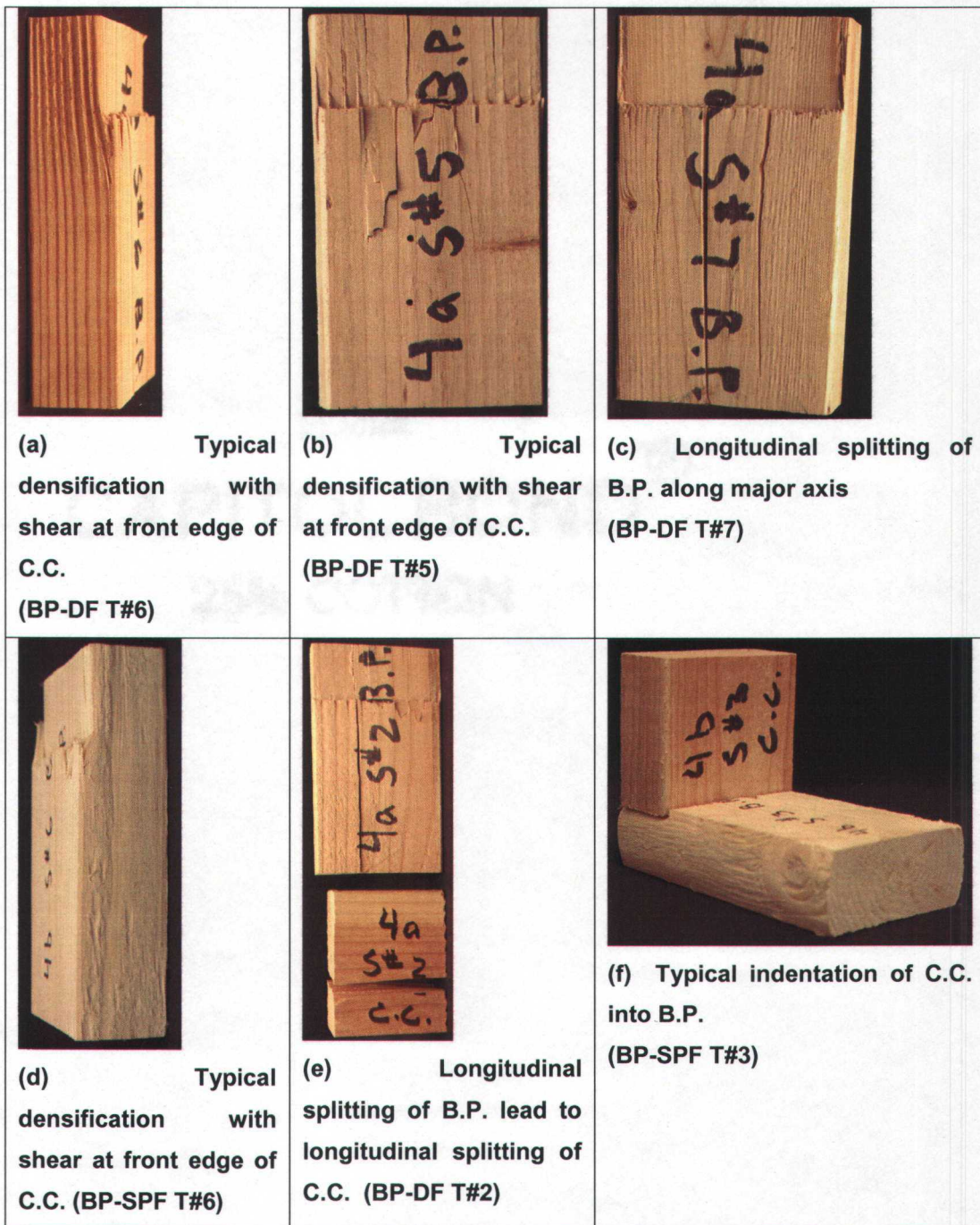


Figure 35: Characteristic compression damage in 2X4 BP assembly members

4.2.6 Comparison Of σ_{max} To $\sigma_{2\%-OS}$

The compression behavior of the ASTM c-perp specimen is that of continuing densification with stress increasing with deflection. Therefore, in c-perp applications it is generally assumed that no ultimate limit state exists, i.e. specimens will exhibit residual load capacity beyond specified deformations. This may be interpreted as an unlimited factor of safety. In order to compare residual load carrying capacity of tested assemblies, σ_{max} was compared to $\sigma_{2\%-OS}$. Table 4 shows $\sigma_{2\%-OS}$, σ_{max} , and the ratio of σ_{max} to $\sigma_{2\%-OS}$ for all assembly tests.

The ratio of σ_{max} to $\sigma_{2\%-OS}$ decreased with increased depth of the main member (Table 4). To illustrate the extremes, BP tests, with the lowest depth of the main member (1.5-in.), exhibited σ_{max} of 1.90 and 1.86 times $\sigma_{2\%-OS}$ for BP-DF and BP-SPF assemblies, respectively. This is as compared with 1.19 and 1.21 times $\sigma_{2\%-OS}$ for BC-2X12-DF and BC-2X12-SPF assemblies respectively. Because 88-percent of the BC-2X12 assemblies failed catastrophically prior to attaining 10-percent system strain, it may be assumed that no post-peak capacity was available in these assemblies. In these tests, it follows that the factor of safety is only in the range of 1.19 to 1.21.

Table 4: Comparisons of σ_{max} to $\sigma_{2\%-OS}$ for all assemblies

Test Assembly	Response Variable		
	$\sigma_{2\%-OS}$ (psi)	σ_{max} (psi)	$\sigma_{max} / \sigma_{2\%-OS}$
BP-DF	642 (20, 34%)	1219 (20, 24%)	1.90
BP-SPF	508 (10, 21%)	947 (10, 15%)	1.86
BC-2X4-DF	691 (20, 27%)	995 (20, 23%)	1.44
BC-2X4-SPF	652 (20, 22%)	944 (20, 19%)	1.45
BC-2X8-DF	773 (17, 23%)	995 (17, 18%)	1.29
BC-2X8-SPF	717 (18, 18%)	976 (18, 15%)	1.36
BC-2X12-DF	700 (20, 26%)	831 (20, 25%)	1.19
BC-2X12-SPF	670 (20, 25%)	811 (20, 25%)	1.21

Note: First number in parenthesis is no. of tests performed and second number is coefficient of variation.

4.3 $F_{c\perp}$ DETERMINATION

Figure 36 shows typical load-deflection diagrams for ASTM and c-perp assemblies tested in this study. As will be shown later, behavior of DF and SPF assemblies are very similar. Therefore for illustration purposes DF tests are depicted in Figure 36 but the same point could be made with depiction of SPF tests. Figure 36 illustrates the extreme differences between the behaviors of ASTM tests and BC and BP assemblies. Load at 0.04-in. deflection for ASTM test and BC and BP assemblies are very different. For instance load at 0.04-in. deflection in the ASTM test is approximately 4300 lb, whereas the BC-2X12 assembly attains a load of approximately 400 lb, and the BP assembly attains a load around 600 lb at the same deflection. The explanation for this extreme difference in $\sigma_{0.04-D}$ is two-fold. First, member depth plays an important role in compressibility of the members. With increasing member depth and multiple members in the connection, depth of the assembly increases. The total depth of BC-2X12 assemblies is 14.25-in. compared with 1.5-in. deep ASTM tests utilized in this study. While 0.04-in. deflection corresponds to 2-percent strain in the standard ASTM specimen and 2.67-percent strain in ASTM members used in this study, this same deflection corresponds to a system strain of less than 0.3-percent in BC-2X12 assemblies. The stress in a member is related to the strain in the member through the modulus of elasticity. Therefore, in order to account for depth of assemblies, it is necessary to base stress values on a specified strain. The 0.04-in. deflection benchmark of the ASTM test corresponds to 2-percent strain. Thus stress at 2-percent strain ($\sigma_{2\%-S}$) should be utilized for comparisons between the different testing configurations and assemblies.

The second reason for the extreme difference in $\sigma_{0.04-D}$ is related to the initial range of non-linearity and upward curvature in the load-deflection diagram. The multiple wood member assemblies examined in this study lead to larger misalignment and settling effects than are present in standard ASTM metal-on-wood tests. This led to correspondingly larger ranges of non-linearity prior to near linearity in the load-deflection graph for these assemblies. This phenomenon was especially apparent in BP tests. Because the BP specimens were cut in a manner deemed to be consistent with construction practice, i.e. cut with a table saw, rough and non-rectilinear surfaces were present at the contact surface between the C.C. and B.P. members. Large settling effects in BP tests led to unusually larger regions of initial misalignment, which pushed the near linear range out farther on the load axis. To adjust for settlement effects in all assemblies, it was determined that an offset strain would be utilized for majority of comparisons between

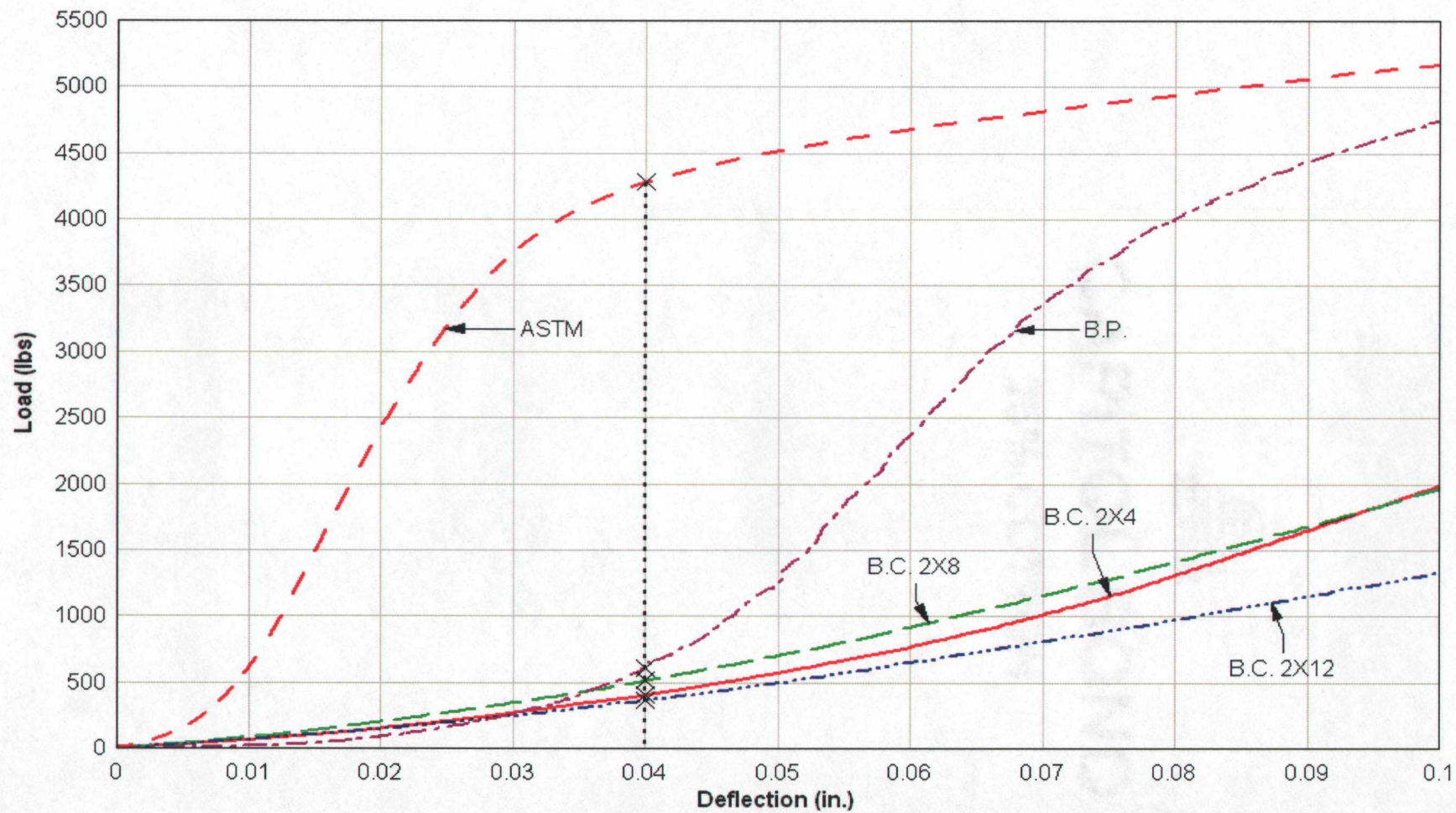


Figure 36: Typical load-deflection diagrams for BC, BP and ASTM tests

testing configurations and assemblies. Figure 37 shows a stress-strain diagram that corresponds to Figure 36.

With the exception of BP assembly, stress values are much closer to each other between testing configurations and geometries when based on a stress at a specified system strain (Figure 37). When $\sigma_{2\%-S}$ is used as the criteria, all BC assemblies are within about 150 psi of one another (about 25-percent), and the ASTM configuration is about 60-percent higher. However, $\sigma_{2\%-S}$ for BP assemblies is very low due to the large initial misalignment region. Since the region of initial misalignment does not represent true material behavior, an offset strain was used to compare all test assemblies in order to compare true material behavior. The $\sigma_{2\%-OS}$ (Figure 37) is recommended to be used as c-perp strength value. Similar to an offset deflection (see background), the offset strain is determined by first fitting a linear regression to the linear range on the stress-strain diagram. The regression is then extended back to zero stress. Two-percent offset strain is calculated as two-percent strain from strain at intersection of the regression line with the strain axis. For the BP assembly (Figure 37), $\sigma_{2\%-OS}$ is just over 600 psi.

To emphasize the difference in range of initial non-linearity and miss-alignment observed in testing as well as the data adjustment being made with use of $\sigma_{2\%-OS}$ it is helpful to compare offset strain values. The offset strain value in this context is defined as the difference in strain between origin and intersection of regression line with strain axis. To illustrate the two extremes, BP and ASTM, are compared. Average offset strain values for DF and SPF ASTM specimens were respectively 0.005 and 0.007 in./in. Average offset values for BP-DF and BP-SPF members were .027 and .022 in./in., respectively.

For these reasons $\sigma_{2\%-OS}$ is recommended to be used as the c-perp strength value. This is the basis for further discussion. In the BP assemblies, calculated deflection attributed to the C.C. members was subtracted from overall system deflection. Calculated deflection was about 3 percent of system deflection and is consistent with the findings of the finite element modeling that showed deflection in C.C. member is less than 3.5-percent. No deflection adjustment was made to BC assemblies.

Tables 5 to 9 illustrate mean values of $\sigma_{0.04-D}$, $\sigma_{2\%-S}$, $\sigma_{0.04-OD}$, and $\sigma_{2\%-OS}$ for all test assemblies along with corresponding ASTM tests of the main member for each assembly.

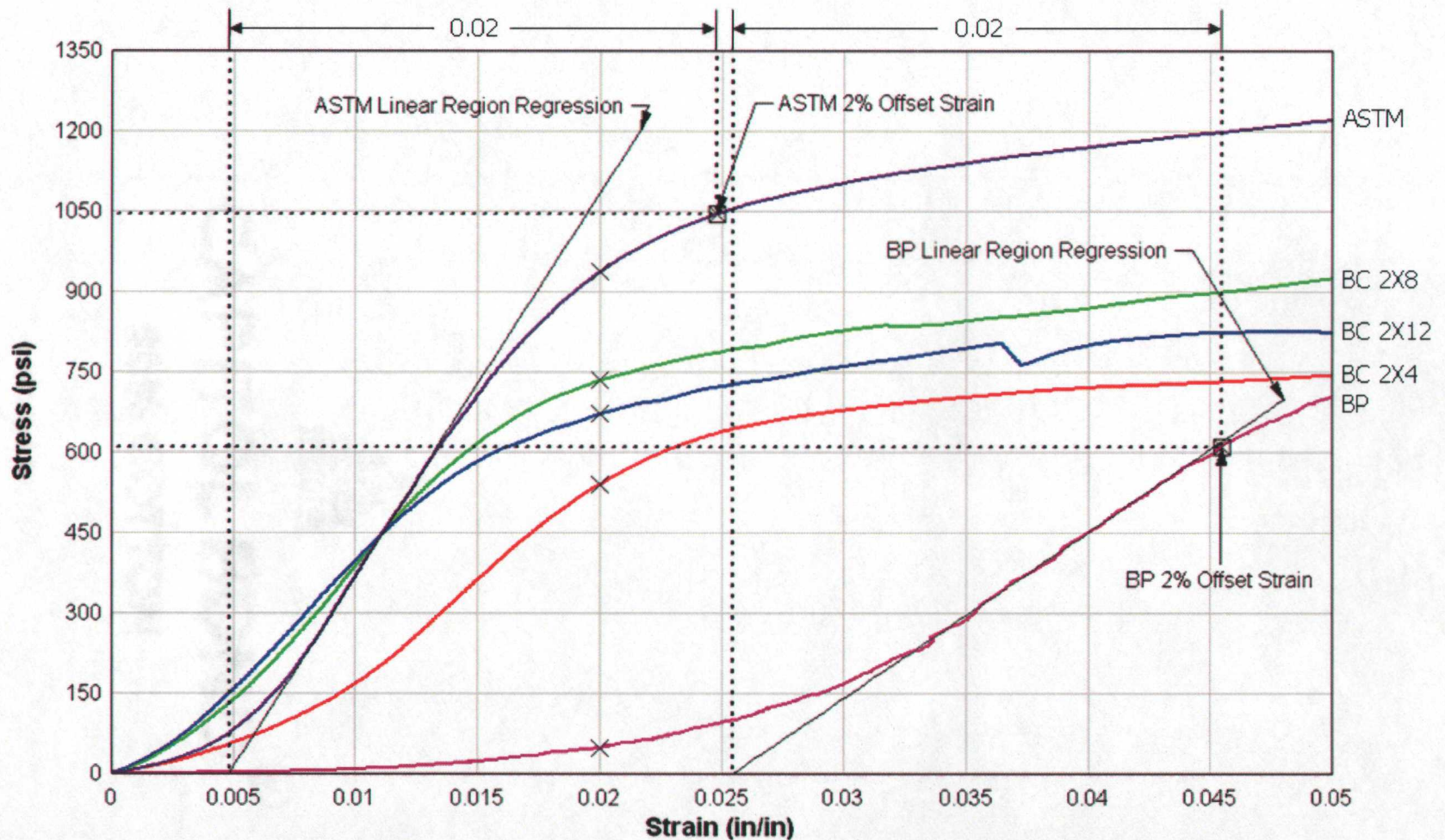


Figure 37: Typical stress-strain diagrams for BC, BP and ASTM tests

Table 5: BC-2X4 and corresponding ASTM means for all response variables

Test Assembly	Response Variable (psi)			
	$\sigma_{0.04-D}$	$\sigma_{2\%-S}$	$\sigma_{0.04-OD}$	$\sigma_{2\%-OS}$
BC-2X4-DF	125 (20, 45%)	625 (20, 32%)	283 (20, 34%)	691 (20, 27%)
BC-2X4-SPF	118 (20, 44%)	595 (20, 21%)	278 (20, 29%)	652 (20, 22%)
ASTM-2X4-DF	964 (20, 22%)	744 (20, 27%)	1053 (20, 24%)	941 (20, 25%)

Note: First number in parenthesis is no. of tests performed and the second number is coefficient of variation.

Table 6: BC-2X8 and corresponding ASTM means for all response variables

Test Assembly	Response Variable (psi)			
	$\sigma_{0.04-D}$	$\sigma_{2\%-S}$	$\sigma_{0.04-OD}$	$\sigma_{2\%-OS}$
BC-2X8-DF	77 (17, 35%)	717 (17, 22%)	202 (17, 25%)	773 (17, 23%)
BC-2X8-SPF	81 (18, 45%)	664 (18, 22%)	200 (18, 28%)	717 (18, 18%)
ASTM-2X8-DF	922 (20, 35%)	614 (20, 37%)	1153 (20, 31%)	995 (20, 32%)

Note: First number in parenthesis is no. of tests performed and the second number is coefficient of variation.

Table 7: BC-2X12 and corresponding ASTM means for all response variables

Test Assembly	Response Variable (psi)			
	$\sigma_{0.04-D}$	$\sigma_{2\%-S}$	$\sigma_{0.04-OD}$	$\sigma_{2\%-OS}$
BC-2X12-DF	61 (20, 46%)	667 (20, 27%)	144 (20, 32%)	700 (20, 26%)
BC-2X12-SPF	55 (20, 48%)	637 (20, 25%)	147 (20, 32%)	670 (20, 25%)
ASTM-2X12-DF	794 (20, 42%)	559 (20, 51%)	1048 (20, 35%)	891 (20, 35%)

Note: First number in parenthesis is no. of tests performed and the second number is coefficient of variation.

Table 8: BP-DF and corresponding ASTM means for all response variables

Test Assembly	Response Variable (psi)			
	$\sigma_{0.04-D}$	$\sigma_{2\%-S}$	$\sigma_{0.04-OD}$	$\sigma_{2\%-OS}$
BP-DF	150 (20, 94%)	77 (20, 99%)	771 (20, 31%)	642 (20, 34%)
ASTM-2X4-DF	964 (20, 22%)	774 (20, 27%)	1053 (20, 24%)	941 (20, 25%)

Note: First number in parenthesis is no. of tests performed and the second number is coefficient of variation.

Table 9: BP-SPF and corresponding ASTM means for all response variables

Test Assembly	Response Variable (psi)			
	$\sigma_{0.04-D}$	$\sigma_{2\%-S}$	$\sigma_{0.04-OD}$	$\sigma_{2\%-OS}$
BP-SPF	252 (10, 59%)	122 (10, 62%)	621 (10, 18%)	508 (10, 21%)
ASTM-2X4-SPF	837 (10, 18%)	673 (10, 33%)	927 (10, 12%)	852 (10, 16%)

Note: First number in parenthesis is no. of tests performed and the second number is coefficient of variation.

The improvement in variability and uniformity of stress values when using $\sigma_{2\%-OS}$ rather than $\sigma_{0.04-D}$ can be seen. The coefficient of variation is lower for the $\sigma_{0.04-D}$ as compared to the $\sigma_{2\%-OS}$ for all test assemblies. This is especially true for BP tests, which exhibited large ranges of initial nonlinearity before the linear behavior in the load-deflection diagram. The Wood Handbook lists average c-perp coefficient of variation (COV) at 28 percent (FPL 1999). COV of ASTM 2X8 and 2X12 tests exceeded 28-percent for $\sigma_{0.04-D}$, $\sigma_{2\%-S}$, $\sigma_{0.04-OD}$, and $\sigma_{2\%-OS}$. This likely resulted from the variable ring angle of ASTM tests conducted in this study whereas the ASTM testing procedure specifies load applied only parallel to the annual rings. Stress values for ASTM and assembly tests are also much closer to one another when based on $\sigma_{2\%-OS}$ rather than $\sigma_{0.04-D}$. Comparisons are discussed in section 4.5.

4.4 INFLUENCE OF WOOD SPECIES

Figure 38 shows difference between mean $\sigma_{2\%-OS}$ for DF and SPF assemblies and corresponding 95-percent confidence intervals (CIs) based on pair-wise comparisons. No statistically significant difference in $\sigma_{2\%-OS}$ was seen between DF and SPF BC tests (Figure 38), i.e. the 95-percent CI for difference in means includes zero. Mean $\sigma_{2\%-OS}$ of the BP-DF tests was found to be 134 psi greater than that of BP-SPF tests in this study. This lead to suggestive but inconclusive evidence of a significant difference between the two tests (p -value = 0.076).

It is believed that c-perp behavior of BC assemblies was dominated by B.C. member. For this reason and because all BC assembly B.C. members were DF no significant difference in mean $\sigma_{2\%-OS}$ was observed between BC-DF and SPF tests. In BP assemblies, B.P. main members were alternately DF and SPF in BP-DF and BP-SPF assemblies. It is believed that if more tests had been conducted a significant difference in mean $\sigma_{2\%-OS}$

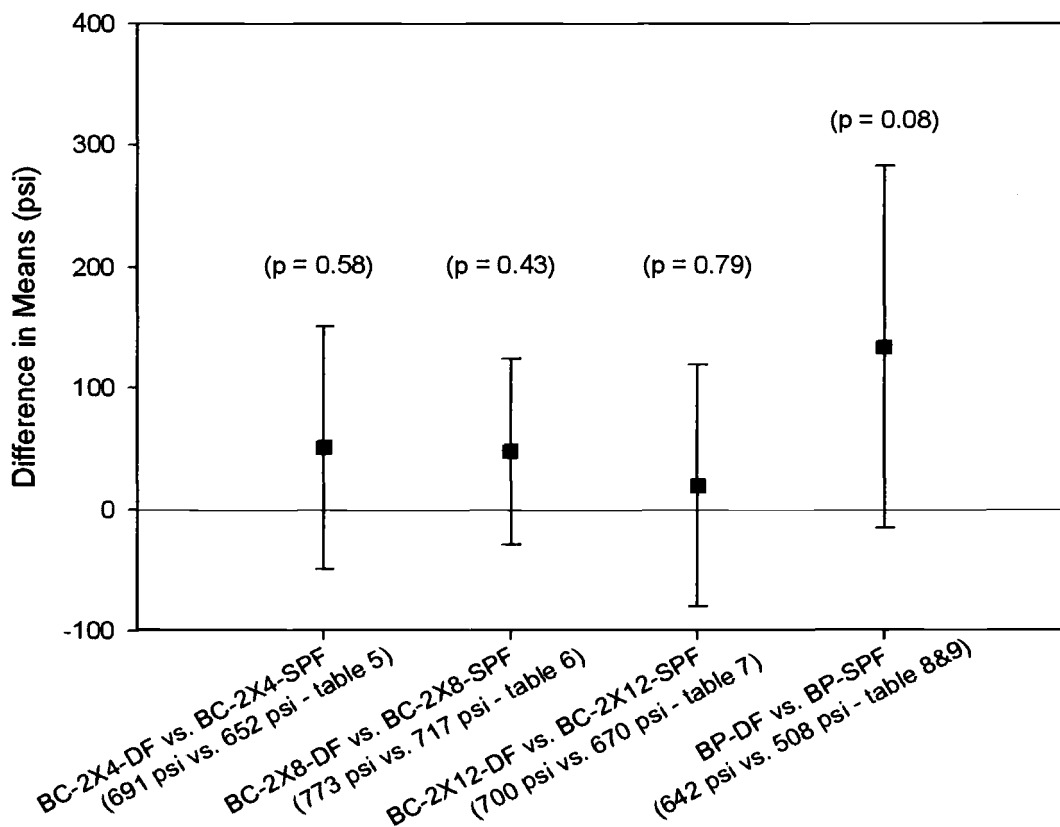


Figure 38: All assemblies 95-percent C.I. for difference in mean $\sigma_{2\%-OS}$

between BP-DF and BP-SPF may have been observed. It is recommended that further studies with larger sample sizes be conducted to determine the influence of wood species on BP assemblies.

The rest of the analysis included adjustment for covariate effect. It was not deemed appropriate to include adjustment for covariate effect in comparisons between DF and SPF tests. This is because member properties specific to wood species were often found to have significant covariate effects. To adjust for these properties would have negated the effect of wood species within these assemblies.

4.5 COMPARISON OF TESTED ASSEMBLIES TO CORRESPONDING ASTM TESTS OF MAIN MEMBER

Figure 39 depicts individual means for $\sigma_{2\%-OS}$ (from tables 5 to 9 except ASTM-DF) and 95-percent CIs for means of all test assemblies before inclusion of covariate effects. No significant difference in $\sigma_{2\%-OS}$ existed between ASTM-DF tests, for 2X4, 2X8, and 2X12 assemblies so these tests are pooled into a single C.I. (Figure 39). In Figure 39, the CIs that do not overlap represent statistically significant differences in mean stress. Combined ASTM-DF tests showed significant differences when compared to all test assemblies with DF main members. ASTM-SPF tests showed significant differences when compared to BP-SPF assemblies as these were the only assemblies with SPF main members. It is believed that ASTM tests are significantly different than corresponding test assemblies because the loading conditions and contact surfaces are different. BC and BP test assemblies were loaded with opposite side end bearing in the main member. This scenario has been shown to be a more severe loading condition than the ASTM c-perp loading (Lum and Karacabeyli 1994, Blass and Gorlacher 2004). These members also represented wood-on-wood bearing. Wood-on-wood bearing has been shown to produce lower stresses as opposed to the metal-on-wood bearing condition present in the ASTM c-perp specimen (Fergus et al. 1981).

Mean $\sigma_{2\%-OS}$ for all test assemblies were compared with corresponding ASTM tests of the main members. Figure 40 shows the difference between means and 95-percent CIs for difference between means (shown in Figure 39 except for combined ASTM-DF 2X4, 2X8 and 2X12) based on pair wise comparisons before inclusion of covariate effects. Figure 40 is similar to Figure 39 except that each assembly is compared to its corresponding ASTM tests, and therefore ASTM-D-fir 2X4, 2X8, and 2X12 are not combined. In Figure 40, CIs that do not include 0 represent statistically significant differences in mean stress.

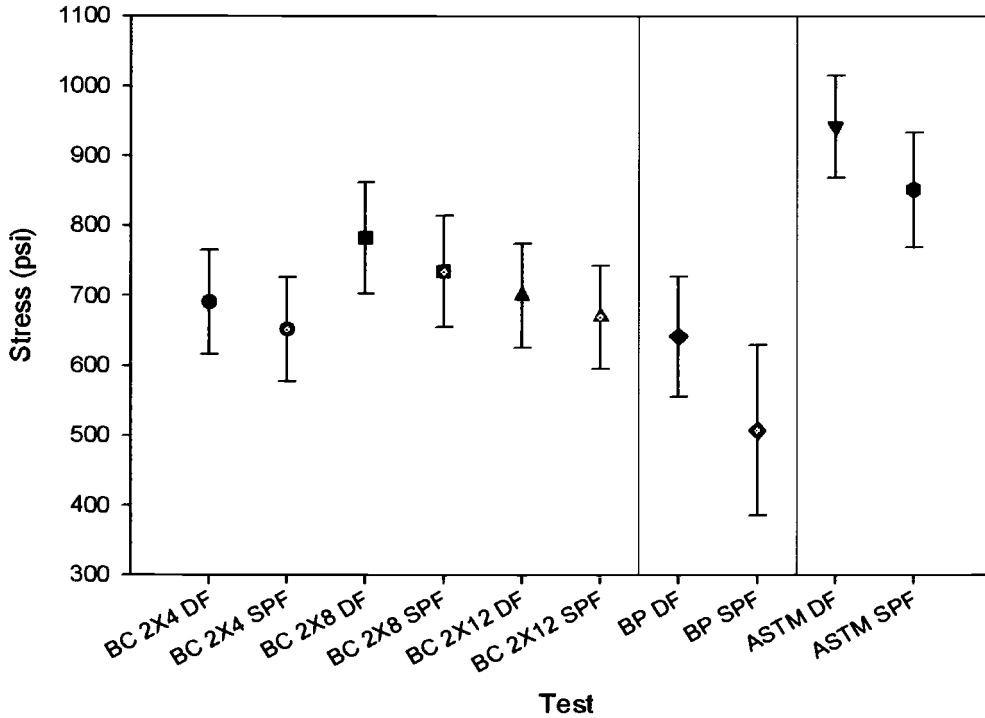


Figure 39: All assemblies 95-percent C.I. for mean $\sigma_{2\%-Os}$

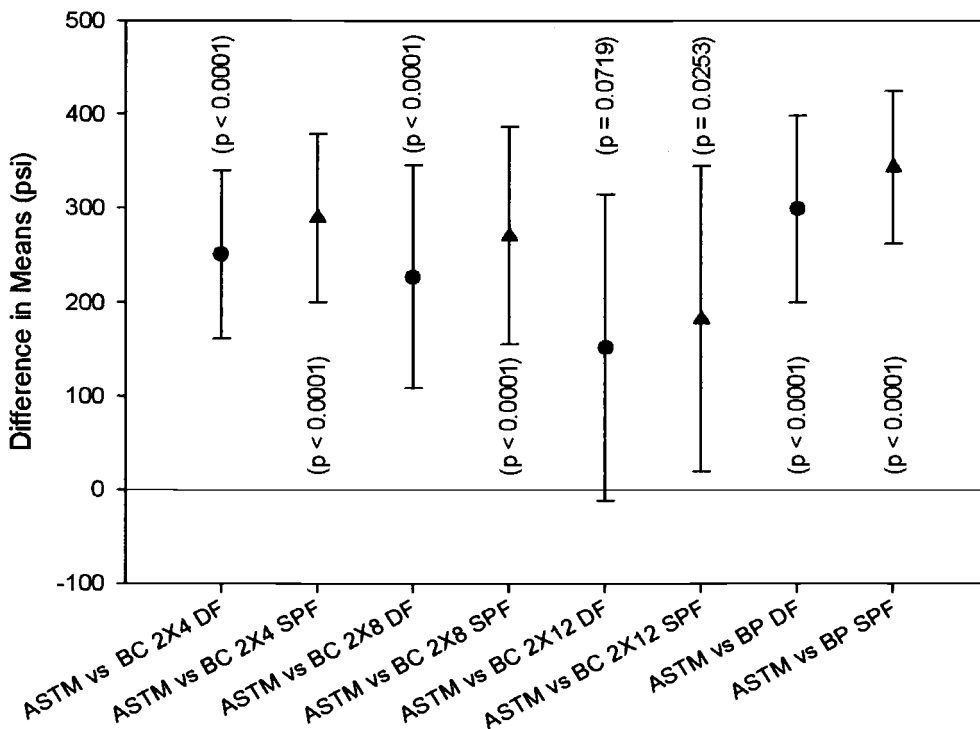


Figure 40: All assemblies vs. corresponding ASTM tests of main member 95-percent C.I. for difference in mean $\sigma_{2\%-Os}$

With the exception of BC-2X12-DF vs. corresponding ASTM tests of the main member which showed a suggestive but inconclusive difference (p-value = 0.07), differences in mean $\sigma_{2\%-OS}$ for all comparisons were found to be statistically significant. However, covariates were found to have an effect on mean $\sigma_{2\%-OS}$. Therefore, mean $\sigma_{2\%-OS}$ for all test assemblies were also compared with corresponding ASTM tests of the main members after accounting for covariate effects (Figure 41). Figure 41 shows difference between means and 95-percent CIs for difference between means based on pair wisecomparisons after adjustment for covariate effects.

Covariates were not found to have significant correlation to $\sigma_{2\%-OS}$ in comparisons of BC-2X4 tests to corresponding ASTM tests of the main member. While ring angle was found to have significant covariate effect in comparison of BC-2X8 and BC-2X12 assemblies to corresponding ASTM tests of the main member, it is believed that the lower aspect ratio of BC-2X4 tests tended to lesson the ring angle covariate effect.

In comparisons of BC-2X8 tests to corresponding ASTM tests of the main member, average ring angle of wood material was found to have significant covariate effect

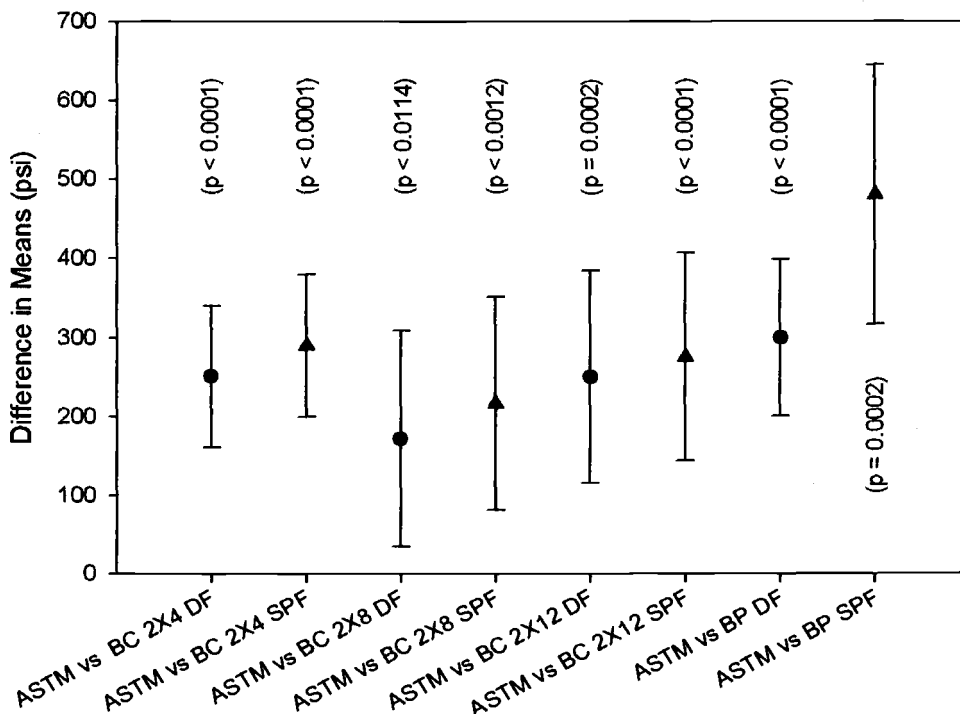


Figure 41: All assemblies vs. corresponding ASTM tests of main member 95-percent C.I. for difference in mean $\sigma_{2\%-OS}$ after adjustment for covariate effects

(respective p-values of 0.0427 and 0.0465 for ring angle and ring angle squared). With inclusion of covariate effect, BC-2X8-DF and BC-2X8-SPF continued to show statistically significant differences in mean $\sigma_{2\%-OS}$ when compared to ASTM tests of the main member (respective p-values of 0.0114 and 0.0012). After accounting for covariate effect, mean $\sigma_{2\%-OS}$ for ASTM tests of main member were estimated to be correspondingly 172 and 216 psi greater than that of BC-2X8-DF and BC-2X8-SPF tests.

For comparisons of BC-2X12 tests to corresponding ASTM tests of the main member, average ring angle as well as member specific gravity were found to have significant covariate effects (all p-values < 0.0001 for ring angle, ring angle squared, and specific gravity). After accounting for covariate effect, both BC-2X12-DF and BC-2X12-SPF tests continued to show statistically significant differences in mean $\sigma_{2\%-OS}$ when compared to ASTM tests of the main member (respective p-values of 0.0002 and < 0.0001). With inclusion of covariate effect, mean $\sigma_{2\%-OS}$ for ASTM tests of the main member were estimated to be correspondingly 250 and 275 psi greater than that of BC-2X12-DF and BC-2X12-SPF assembly tests.

When comparing BP-DF tests to corresponding ASTM tests of the main member, covariates were not found to have significant correlation to $\sigma_{2\%-OS}$. Lum and Karacabeyli (1994) suggested that for loading over the wide face of a member, (as was the case for B.P. member in BP assemblies) because ring angle across the width of the member varies, allowable c-perp design value can be increased. The rationale behind this suggested increase was that varying ring angle will produce a less pronounced ring angle effect and worst case ring angle scenario (about 45 degrees) does not have to be accounted for. This variability in ring angle across the wide face may have accounted for the fact that ring angle did not show significant covariate effect in comparison of BP-DF tests to corresponding ASTM tests. However average ring angle was found to have significant covariate effect on BP-SPF vs. corresponding ASTM tests of main member comparisons (respective p-value of 0.0605 and 0.0698 for ring angle and ring angle squared). The SPF 2X4s used in BP SPF tests were cut from veneer core stock. Most B.P. members therefore included pith. It may be that when pith is present ring angle has greater effect on c-perp behavior. It may also be the case that ring angle has greater effect on c-perp behavior of the SPF B.P. members in BP-SPF tests as opposed to the DF B.P. members in BP-DF tests. After accounting for covariate effect, BP-SPF tests continued to show statistically significant differences in mean $\sigma_{2\%-OS}$ when compared to ASTM tests of main member (p-values = 0.0002). After accounting for covariate effect,

mean $\sigma_{2\%-OS}$ for ASTM tests of main member was estimated to be 481 psi greater than that of BP-SPF tests.

Therefore after adjustment for covariate effect ASTM tests are significantly different from all corresponding assembly tests. The ASTM c-perp specimen does not adequately represent main members in BC and BP assemblies. As suggested by Lum and Karacabeyli (1994) and Blass and Goerlacher (2004), it seems that the ASTM c-perp specimen has limited applicability to the opposite side end bearing condition of BC and BP assembly tests. The wood-on-wood bearing present in these assembly tests likely also contributed to the lower stress value associated with BC and BP tests (Fergus et al. 1981). It is therefore necessary to adjust from ASTM c-perp stress values to c-perp stress values appropriate for these construction applications. This adjustment should include an adjustment factor for opposite side end bearing as well as an adjustment factor for wood-on-wood bearing.

4.6 COMPARISON OF DATA WITH LITERATURE

Table 10 gives ratios of assembly performance to performance of corresponding ASTM tests of the main member based on mean $\sigma_{2\%-OS}$. Also shown are predicted ratios of assembly to ASTM test performance based on design procedures proposed by Lum and Karacabeyli (1994) as well as Blass and Goerlacher (2004) and determined from the loading condition of the main member in each assembly. For each assembly the design procedure proposed by Lum and Karacabeyli comes closer to predicting actual $\sigma_{2\%-OS}$ attained in testing and is therefore bolded.

It is noted that for each design procedure the predicted ratio is based on loading condition of the main member alone. In BC assemblies, T.P. members would have a different predicted ratio and this likely contributes to at least some of the discrepancy between the theoretical ratios and those produced in testing. This is because the T.P. members in BC assembly tests contributed to the c-perp behavior of the assembly but the ratios shown in table 9 are based on the loading condition of the B.C. member alone. Of all assembly tests performed, the BP assembly comes closest to idealizing the loading condition upon which these ratios are predicated. This is because theoretical deflection in the C.C. member was adjusted out of the data, and it is also predicted to be very small. In BP testing assemblies, it is believed that the lower stress values achieved in testing (as compared with those predicted by Lum and Karacabeyli (1994) and Blass and Goerlacher

Table 10: Ratio of assembly performance to corresponding ASTM test performance with predicted ratios from literature

Assembly	Ratio Assembly/ ASTM (%)	Lum and Karacabeyli Predicted (%)	Blass and Goerlacher Predicted (%)
BC 2X4 D-fir	73	66	61
BC 2X4 SPF	69	66	61
BC 2X8 D-fir	78	66	61
BC 2X8 SPF	72	66	61
BC 2X12 D-fir	79	66	61
BC 2X12 SPF	75	66	61
BP D-fir	68	77	82
BP SPF	60	77	82

(2004)) are likely due to the wood-on-wood contact involved in these assemblies (Fergus et al. 1981). Non-parallelism of the specimens may also have contributed to these discrepancies

4.7 RELATIONSHIP BETWEEN ASPECT RATIO AND C-PERP BEHAVIOR INCLUDING ULTIMATE LIMIT STATE

4.7.1 STRESS AT 2-PERCENT OFFSET STRAIN ($\sigma_{2\%-OS}$)

Mean $\sigma_{2\%-OS}$ of all BC tests was compared across assemblies (Figure 42). Figure 42 shows difference between means and 95-percent CIs for difference between means based on pair wise comparisons both before and after inclusion of covariate effects. As discussed in the influence of wood species section, significant differences in mean $\sigma_{2\%-OS}$ between BC-DF and BC-SPF assemblies were not present. Therefore, BC-DF and BC-SPF tests are combined in Figure 42. Based on 95-percent CIs for specified linear combinations, no statistically significant difference in $\sigma_{2\%-OS}$ was seen between any BC assemblies before inclusion of covariate effects (i.e. all 95-percent confidence intervals include 0). However with inclusion of covariate effects the phenomenon changed.

Significant covariates in the model were found to include average ring angle of the bottom chord, as well as specific gravity of both T.P. and B.C. member wood material (respective p-values of .005 and .0185). After adjustment for covariate effect, mean $\sigma_{2\%-OS}$ of BC-2X4 tests was significantly lower than that of BC-2X8 tests (p-value = .0037). Mean stress of

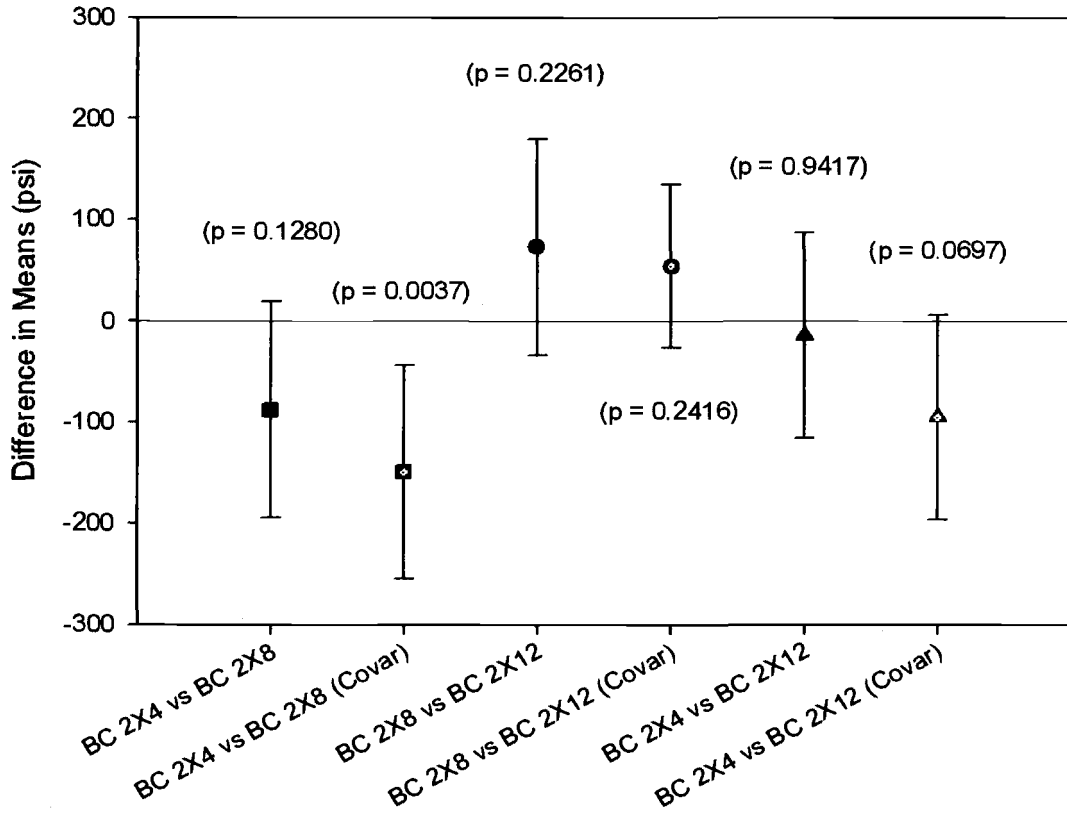


Figure 42: BC tests all - 95% C.I. for difference in mean $\sigma_{2\%-OS}$ before and after accounting for covariate effect

BC-2X4 tests was estimated to be 149 psi lower than that of BC-2X8 tests. There was also suggestive but inconclusive evidence that mean stress of BC-2X4 tests is lower than that of BC-2X12 tests (p -value = .0697). No significant difference in mean stress at 2-percent system offset strain was observed between test BC-2X8 and BC-2X12 assembly tests.

This data suggests that associated with higher aspect ratio in BC-2X8 assemblies as opposed to BC-2X4 assemblies is a mean increase in $\sigma_{2\%-OS}$. Initially this seems to be counterintuitive given the fact that larger aspect ratios lead to higher probability of catastrophic failure. However, most B.C. members in BC assemblies failed catastrophically only after attaining $\sigma_{2\%-OS}$. Those that did not fail after attaining $\sigma_{2\%-OS}$, were within a few percent of $\sigma_{2\%-OS}$ at time of failure. It is suggested that the greater $\sigma_{2\%-OS}$ in BC-2X8 assemblies as compared with that of BC-2X4 assemblies is related to the stress distribution within B.C. members. As previously discussed, finite element analysis revealed that wood material within 2X12 B.C. members adjacent to but outside of the region directly between top and bottom T.P. members, provided support with

corresponding strain in the material. This additional strained area increases toward mid-depth in the B.C. member. It follows that the stressed cross section at mid depth is larger in deeper members. Therefore stress is distributed across a larger average cross section in deeper members. 2X8 B.C. members have stress distributed across a larger average cross-sectional area than do 2X4 B.C. members.

While mean $\sigma_{2\%OS}$ of BC-2X12 is not greater than that of BC-2X8 members, it is believed that the tendency of BC-2X12 members to buckle overshadowed the effect of the increased depth in the members. When cross-grain bending occurs, this mode of compressive deflection dominates compressive behavior. Compressive deflection occurs predominantly through further cross-grain bending in the B.C. member, rather than compressive deflection throughout the depth of the members. It is suggested that further study into the relationship between member depth and stress at specified strain in partially surface c-perp loading should be conducted.

4.7.2 MAXIMUM STRESS AND STRAIN AT MAXIMUM STRESS

In order to determine the influence of aspect ratio on maximum stress, mean σ_{max} for the three BC assemblies were compared. Figure 43 illustrates difference between mean σ_{max} and 95-percent CIs for difference between mean σ_{max} for multiple comparisons of BC assembly tests both before and after adjustment for covariate effects. Species of T.P. material was not found to have a statistically significant impact on σ_{max} (respective p-values of 0.36 and 0.31 before and after inclusion of covariate effects). Therefore, BC-DF and BC-SPF tests are combined (Figure 43).

As shown in Figure 43, without covariate effects included, no significant difference in mean σ_{max} is present between BC-2X4 and BC-2X8 tests (i.e. 95-percent C.I. includes 0). Both BC-2X4 and BC-2X8 tests have significantly different mean σ_{max} as compared with BC-2X12 (respective p-values of .02 and .0075). Mean σ_{max} of BC-2X4 and BC-2X8 was found to be respectively 149 and 178 psi higher than that of BC-2X12.

Average ring angle of BC member was found to have a significant covariate effect for all BC assemblies (p-value = .0199). After adjusting for covariate effect, the difference in mean σ_{max} between BC-2X4 and BC-2X12 was no longer significant. However the difference between BC-2X8 and BC-2X12 remained significant (p-value = .0165). The

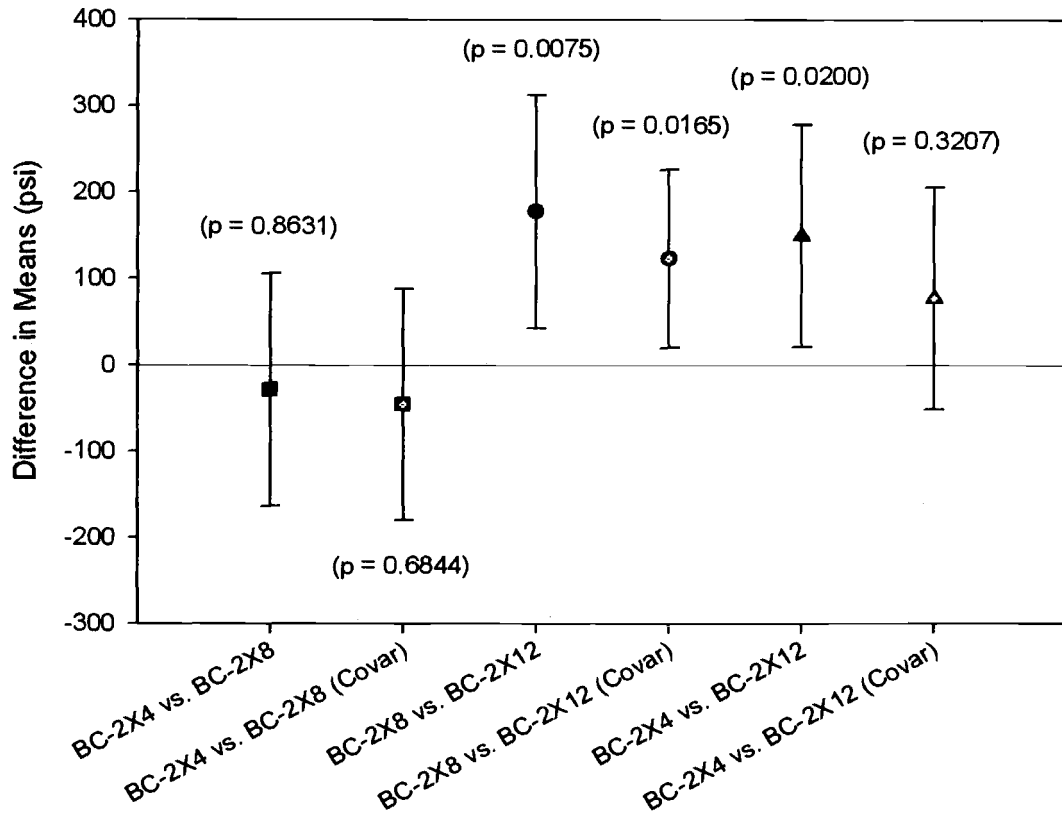


Figure 43: BC assemblies σ_{\max} before and after adjustment for covariate effects

mean difference between BC-2X8 and BC-2X12 was estimated to be 123 psi after adjustment for covariate effect.

As previously noted, the finite element analysis suggests that deeper B.C. members had stress distributed across a larger average cross-section. This is due to the fact that more support is provided by material away from the loaded longitudinally end of the B.C. member in deeper B.C. members. This phenomenon may be responsible for the fact that BC-2X4 assemblies did not significantly outperform BC-2X12 assemblies based on σ_{\max} . It is believed that the significant difference in mean σ_{\max} between BC-2X12 and BC-2X8 assemblies is due to the increased aspect ratio of BC-2X12 B.C. members over that of BC-2X8 B.C. members. As discussed in the compression behavior section, BC-2X12 B.C. members exhibited higher instances of cross-grain bending as well as higher probability of catastrophic failure prior to 10-percent system strain.

Figures 44 to 46 show histograms of the number of assemblies reaching various fractions of the NDS c-perp design value for DF ($F_{c\perp}$). BC-2X4-DF and BC-2X4-SPF test # 3 failed to reach $F_{c\perp}$ (B.C. member in both tests was cut from same board). In these two tests, the B.C. member was cut from near the pith and had annual rings with a low radius of curvature (Figure 32(e)). These two B.C. members exhibited rolling shear along the earlywood/latewood interface combined with tension perpendicular to grain cracking. However this was not uncommon in BC-2X4 tests and the reason for the unusually low σ_{max} is not clear. The majority of BC-2X4 assemblies reached σ_{max} values between 125 and 175 percent of $F_{c\perp}$. The trend was similar for BC-2X8 assemblies with all assemblies reaching $F_{c\perp}$ and the majority of assemblies attaining between 125 and 175 percent of $F_{c\perp}$. However, with increased aspect ratio of the B.C. member in BC-2X12 members, six assemblies failed to reach $F_{c\perp}$ due to premature failure of the B.C. member. These failures were initiated by cross-grain bending in the B.C. member that led to rolling shear and or tension perpendicular to grain damage with corresponding failure. Despite this phenomenon, the majority of BC-2X12 assemblies attained between 100 and 150-percent of $F_{c\perp}$.

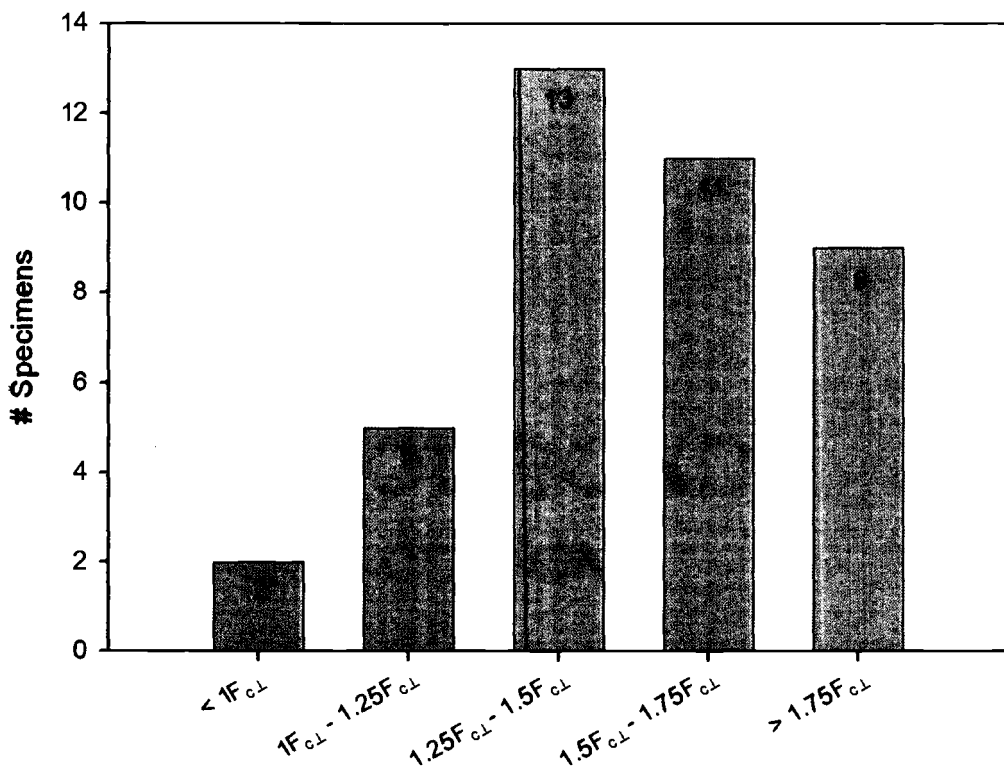


Figure 44: BC-2X4 assembly σ_{max} as ratio of NDS base design value ($F_{c\perp}$)

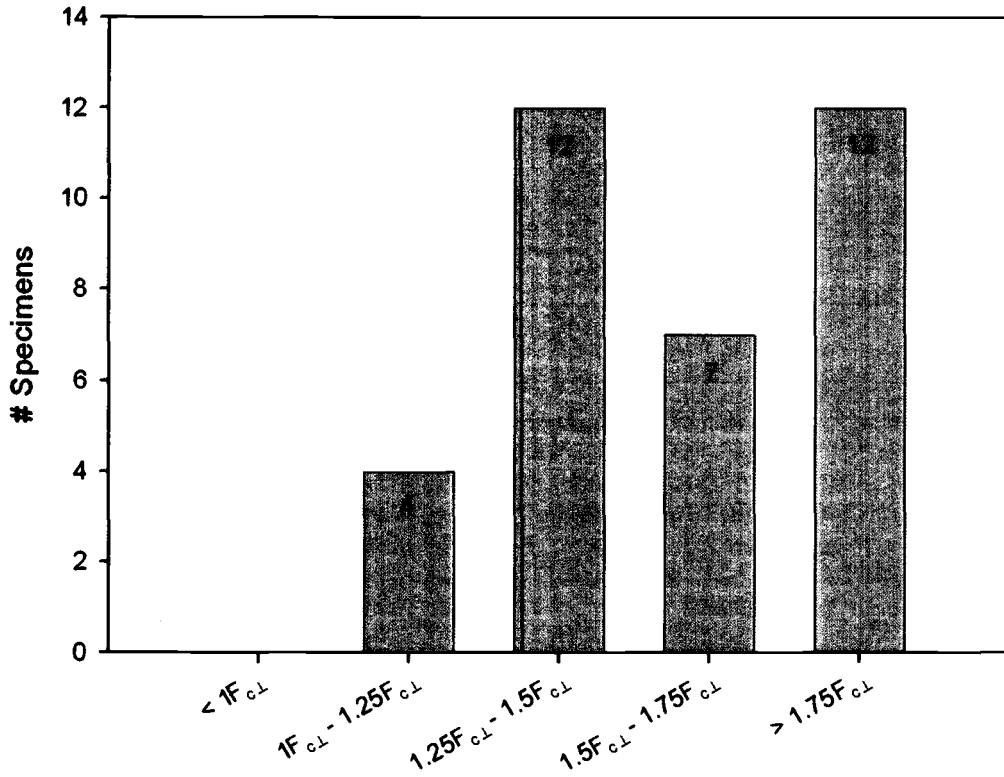


Figure 45: BC-2X8 assembly σ_{\max} as ratio of NDS design value ($F_{c\perp}$)

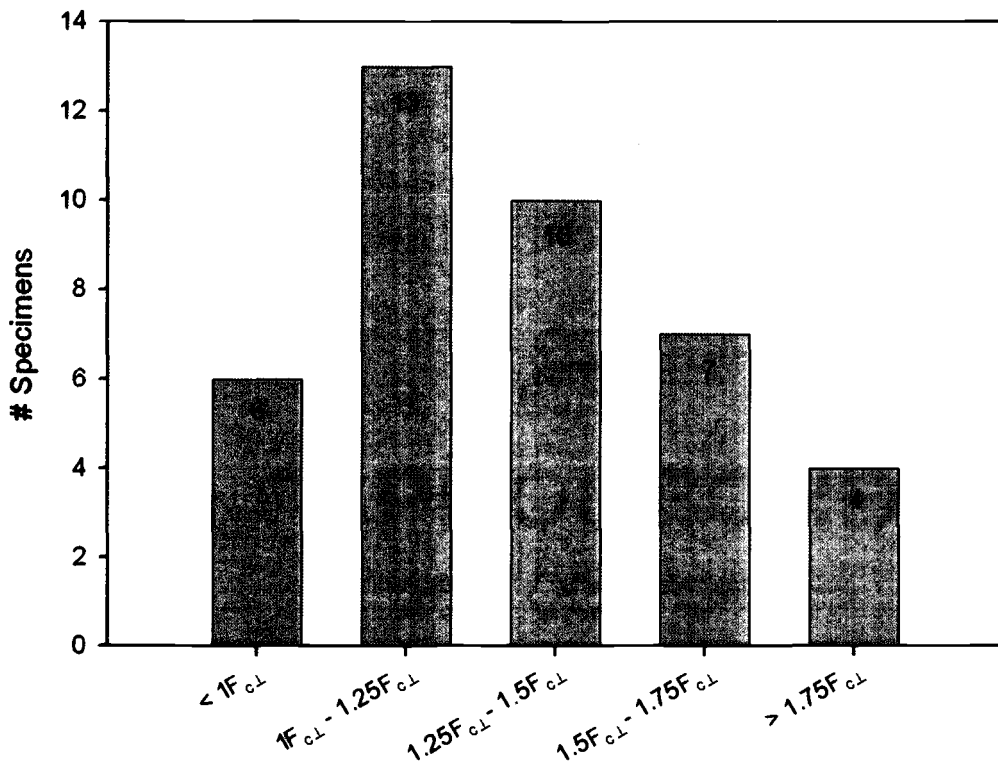


Figure 46: BC-2X12 assembly σ_{\max} as ratio of NDS design value ($F_{c\perp}$)

Figures 47 through 49 show the range of strain values attained by BC assemblies where strain is measured from the offset strain for the particular test in question. From Figures 47 through 49, the trend of decreasing strain at σ_{max} with increasing aspect ratio can be seen. As shown in Figure 47, 39 of the 40 BC-2X4 assemblies attained σ_{max} at offset strain near 10-percent. Nineteen of the 40 assembly tests were continuing to densify with increasing stress capacity at 10-percent system offset strain. Sixteen of the 35 BC-2X8 assemblies attained σ_{max} at offset strain near 10-percent. Ten of these 35 assemblies were continuing to densify with increasing stress at conclusion of testing. While the majority of BC-2X12 assemblies attained σ_{max} at between 2 and 6-percent system offset strain, two BC-2X12 assemblies failed catastrophically in the B.C. member immediately prior to attaining 2-percent system offset strain (within 2-percent of 2-percent system offset stress). For these tests $\sigma_{2\%-OS}$ was the same as σ_{max} . The BC-2X12-SPF test #18 was continuing to densify with increasing stress at the conclusion of testing.

This phenomenon of decreased strain at σ_{max} with increased aspect ratio is related to changes in compressive behavior with increasing aspect ratio of the B.C. member as described in the compression behavior section. The lower aspect ratio B.C. members in BC-2X4 assemblies continue to densify with increasing stress (often times up to or near 10-percent system offset strain). These assemblies behave much more like the ASTM

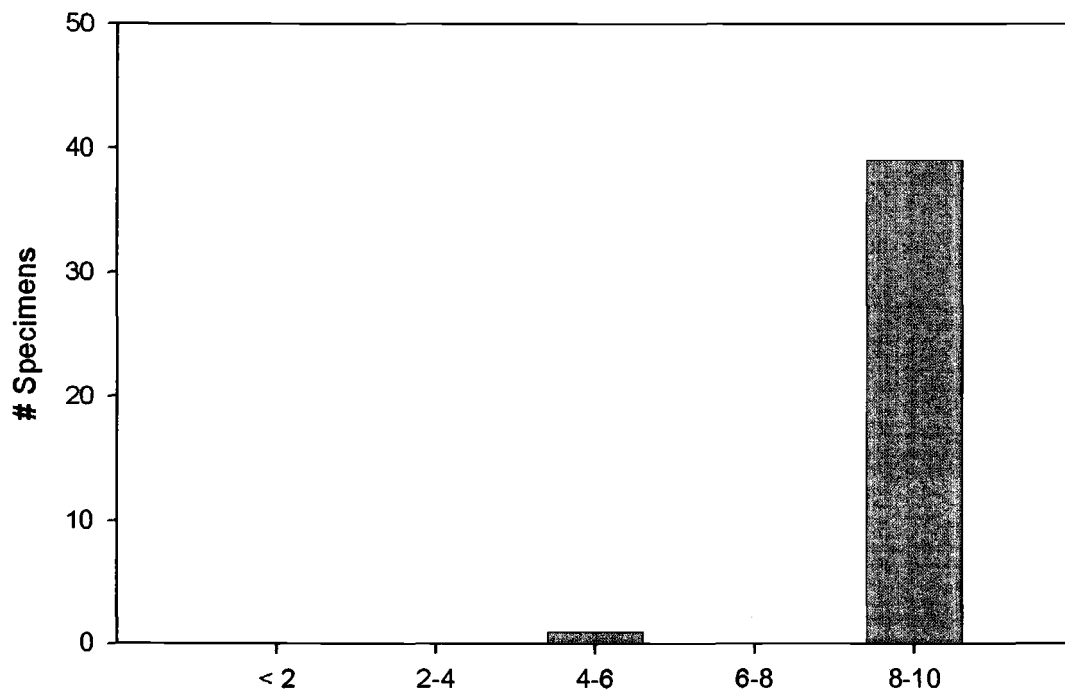


Figure 47: Histogram of percent strain from offset at σ_{max} for BC-2X4 assemblies

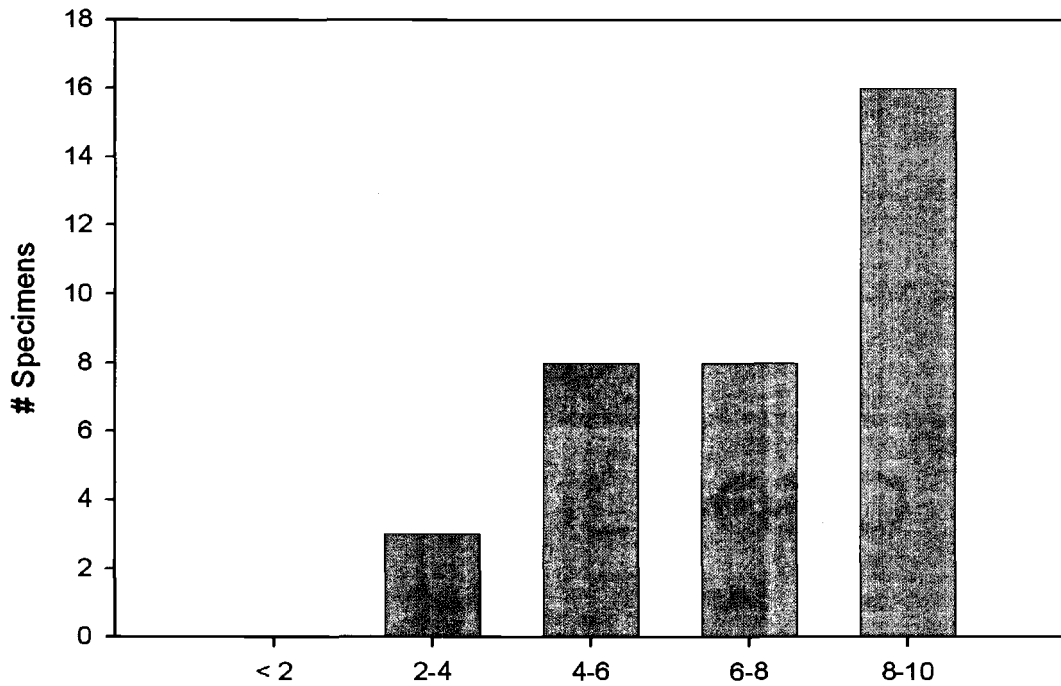


Figure 48: Histogram of percent strain from offset at σ_{max} for BC-2X8 assemblies

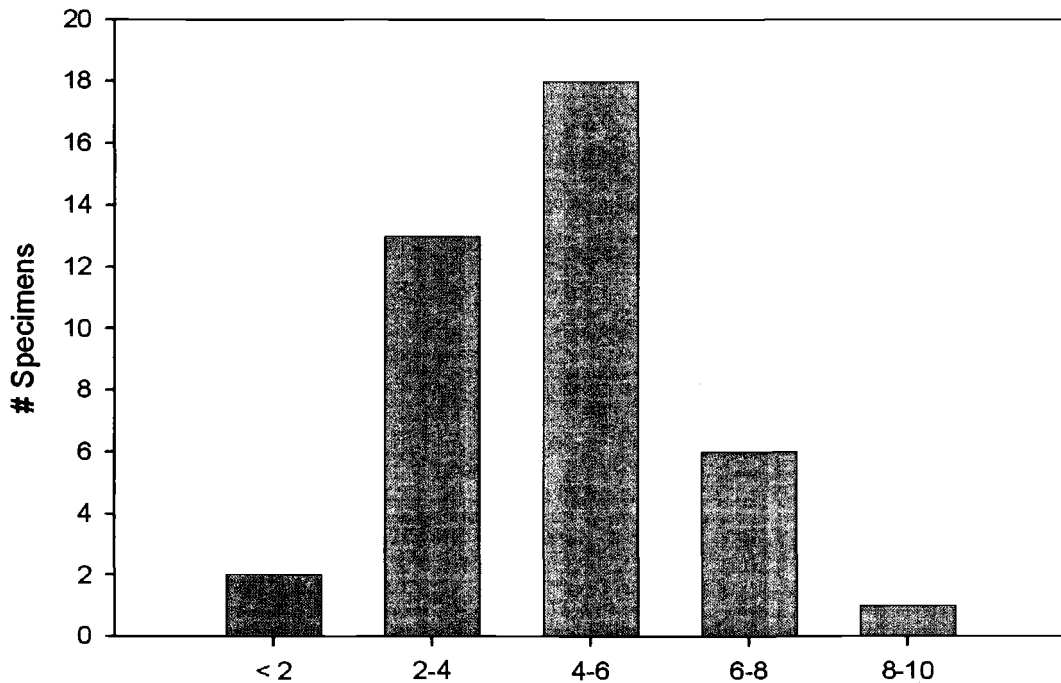


Figure 49: Histogram of percent strain from offset at σ_{max} for BC-2X12 assemblies

specimen in terms of continued densification with increasing load. Even when cross-grain bending of the B.C. member occurs the assemblies generally continue to support increasing loads. Increasing aspect ratio leads to increased cross-grain bending of B.C. members. As aspect ratio increases the continued densification associated with the ASTM c-perp specimen becomes less and less representative of the behavior of B.C. members. With increasing aspect ratio, members that exhibit cross-grain bending tend to begin supporting lower loads with increased strain. This leads to stress dropping off earlier in the stress strain diagram and often results in catastrophic failure at much lower strains.

4.7.3 PROBABILITY OF CATASTROPHIC FAILURE

Catastrophic failures were observed only in BC-2X8 and BC-2X12 assemblies and the catastrophic failures always occurred in the B.C. member. A logistic regression was performed that includes covariate effects and estimates probability of catastrophic failures of the B.C. member in these two assemblies. Based on a best fit, it is estimated that a 2X12-B.C. member in a BC-2X12 assembly is 72 times more likely to fail catastrophically than the 2X8-B.C. member in a BC-2X8 assembly (95-percent CI between 16 and 327 times more likely to fail). This data leads to the conclusion that c-perp is a system stability / life safety issue in high aspect ratio members rather than serviceability issue. An adjustment factor, and/or adjustment factors, are therefore necessary to adjust c-perp stress values obtained from the ASTM specimen to appropriate stress values for applications in which load is applied to wood members with aspect ratios larger than 1. Standard dimensional lumber was used in this study, and these conclusions can not be extrapolated to engineered wood products. Further studies are appropriate to establish the relationship between aspect ratio and c-perp behavior of engineered wood products.

Probability of catastrophic failure of BC-2X8 assemblies was found to have a significant relationship with average ring angle of B.C. member at interface with T.P. members. For 2X8 B.C. member probability of catastrophic failure is estimated from the logistic regression as;

$$P.F. = e^{(-.397 \cdot R.A._{T\&B} + 4.866)} / (1 + e^{(-.397 \cdot R.A._{T\&B} + 4.866)}) \quad \text{eq(1)}$$

Where P.F. = probability of catastrophic failure, $R.A._{T\&B}$ = Average ring angle of B.C. member at interface with top plate members, and e = natural logarithm (Figure 50). The

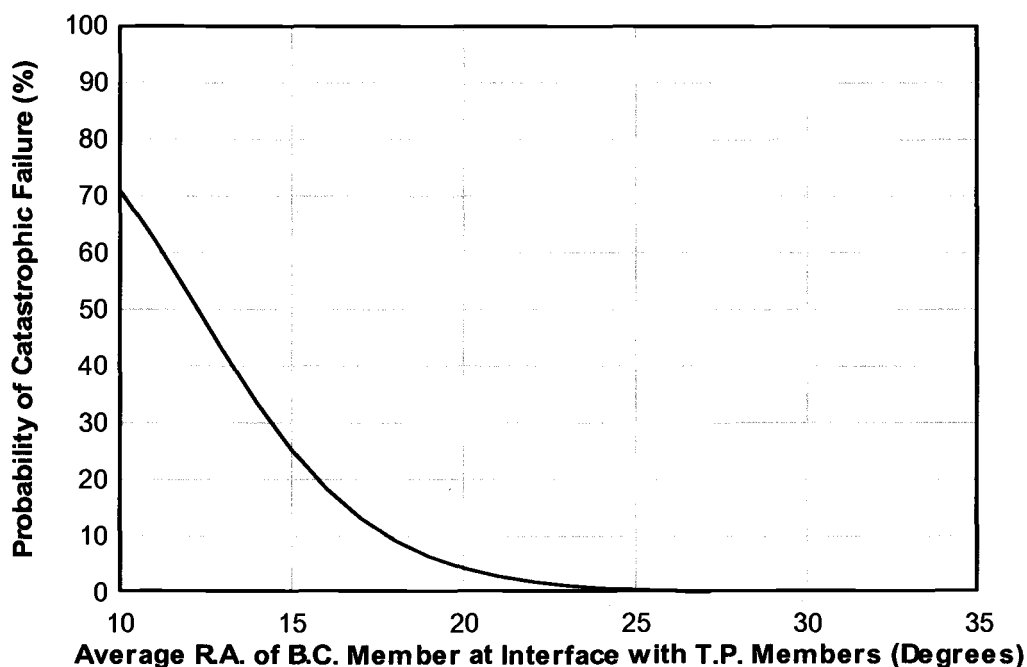


Figure 50: Calculated probability of catastrophic failure of 2X8-B.C. member as a function of average ring angle of B.C. member at interface with T.P. members

probability of catastrophic failure of BC-2X12 assemblies was not found to have a significant relationship with covariates. This was due to the high instance of failure in these members (86-percent failed catastrophically prior to 10-percent system strain).

In Figure 50, the average ring angle of the B.C. member at interface with T.P. members ($RA_{T\&B}$) is the average ring angle at the top and bottom narrow faces of the B.C. member (faces in contact with T.P. members, Figure 51). The highest probability of catastrophic failure for B.C. 2X8 members occurs at $RA_{T\&B}$ near 10 degrees with probability of catastrophic failure decreasing to 0 for $RA_{T\&B}$ near 25 degrees (Figure 50).

In BC-2X8 assemblies 3 catastrophic failures were observed. The B.C. members cut from 2X8-DF board number 9 failed catastrophically in both BC-2X8-DF and BC-2X8-SPF test number 9 (Figure 51(a)). In both cases, the B.C. member had $RA_{T\&B}$ of 10 degrees. The B.C. member cut from 2X8-DF board number 11 failed catastrophically in BC-2X8-DF test #11 (Figure 51(b)). This B.C. member had $RA_{T\&B}$ of 15 degrees. It is believed that in these assemblies low $RA_{T\&B}$ in B.C. member prevented localized annual ring buckling near the interface of the B.C. member with T.P. members. This forced annual ring buckling near mid depth of the B.C. members. Corresponding cross-grain bending of the

B.C. members lead to a combination of rolling shear, and tension perpendicular to grain damage, that eventually lead to catastrophic failure in the B.C. members.

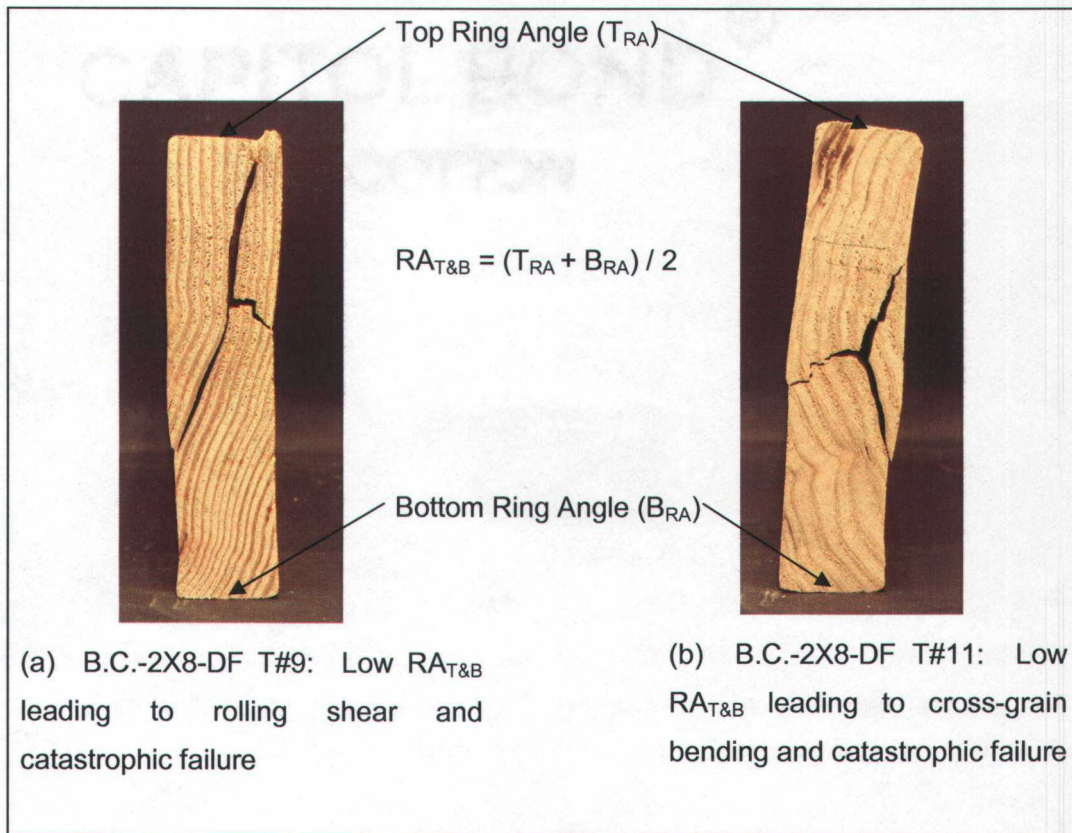


Figure 51: Characteristic $RA_{T\&B}$ which led to catastrophic failure of B.C. member in BC-2X8 assemblies

CHAPTER 5. CONCLUSIONS AND RECOMMENDATIONS

5.1 CONCLUSIONS

- 1.) Finite element modeling showed that, in BC assemblies, strain is more uniform throughout the depth of the B.C. member in radial compression than in tangential compression. Also, the majority of system strain occurs in the B.C. member and c-perp behavior is dominated by B.C. member. In BP assemblies, the vast majority of system strain occurs in the B.P. member. Modeling results indicate that 12-percent of total system strain occurs in T.P. members for BC assemblies and that 3.5-percent of total system strain occurs in C.C. member in BP assemblies
- 2.) The compression in T.P. members was similar to that seen in the ASTM specimen. However, the compression was uneven with more densification on the side of the T.P. member away from loaded end of the B.C. member. This behavior shows that the adjacent unloaded material in the B.C. member provides support to the volume directly under the T.P. bearing surface. This is consistent with FEM results.
- 3.) When loaded tangentially, B.C. members buckle in the direction of annual ring curvature. This phenomenon was attributed to latewood layers acting as reinforcing columns in this orientation. High aspect ratios accentuate this effect and when combined with high aspect ratio, the combination of ring curvature and aspect ratio had a tendency to produce rolling shear failure in B.C. members along the earlywood-latewood interface.
- 4.) B.C. members had a tendency to split longitudinally in along their major axis. The splitting was attributed to transverse tensile forces that develop in the B.C. member as one longitudinal end is compressed. High aspect ratio accentuated this effect. This phenomenon did not lead to immediate catastrophic failure of B.C. members but it may have contributed to global failure. It is believed that this longitudinal splitting was due to relatively short pieces used in testing and that full sized members may not have exhibited this behavior.

- 5.) B.P. members had a tendency to split longitudinally along their major axis. In this case, the phenomenon was attributed to transverse tensile forces that develop within the B.P. member as it densifies. It is believed that for B.P. tests this longitudinal splitting along the major axis was due to the relatively short pieces used in testing. As discussed for B.C. members, full-sized B.P. members used in construction application may not exhibit this behavior.
- 6.) In order to account for assembly depth, stress values were based on system strain. A 0.04-in. deflection corresponds to a 2-percent strain in the 2-in. deep ASTM specimen, and stress in the assemblies was based on 2-percent system strain. Large settlement effects (initial misalignment region) were observed in the wood-on-wood test assemblies. It was concluded that when wood members are rough cut and/or not perfectly rectilinear (as is the case in most construction applications), wood-on-wood bearing settlement effects are cumulative and are accentuated by surface roughness and non-parallel contact surfaces. An offset strain successfully adjusts for these effects. Thus an offset strain was adopted as the method for determining and comparing stress values across differing assemblies and configurations tested. Therefore an offset strain is recommended for determination of c-perp design values.
- 7.) Within BC assembly tests, top plate wood species was not found to have a significant impact on stress at 2-percent offset strain. This was due to the overwhelming influence of the truss B.C. main members, i.e. c-perp behavior was dominated by the B.C. member. Within BP assembly tests, a suggestive but inconclusive effect of bottom plate wood species on stress at 2-percent offset strain was observed (p-value = 0.076).
- 8.) Mean stress at 2-percent offset strain of all assemblies were significantly lower than corresponding ASTM tests of the main member. This was attributed to the opposite side longitudinal end bearing and wood-on-wood bearing of tested assemblies. The ASTM test does not adequately represent these testing configurations and adjustment to design value is necessary for determining allowable c-perp stress values.
- 9.) It is therefore recommended that a c-perp adjustment factor (for example $C_{\text{end-bearing}}$) be incorporated into the NDS for the case of opposite side longitudinal

end bearing in wood members, and that this factor be used in determining allowable c-perp design stress ($F_{c\perp}'$)

- 10.) It is therefore also recommended that a c-perp adjustment factor (for example $C_{\text{wood-bearing}}$) be incorporated into the NDS for the case of wood-on-wood bearing, and that this factor be used in determining allowable c-perp design stress ($F_{c\perp}'$)
- 11.) Data from this study supports the 2/3 reduction factor used in Canadian design for c-perp when load is applied to opposite sides of a member near the longitudinal end of the member. Data from this study does not agree as closely with the German design approach in which the allowable c-perp is based on full surface compression that is adjusted upward based on effective contact length parallel to grain. For assembly tests conducted in this study, the aforementioned design procedures could only be applied to the loading condition of the main member. T.P. members in BC assemblies obscure conclusions with respect to the accuracy of these design procedures in predicting c-perp behavior of B.C. members.
- 12.) Aspect ratio affects c-perp behavior of wood members. While the higher aspect ratios examined in this study do not lead to lower stress values (when based on the stress at 2-percent offset strain), higher aspect ratios lead to instability of the member. A 2X12 may fail catastrophically prior to 2-percent system offset strain. The BC-2X12 assemblies attain lower maximum stresses than BC-2X8 assemblies. The 2X12 members may not attain allowable stress values listed in the NDS.
- 13.) C-perp is a system stability / life safety issue in high aspect ratio members rather than a serviceability issue alone.
- 14.) It is therefore recommended that a c-perp adjustment factor (for example C_{aspect}) be incorporated into the NDS for the case of c-perp loading of high aspect ratio members which may exhibit aspect ratio related instability, and that this factor be used in determining allowable c-perp design stress ($F_{c\perp}'$)
- 15.) This study involved standard dimensional lumber, and these conclusions can not be extrapolated to engineered wood products.

5.2 RECOMMENDATIONS FOR FUTURE STUDY

- 1.) It is recommended that further studies with larger sample sizes be conducted to determine the influence of wood species on BP assemblies.
- 2.) It is recommended that further studies be conducted to determine an appropriate adjustment factor to be used in calculating allowable c-perp design value ($F_{c\perp}'$) for the case of opposite side longitudinal end bearing in wood members.
- 3.) It is recommended that further studies be conducted to determine an appropriate adjustment factor to be used in calculating allowable c-perp design value ($F_{c\perp}'$) for the case of wood-on-wood bearing.
- 4.) It is recommended that further studies into the relationship between member depth and stress at specified strain in partially surface c-perp loading be conducted.
- 5.) It is recommended that further studies be conducted to better understand the relationship between aspect ratio and member instability in c-perp loading. It is further suggested that these studies focus on determining an appropriate adjustment factor and/or adjustment factors to be used in calculating allowable c-perp design value ($F_{c\perp}'$) for members with aspect ratios greater than 1.
- 6.) It is recommended that further studies into the relationship between aspect ratio and c-perp behavior of engineered wood products be conducted.

CHAPTER 6. BIBLIOGRAPHY

American Forest and Paper Association. 1993. ANSI/NFoPA. 1997. National design specification for wood construction. AF&PA, Washington, D.C. 53-73.

American Forest and Paper Association. 2001. National design specification for wood construction. AF&PA, Washington, D.C. 53-73. 174 pp.

American Society for Testing and Materials (ASTM). 2000. Standard methods of testing small clear specimens of timber. Designation D 143-94. American Society of Testing and Materials, West Conshohocken, PA. 708 pp.

American Society for Testing and Materials (ASTM). 2000. Standard methods for specific gravity of wood and wood-based materials. Designation D 2395. American Society of Testing and Materials, West Conshohocken, PA. 708 pp.

American Society for Testing and Materials (ASTM). 2000. Standard methods for direct moisture content measurement of wood and wood-base materials. Designation D 4442. American Society of Testing and Materials, West Conshohocken, PA. 708 pp.

Bendtsen, B.A., J.H. Haskell, and W.L. Galligan. 1978. Characterizing the stress-compression relationship of wood in compression perpendicular to grain. *Wood Sci.* 10(3):111-121.

Bendtsen, B.A. and W.L. Galligan. 1979. Modeling of the stress-compression relationship in wood in compression perpendicular to grain. *Forest Prod. J.* 29(2):42-48.

Blass, H.J., and I.R. Gortlacher. 2004. Compression perpendicular to the grain. *Proceedings of the 8th World Conference of Timber Engineering.* 2:435-440.

Bodig, J. 1963. The peculiarity of compression of conifers in radial direction. *Forest Prod. J.* 13(10):438.

Bodig, J. 1965. Initial stress-strain relationship in transverse compression. *Forest Prod. J.* 15(5):197-202.

Bodig, J. 1969. Improved load-carrying capacity of wood in transverse compression. *Forest Prod. J.* 19(12):39-44.

Breyer, D.E., K.J. Fridley, D.G. Pollock, and K.E. Cobeen. 2003. Design of wood structures. The McGraw-Hill Companies, Inc. 996 pp.

Bulmanis, N.S., H.A. Latos, and F.J. Keenan. 1983. Improving the bearing strength of supports of light wood trusses. *Can. J. Civ. Eng.* 10:306-312.

Easterling, K.E., R. Harrysson, L.J. Gibson, and M.F. Ashby. 1982. On the mechanics of balsa and other woods. *In: Proceedings of the Royal Society of London. Series A. Mathematical and Physical Sciences.* 383(1784):31-41.

Ethington, R.L., V. Eskelsen, and R. Gupta. 1996. Relationship between compression strength perpendicular to grain and ring orientation. *Forest Prod. J.* 46(1):84-86.

Fergus, D.A., J.F. Senft, and S.K. Suddarth. 1981. Recommended bearing stresses for design in light-frame construction. *Forest Prod. J.* 31(4):50-57.

Forest Products Laboratory. 1999. Wood Handbook--Wood as an engineering material. Gen. Tech. Rep. FPL-GTR-113. Madison, WI: 463 pp.

Gibson, L.J., K.E. Easterling, and M.F. Ashby. 1981. The Structure and Mechanics of Cork. *In: Proceedings of the Royal Society of London. Series A. Mathematical and Physical Sciences.* 377(1769):99-117.

Gibson, L.J., M.F. Ashby, G.S. Schajer, and C.I. Robertson. 1982. The Mechanics of two-dimensional Cellular Materials. *In: Proceedings of the Royal Society of London. Series A. Mathematical and Physical Sciences.* 382(1782):25-42.

Haygreen, J.G., R. Shmulsky, and J.L. Bowyer. 2003. Forest Products and Wood Science. Iowa State University Press, Ames, IA. 554 pp.

Johnson, J.W. 1983. Compression perpendicular to the grain in dry Douglas-fir and hem-fir. *Forest Prod. J.* 33(3):55-63.

Kennedy, R.W. 1968. Wood in transverse compression – Influence of some anatomical variables and density on behavior. *Forest Prod. J.* 18(3):36-40.

Kretschmann, D.E., S.M. Cramer, R. Lakes, and T.S. Schmidt. 2003. Selected mesostructure properties in loblolly pine from Arkansas plantations, Characterization of the cellulosic cell wall proceedings, Grand Lake, CO. (Copy of paper received from authors).

Kunesh, R.H. 1961. The inelastic behavior of wood. A new concept for improved panel forming processes. *Forest Prod. J.* 11:395-406.

Kunesh, R.H. 1968. Strength and elastic properties of wood in transverse compression. *Forest Prod. J.* 18(1):65-72.

Leicester, R.H., H. Fordham, and H. Breiting. 1998. Bearing strength of timber beams. *In: International Council For Building Research Studies and Documentation, Working Commission W18 – Timber Structures. Meeting thirty-one. CSIRO Building, Construction and Engineering. Melbourne, Australia. 12 pp.*

Lum, C. 1995. Compression perpendicular-to-grain design in CSA-086.1-M94. Forintek Canada Corp, Vancouver B.C. 37 pp.

Lum, C. and E. Karacabeyli. 1994. Development of the "critical bearing" design clause in CSA-086.1. *In: CIB Working Commission (W18A) – Timber Structures in Sydney, Australia. Forintek Canada Corp, Vancouver B.C. 17 pp.*

Lum, C. and E. Varoglue. 1988. Testing and analysis of parallel chord trusses, *In: Proceedings of the 1988 International Conference on Timber Engineering. Forest Products Research Society. 1:460-466.*

Pellicane, P.J., J. Bodig, and A.L. Mrema. 1994. Modeling wood in tranverse compression. *Journal of Testing and Evaluation.* 22(4):376-382.

Pellicane, P.J., J. Bodig, and A.L. Mrema. 1994. Behavior of wood in tranverse compression. *Journal of Testing and Evaluation.* 22(4):383-387.

Rose, J.D. 1998. Preliminary testing of wood structural panel shear walls under cyclic (reversed) loading, *In: Laboratory Report 158*. APA-The Engineered Wood Association, Engineered Wood Systems. Tacoma, WA.

Rose, J.D., and E.D. Keith. 1996. Wood structural panel shear walls with gypsum wallboard and window/door openings. Laboratory Report 157. APA-The Engineered Wood Association. Tacoma, WA.

Shiari, B., and P.M. Wild. 2004. Finite element analysis of individual wood-pulp fibers subjected to transverse compression. *Wood and Fiber Science*. 36(2):135-142.

Stanzl-Tschegg, S.E., D.M. Tan, and E.K. Tschegg. 1995. New splitting method for wood fracture characterization. *Wood Science and Technology*. 29:31-50.

Tabarsa, T. and Y.H. Chui. 1999. Microscopic observation of wood behavior in radial compression. *In: Proc. Fourth international conference on the development of wood science, wood technology and forestry*. Chilterns University College, Buckinghamshire, England. 463-470.

Tabarsa, T., and Y.H. Chui. 2000. Stress-strain response of wood under radial compression. Part I. Test method and influences of cellular properties. *Wood and Fiber Sci*. 32(2):144-152.

Tabarsa, T. and Y.H. Chui. 2001. Characterizing microscopic behavior of wood under transverse compression. Part II. Effect of species and loading direction. *Wood and Fiber Sci*. 33(2):223-232.

Tissell, J.R. 1996. Structural panel shear walls. Laboratory Report 154. APA-The Engineered Wood Association, Tacoma, WA.

Wanbing, L., and E.W. Robert. 1996. Mechano-sorptive behavior of solid wood stressed in compression perpendicular to the grain. *Forest Prod. J*. 46(4):63-68.

Wolcott, M.P., B. Kasal, F.A. Kamke, and D.A. Dillard, 1989. Testing small wood specimens in transverse compression. *Wood and Fiber Sci*. 21(3):320-329.

Wolfgang, G, M. Ulrich, and T. Alfred. 2003. Transverse compressive strength and fracture of spruce wood modified by melamine-formaldehyde impregnation of cell walls. *Wood and Fiber Science*. 35(2):239-246.

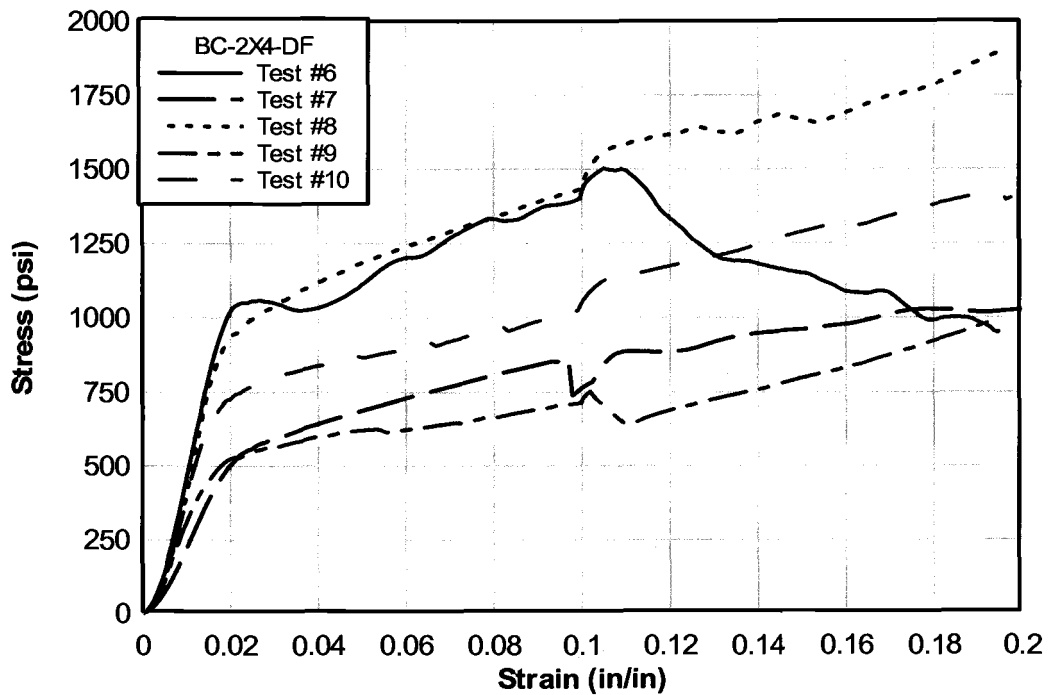
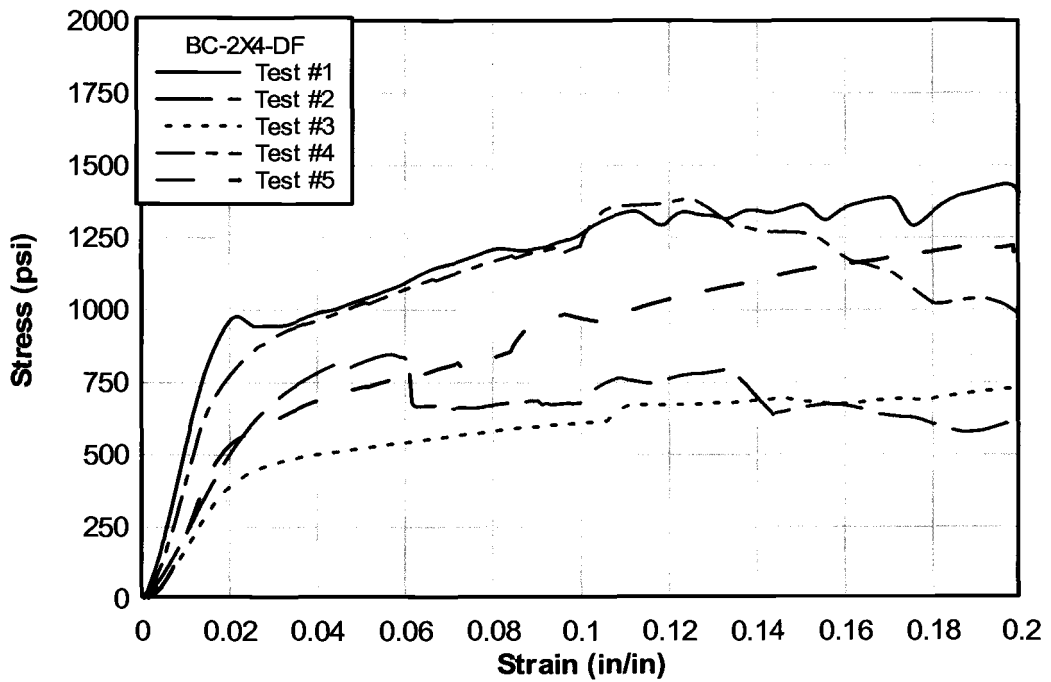
CHAPTER 7. APPENDICES

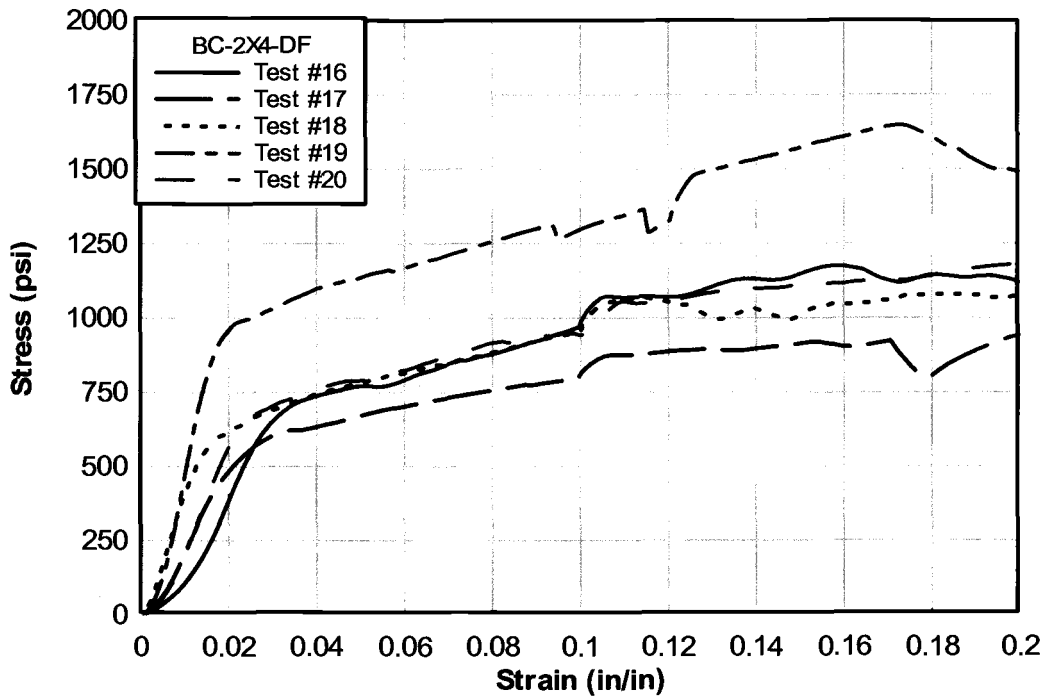
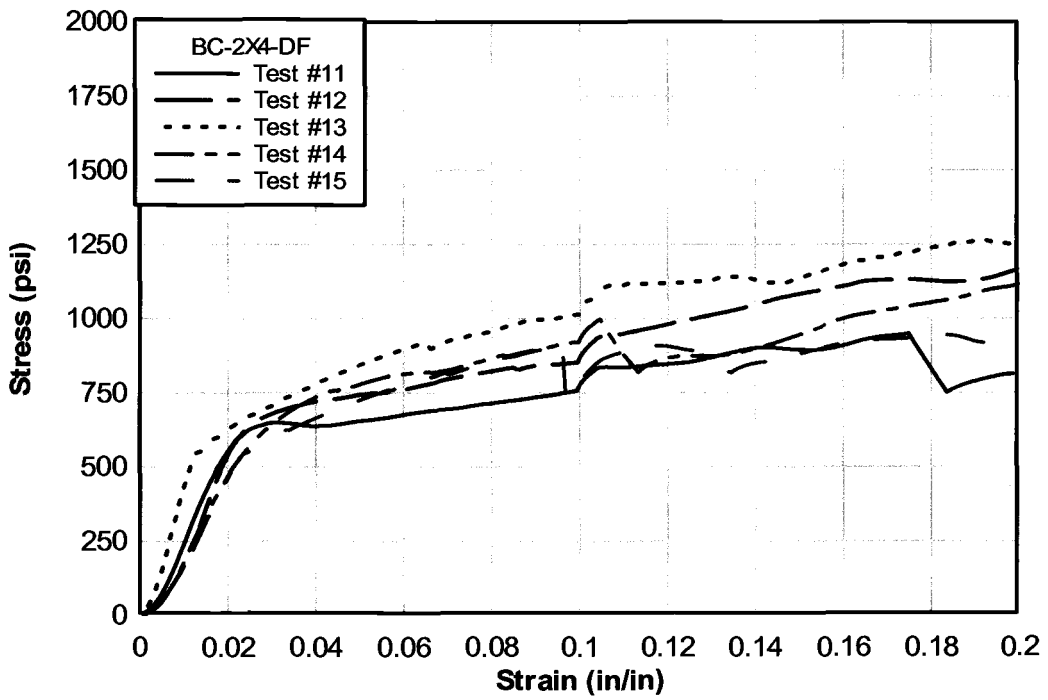
7.1 APPENDIX A: NOTATION

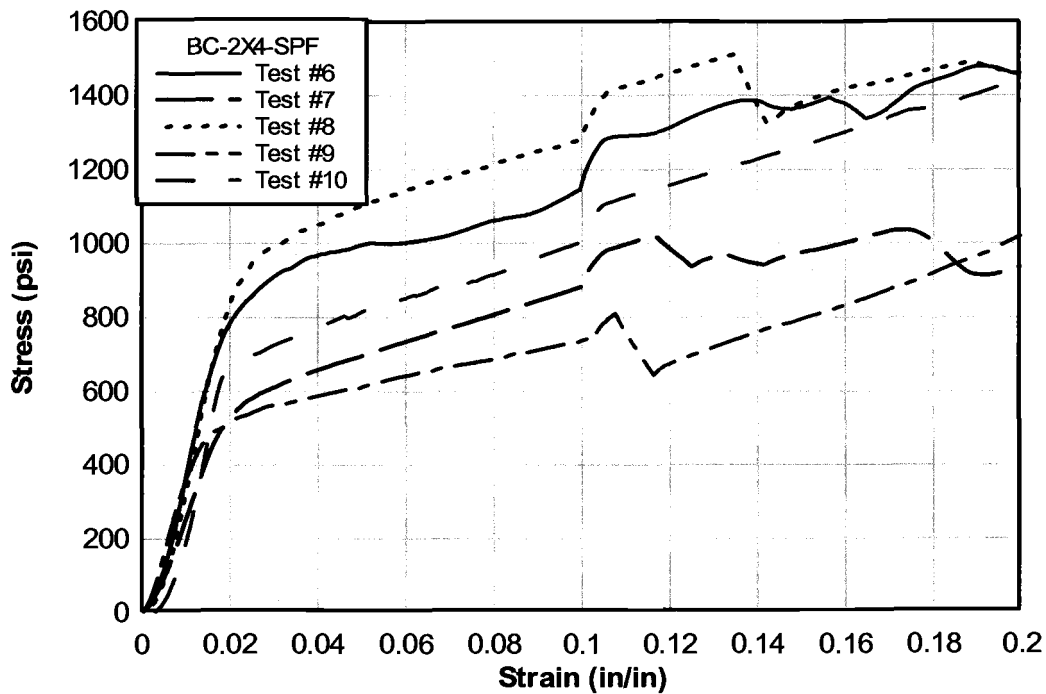
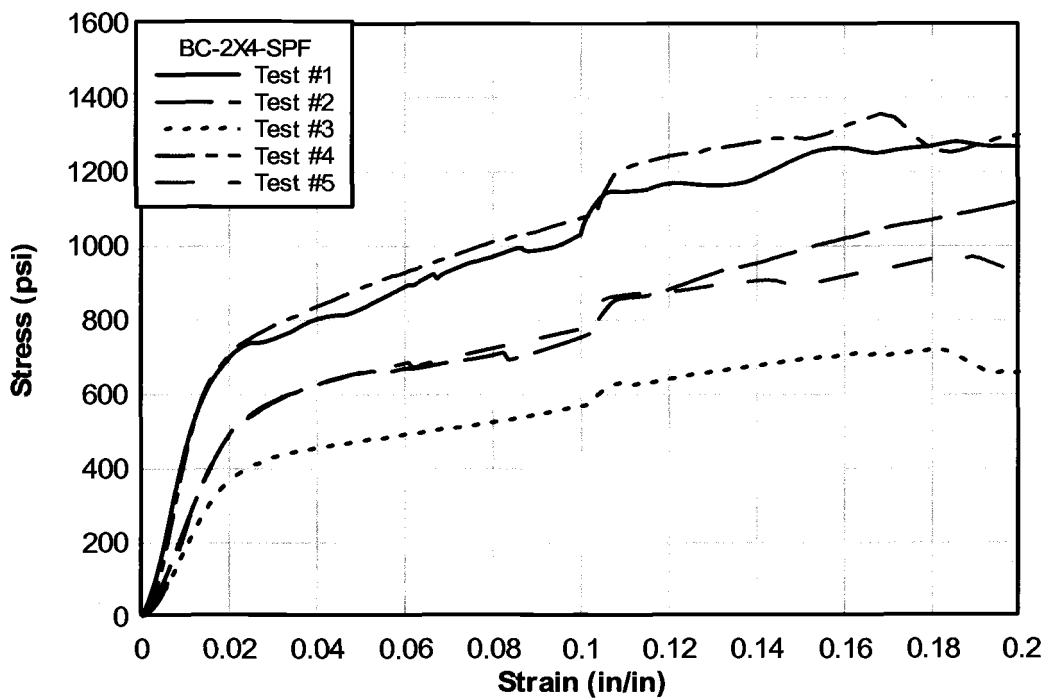
- B_{RA} – Ring angle at bottom surface of B.C. member where B.C. member contacts T.P. member
- BC – Abbreviation for the scenario of the bottom chord of a truss bearing on the top plate of a wall. Abbreviation for this testing assembly.
- B.C. – Abbreviation for member representing bottom chord of truss in BC assembly
- BP – Abbreviation for the scenario of the compression chord of a wall bearing on the bottom sill plate of a wall. Abbreviation for this testing assembly.
- B.P. – Abbreviation for member representing bottom plate of wall in BP testing assembly
- Catastrophic failure - System strain at which stress dropped to 50 percent of maximum stress and exhibited negative slope in the stress-strain diagram or such time as complete destruction of the bottom chord led to failure to support any stress whatsoever.
- C-perp – Compression perpendicular-to-grain
- C.C. – Abbreviation for the compression chord of a shear wall
- DF – Douglas-fir
- $F_{c\perp}$ – Allowable stress design value in c-perp
- $F_{c\perp}'$ – Factor adjusted allowable stress design value in c-perp
- FEM – Abbreviation for finite element analysis
- Main member – Member in configuration in which majority of deformation occurs. Refers to B.C. members in BC tests. Refers to B.P. member in BP tests. Refers to ASTM members in ASTM tests.
- Offset strain value - The difference in strain between origin and intersection of linear regression line with strain axis.
- σ_{max} – Refers to maximum stress attained between 0 and 10 percent system strain in BC tests. Refers to maximum stress attained between 0 and 10 percent strain of B.P. member in BP tests.
- $RA_{T\&B}$ – Average of T_{RA} and B_{RA}
- Radial compression – C-perp load applied perpendicular to annual rings
- Residual load carrying capacity – Ability of assembly to carry load beyond $\sigma_{2\%-OS}$. Percentage increase in load carrying capacity from $\sigma_{2\%-OS}$ to σ_{max} .
- Ring angle – Annual ring orientation measured with respect to applied load

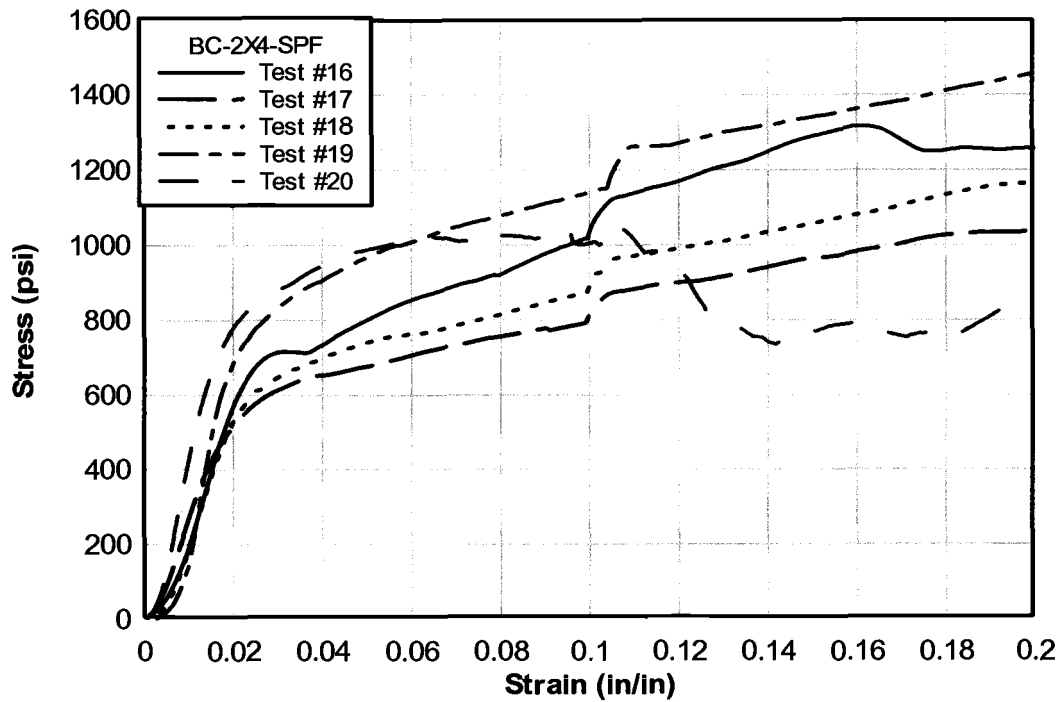
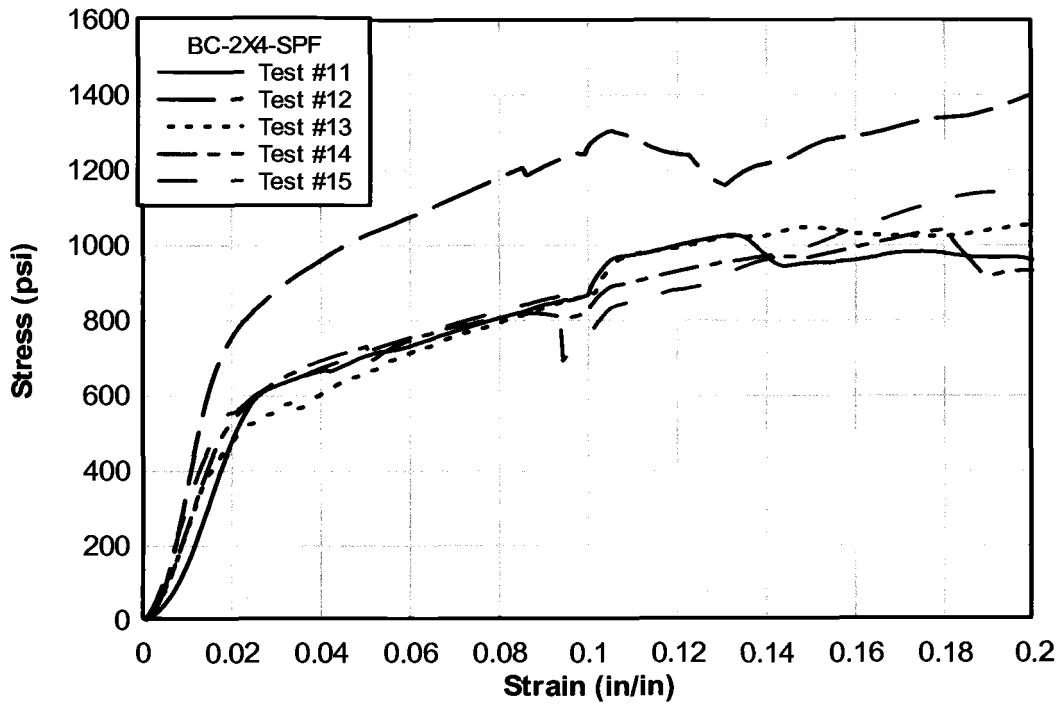
- S# – As seen in test pictures – Corresponds to testing number within assembly
- System strain – Total deflection of assembly divided by depth of assembly
- Tangential compression – c-perp load applied parallel to annual rings
- SPF – Spruce-Pine-Fir
- T_{RA} – Ring angle at top surface of B.C. member where B.C. member contacts T.P. member
- Ultimate limit state – Stress at such time as c-perp stresses induced in a member lead to complete or catastrophic failure of a system
- $\sigma_{0.04-D}$ – Stress at 0.04 in system deflection in BC tests. Stress at 0.04 in deflection of B.P. member in BP tests. Stress at 0.04 in deflection in ASTM tests.
- $\sigma_{0.04-OD}$ – Stress at 0.04 in system offset deflection in BC tests. Stress at 0.04 in offset deflection of B.P. member in BP tests. Stress at 0.04 in offset deflection in ASTM tests.
- $\sigma_{2\%-S}$ – Stress at 2 percent system strain in BC tests. Stress at 2 percent strain of B.P. member in BP tests. Stress at 2 percent strain in ASTM tests.
- $\sigma_{2\%-OS}$ – Stress at 2 percent system offset strain in BC tests. Stress at 2 percent offset strain of B.P. member in BP tests. Stress at 2 percent offset strain in ASTM tests.

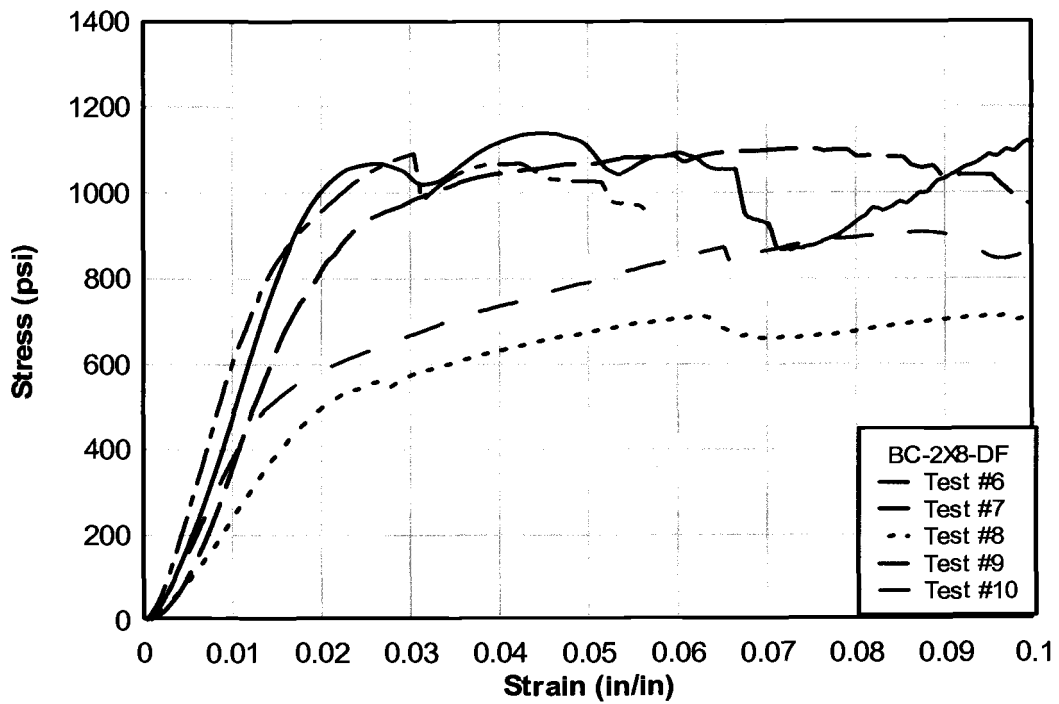
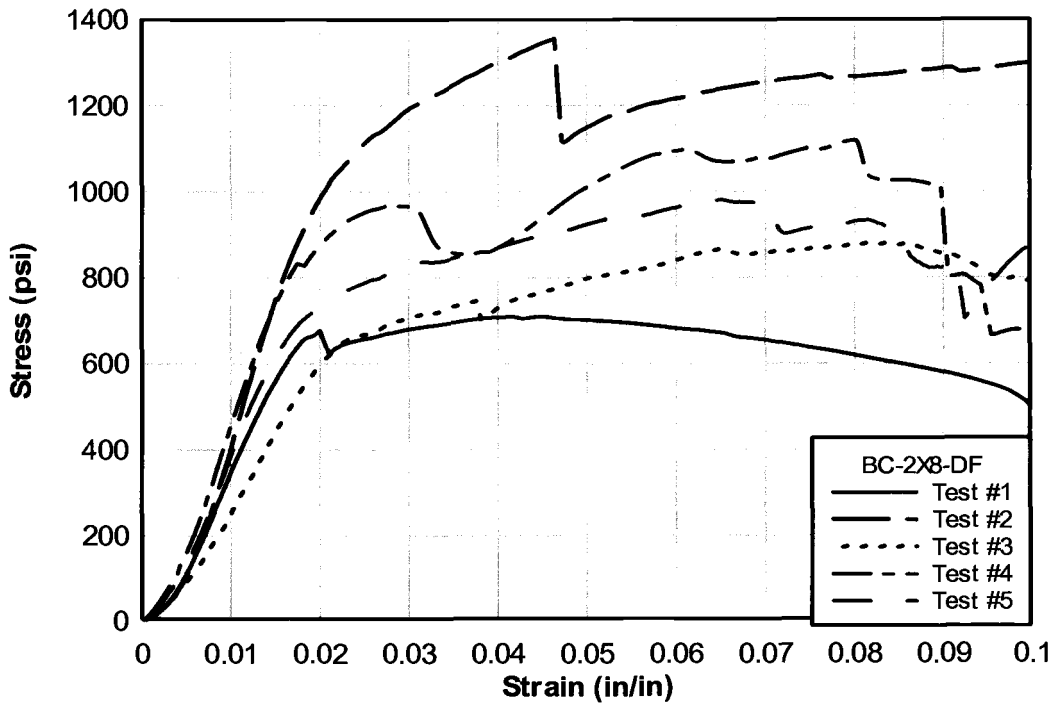
7.2 APPENDIX B: STRESS-STRAIN DIAGRAMS

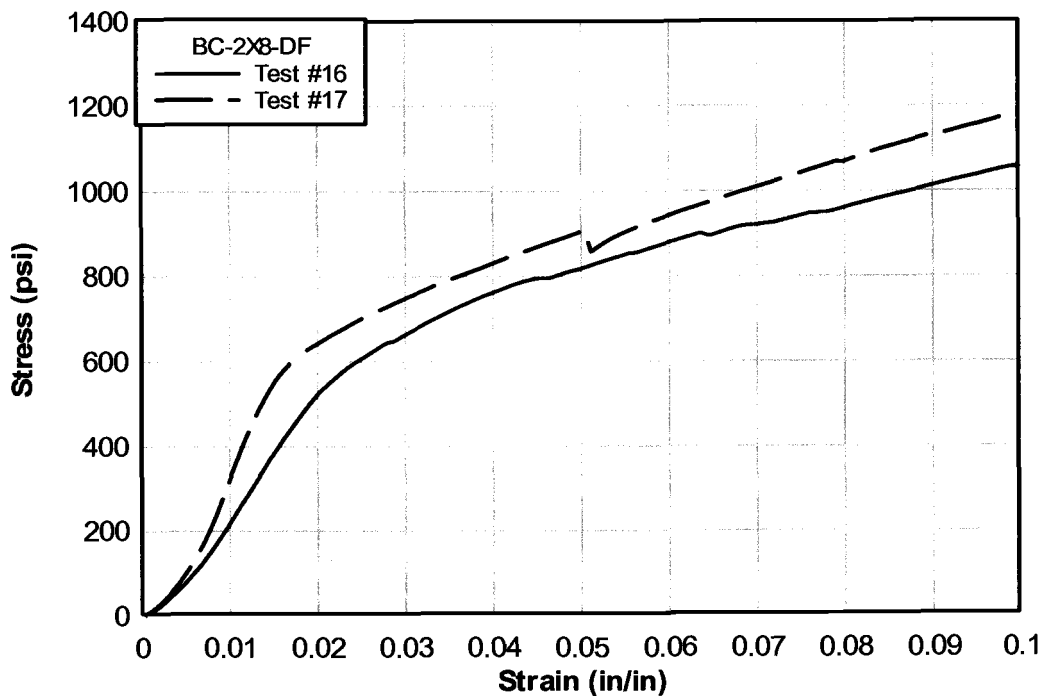
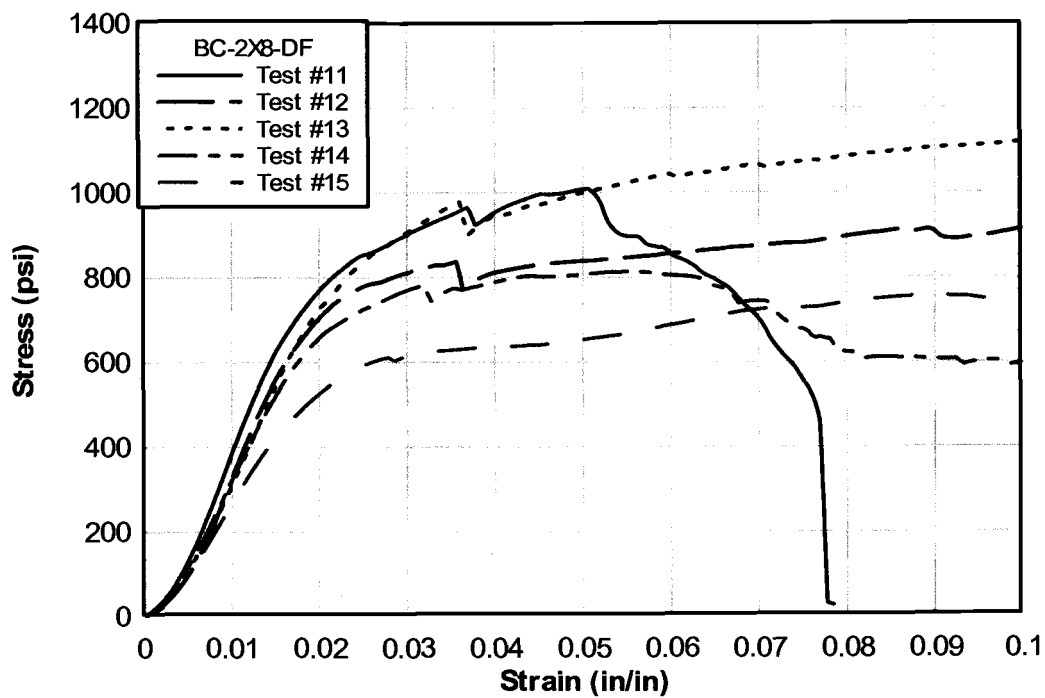


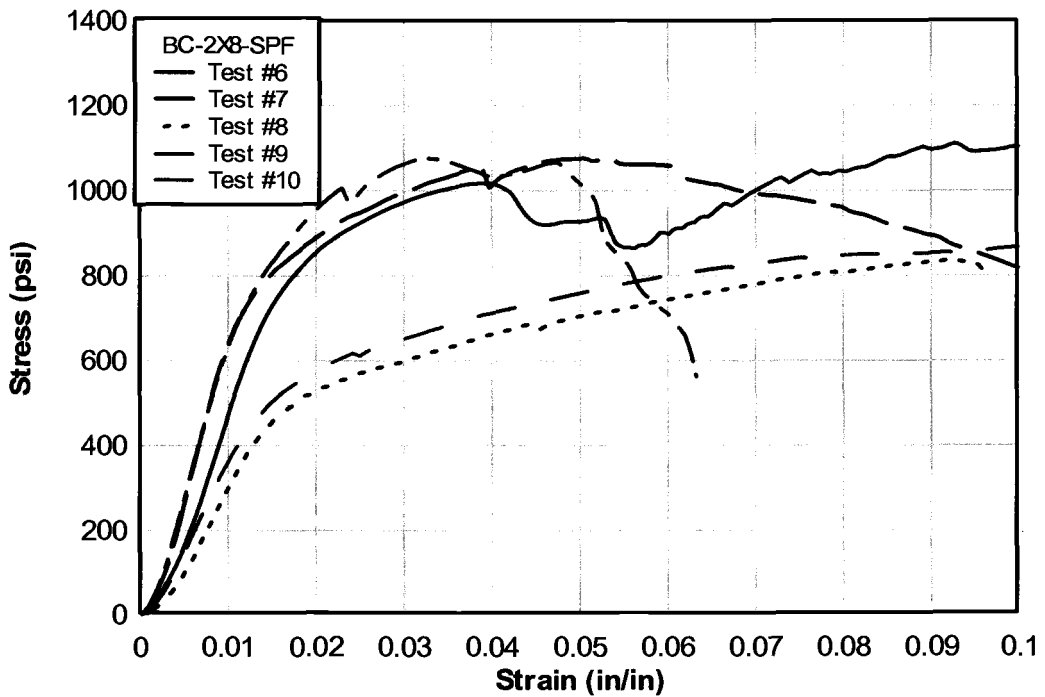
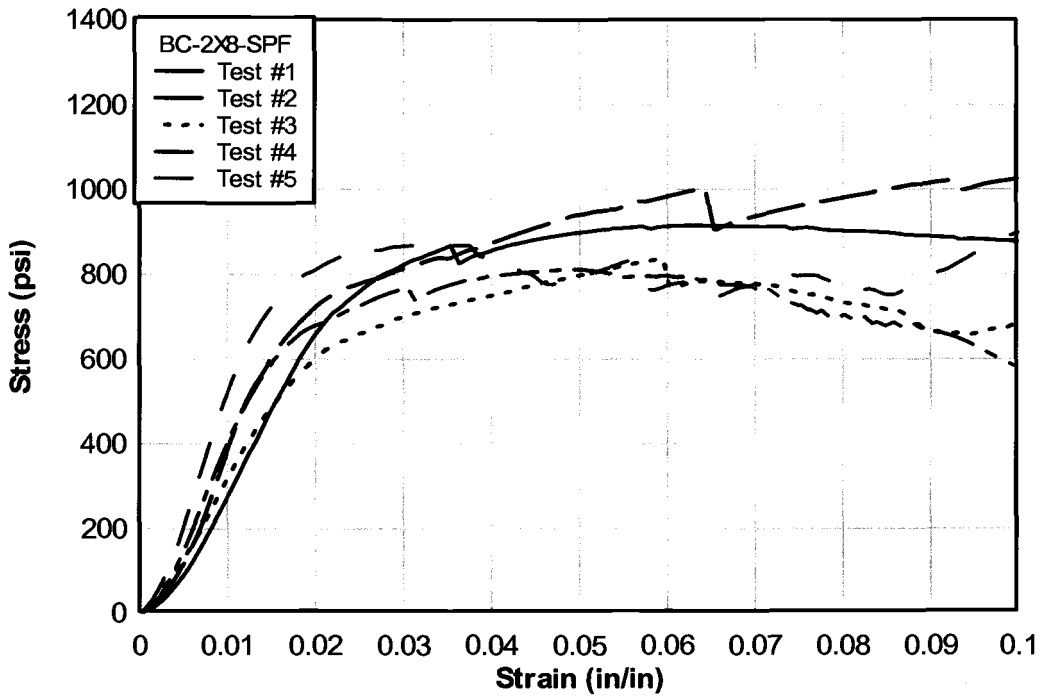


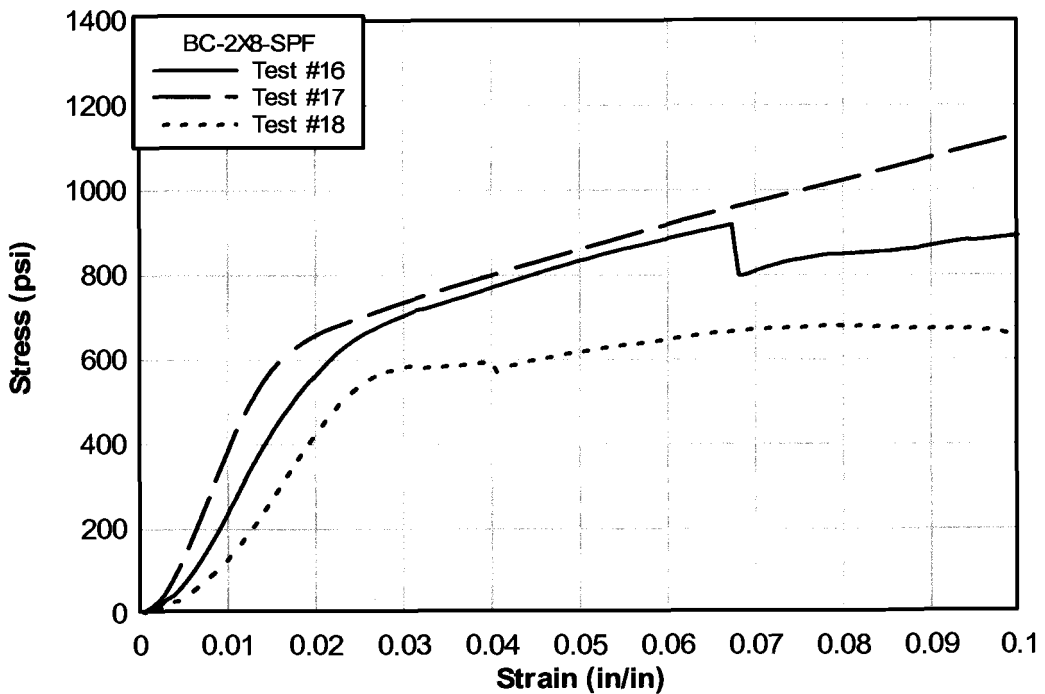
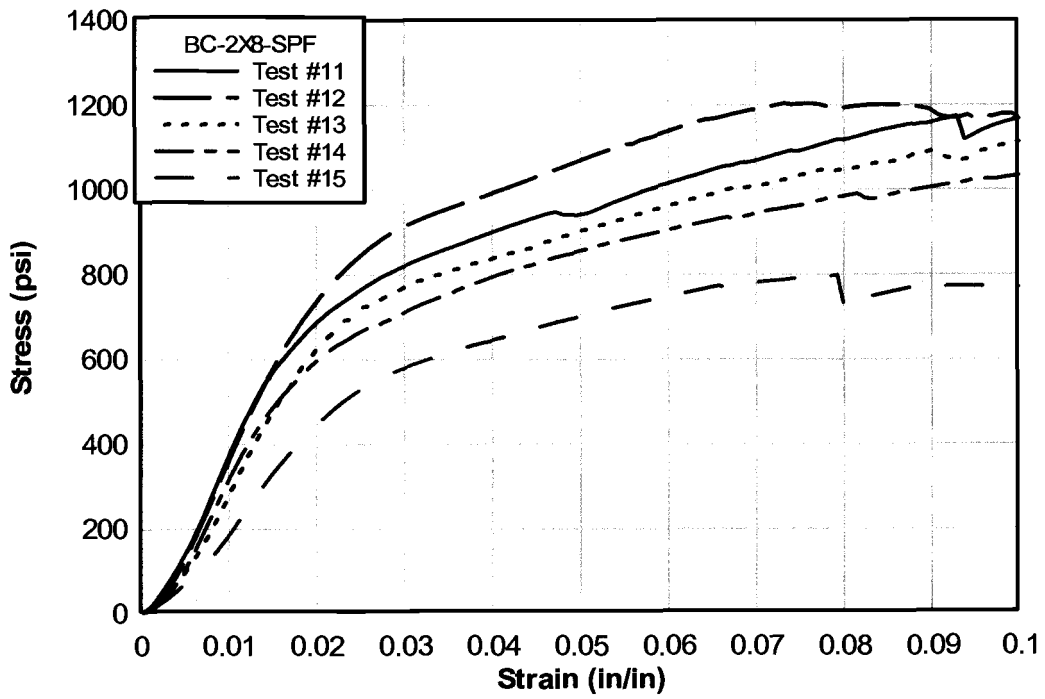


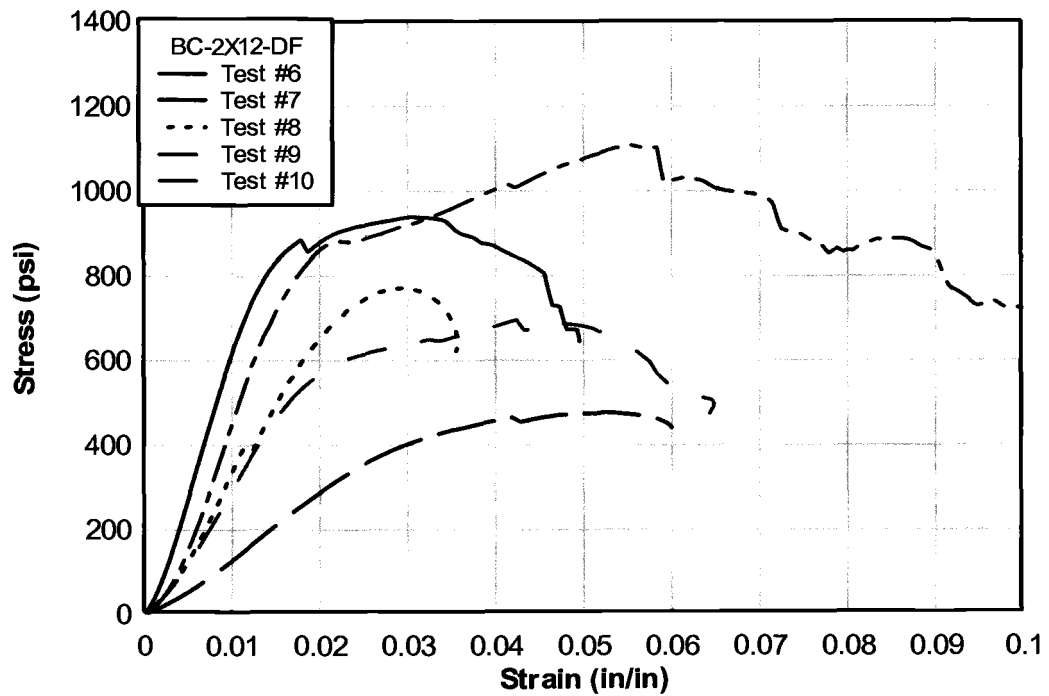
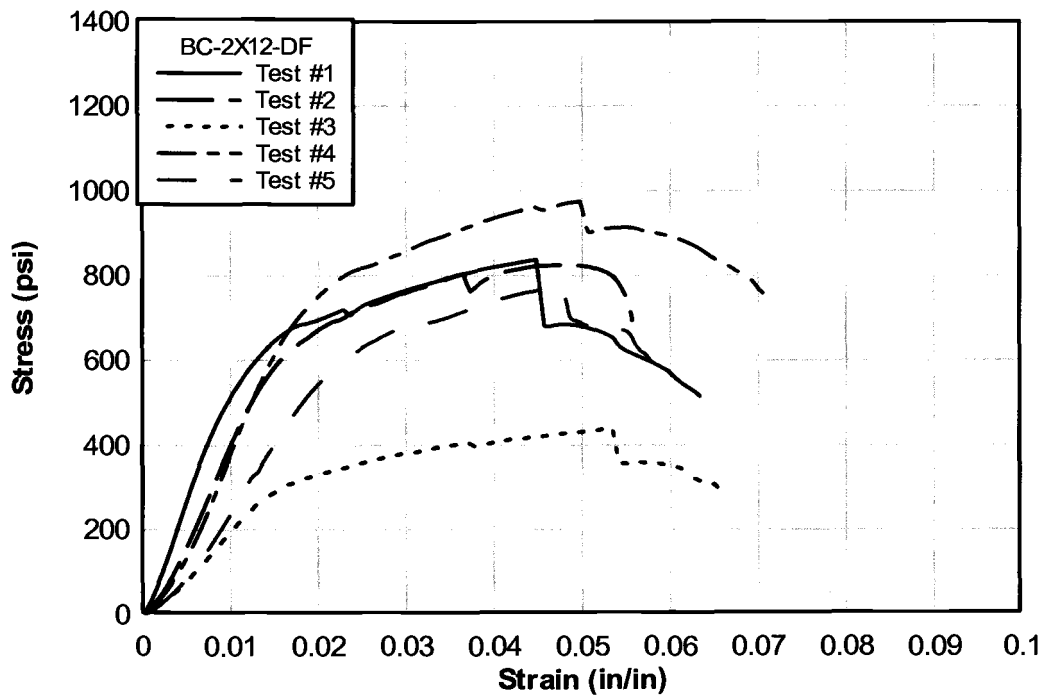


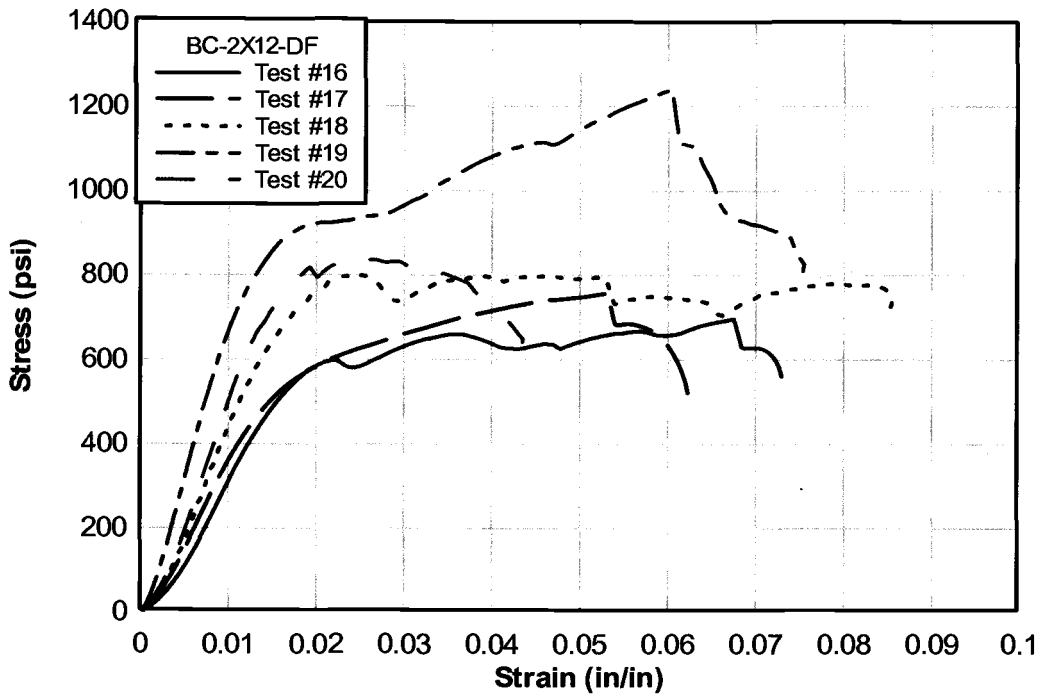
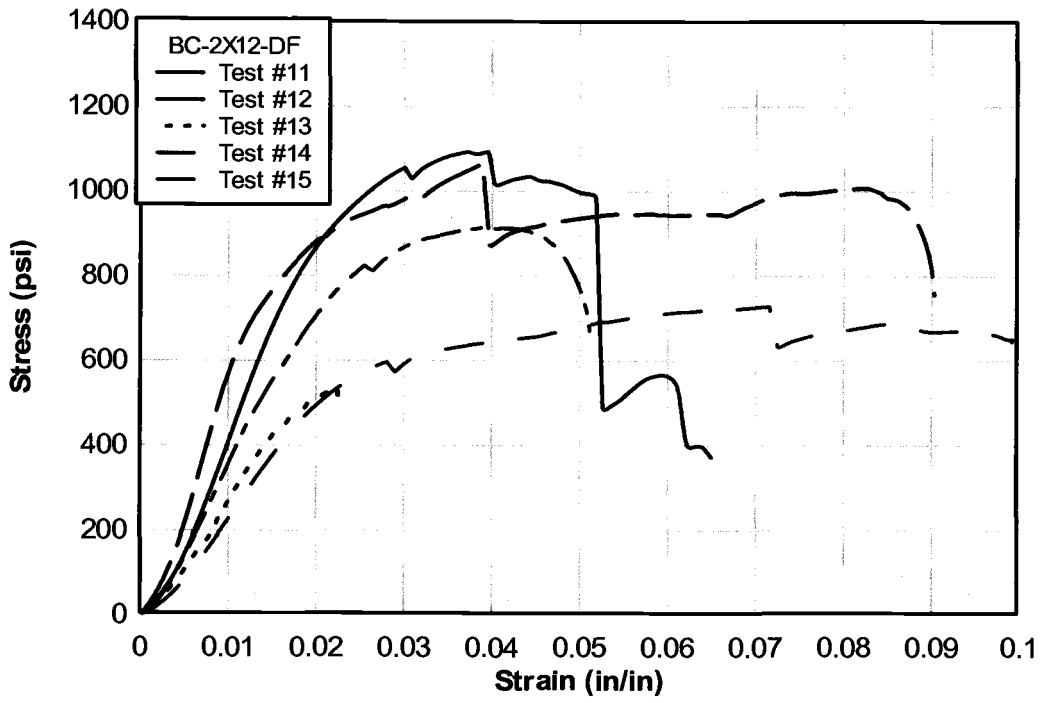


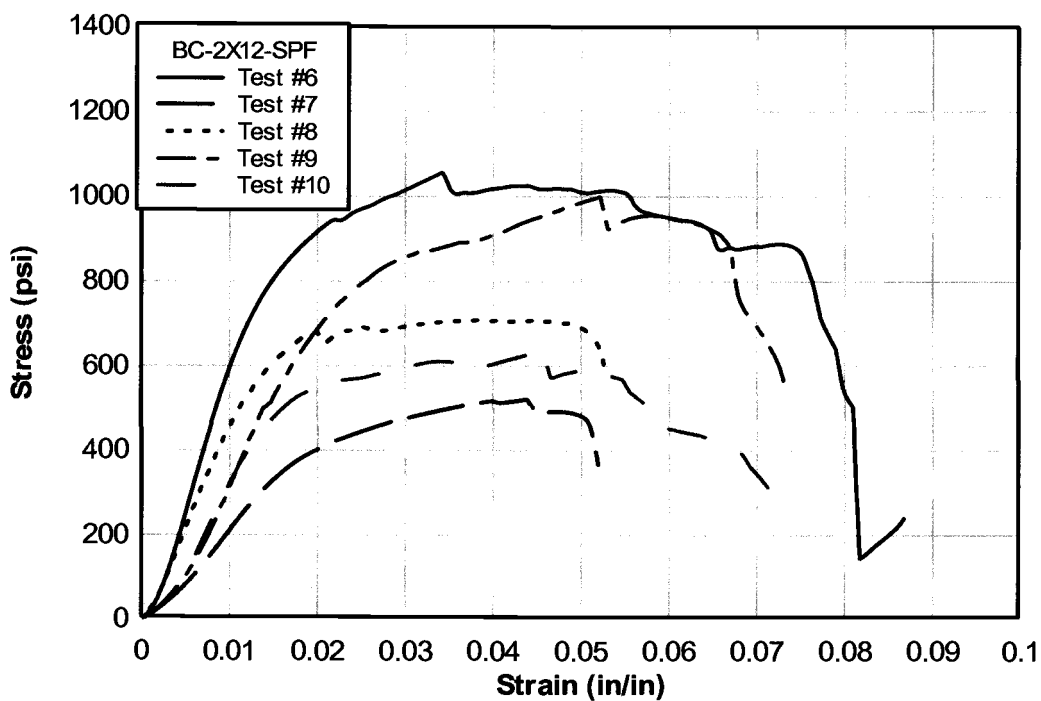
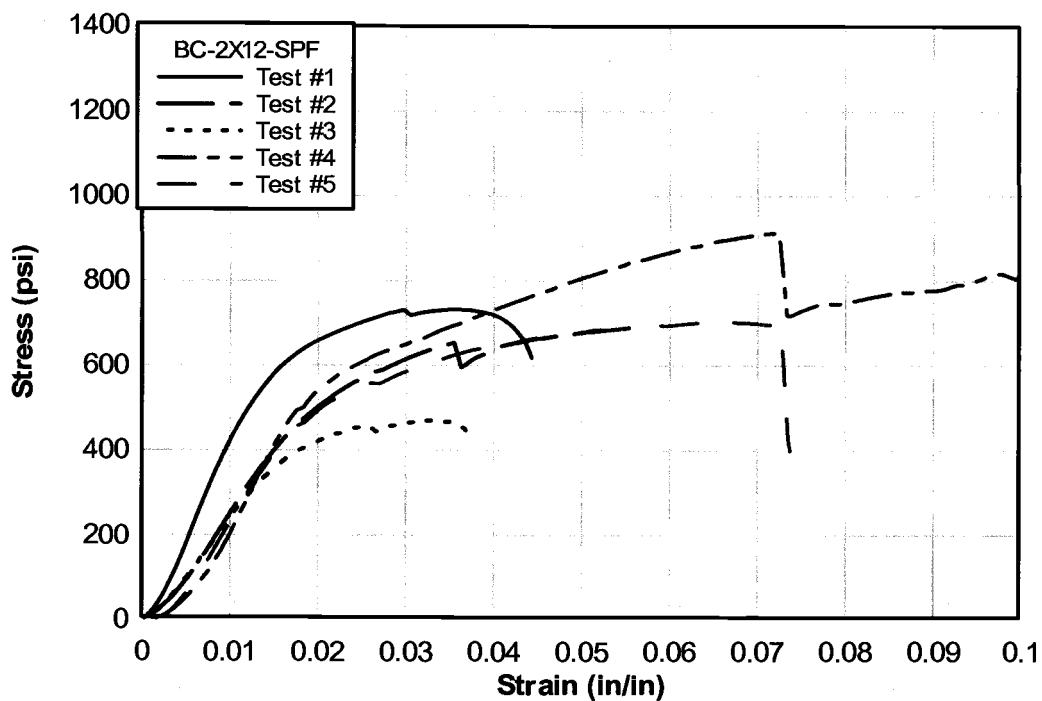


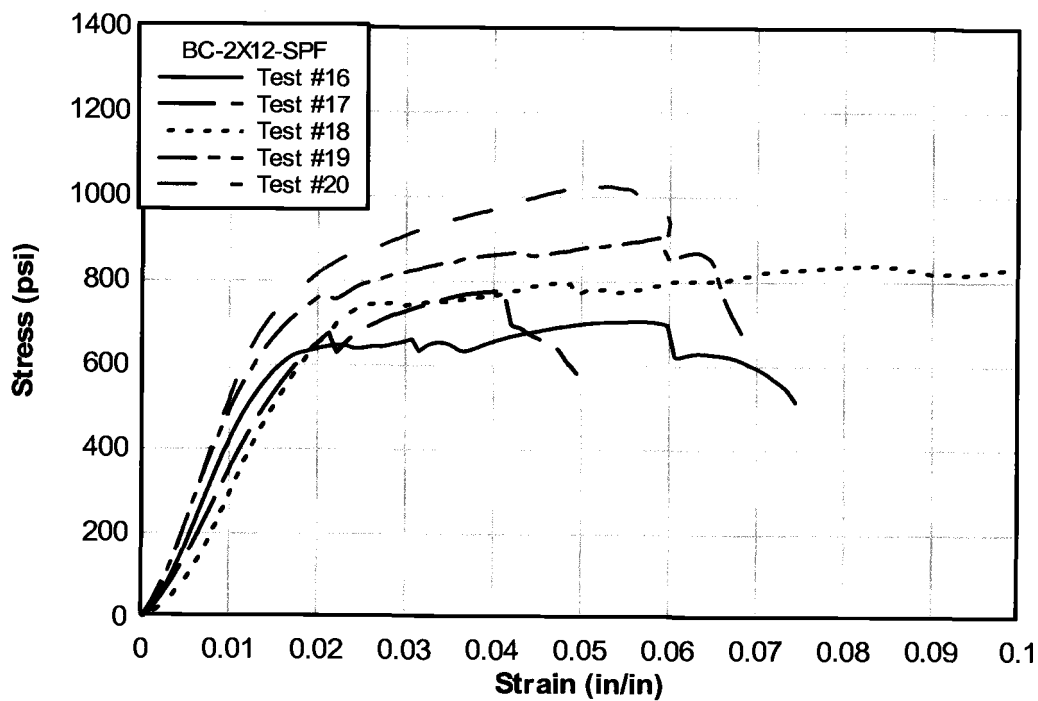
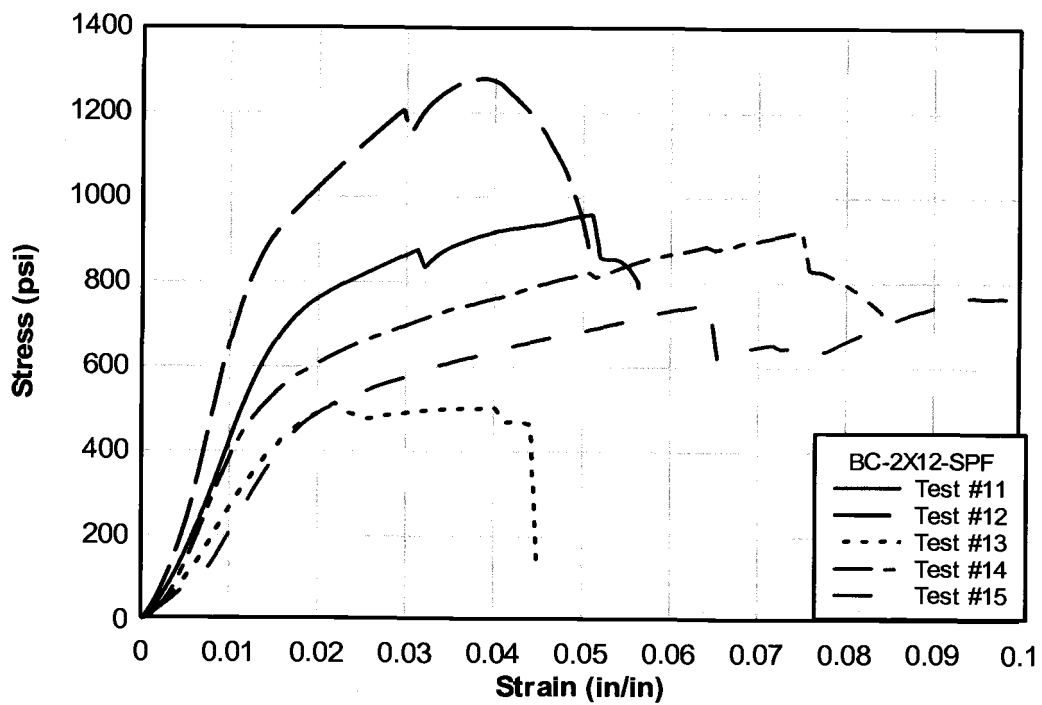


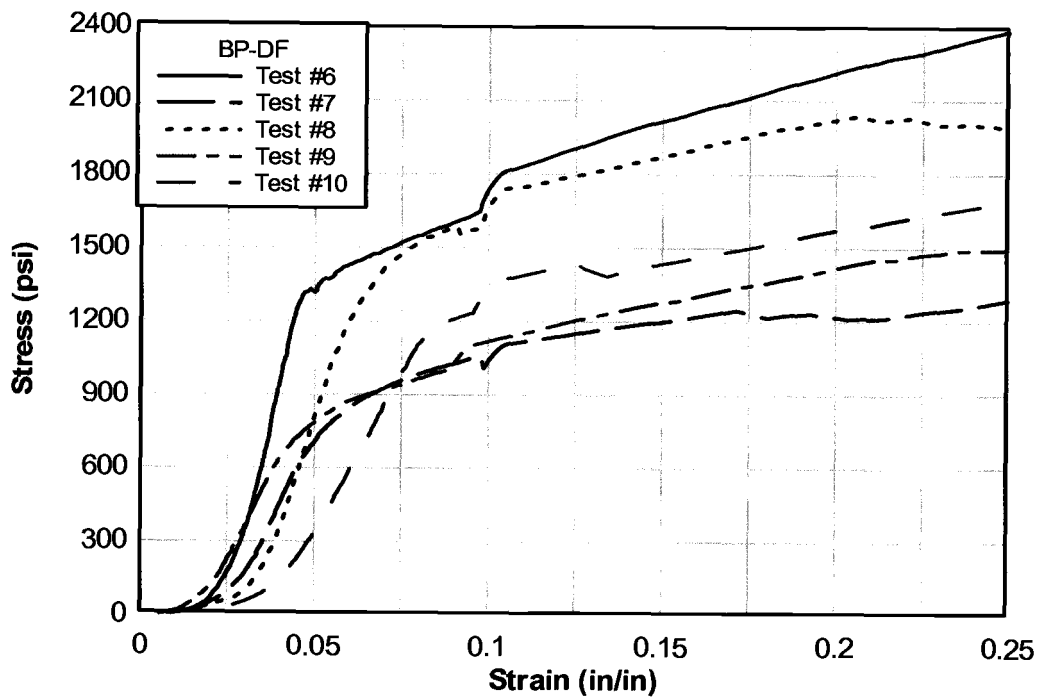
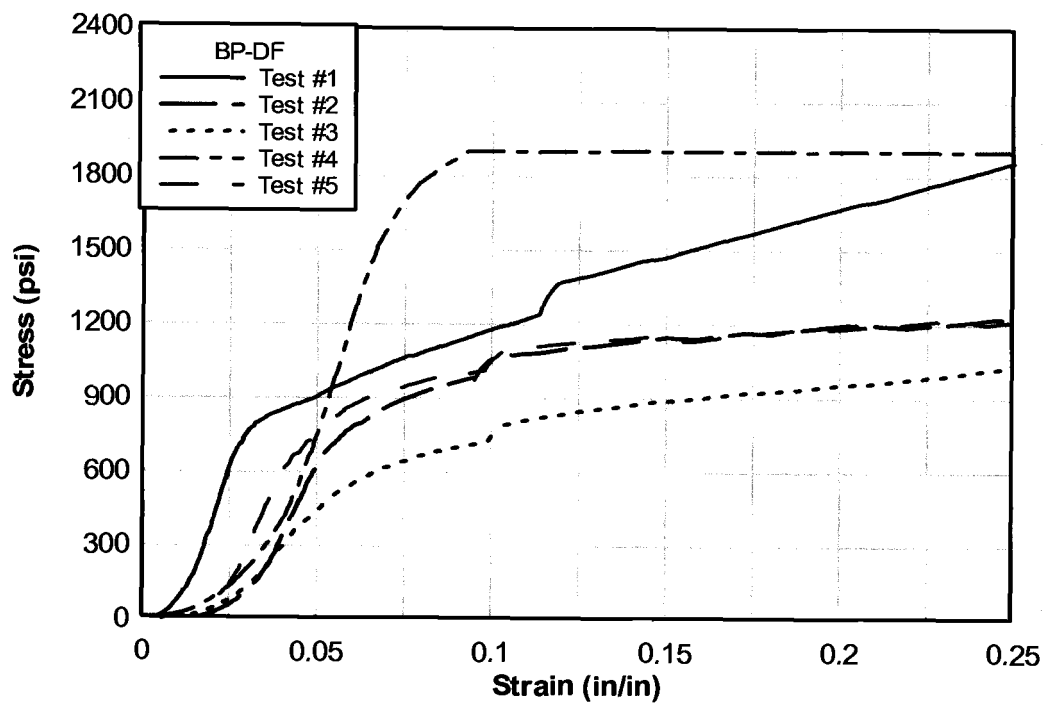


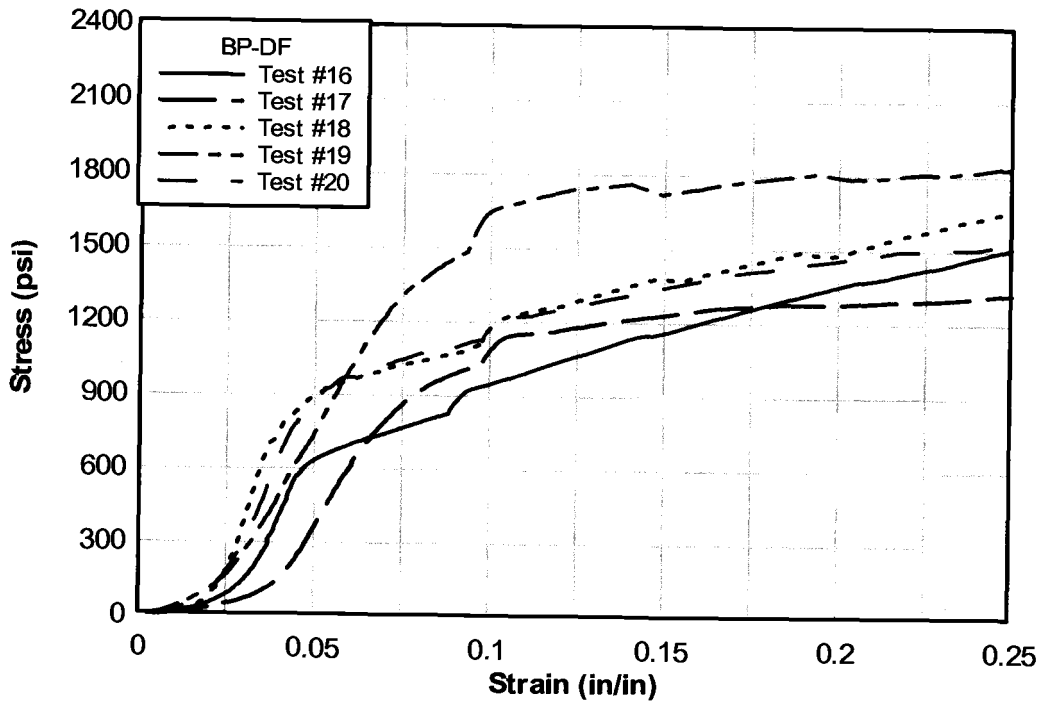
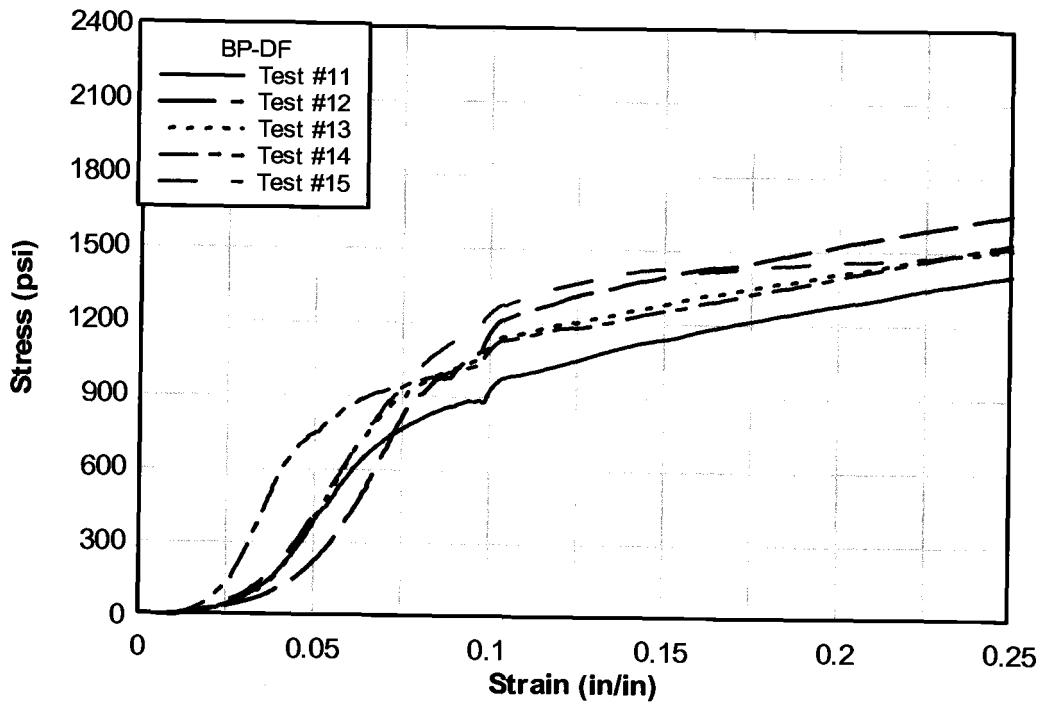


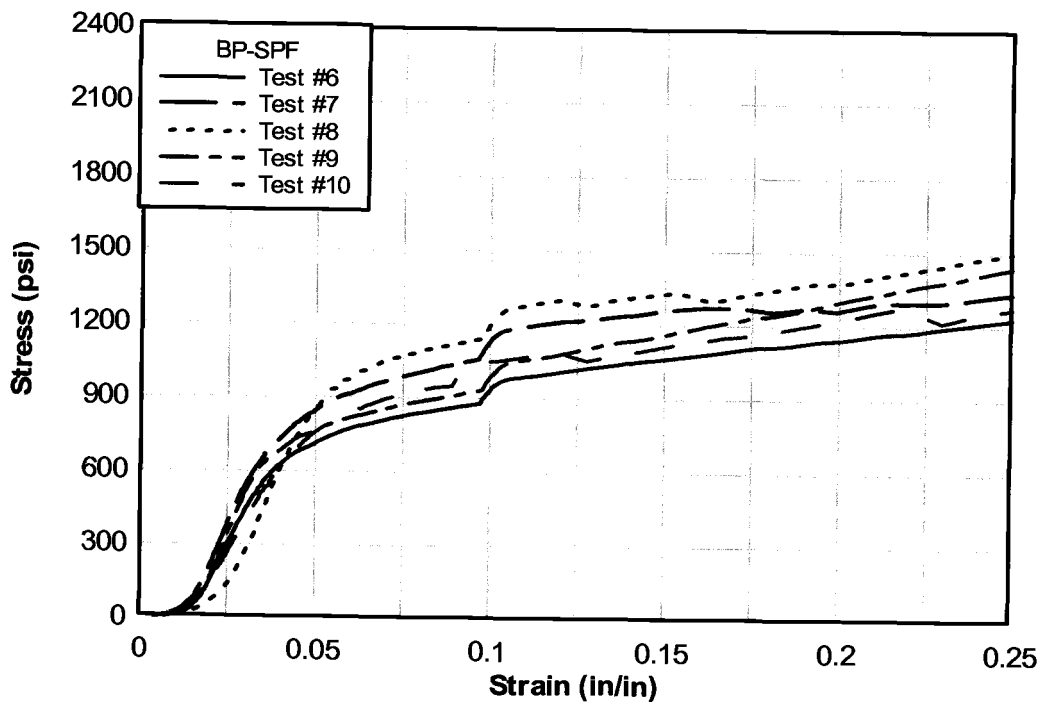
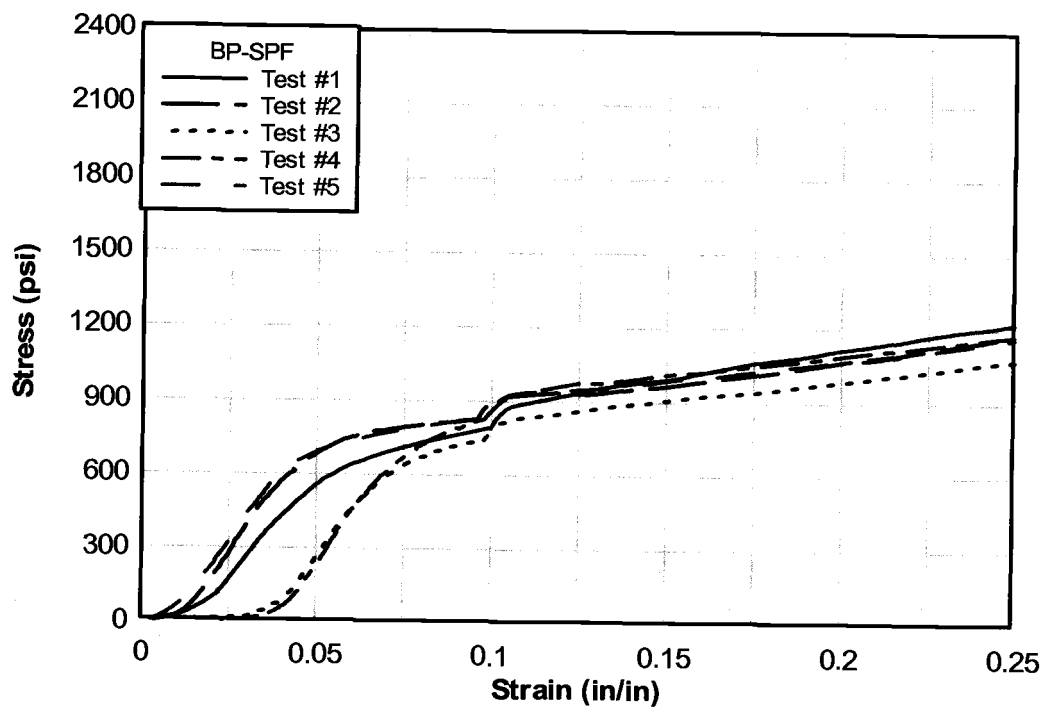


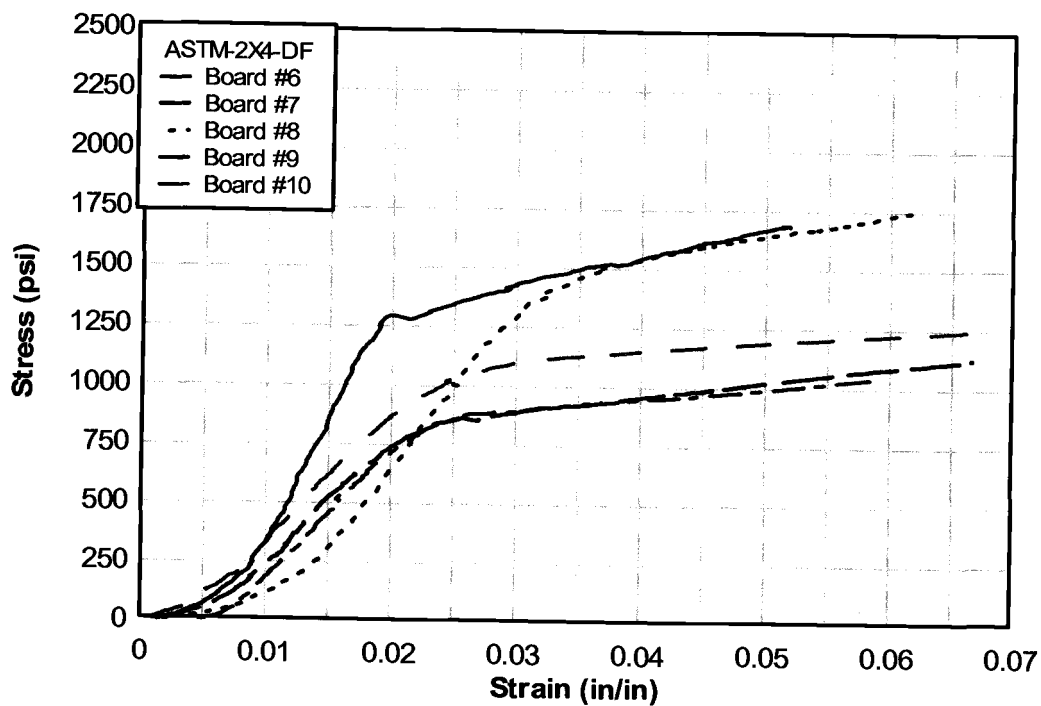
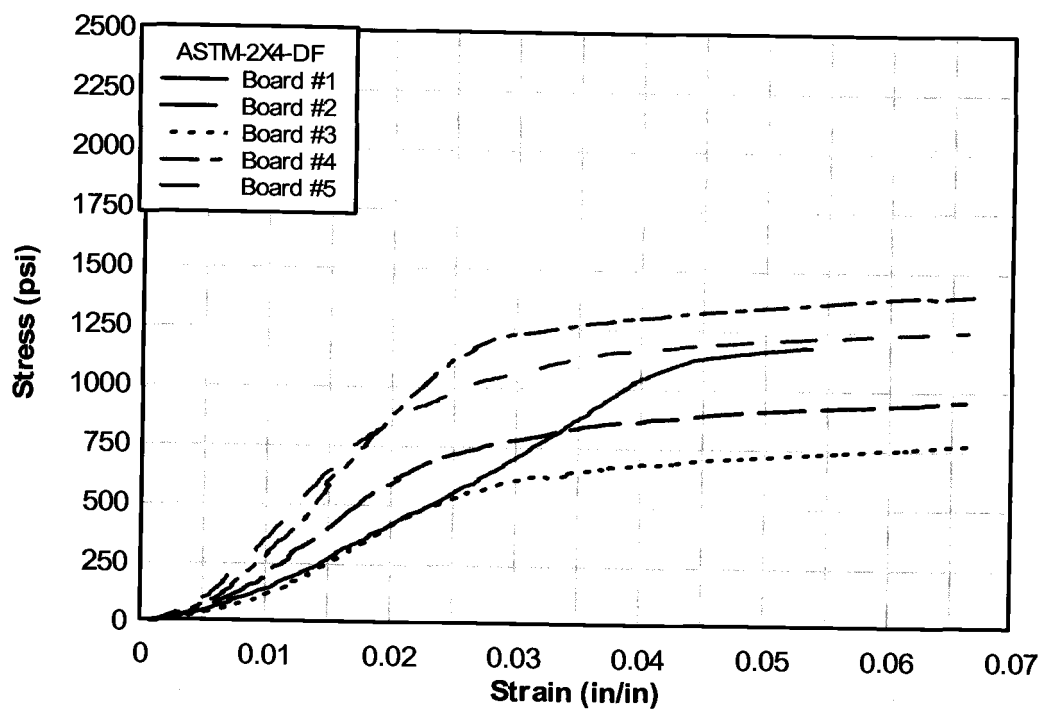


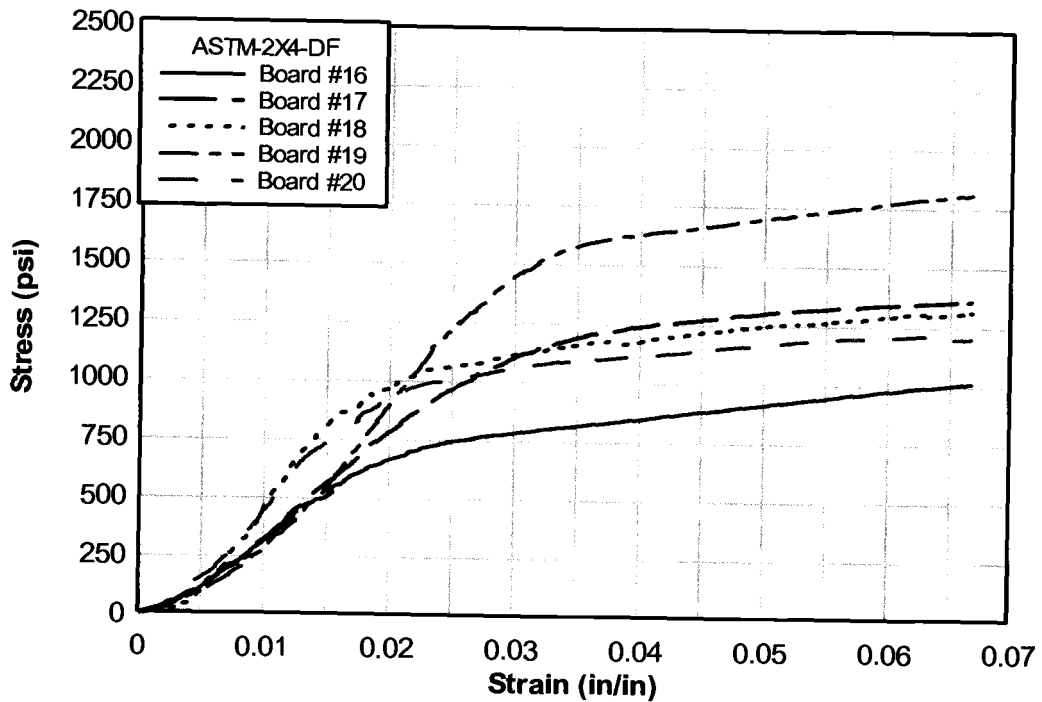
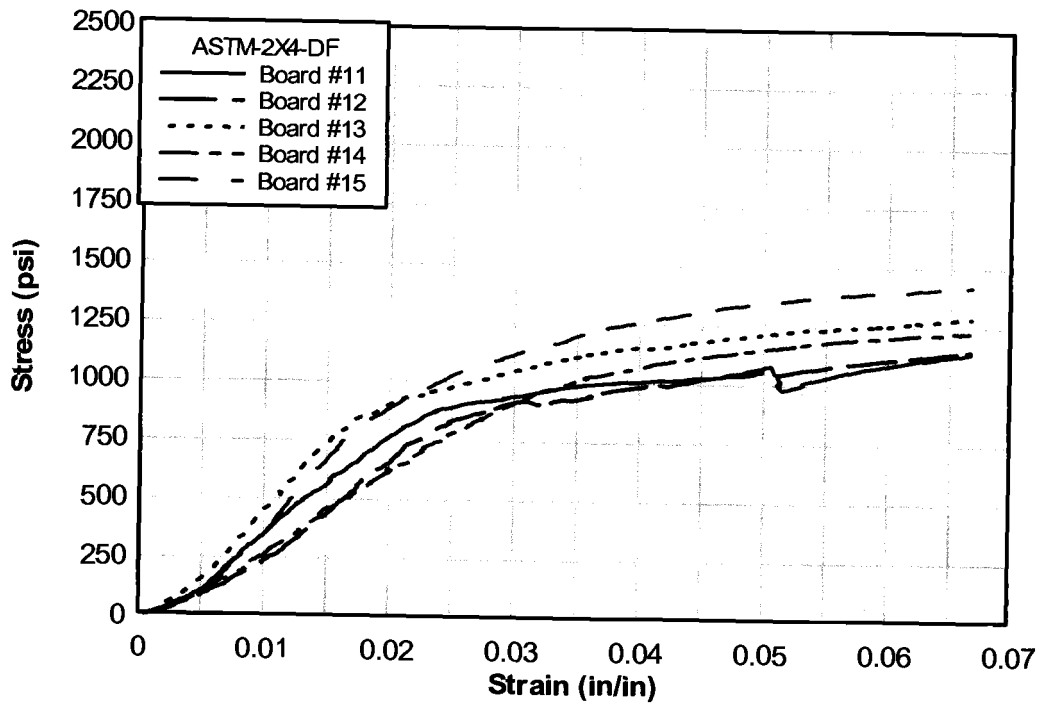


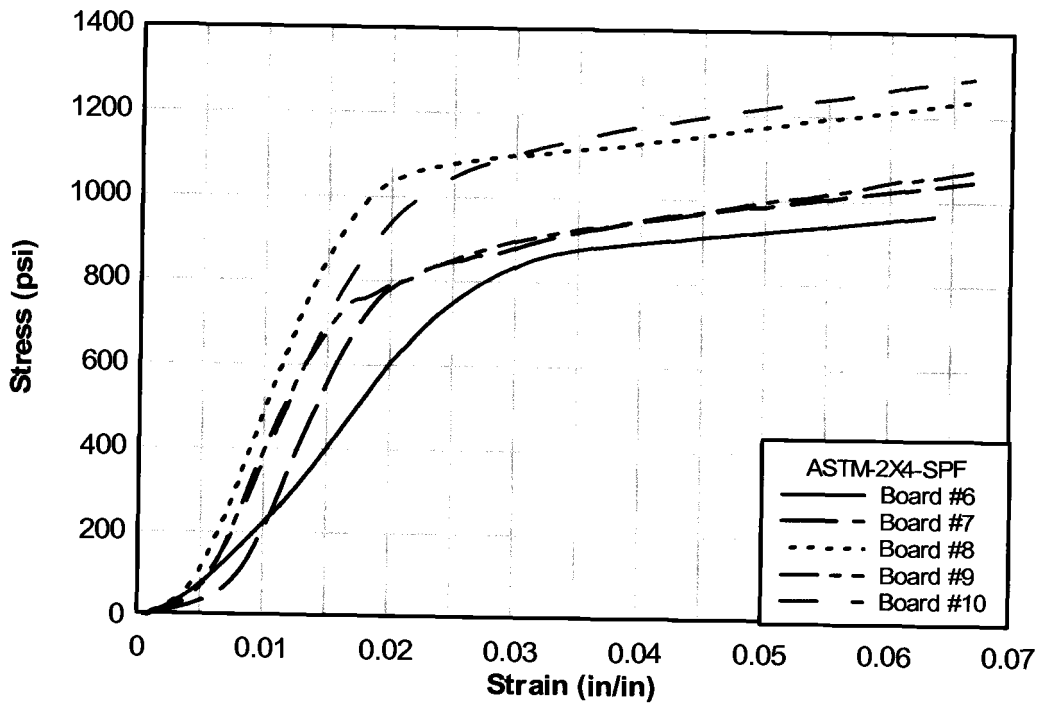
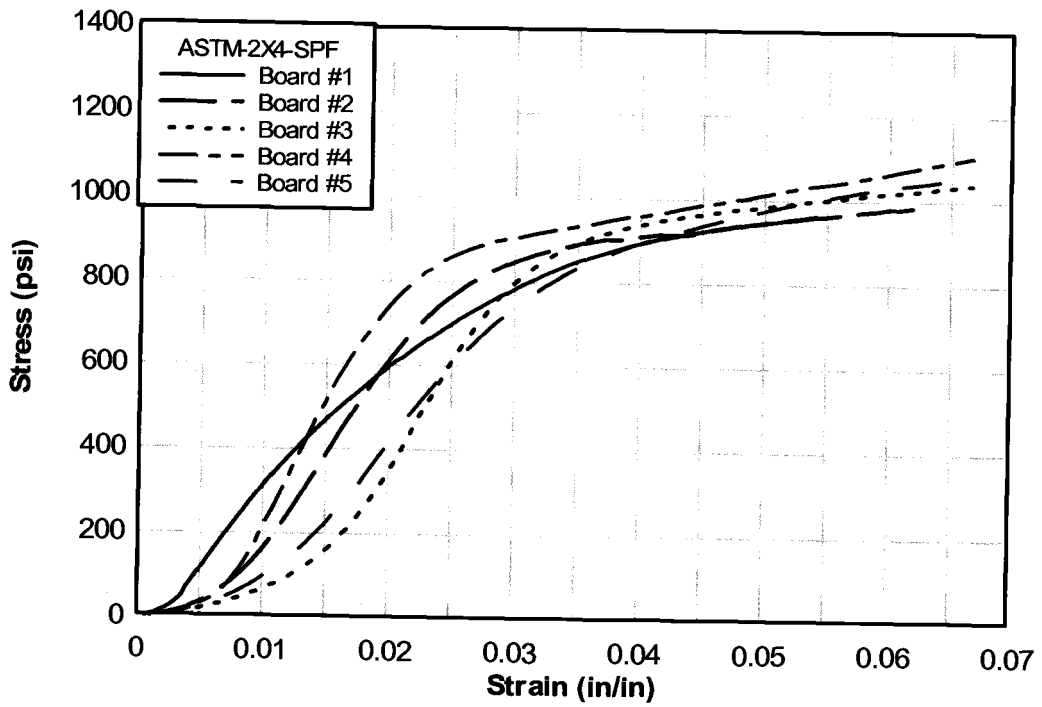


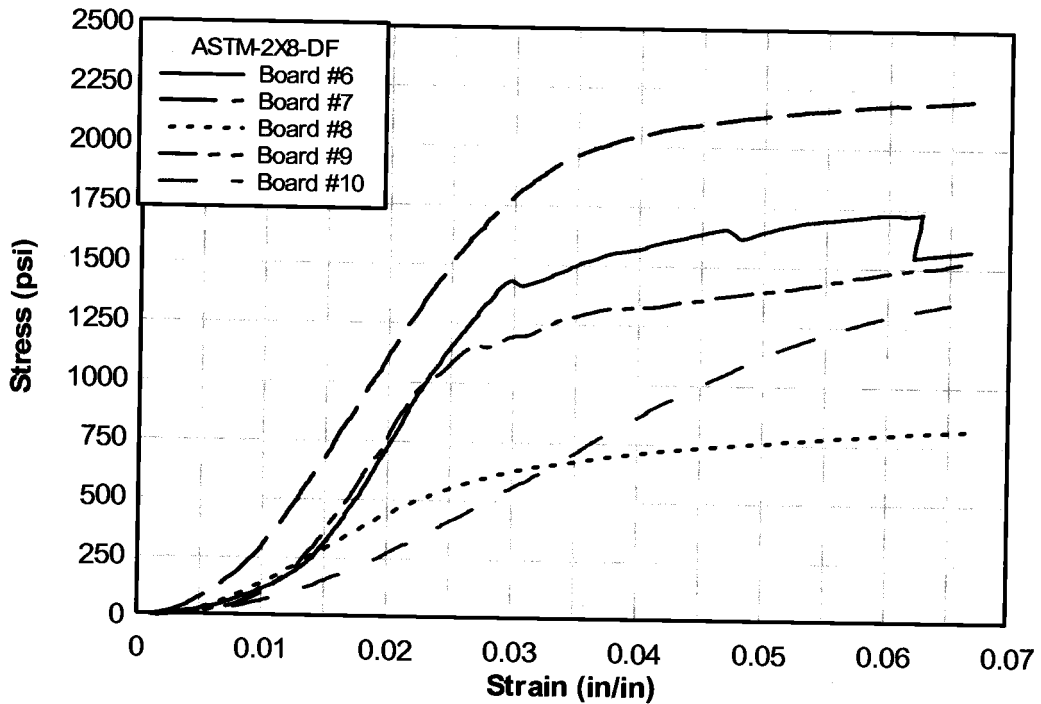
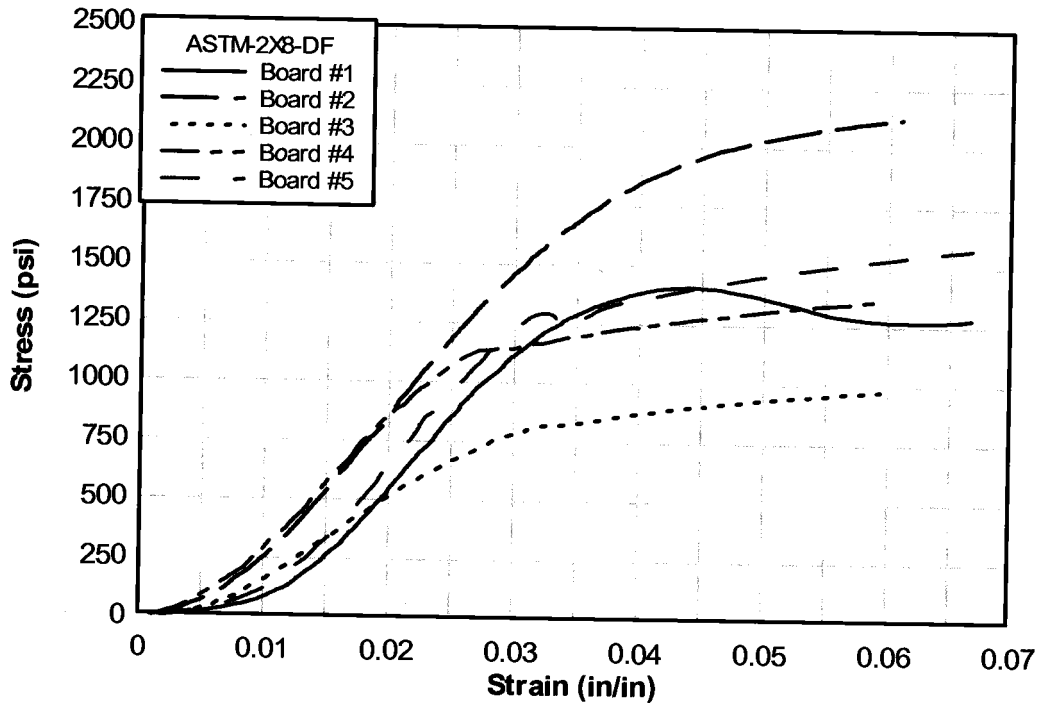


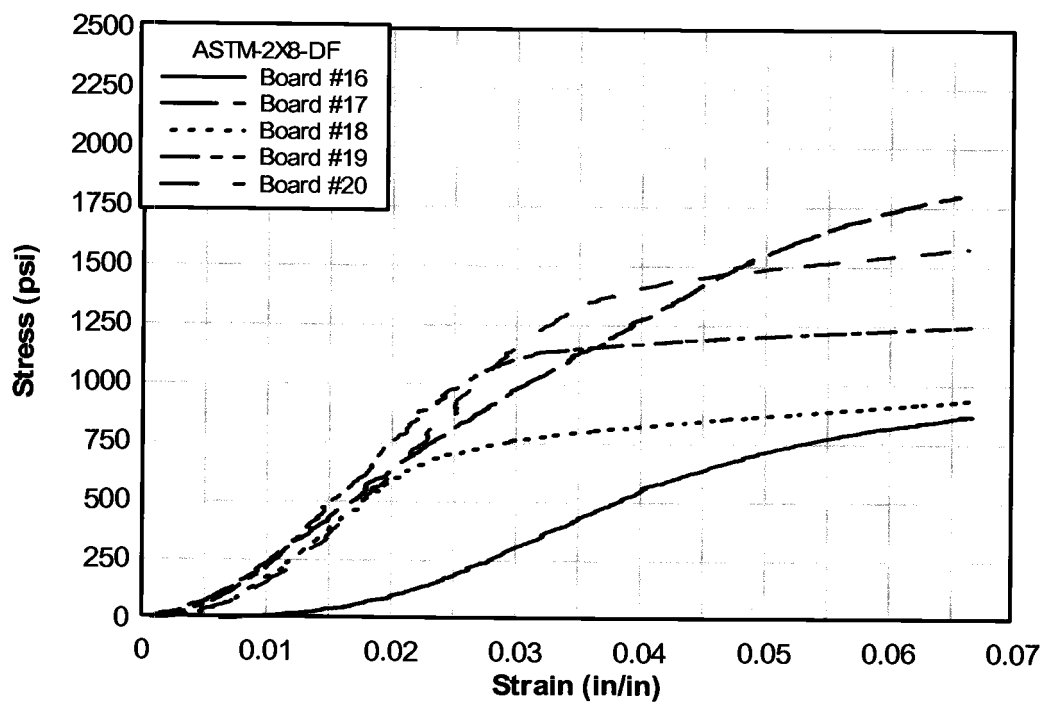
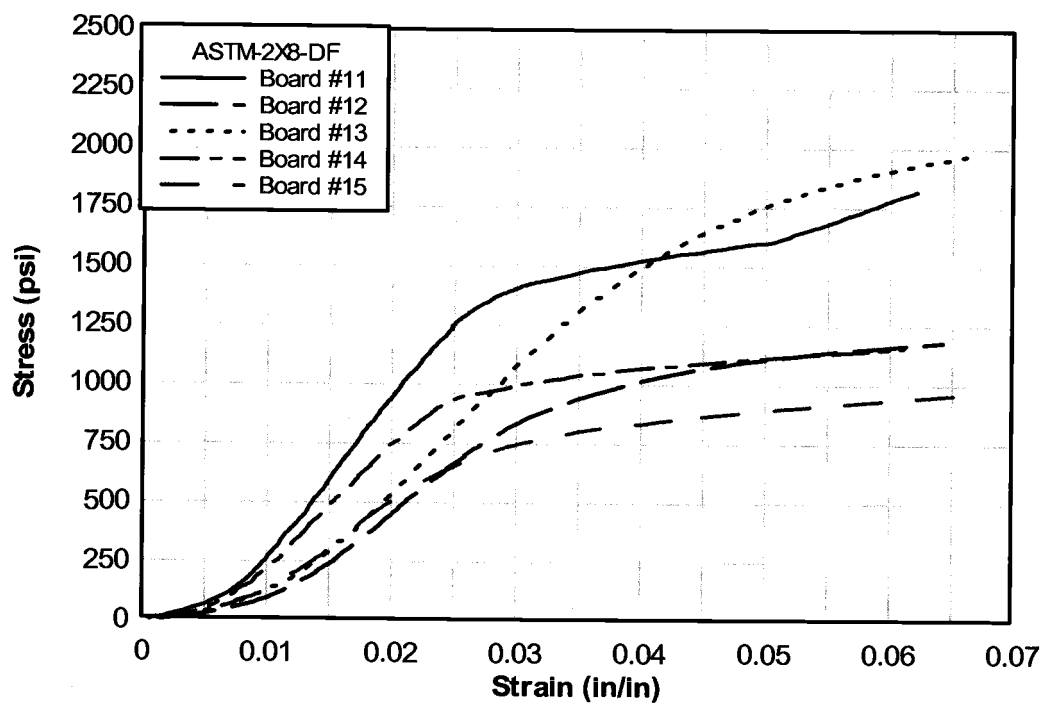


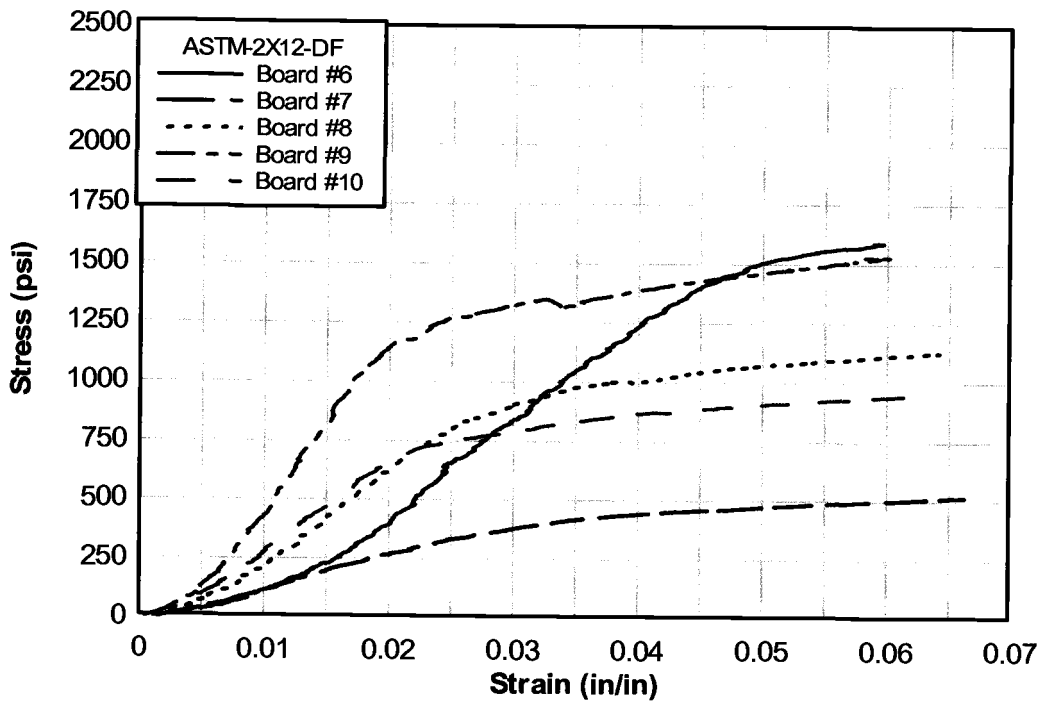
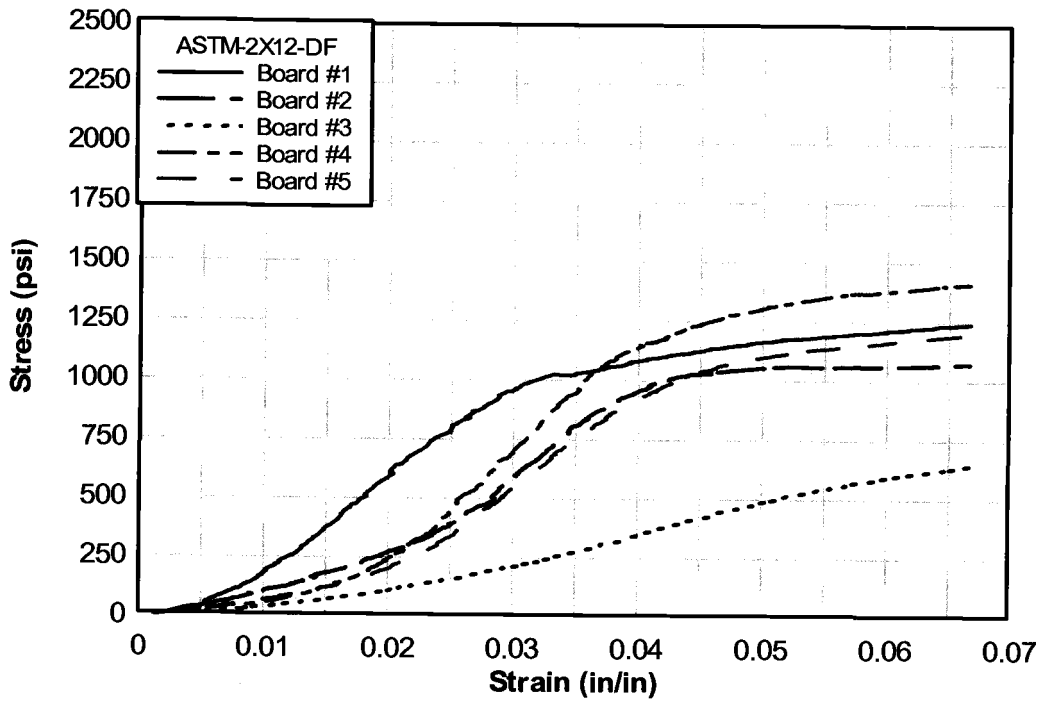


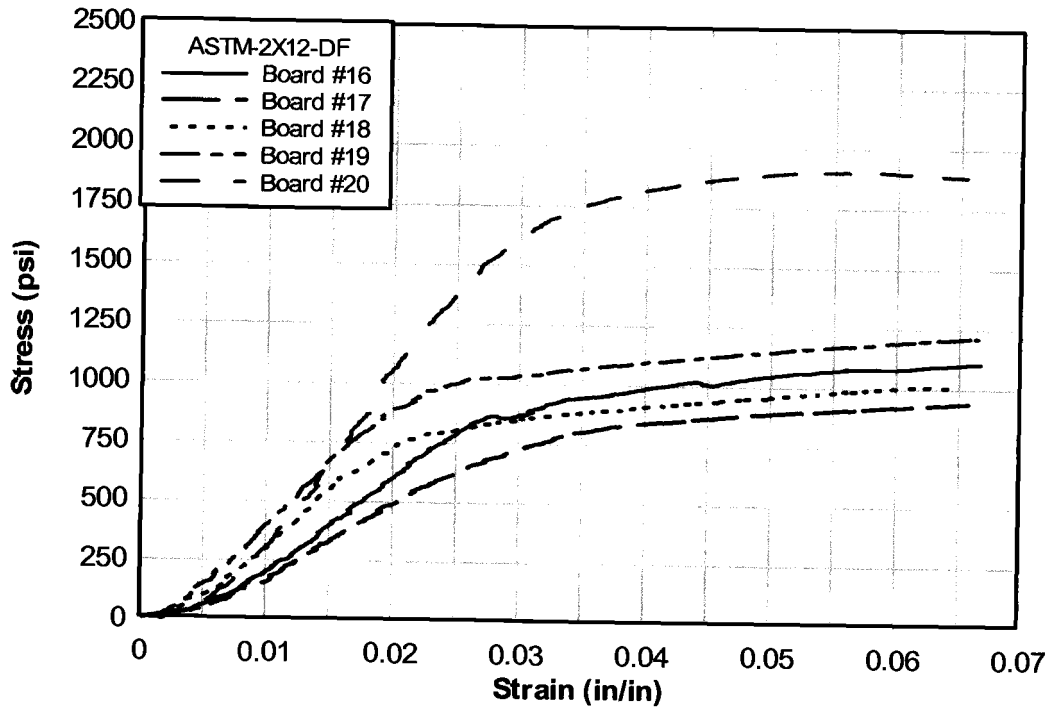
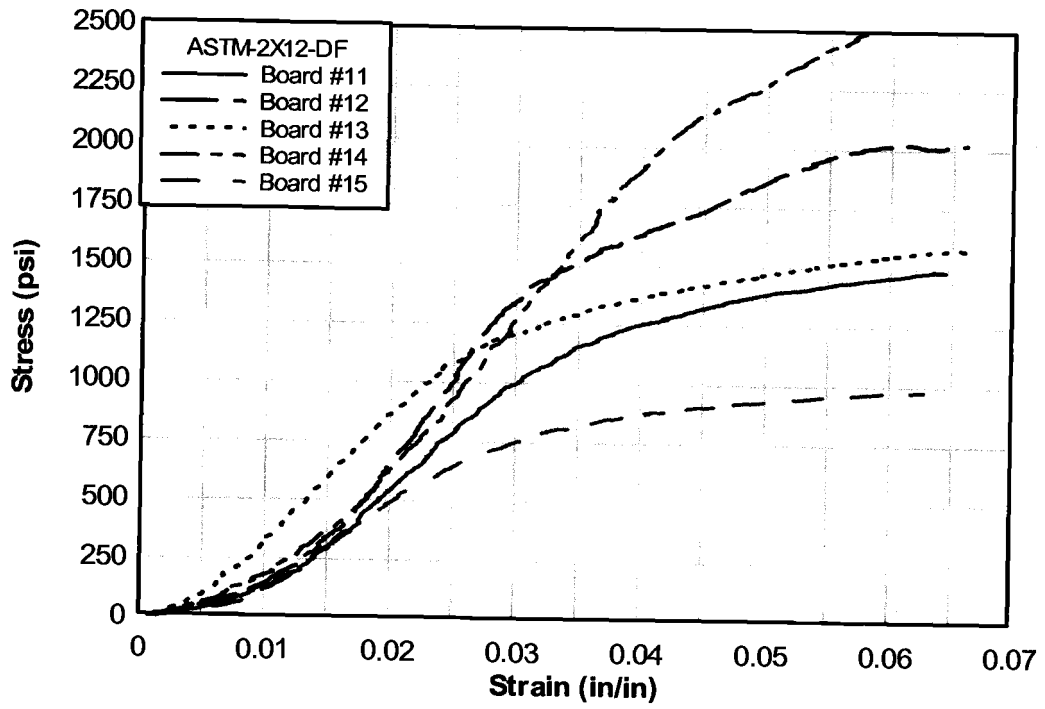




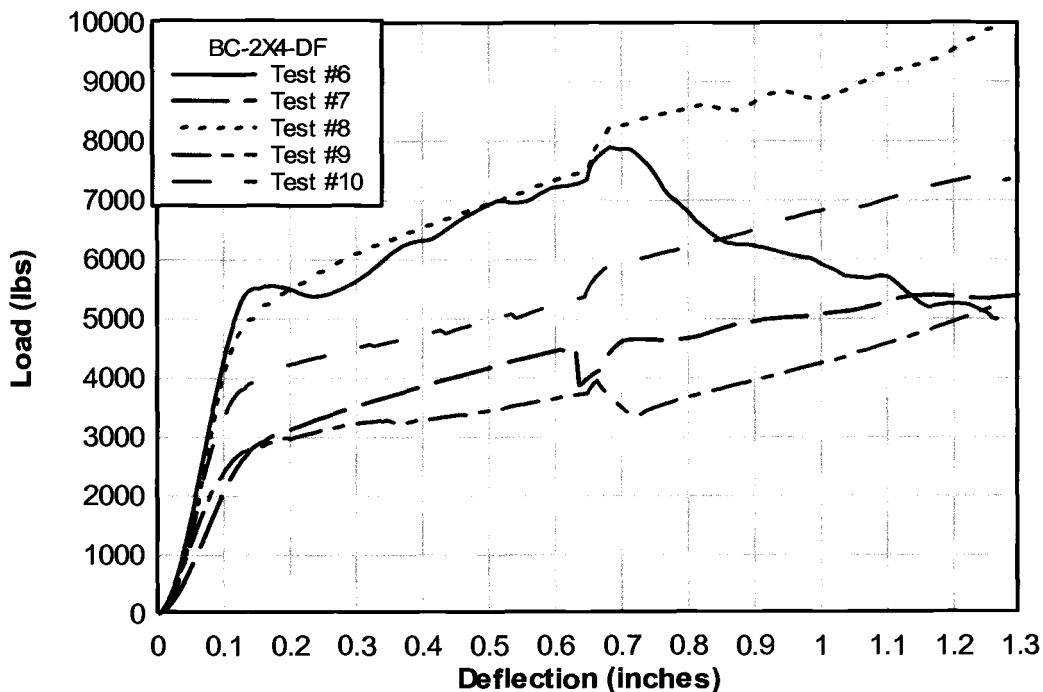
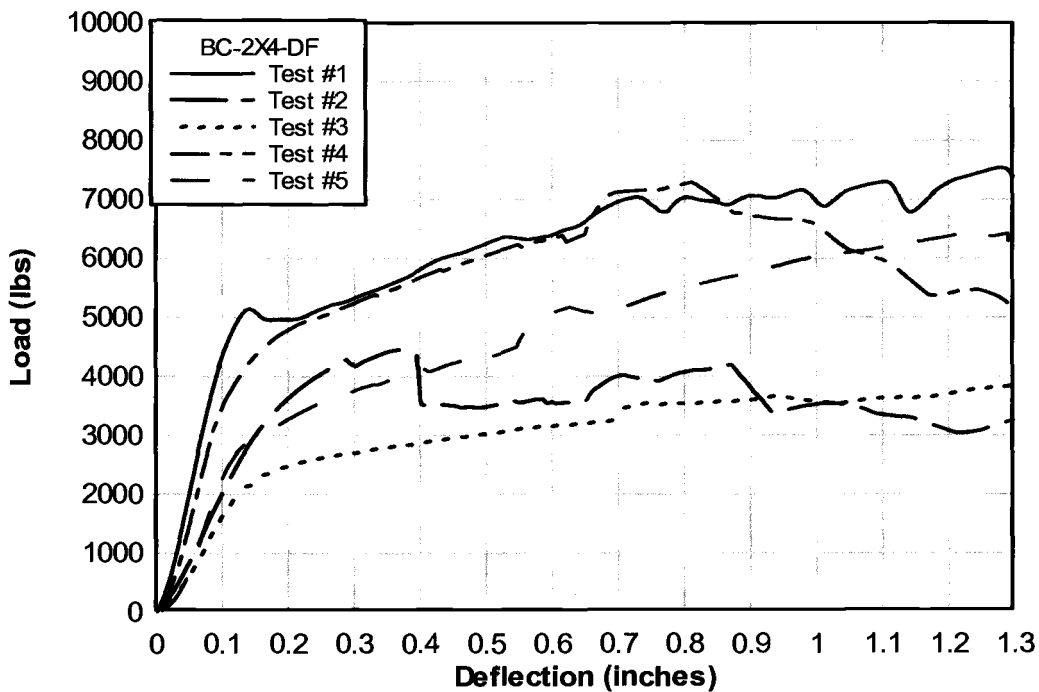


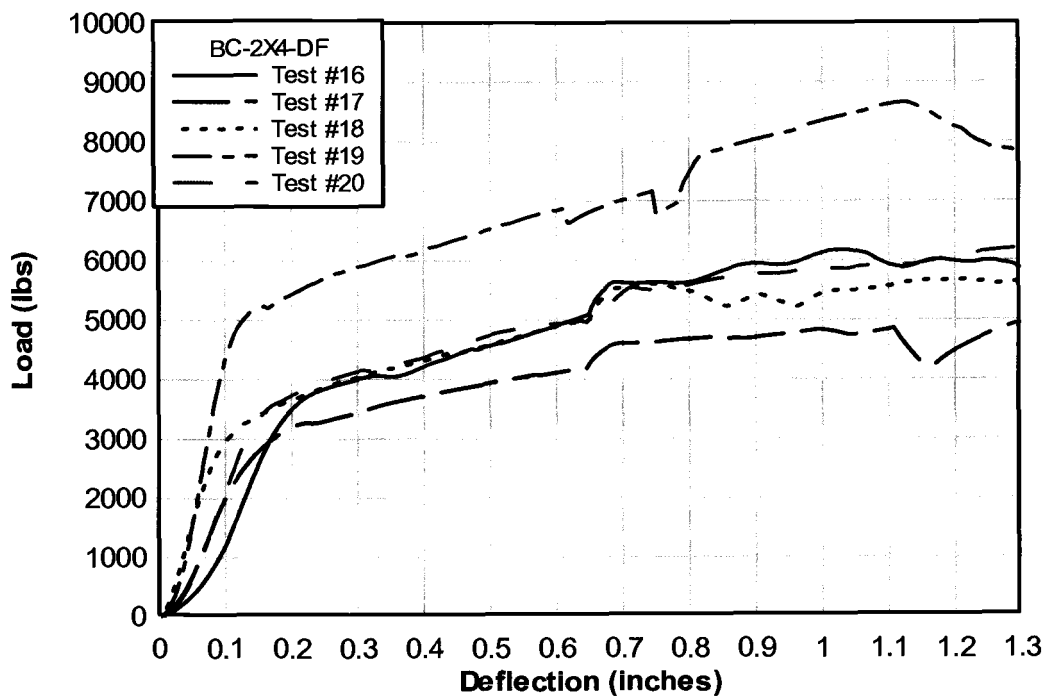
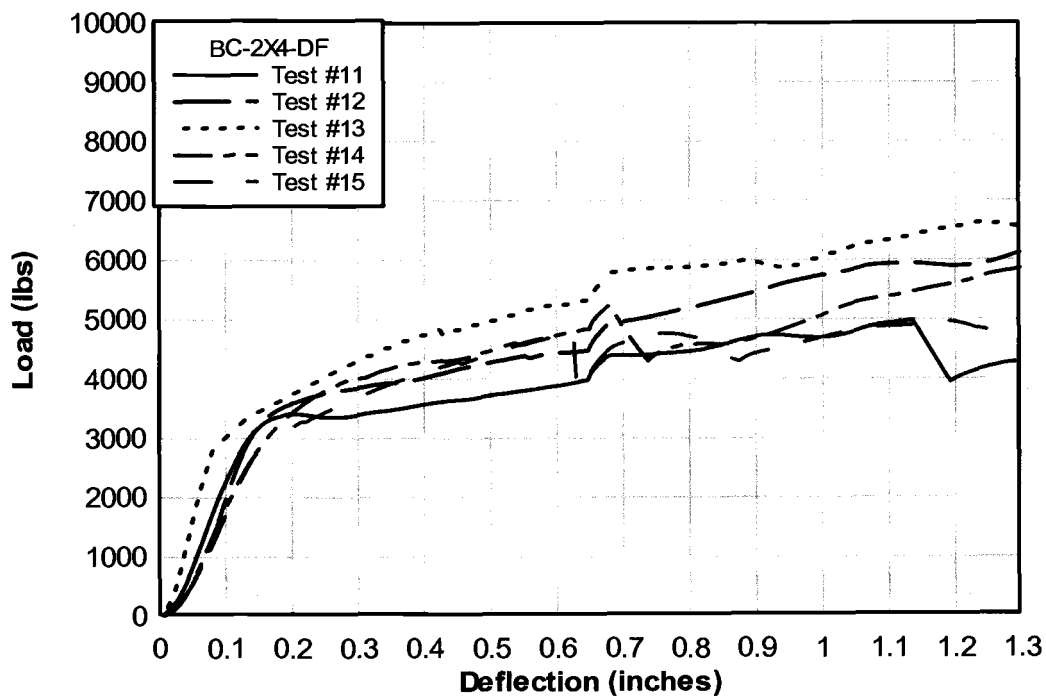


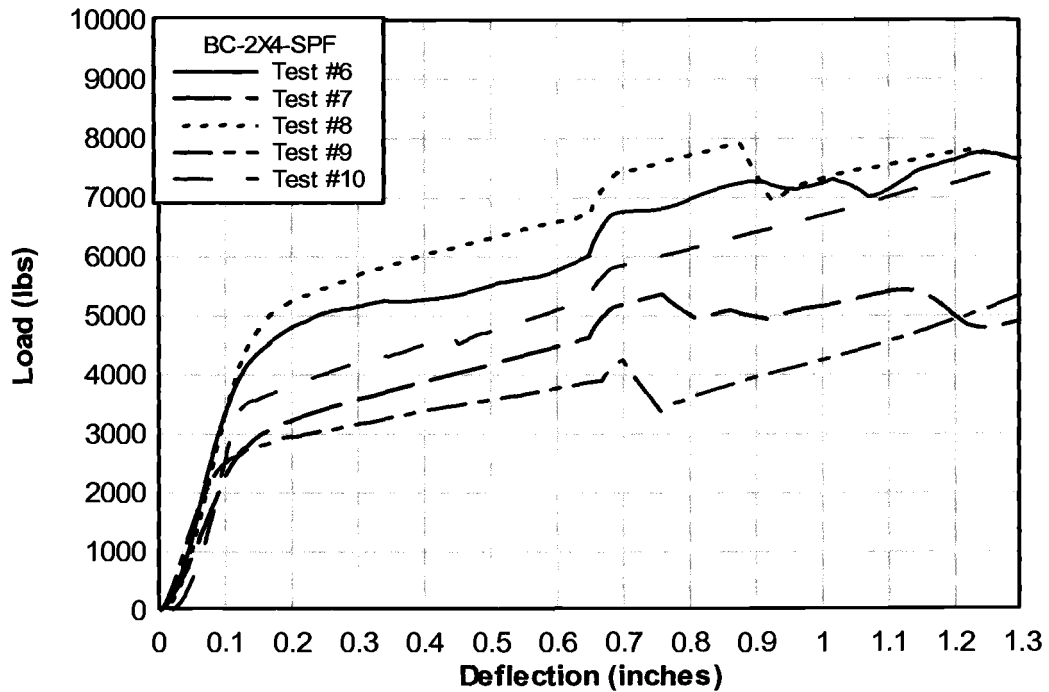
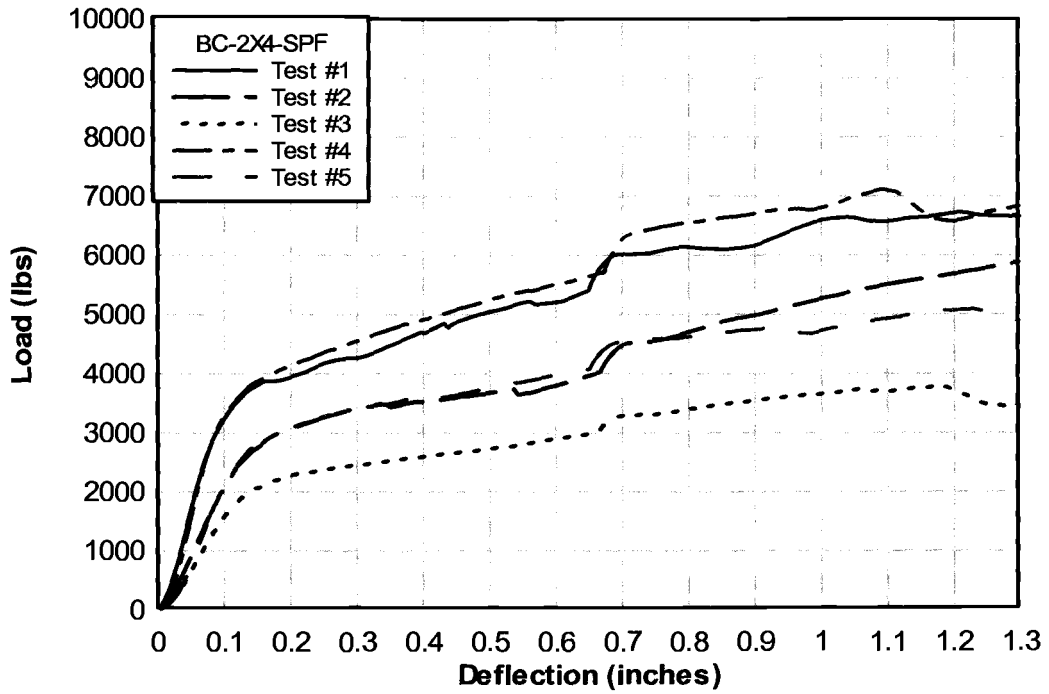


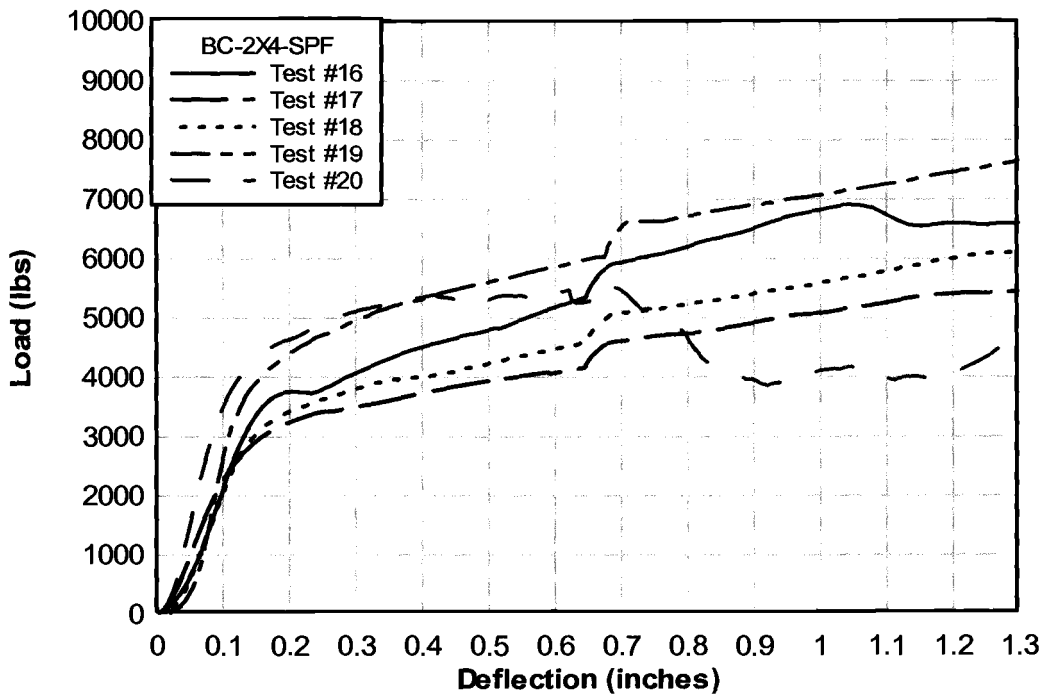
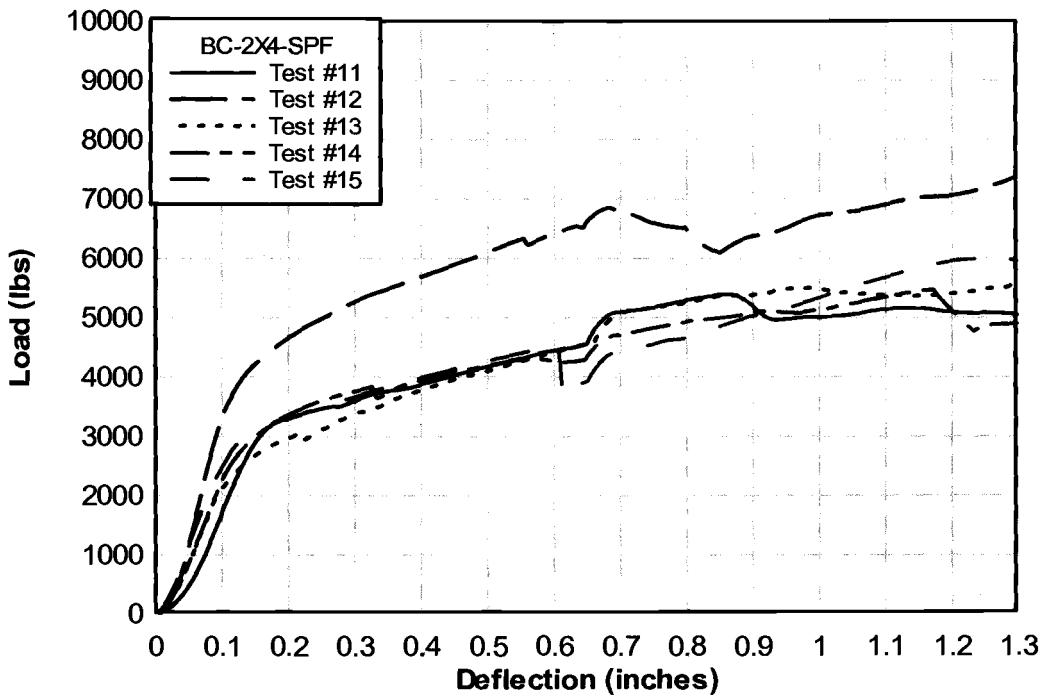


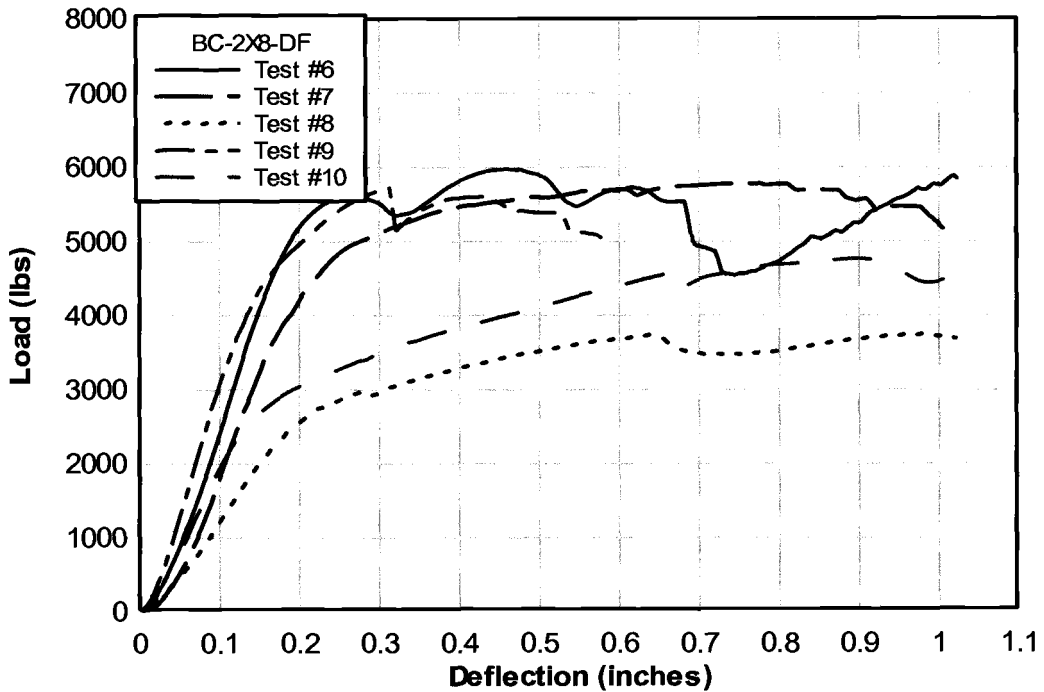
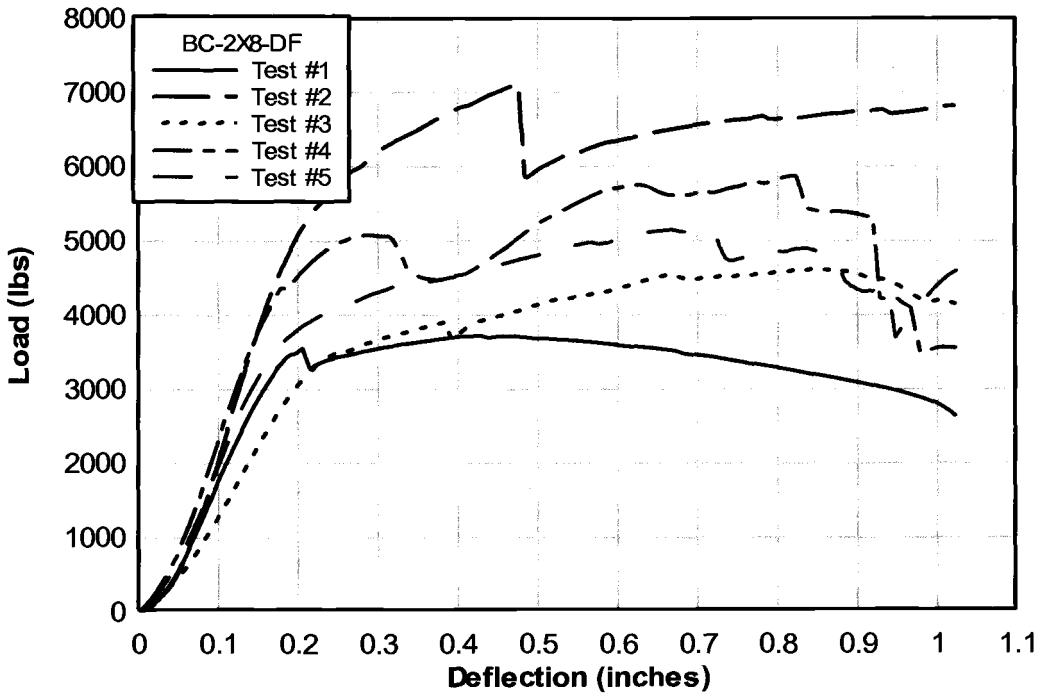
7.3 APPENDIX C: LOAD -DEFLECTION DIAGRAMS

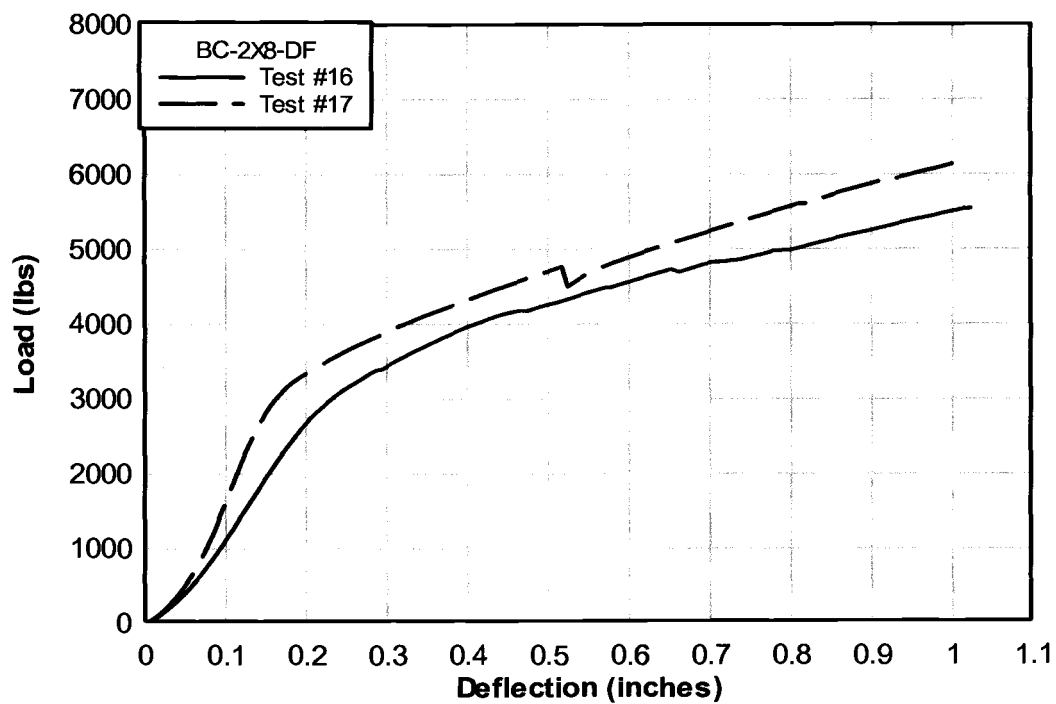
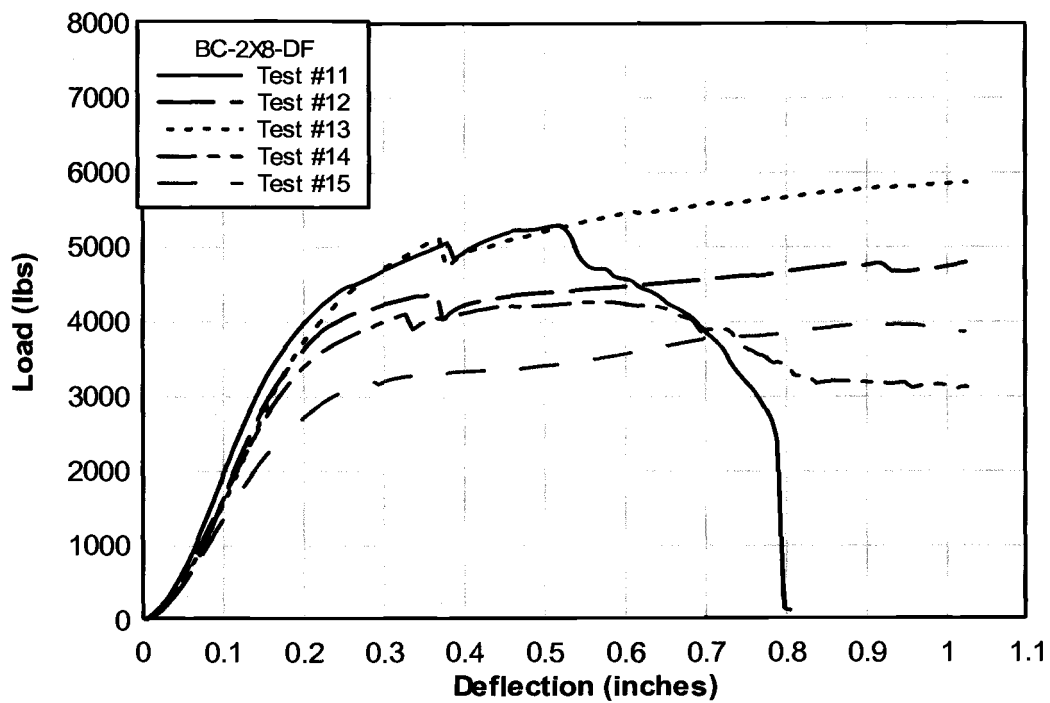


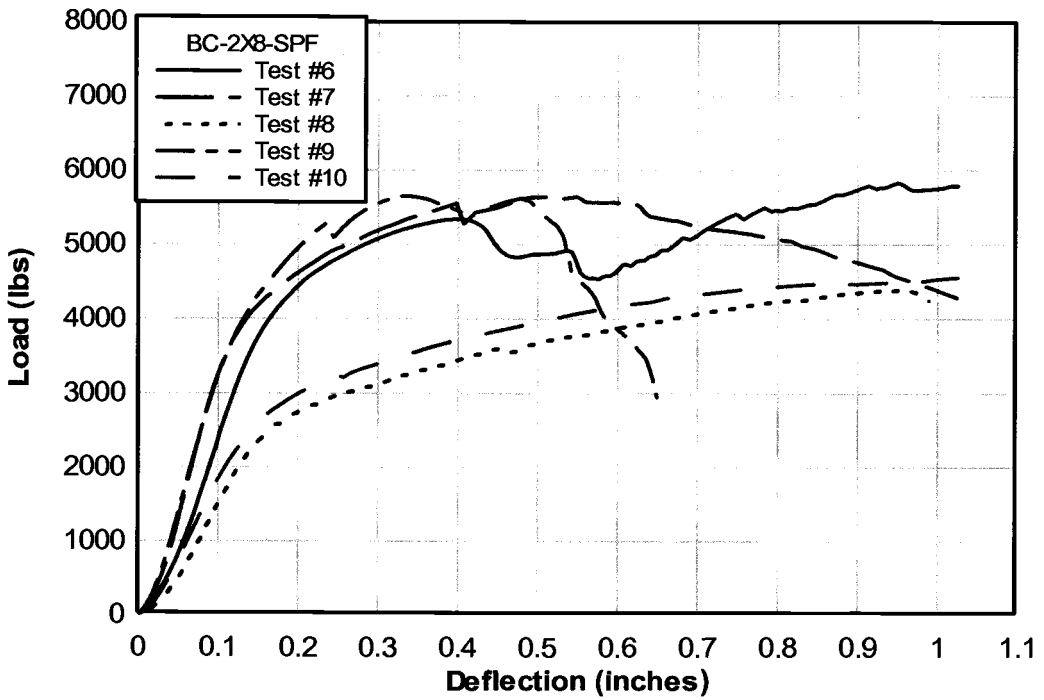
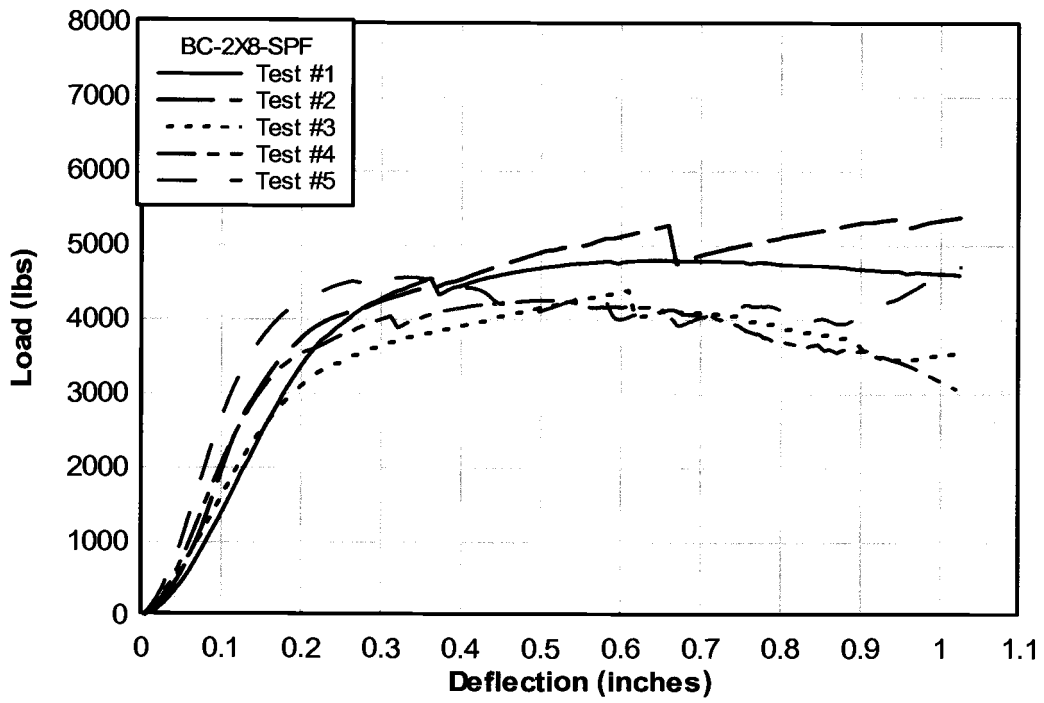


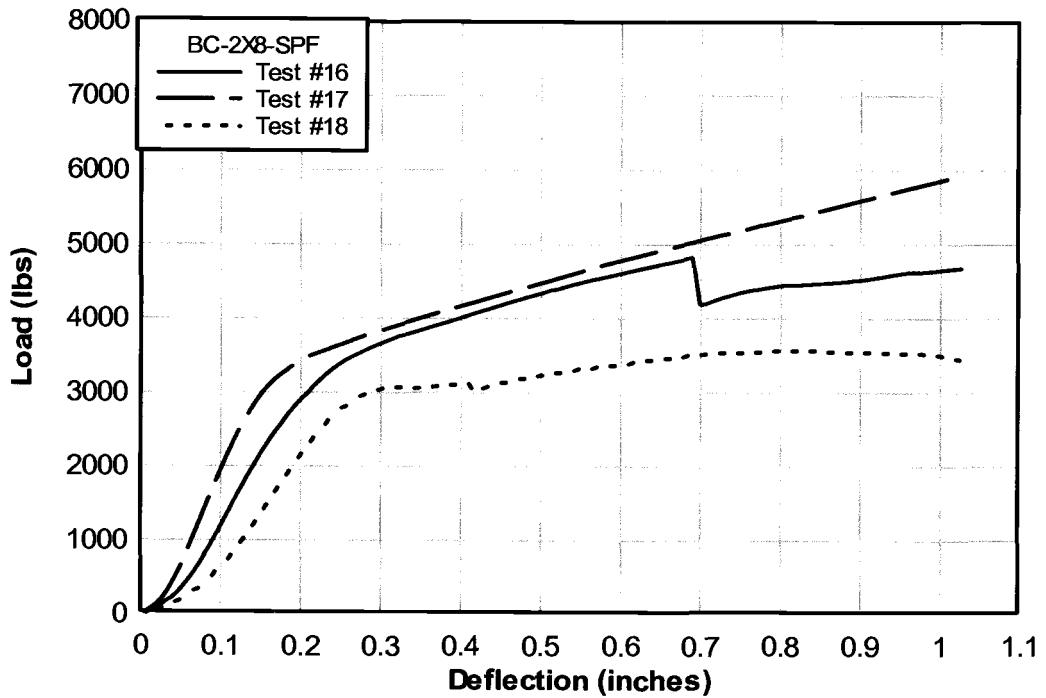
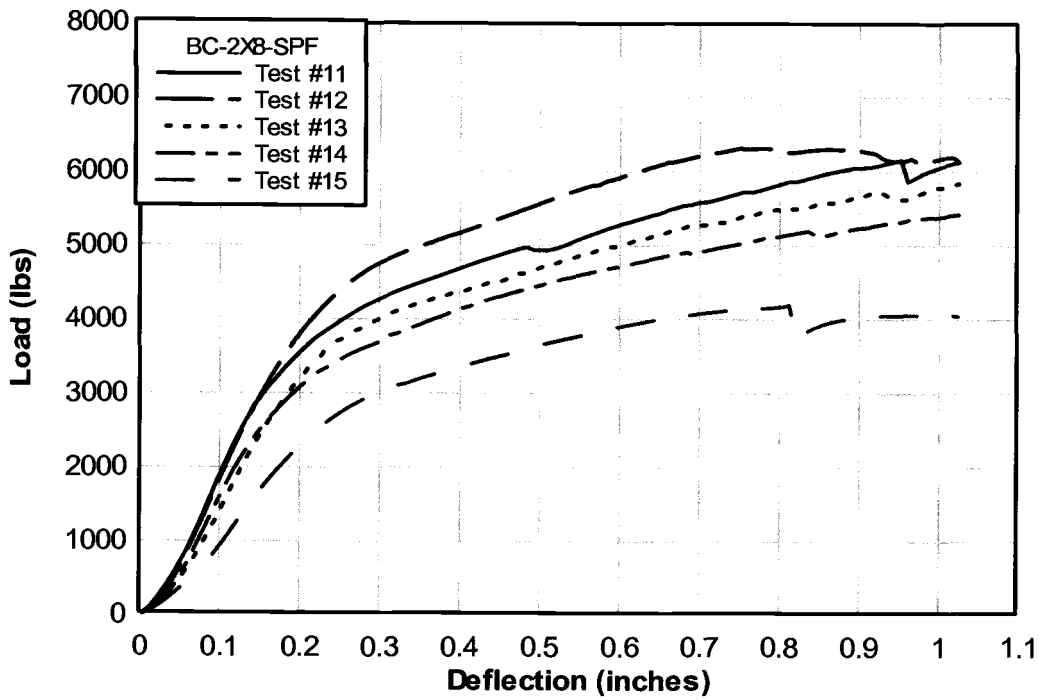


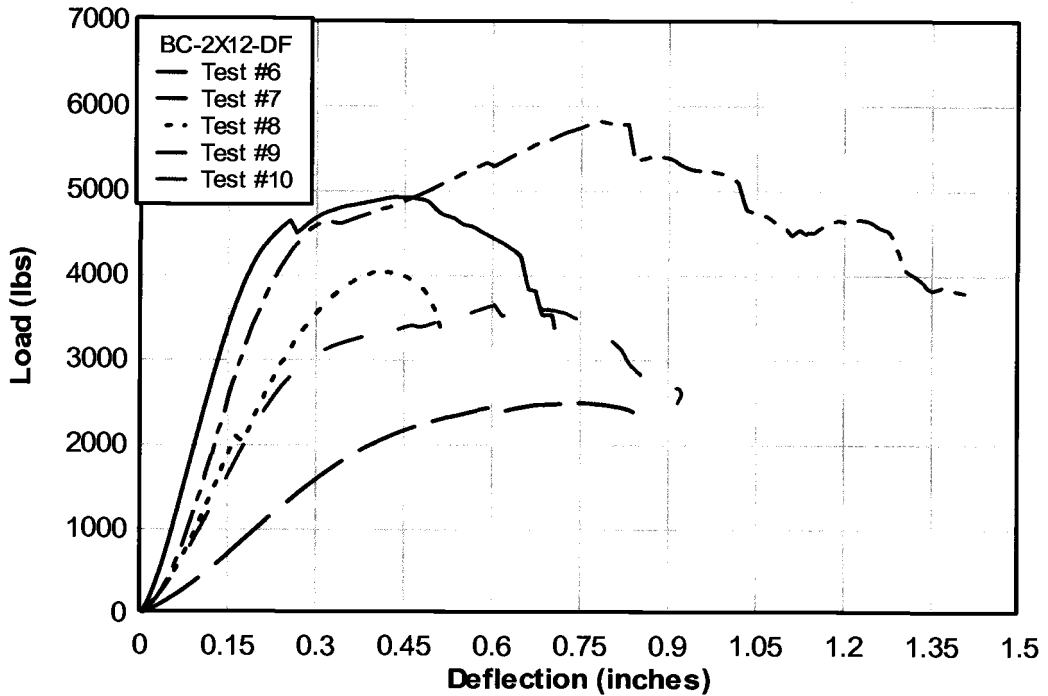
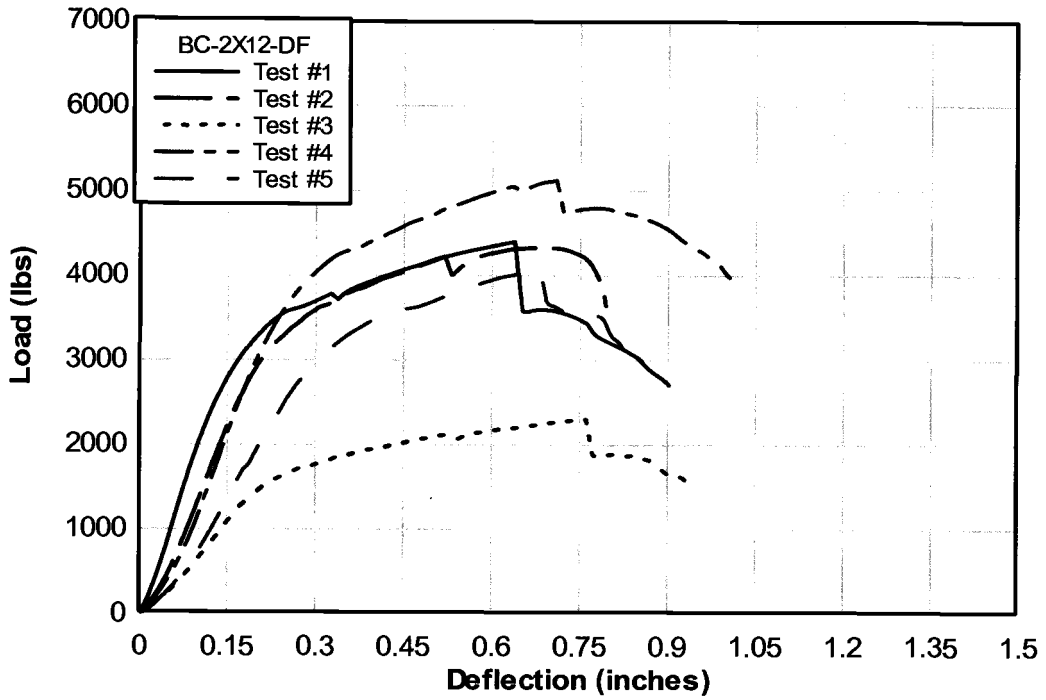


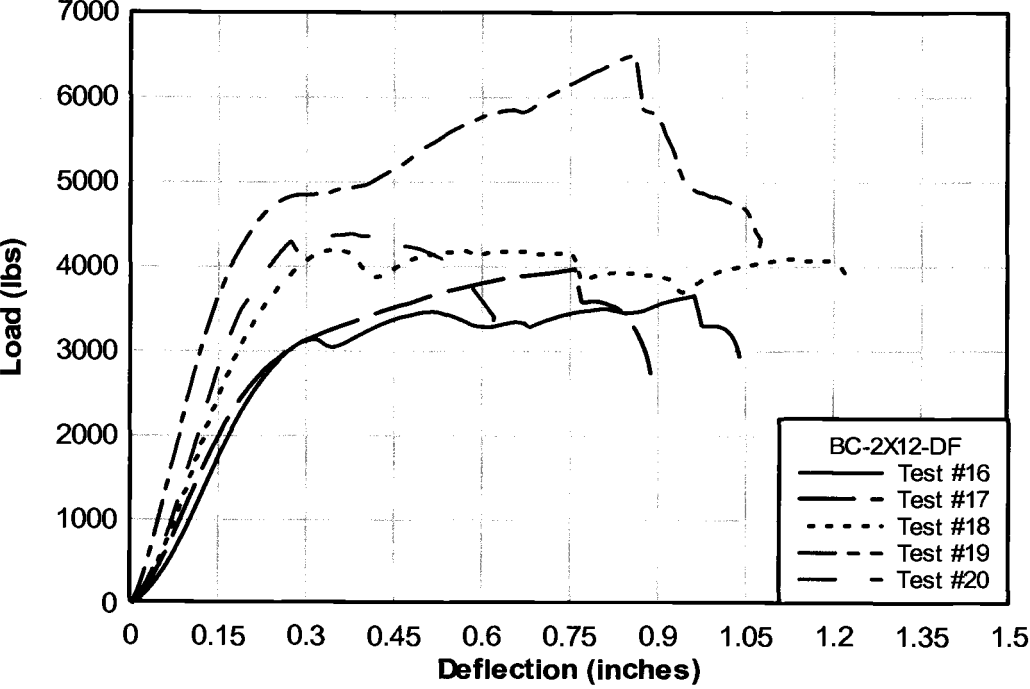
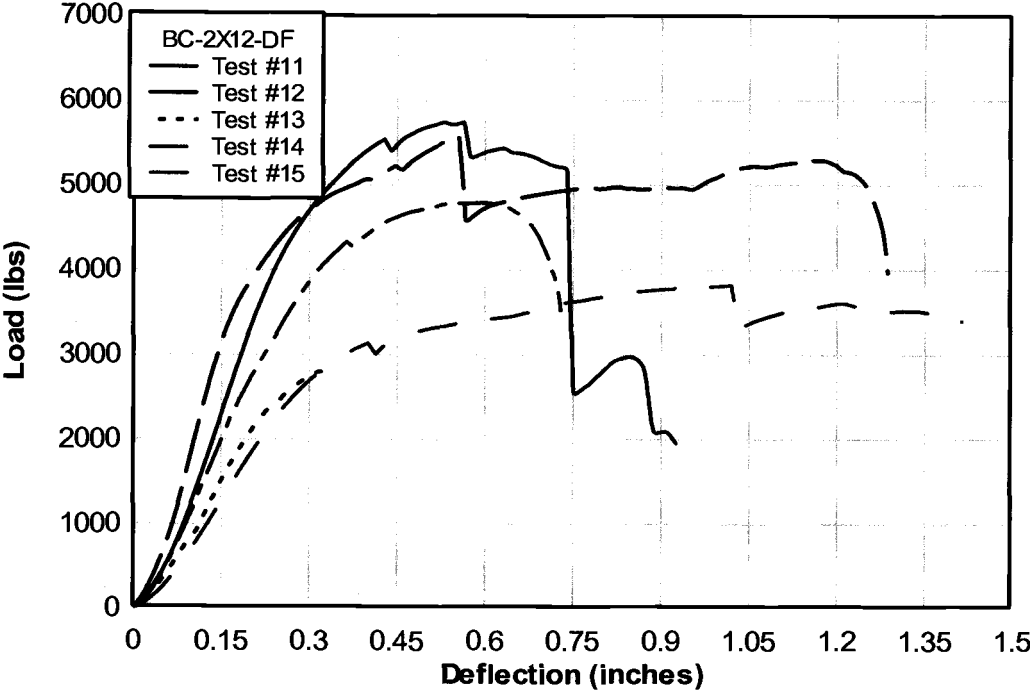


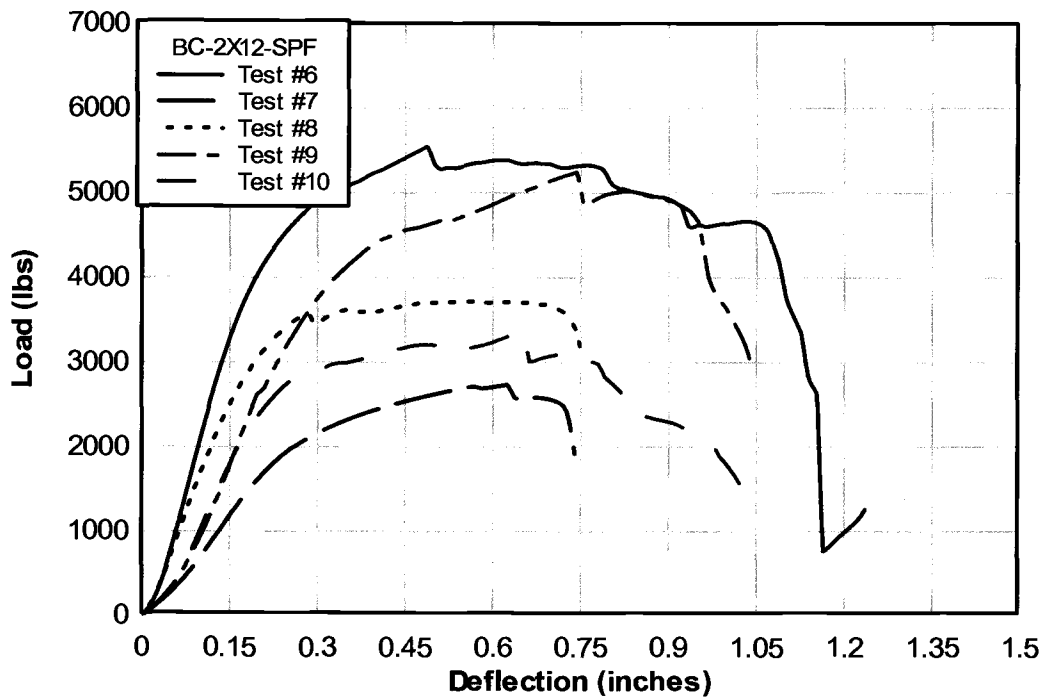
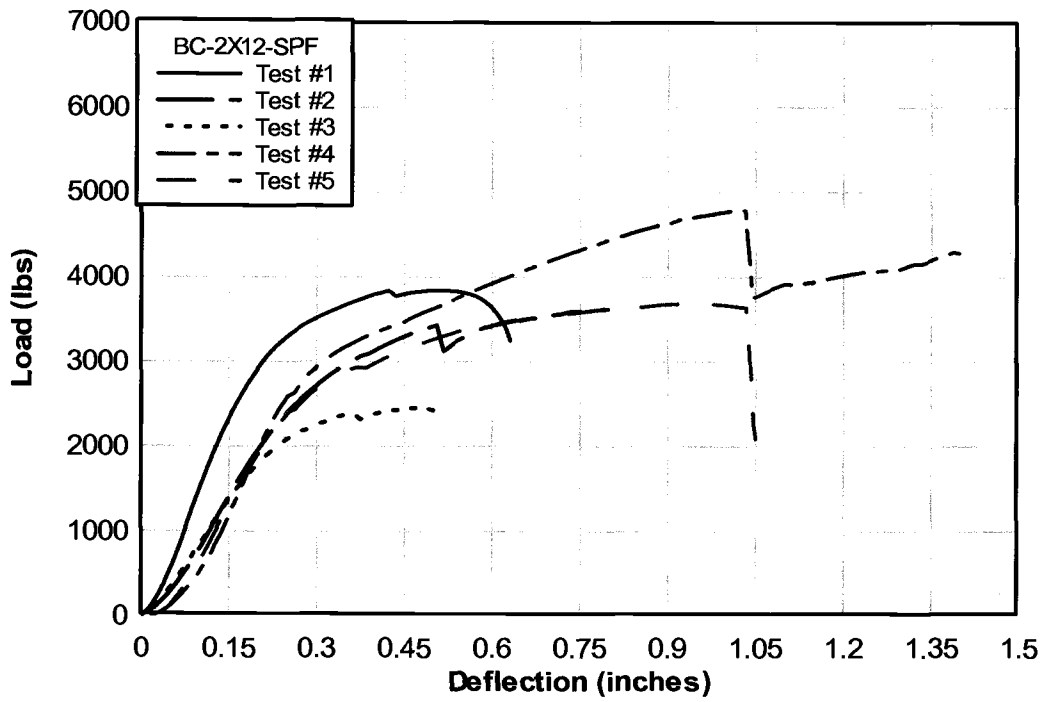


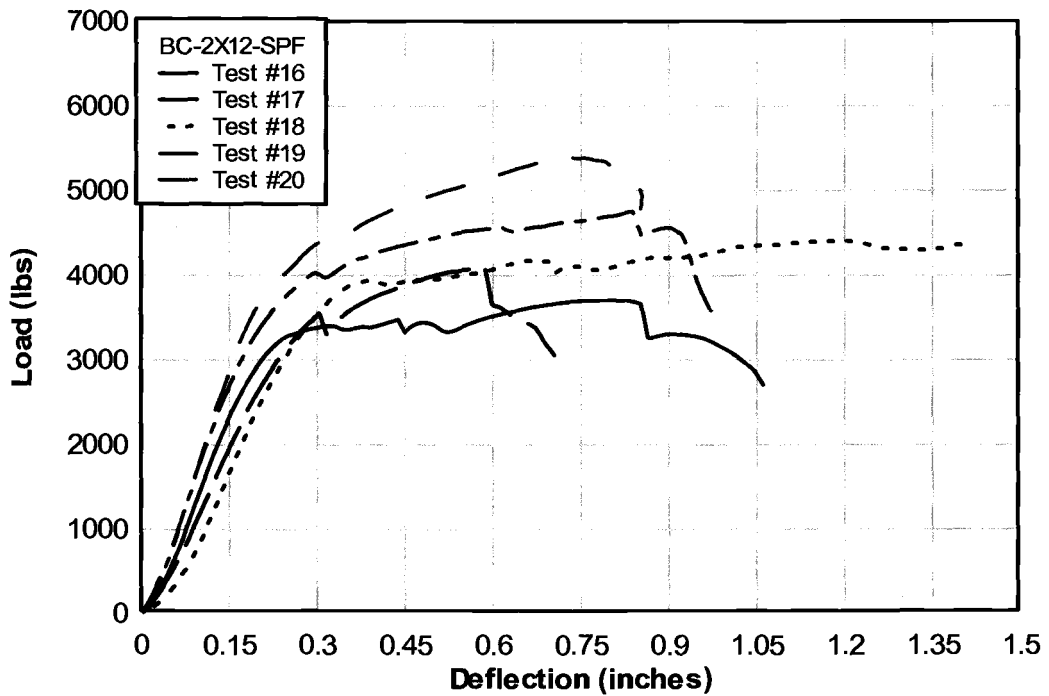
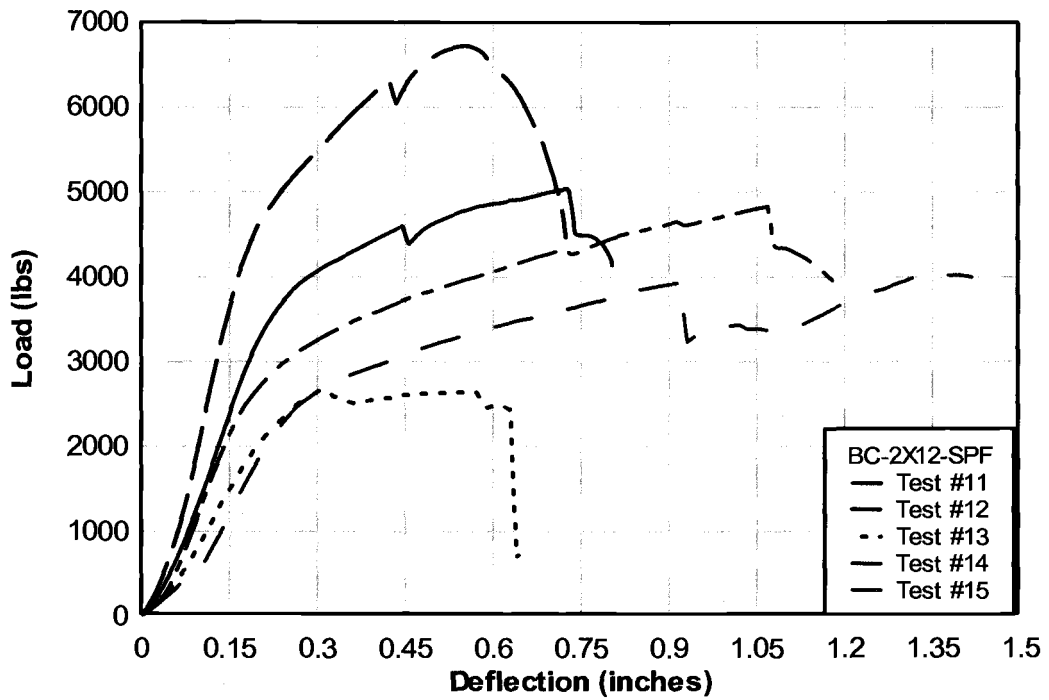


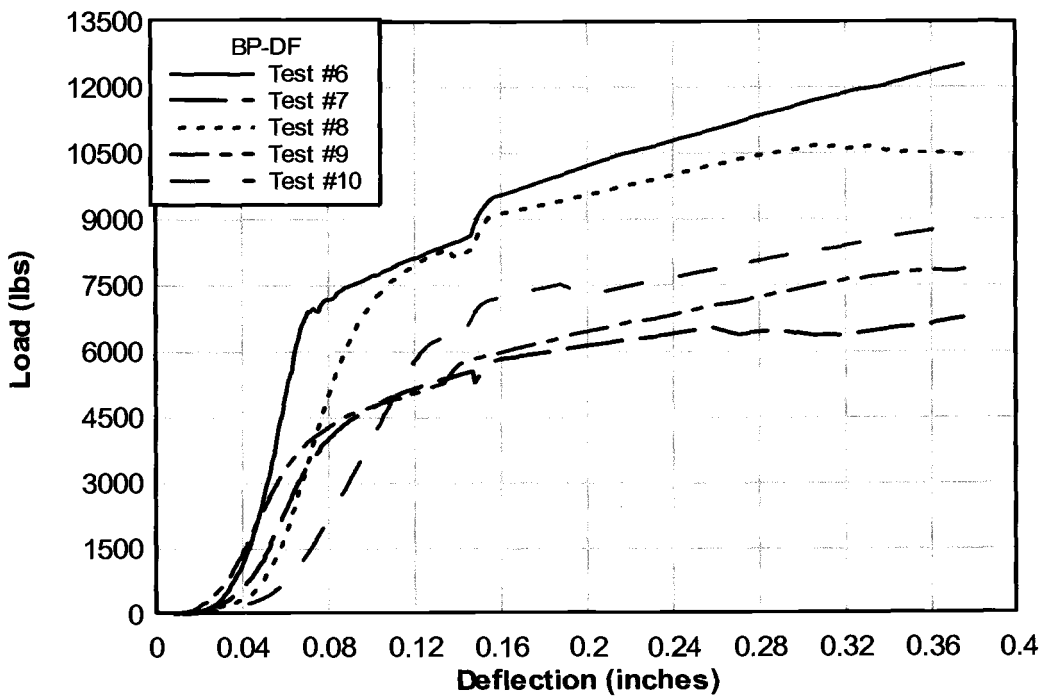
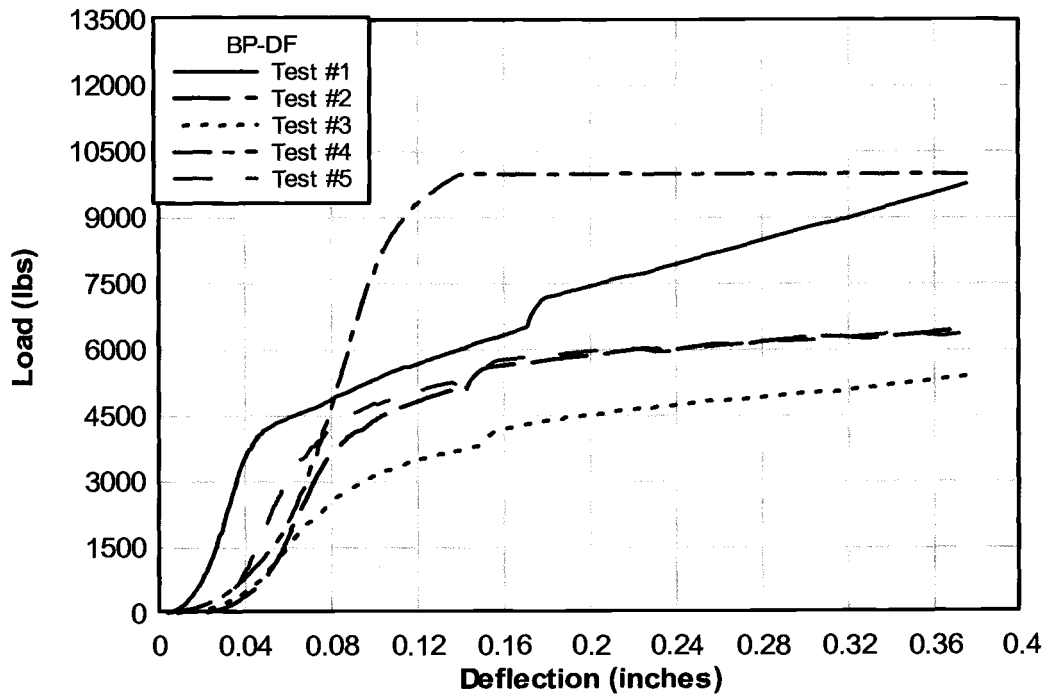
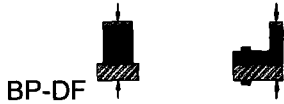


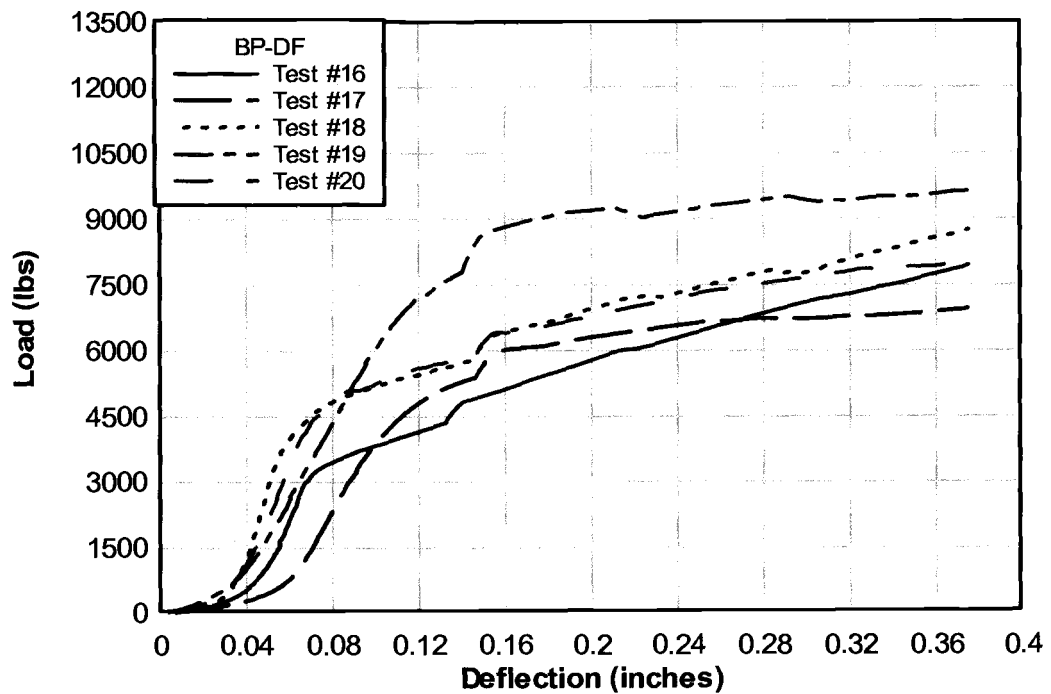
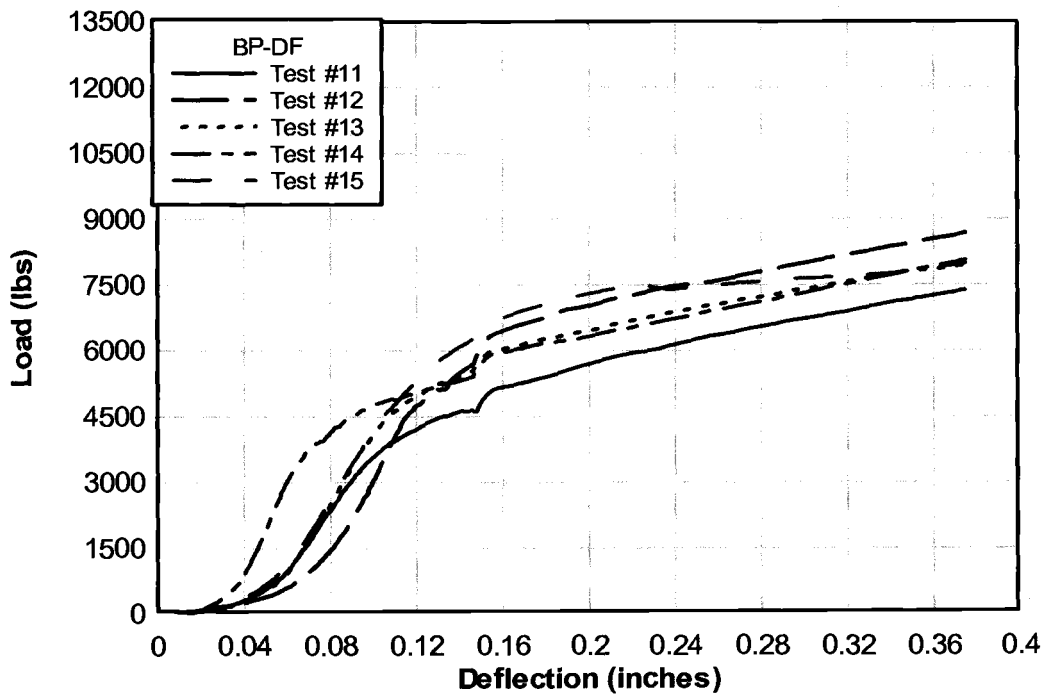


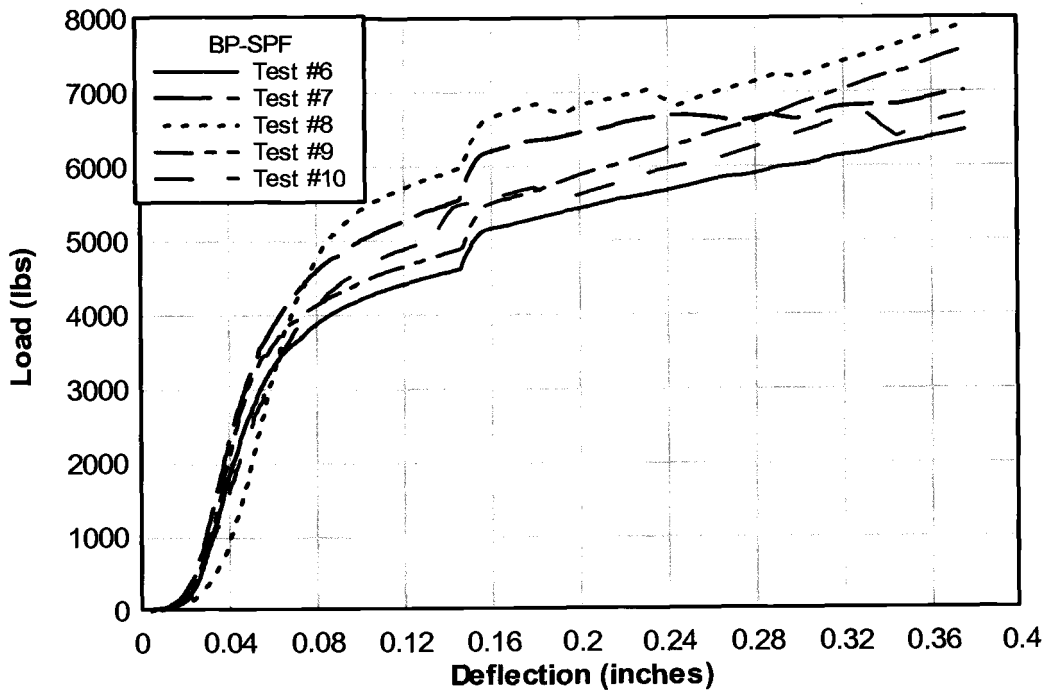
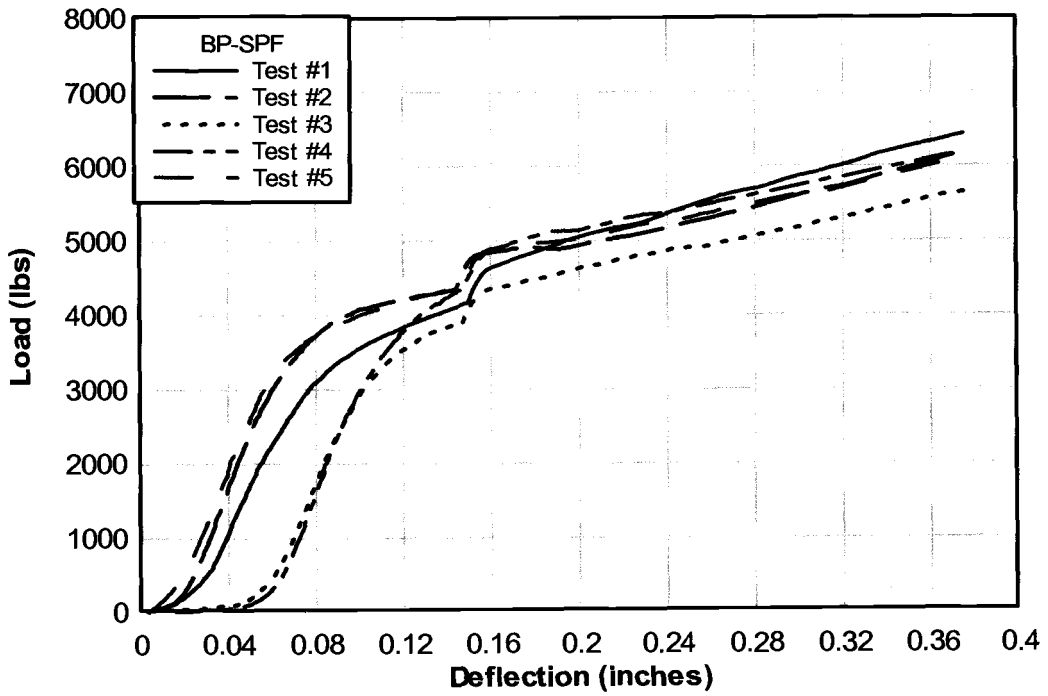


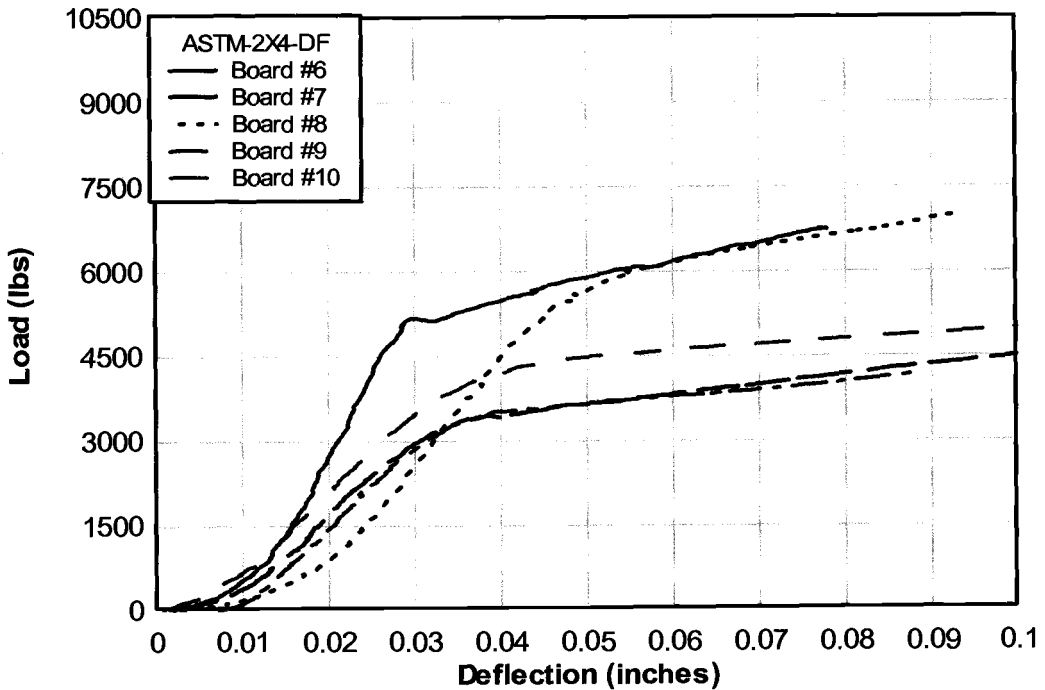
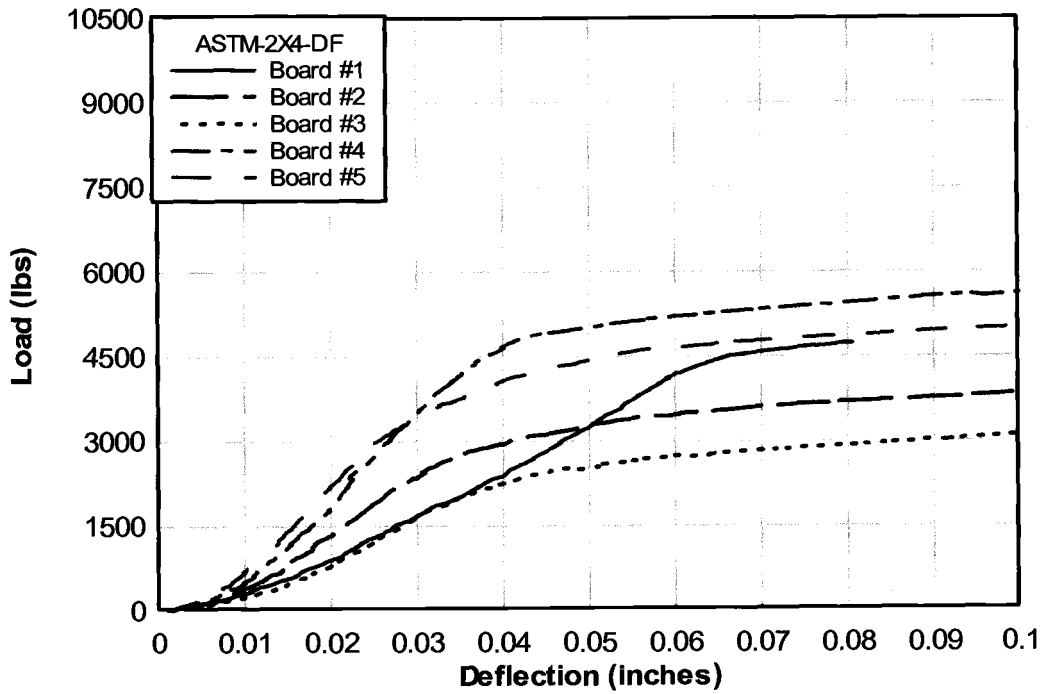


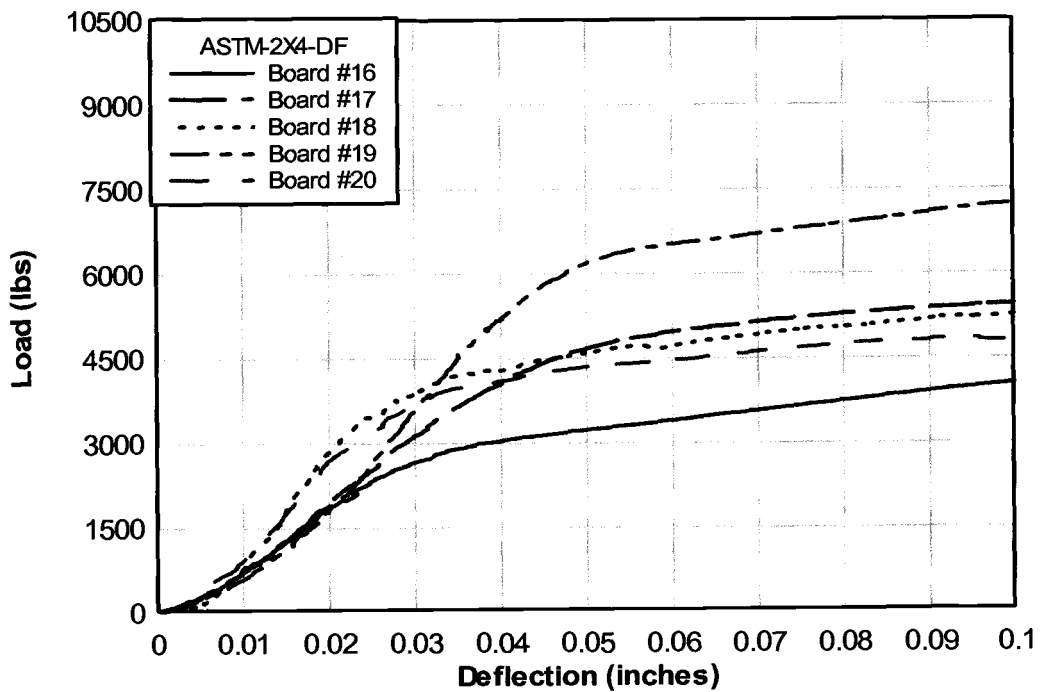
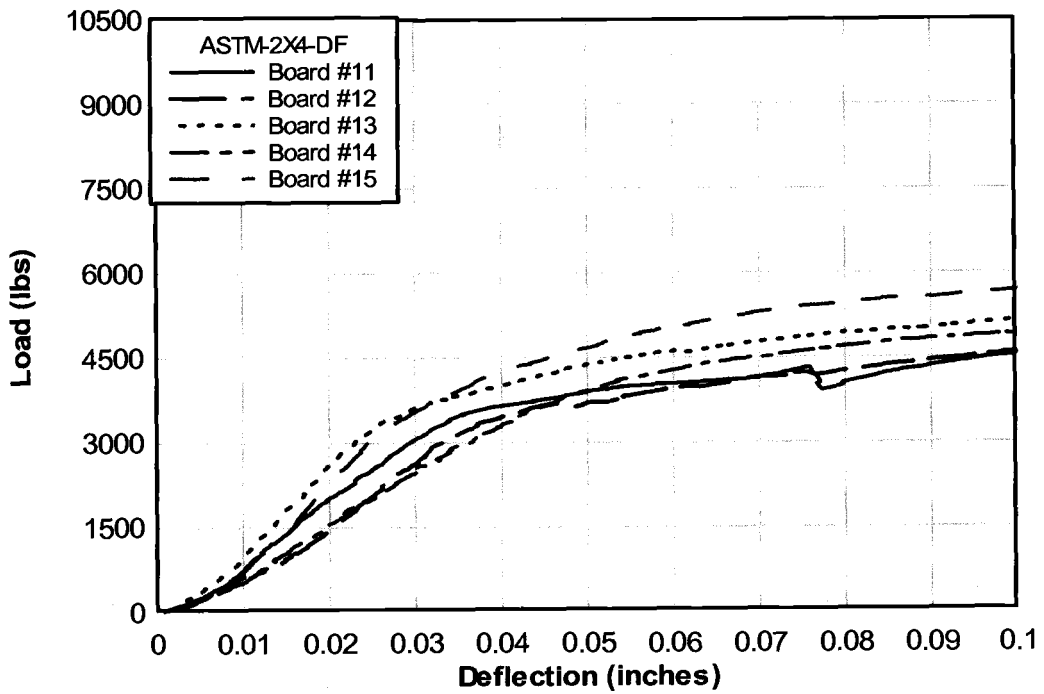


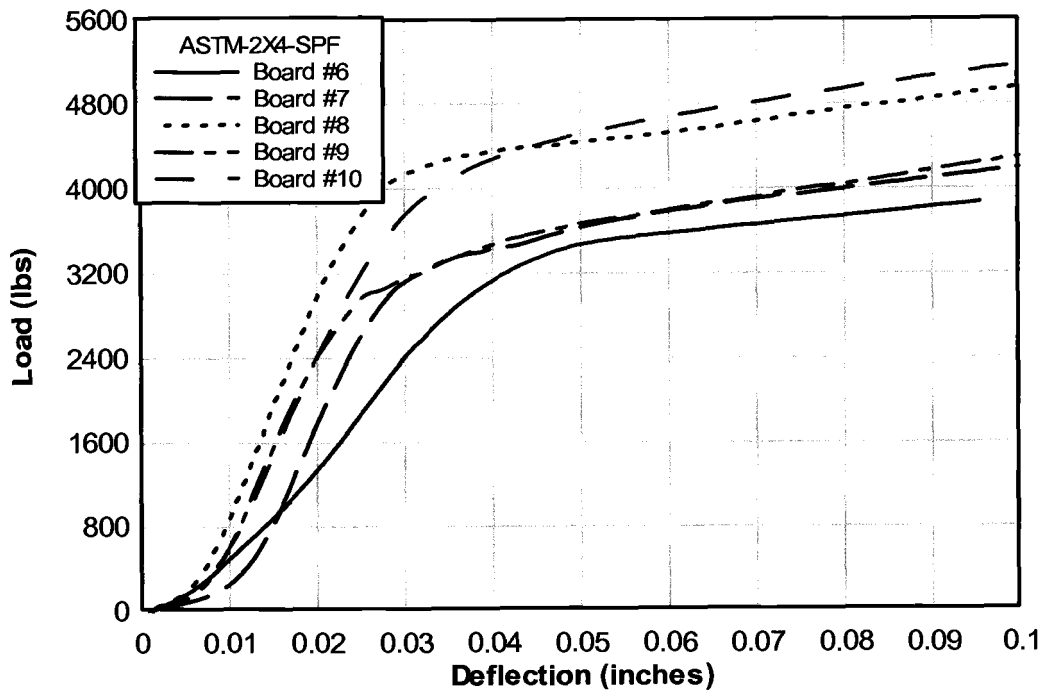
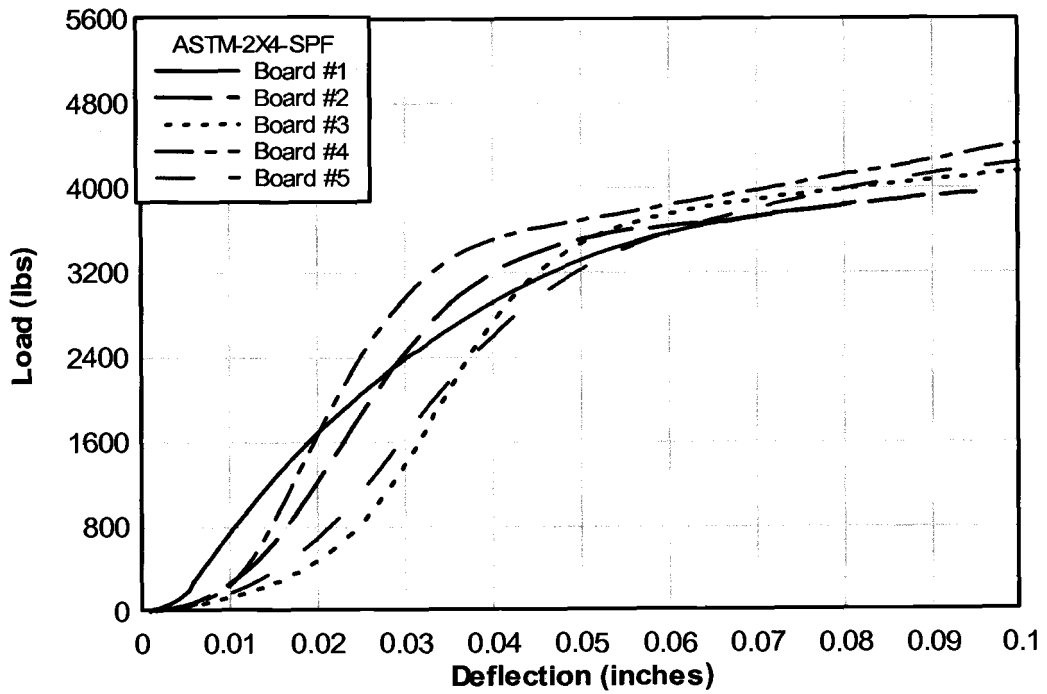


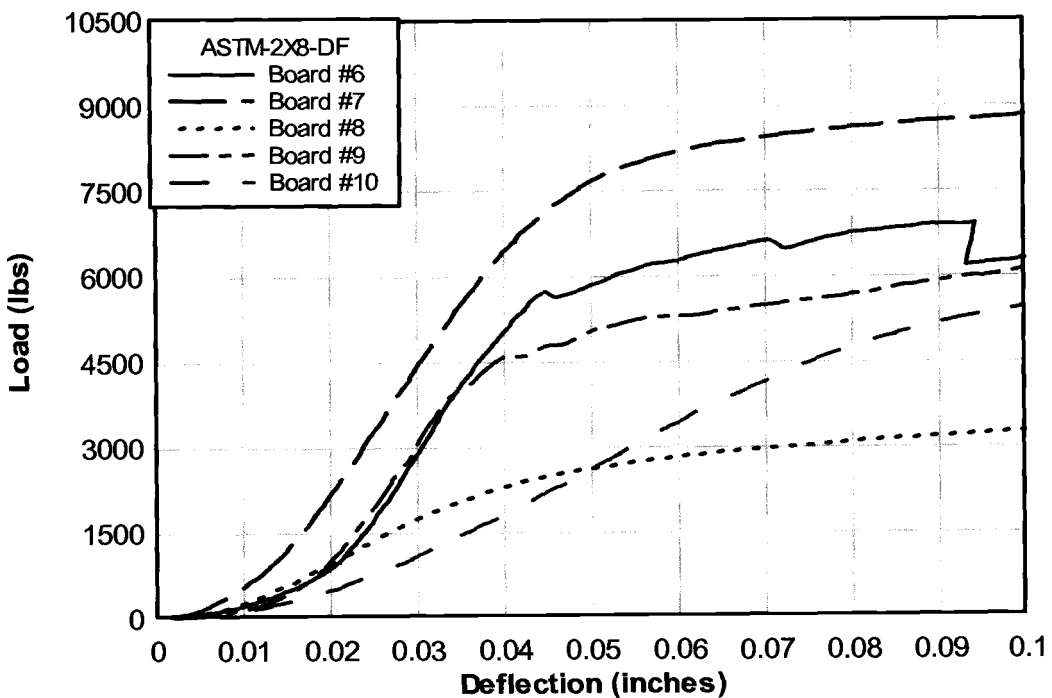
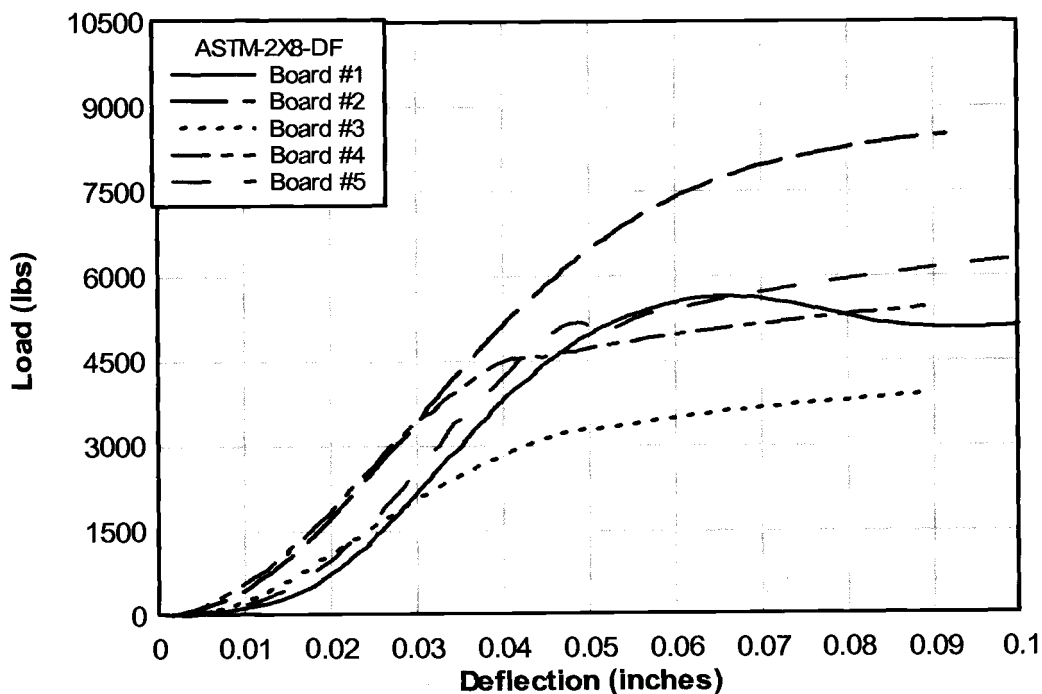


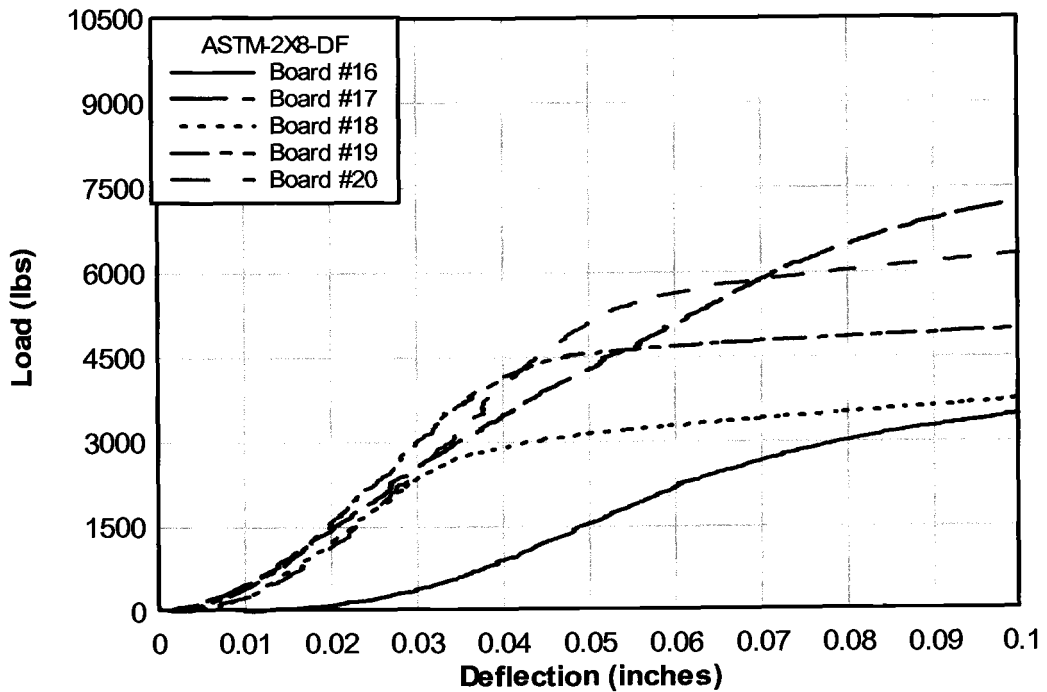
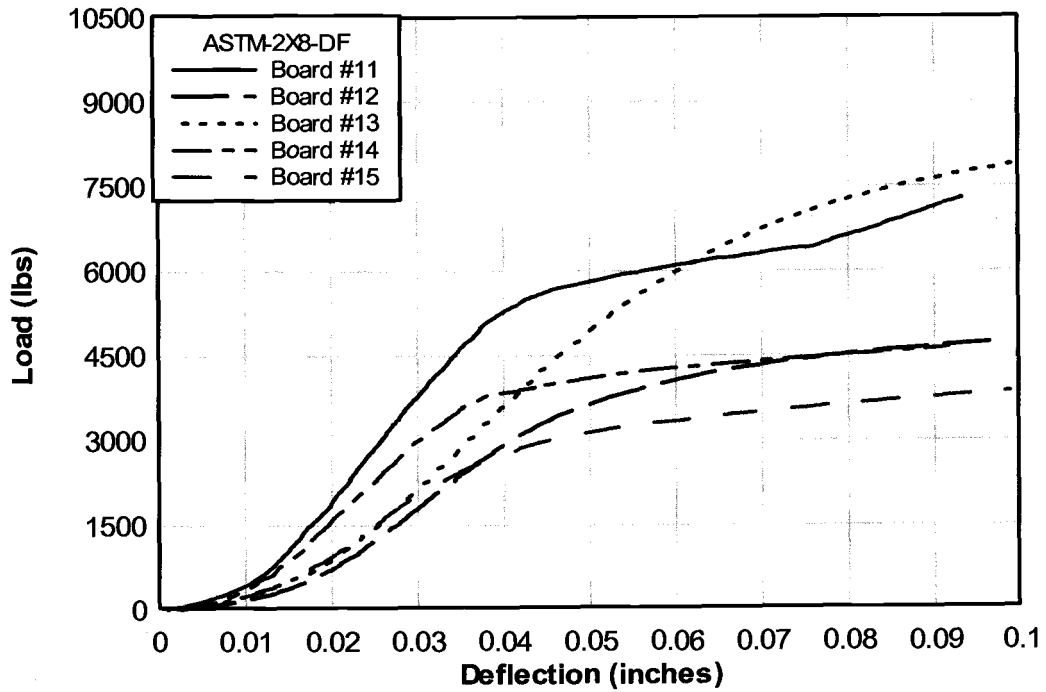


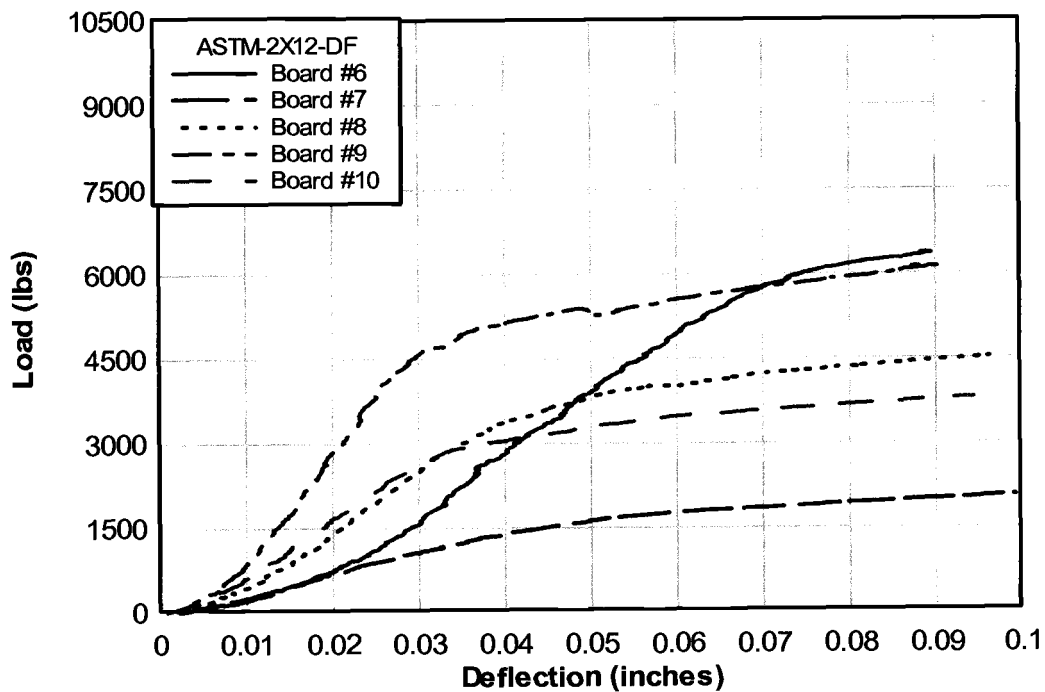
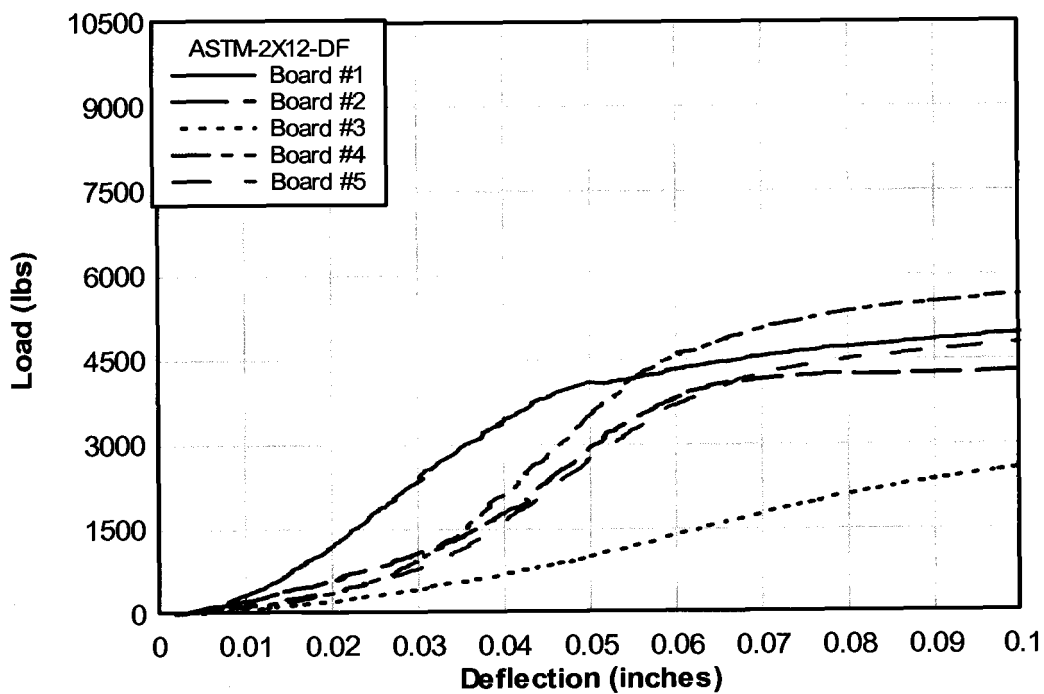


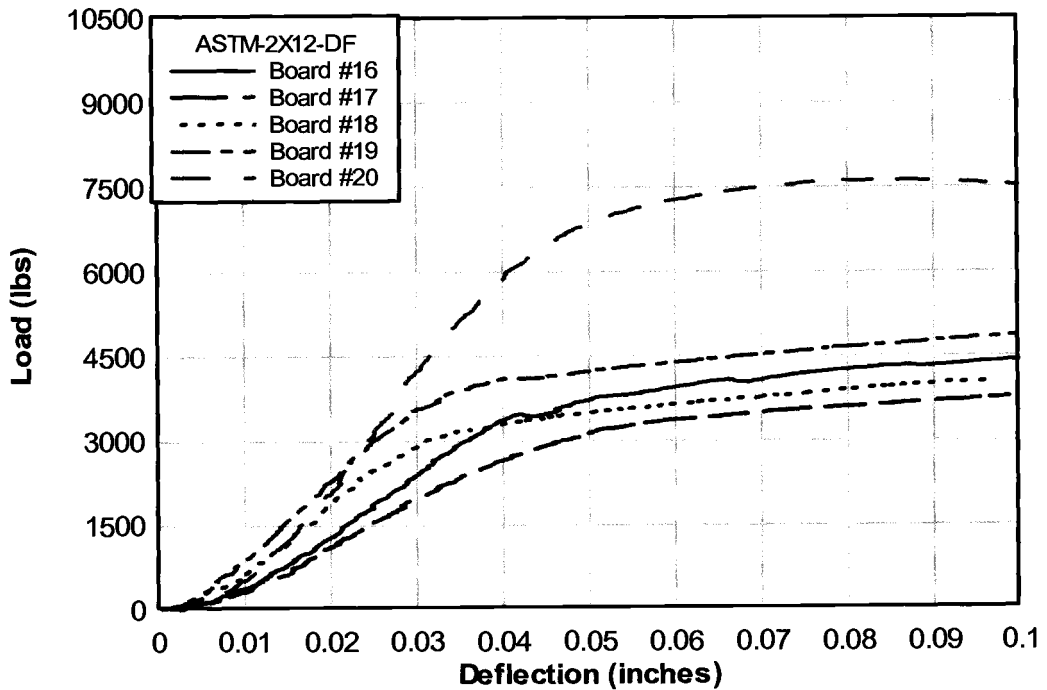
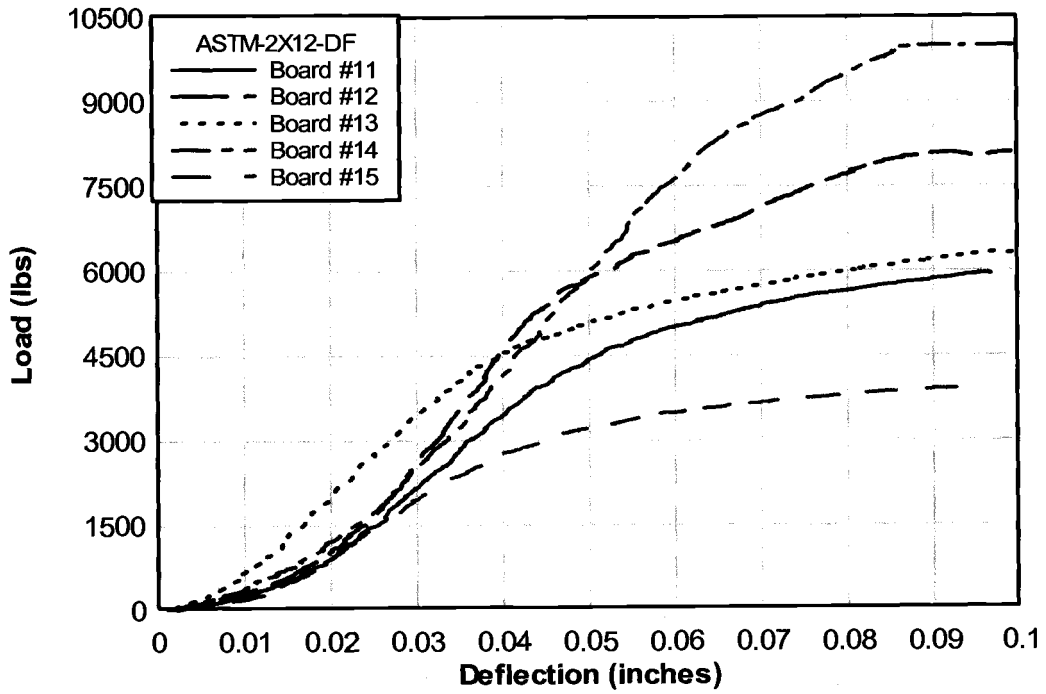












7.4 APPENDIX D: RAW DATA

BC-2X4-DF



Test #	$\sigma_{0.04-D}$	$\sigma_{0.04-OD}$	$\sigma_{2\%-S}$	$\sigma_{2\%-OS}$	σ_{max}	Slope of Linear Region	Catastrophic Failure
	psi	psi	psi	psi	psi	psi	Yes/No
1	220	394	963	1006	1463	65004	No
2	114	181	499	553	852	29234	No
3	82	156	391	428	734	25444	No
4	171	342	768	824	1394	55617	No
5	73	258	530	584	1224	41946	No
6	192	429	1018	1056	1508	69825	No
7	94	203	497	550	1031	33025	No
8	163	439	933	994	1888	72116	No
9	156	227	528	533	980	36702	No
10	132	350	728	762	1415	59325	No
11	100	221	548	610	952	36279	No
12	73	254	534	653	1166	41377	No
13	209	352	635	655	1269	57208	No
14	67	199	466	562	1117	32126	No
15	72	198	463	556	948	31976	No
16	49	227	372	639	1179	35044	No
17	80	208	477	543	925	33654	No
18	217	299	625	639	1085	48369	No
19	166	479	957	1000	1500	77775	No
20	78	236	560	664	1179	38418	No
Average	125	283	625	691	1190	46023	
COV (%)	45	34	32	27	23	35	

BC-2X4-SPF



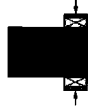
Test #	$\sigma_{0.04-D}$	$\sigma_{0.04-OD}$	$\sigma_{2\%-S}$	$\sigma_{2\%-OS}$	σ_{max}	Slope of Linear Region	Catastrophic Failure
	psi	psi	psi	psi	psi	psi	Yes/No
1	227	350	698	723	1287	56798	No
2	119	189	492	524	1115	30855	No
3	85	153	368	392	722	24802	No
4	192	362	705	739	1300	58205	No
5	88	218	482	531	972	35334	No
6	152	352	782	845	1483	56945	No
7	117	209	528	562	1040	34066	No
8	117	352	826	930	1511	57686	No
9	200	270	520	532	1001	43851	No
10	44	375	662	709	1428	60736	No
11	61	209	470	601	1029	34065	No
12	122	361	750	814	1387	58413	No
13	109	211	476	511	1056	34363	No
14	118	222	531	574	1045	35883	No
15	148	235	559	571	1146	38165	No
16	77	243	562	681	1320	39736	No
17	117	215	513	552	1037	35038	No
18	70	234	533	609	1165	37990	No
19	29	418	673	811	1449	67779	No
20	165	373	771	822	1063	60619	No
Average	118	278	595	652	1178	45066	
COV (%)	44	29	21	22	18	29	

BC-2X8-DF



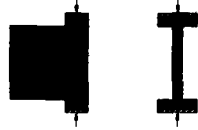
Test #	$\sigma_{0.04-D}$	$\sigma_{0.04-OD}$	$\sigma_{2\%-S}$	$\sigma_{2\%-OS}$	σ_{max}	Slope of Linear Region	Catastrophic Failure
	psi	psi	psi	psi	psi	psi	Yes/No
1	62	186	673	648	713	47942	No
2	59	281	974	1097	1358	70837	No
3	61	153	590	659	882	37209	No
4	104	256	871	933	1125	63733	No
5	91	222	733	772	984	55050	No
6	106	269	996	1056	1143	66329	No
7	53	233	805	916	1102	58991	No
8	61	132	495	534	717	32021	No
9	158	276	955	987	1098	70757	Yes
10	98	178	586	604	913	45794	No
11	81	211	765	826	1013	53918	Yes
12	59	199	700	766	916	51131	No
13	64	179	718	800	1121	44701	No
14	78	168	655	698	819	42523	No
15	62	140	523	566	760	35261	No
16	54	133	517	585	1060	32384	No
17	61	213	640	693	1184	53562	No
18	NA	NA	NA	NA	NA	NA	NA
19	NA	NA	NA	NA	NA	NA	NA
20	NA	NA	NA	NA	NA	NA	NA
Average	77	202	717	773	995	50714	
COV (%)	35	25	22	23	18	25	

BC-2X8-SPF



Test #	$\sigma_{0.04-D}$	$\sigma_{0.04-OD}$	$\sigma_{2\%-S}$	$\sigma_{2\%-OS}$	σ_{max}	Slope of Linear Region	Catastrophic Failure
	psi	psi	psi	psi	psi	psi	Yes/No
1	54	172	648	735	920	41732	No
2	69	239	717	770	1026	61232	No
3	90	177	601	634	842	39366	No
4	88	200	680	700	815	51578	No
5	129	258	812	837	902	66153	No
6	103	249	855	902	1118	63533	No
7	150	335	889	920	1082	85470	No
8	56	162	527	558	839	41831	No
9	161	305	951	989	1084	78790	Yes
10	87	175	576	598	871	45027	No
11	90	196	684	731	1177	49588	No
12	76	188	729	798	1206	48049	No
13	59	159	616	689	1115	39881	No
14	57	169	593	642	1036	43618	No
15	47	128	443	516	802	30065	No
16	43	155	559	642	922	38881	No
17	71	200	656	683	1130	51169	No
18	26	137	418	560	682	31647	No
19	NA	NA	NA	NA	NA	NA	NA
20	NA	NA	NA	NA	NA	NA	NA
Average	81	200	664	717	976	50423	
COV (%)	45	28	22	18	15	30	

BC-2X12-DF



Test #	$\sigma_{0.04-D}$	$\sigma_{0.04-OD}$	$\sigma_{2\%-S}$	$\sigma_{2\%-OS}$	σ_{max}	Slope of Linear Region	Catastrophic Failure
	psi	psi	psi	psi	psi	psi	Yes/No
1	116	179	706	714	851	63564	Yes
2	64	143	671	697	830	49053	Yes
3	35	69	334	344	443	23358	Yes
4	53	160	746	801	980	52974	Yes
5	35	107	539	601	775	33808	Yes
6	106	201	881	902	948	71440	Yes
7	24	55	285	322	479	16637	Yes
8	52	133	647	707	775	44122	Yes
9	51	184	858	887	1113	62424	No
10	50	109	568	595	702	35853	Yes
11	60	173	864	941	1100	56734	Yes
12	81	218	880	919	1071	75777	Yes
13	47	125	510	515	538	37083	Yes
14	51	132	698	761	916	44710	Yes
15	32	90	489	537	731	30030	No
16	43	125	587	602	703	42061	Yes
17	58	124	585	606	763	43840	Yes
18	62	159	757	791	805	55257	Yes
19	129	220	930	932	1248	78506	Yes
20	72	179	813	828	842	62782	Yes
Average	61	144	667	700	831	49001	
COV (%)	46	32	27	26	25	35	

BC-2X12-SPF



Test #	$\sigma_{0.04-D}$	$\sigma_{0.04-OD}$	$\sigma_{2\%-S}$	$\sigma_{2\%-OS}$	σ_{max}	Slope of Linear Region	Catastrophic Failure
	psi	psi	psi	psi	psi	psi	Yes/No
1	69	152	661	678	737	53547	Yes
2	37	100	499	540	693	32960	Yes
3	45	83	423	436	470	28817	Yes
4	11	131	536	613	914	42176	No
5	10	104	489	541	704	36071	Yes
6	90	209	917	947	1062	74018	Yes
7	38	83	402	426	526	26995	Yes
8	88	221	681	670	716	54071	Yes
9	42	156	681	741	1005	49380	Yes
10	40	126	552	569	642	44238	Yes
11	69	174	764	796	965	55855	Yes
12	94	268	1024	1085	1289	92121	Yes
13	43	107	491	511	517	35355	Yes
14	45	153	608	639	924	52852	Yes
15	40	110	489	543	771	36516	No
16	64	147	643	651	711	51678	Yes
17	57	127	651	663	784	42760	Yes
18	35	137	647	725	841	45885	No
19	85	168	760	774	913	59617	Yes
20	98	174	820	843	1035	60468	Yes
Average	55	147	637	670	811	48769	
COV (%)	48	32	25	25	25	32	

BP-DF



Test #	$\sigma_{0.04-D}$	$\sigma_{0.04-OD}$	$\sigma_{2\%-S}$	$\sigma_{2\%-OS}$	σ_{max}	Slope of Linear Region	Catastrophic Failure
	psi	psi	psi	psi	psi	psi	Yes/No
1	675	841	375	782	1843	46048	No
2	197	722	92	591	1225	29630	No
3	96	428	46	344	1030	17022	No
4	149	1264	78	946	1902	47297	No
5	177	731	72	625	1220	32990	No
6	212	1366	67	1272	2387	64590	No
7	93	744	39	600	1287	30383	No
8	72	1171	42	923	2037	46236	No
9	254	707	112	562	1499	28199	No
10	40	698	23	520	1693	26066	No
11	63	541	32	412	1407	20122	No
12	49	730	32	543	1652	27197	No
13	59	644	31	481	1511	24077	No
14	176	738	70	625	1536	31540	No
15	73	610	44	455	1519	22795	No
16	98	669	51	615	1511	33224	No
17	55	667	33	517	1324	25864	No
18	58	630	78	796	1668	48142	No
19	194	662	110	516	1836	25350	No
20	212	859	111	707	1533	35149	No
Average	150	771	77	642	1581	33096	
COV (%)	94	31	99	34	20	35	

BP-SPF



Test #	$\sigma_{0.04-D}$	$\sigma_{0.04-OD}$	$\sigma_{2\%-S}$	$\sigma_{2\%-OS}$	σ_{max}	Slope of Linear Region	Catastrophic Failure
	psi	psi	psi	psi	psi	psi	Yes/No
1	199	460	94	369	1226	18573	No
2	306	556	161	443	1177	22488	No
3	19	525	11	415	1073	20741	No
4	11	571	8	459	1175	23419	No
5	350	538	216	416	1163	20625	No
6	335	649	142	545	1236	29734	No
7	447	740	219	628	1336	34401	No
8	177	827	69	665	1503	33635	No
9	381	710	156	632	1444	35296	No
10	294	632	139	505	1281	25058	No
Average	252	621	122	508	1261	26397	
COV (%)	59	18	62	21	11	24	

ASTM-2X4-DF



Board #	$\sigma_{0.04-D}$	$\sigma_{0.04-OD}$	$\sigma_{2\%-S}$	$\sigma_{2\%-OS}$	Slope of Linear Region	Catastrophic Failure
	psi	psi	psi	psi	psi	Yes/No
1	591	779	403	573	29161	No
2	738	800	584	721	40598	No
3	561	632	402	569	31600	No
4	1183	1252	900	1148	65315	No
5	1020	1072	851	955	57337	No
6	1373	1481	1297	1384	107296	No
7	860	916	733	868	57093	No
8	1121	1518	642	1360	72913	No
9	885	921	697	890	56633	No
10	1057	1112	871	1005	56335	No
11	915	931	752	827	43103	No
12	860	913	651	846	45959	No
13	1010	1042	911	950	60543	No
14	813	899	607	706	36040	No
15	1055	1141	868	1006	61908	No
16	764	788	660	718	41430	No
17	1004	1100	768	907	46974	No
18	1077	1130	968	1066	78177	No
19	1358	1565	977	1323	69821	No
20	1034	1070	940	1005	67715	No
Average	964	1053	774	941	56298	
COV (%)	22	24	27	25	33	

ASTM-2X4-SPF



Board #	$\sigma_{0.04-D}$	$\sigma_{0.04-OD}$	$\sigma_{2\%-S}$	$\sigma_{2\%-OS}$	Slope of Linear Region	Catastrophic Failure
	psi	psi	psi	psi	psi	Yes/No
1	728	766	591	643	40459	No
2	795	882	567	805	47792	No
3	671	941	331	872	52959	No
4	877	925	729	879	61218	No
5	640	854	402	733	40374	No
6	779	858	590	749	39772	No
7	858	912	774	863	70004	No
8	1089	1105	1031	1077	81270	No
9	863	906	786	849	73053	No
10	1068	1117	924	1046	70595	No
Average	837	927	673	852	57750	
COV (%)	18	12	33	16	27	

ASTM-2X8-DF



Board #	$\sigma_{0.04-D}$	$\sigma_{0.04-OD}$	$\sigma_{2\%-S}$	$\sigma_{2\%-OS}$	Slope of Linear Region	Catastrophic Failure
	psi	psi	psi	psi	psi	Yes/No
1	947	1353	532	1165	61625	No
2	1237	1629	798	1297	64964	No
3	701	822	500	688	36358	No
4	1124	1172	853	1094	60385	No
5	1043	1301	642	1220	63151	No
6	1245	1567	699	1439	92253	No
7	1595	1930	1085	1635	85840	No
8	575	651	432	559	30296	No
9	1141	1316	719	1203	76424	No
10	454	794	271	583	29229	No
11	1316	1456	933	1325	71849	No
12	725	964	443	828	43728	No
13	897	1380	526	1091	54653	No
14	962	1018	748	951	51433	No
15	686	795	498	703	40849	No
16	226	627	91	485	24298	No
17	821	1018	588	795	41197	No
18	721	784	577	719	41966	No
19	1048	1143	766	1007	52466	No
20	972	1344	586	1111	56281	No
Average	922	1153	614	995	53962	
COV (%)	35	31	37	32	34	

ASTM-2X12-DF



Board #	$\sigma_{0.04-D}$	$\sigma_{0.04-OD}$	$\sigma_{2\%-S}$	$\sigma_{2\%-OS}$	Slope of Linear Region	Catastrophic Failure
	psi	psi	psi	psi	psi	Yes/No
1	846	1025	575	847	43609	No
2	429	1018	256	865	43503	No
3	175	395	111	295	14810	No
4	519	1192	226	1016	50065	No
5	397	1002	198	817	40939	No
6	697	1045	391	775	38689	No
7	346	375	268	306	16369	No
8	758	926	494	793	41081	No
9	1281	1343	1130	1264	79400	No
10	766	790	646	730	39288	No
11	852	1172	531	975	49512	No
12	1102	1585	601	1405	72178	No
13	1129	1218	855	1043	54236	No
14	1014	1780	605	1329	66343	No
15	690	811	478	704	38740	No
16	845	915	593	807	41101	No
17	661	753	489	616	32109	No
18	833	866	733	804	49555	No
19	1031	1037	893	972	54138	No
20	1518	1704	1111	1451	75092	No
Average	794	1048	559	891	47038	
COV (%)	42	35	51	35	36	

7.5 APPENDIX E: MEMBER PROPERTIES

BC-2X4-DF (B.C. 2X4 Members)

Board #	Rings/ln.	L.W.	Ring Angle w/ Respect to Load	M.C.	S.G.	M.O.E.
		%	Degrees	%		X 10 ⁶ psi
1	16	40	0	11.5	0.56	2.55
2	4	20	20	12.1	0.41	1.64
3	5	20	0	11.7	0.32	1.21
4	3.5	25	80	11.3	0.43	1.19
5	4.5	25	0	12.0	0.38	1.3
6	8	35	10	10.9	0.53	2.04
7	9.5	25	0	11.9	0.42	1.92
8	9	30	90	11.7	0.53	2.24
9	12	35	45	10.9	0.53	2.72
10	3.5	20	90	10.8	0.43	1.42
11	6.5	25	0	11.5	0.47	2
12	10	40	0	11.1	0.47	2.09
13	3	20	10	11.5	0.44	1.72
14	15	40	0	11.1	0.51	2.3
15	4	35	20	10.9	0.45	2.18
16	8.5	35	0	11.8	0.53	2.44
17	3.5	25	30	11.4	0.42	1.57
18	5.5	35	0	10.4	0.46	1.79
19	4.5	35	90	10.8	0.46	1.35
20	4	15	0	11.1	0.38	NA
Average	7	29	24	11.3	0.46	1.88
COV (%)	56	27	143	4	13	25

BC-2X4-DF (T.P. 2X4 Members)

Board #	Rings/In.	L.W.	Ring Angle w/ Respect to Load	M.C.	S.G.	M.O.E.
		%	Degrees	%		X 10 ⁶ psi
1T	15	40	90	11.3	0.55	2.55
1B	12	35	90	9.7	0.53	2.55
2T	3.5	25	30	11.0	0.42	1.64
2B	3.5	20	30	10.6	0.41	1.64
3T	4	25	90	9.9	0.32	1.21
3B	5	25	90	9.7	0.31	1.21
4T	3	15	0	10.6	0.40	1.19
4B	3	15	0	10.3	0.39	1.19
5T	3.5	20	90	11.3	0.42	1.3
5B	4	20	90	10.2	0.39	1.3
6T	9.5	35	90	10.2	0.53	2.04
6B	9	35	80	10.3	0.52	2.04
7T	11	35	90	10.2	0.43	1.92
7B	10	35	90	9.9	0.43	1.92
8T	9.5	35	0	10.0	0.54	2.24
8B	9.5	35	0	9.8	0.54	2.24
9T	14	35	45	9.7	0.53	2.72
9B	16.5	35	45	10.9	0.53	2.72
10T	4	15	0	10.3	0.39	1.42
10B	3.5	15	0	10.2	0.43	1.42
11T	6	25	90	11.2	0.45	2
11B	6	25	90	9.5	0.44	2
12T	10.5	35	90	9.8	0.46	2.09
12B	10.5	35	90	10.0	0.47	2.09
13T	3.5	20	90	10.3	0.47	1.72
13B	3	20	90	10.4	0.44	1.72
14T	13	35	90	10.6	0.50	2.3
14B	12	35	90	9.8	0.51	2.3
15T	4	30	30	12.6	0.46	2.18
15B	4	35	30	11.2	0.45	2.18
16T	9.5	30	90	11.8	0.53	2.44
16B	9.5	30	90	12.9	0.52	2.44
17T	4.5	25	45	11.5	0.40	1.57
17B	4	20	30	12.4	0.40	1.57
18T	5.5	25	90	12.6	0.43	1.79
18B	5.5	30	90	11.7	0.44	1.79
19T	5.5	20	0	11.5	0.47	1.35
19B	5	20	0	11.7	0.47	1.35
20T	3.5	15	90	12.9	0.39	NA
20B	3.5	15	80	12.3	0.37	NA
Average	7	27	61	11	0.45	1.88
COV (%)	55	29	62	9	13	24

BC-2X4-SPF (B.C. 2X4 Members)

Board #	Rings/In.	L.W.	Ring Angle w/ Respect to Load	M.C.	S.G.	M.O.E.
		%	Degrees	%		X 10 ⁶ psi
1	16	40	0	11.1	0.55	2.55
2	4	20	30	11.4	0.41	1.64
3	5	33	10	11.2	0.32	1.21
4	2	15	0	10.4	0.44	1.19
5	5	20	0	11.1	0.39	1.3
6	9	33	10	10.0	0.55	2.04
7	15	33	0	10.4	0.44	1.92
8	9	40	90	10.4	0.53	2.24
9	12	40	45	10.4	0.53	2.72
10	4	30	90	10.1	0.41	1.42
11	6	33	0	11.5	0.44	2
12	10	25	0	10.9	0.48	2.09
13	3	20	0	10.9	0.47	1.72
14	16	40	0	11.0	0.51	2.3
15	4	30	20	10.9	0.45	2.18
16	10	40	0	11.1	0.54	2.44
17	3	20	45	11.0	0.43	1.57
18	5	30	0	10.1	0.46	1.79
19	5.5	25	90	10.8	0.49	1.35
20	4	20	20	12.3	0.39	NA
Average	7	29	23	10.9	0.46	1.88
COV (%)	61	28	145	5	13	25

BC-2X4-SPF (T.P. 2X4 Members)



Board #	Rings/In.	L.W.	Ring Angle w/ Respect to Load	M.C.	G	M.O.E.
		%	Degrees	%		X 10 ⁶ psi
1T	7	33	0	14.6	0.36	1.43
1B	8	25	0	14.4	0.38	1.43
2T	5.5	20	90	14.0	0.36	1.15
2B	5.5	25	80	13.8	0.33	1.15
3T	7	25	90	15.4	0.35	1.17
3B	6.5	20	90	14.1	0.35	1.17
4T	7	25	90	14.4	0.36	1.29
4B	6.5	35	90	13.5	0.37	1.29
5T	7	35	70	13.9	0.36	1.32
5B	7	35	70	13.3	0.36	1.32
6T	8	25	90	12.6	0.40	1.42
6B	6	30	90	14.1	0.36	1.42
7T	12	30	0	12.2	0.39	1.48
7B	12	30	0	13.6	0.38	1.48
8T	7	25	90	12.1	0.39	1.01
8B	5.5	25	90	14.0	0.41	1.01
9T	12	35	90	15.1	0.38	1.48
9B	12	35	90	14.6	0.41	1.48
10T	19	40	0	14.4	0.35	0.64
10B	18	40	0	13.5	0.37	0.64
11T	6	33	90	14.2	0.33	1.05
11B	7	25	90	13.5	0.35	1.05
12T	9	35	0	14.6	0.40	0.978
12B	11	35	0	14.4	0.39	0.978
13T	7	30	0	13.9	0.35	1.44
13B	7.5	20	0	13.5	0.36	1.44
14T	8	25	0	15.8	0.31	1.22
14B	8	20	0	13.6	0.33	1.22
15T	5.5	25	0	11.6	0.36	1.18
15B	5	20	0	13.7	0.35	1.18
16T	5	20	0	13.8	0.33	0.956
16B	5	20	0	13.5	0.33	0.956
17T	7	20	0	13.7	0.35	1.4
17B	7.5	20	0	14.1	0.35	1.4
18T	9	20	0	14.0	0.35	0.683
18B	11	25	0	13.6	0.34	0.683
19T	5.5	20	90	13.5	0.36	1
19B	7	20	90	14.4	0.37	1
20T	6.5	20	90	13.9	0.36	1.1
20B	6.5	20	90	14.3	0.37	1.1
Average	8	27	44	14	0.36	1.17
COV (%)	39	24	102	6	6	21

BC-2X8-DF (B.C. 2X8 Members)

Board #	Rings/ In.	L.W.	Ring Angle w/ Respect to Load			M.C. %	S.G.	M.O.E. X 10 ⁶ psi
			Top	Middle	Bottom			
1	8	35	80	0	90	10.8	0.46	2.11
2	8	15	80	0	90	10.0	0.54	1.75
3	3.5	25	20	20	40	10.9	0.47	1.91
4	3	15	45	0	10	9.6	0.44	1.3
5	3.5	25	10	0	10	9.6	0.47	1.75
6	5	15	10	10	20	11.0	0.42	1.49
7	7	25	90	0	90	10.9	0.52	1.56
8	3	20	30	20	45	10.3	0.37	1.54
9	7.5	35	0	20	20	11.6	0.54	1.07
10	4	35	80	20	30	10.2	0.48	1.13
11	4.5	30	10	10	20	10.5	0.45	1.29
12	5.5	35	45	10	30	10.4	0.55	2.22
13	5.5	20	20	20	70	10.0	0.47	1.6
14	4	30	45	10	30	11.6	0.48	1.88
15	8.5	35	30	0	30	12.5	0.50	2
16	3.5	20	60	10	80	10.4	0.38	1.3
17	6.5	60	60	0	60	11.6	0.66	2.3
18	5.5	25	40	0	40	1.1	0.51	2.06
19	4.5	25	90	0	90	10.2	0.37	1.52
20	4.5	25	80	0	80	10.1	0.41	1.48
Average	5	28	46	8	49	10.2	0.47	1.66
COV (%)	34	38	64	113	60	22	15	22

BC-2X8-DF (T.P. 2X4 Members)

Board #	Rings/ In.	L.W.	Ring Angle w/ Respect to Load	M.C.	S.G.	M.O.E.
		%	Degrees	%		X 10 ⁶ psi
1T	11	35	90	11.6	0.53	2.55
1B	14	30	90	12.2	0.54	2.55
2T	3.5	25	45	12.1	0.41	1.64
2B	3.5	30	45	10.4	0.42	1.64
3T	4.5	25	90	12.7	0.30	1.21
3B	4	25	90	12.9	0.33	1.21
4T	3	20	45	11.5	0.48	1.19
4B	3	20	0	12.7	0.39	1.19
5T	4	30	0	12.4	0.38	1.3
5B	4	30	0	13.3	0.38	1.3
6T	8	30	90	10.4	0.52	2.04
6B	9	30	90	10.6	0.53	2.04
7T	11.5	35	0	11.1	0.44	1.92
7B	12	35	0	11.3	0.42	1.92
8T	10	30	0	12.0	0.52	2.24
8B	10	25	0	11.0	0.52	2.24
9T	13	35	45	10.8	0.53	2.72
9B	13	35	45	11.1	0.53	2.72
10T	3.5	20	0	10.7	0.39	1.42
10B	3.5	20	0	11.2	0.39	1.42
11T	6.5	20	90	11.7	0.44	2
11B	6.5	20	90	11.0	0.44	2
12T	10	20	90	12.5	0.45	2.09
12B	10	20	90	12.5	0.46	2.09
13T	3.5	20	80	11.5	0.45	1.72
13B	3	20	80	11.2	0.44	1.72
14T	10	25	90	11.3	0.48	2.3
14B	11	25	90	11.8	0.52	2.3
15T	4	25	45	11.5	0.44	2.18
15B	4.5	25	45	12.0	0.45	2.18
16T	9.5	35	90	12.2	0.55	2.44
16B	9	35	90	12.4	0.50	2.44
17T	4.5	25	45	11.7	0.39	1.57
17B	4	25	45	12.2	0.39	1.57
18T	5.5	25	90	15.3	0.45	1.79
18B	5.5	25	90	12.4	0.45	1.79
19T	5	20	0	12.0	0.46	1.35
19B	5	20	0	11.7	0.46	1.35
20T	3.5	15	90	11.7	0.38	NA
20B	3.5	15	90	11.8	0.37	NA
Average	7	26	55	12	0.45	1.88
COV (%)	51	23	70	8	14	24

BC-2X8-SPF (B.C. 2X8 Members)

Board #	Rings/ In.	L.W. %	Ring Angle w/ Respect to Load (Degrees)			M.C. %	S.G.	M.O.E. X 10 ⁶ psi
			Top	Middle	Bottom			
1	8	30	80	0	90	9.7	0.47	2.11
2	8.5	25	20	0	20	10.1	0.51	1.75
3	3.5	20	10	10	40	10.8	0.47	1.91
4	3	25	10	10	40	9.0	0.44	1.3
5	4.5	20	30	10	10	9.9	0.44	1.75
6	5	15	20	10	10	10.1	0.43	1.49
7	9	30	80	0	90	10.8	0.52	1.56
8	3	20	60	10	45	9.9	0.38	1.54
9	8	35	20	20	0	10.1	0.54	1.07
10	4	35	30	20	70	10.2	0.48	1.13
11	4	25	10	10	45	10.7	0.46	1.29
12	5.5	35	45	10	30	9.9	0.56	2.22
13	4	35	90	20	80	8.5	0.54	1.6
14	5	25	45	0	45	10.4	0.47	1.88
15	9	35	30	0	45	11.1	0.51	2
16	3	25	80	0	80	9.4	0.47	1.3
17	7	70	60	0	30	10.3	0.66	2.3
18	6.5	20	40	10	45	10.0	0.48	2.06
19	6	20	90	0	90	10.6	0.37	1.52
20	5.5	20	80	0	80	9.6	0.41	1.48
Average	6	28	47	7	49	10.1	0.48	1.66
COV (%)	37	42	62	105	58	6	14	22



BC-2X8-SPF (T.P. 2X4 Members)



Board #	Rings/ In.	L.W.	Ring < w/ Respect to Load	M.C.	S.G.	M.O.E.
		%	Degrees	%		X 10 ⁶ psi
1T	9	25	90	13.5	0.30	1.43
1B	7	25	90	14.0	0.37	1.43
2T	6	15	0	14.1	0.34	1.15
2B	5.5	15	0	14.9	0.33	1.15
3T	7.5	20	0	16.9	0.34	1.17
3B	7	20	0	15.2	0.35	1.17
4T	7.5	20	0	14.5	0.36	1.29
4B	7.5	20	0	15.0	0.37	1.29
5T	6.5	25	0	14.9	0.39	1.32
5B	7	25	0	12.7	0.37	1.32
6T	7.5	25	0	15.6	0.37	1.42
6B	7	20	0	14.3	0.37	1.42
7T	10	30	0	14.1	0.39	1.48
7B	10	25	0	13.9	0.38	1.48
8T	6.5	30	0	14.3	0.41	1.01
8B	7.5	25	0	16.1	0.40	1.01
9T	10	30	0	14.9	0.39	1.48
9B	10	35	0	16.8	0.38	1.48
10T	22	45	0	15.6	0.33	0.64
10B	22	45	0	15.7	0.36	0.64
11T	6.5	25	0	14.9	0.35	1.05
11B	6	25	0	15.6	0.32	1.05
12T	11	35	0	15.5	0.40	0.978
12B	12	35	0	14.6	0.39	0.978
13T	7.5	25	0	14.9	0.35	1.44
13B	8	25	0	16.8	0.36	1.44
14T	8	15	0	14.8	0.32	1.22
14B	8	15	0	14.4	0.31	1.22
15T	5.5	15	0	13.1	0.37	1.18
15B	5.5	15	0	13.0	0.36	1.18
16T	5.5	10	0	12.9	0.34	0.956
16B	5	10	0	13.6	0.35	0.956
17T	7.5	15	0	15.2	0.35	1.4
17B	8	20	0	15.3	0.34	1.4
18T	10	20	0	15.9	0.31	0.683
18B	11	20	0	15.5	0.35	0.683
19T	6.5	15	0	14.0	0.39	1
19B	7	15	0	15.5	0.36	1
20T	6.5	15	0	15.0	0.37	1.1
20B	5.5	15	0	15.1	0.38	1.1
Average	8	23	5	15	0.36	1.17
COV (%)	43	37	441	7	7	21

BC-2X12-DF (B.C. 2X12 Members)

Board #	Rings/ In.	L.W.	Ring Angle w/ Respect to Load (Degrees)			M.C.	S.G.	M.O.E.
			Top	Middle	Bottom			
		%						
1	5	30	45	0	45	10.4	0.49	1.51
2	7	25	60	10	45	10.4	0.45	1.6
3	3.5	15	40	10	60	11.1	0.36	1.02
4	3.5	30	30	0	30	10.4	0.43	1.23
5	4.5	35	30	0	45	10.0	0.44	1.13
6	3.5	25	10	10	30	11.2	0.43	1.18
7	4	15	45	0	45	11.1	0.34	1.17
8	6	35	45	10	40	9.7	0.47	1.74
9	7	40	30	0	40	11.7	0.52	1.69
10	5	30	30	0	30	9.7	0.44	1.45
11	5	35	20	10	30	10.8	0.51	1.82
12	5	30	20	20	30	9.7	0.45	1.29
13	5	20	45	0	60	10.6	0.43	1.28
14	7	30	50	0	30	11.6	0.58	2.11
15	4.5	35	60	10	45	10.1	0.48	2.11
16	9	30	30	10	30	11.0	0.47	1.73
17	5	30	40	0	40	10.6	0.47	1.88
18	6	35	20	10	30	10.4	0.45	1.8
19	5	30	45	0	45	10.6	0.48	1.45
20	7	35	80	80	80	10.8	0.55	1.21
Average	5	30	39	9	42	10.6	0.46	1.52
COV (%)	27	23	43	197	32	6	12	22

BC-2X12-DF (T.P. 2X4 Members)

Board #	Rings/ In.	L.W.	Ring Angle w/ Respect to Load	M.C.	S.G.	M.O.E.
		%	Degrees	%		X 10 ⁶ psi
1T	14	35	90	11.5	0.55	2.55
1B	13.5	35	90	10.6	0.55	2.55
2T	4	20	60	11.5	0.40	1.64
2B	3.5	25	60	10.8	0.48	1.64
3T	4.5	20	90	12.1	0.30	1.21
3B	4	20	90	11.4	0.31	1.21
4T	3	25	70	12.1	0.49	1.19
4B	3	25	70	11.1	0.44	1.19
5T	4	25	0	12.8	0.38	1.3
5B	4	25	0	13.0	0.37	1.3
6T	8	30	90	12.0	0.51	2.04
6B	9	35	90	11.6	0.53	2.04
7T	13	35	0	13.1	0.42	1.92
7B	11.5	35	0	13.4	0.41	1.92
8T	10	25	0	11.8	0.51	2.24
8B	9.5	30	0	11.8	0.49	2.24
9T	18	35	45	11.3	0.52	2.72
9B	17	35	45	10.9	0.53	2.72
10T	3.5	20	0	11.2	0.39	1.42
10B	3.5	20	0	10.8	0.41	1.42
11T	6.5	20	90	12.3	0.44	2
11B	6.5	25	90	11.8	0.47	2
12T	10.5	25	90	12.3	0.45	2.09
12B	11	30	90	11.7	0.49	2.09
13T	3	20	90	10.8	0.44	1.72
13B	3	15	90	11.7	0.46	1.72
14T	11	35	90	11.2	0.47	2.3
14B	10	30	90	11.2	0.50	2.3
15T	3.5	25	45	11.4	0.44	2.18
15B	3.5	25	45	10.8	0.46	2.18
16T	9.5	30	90	11.5	0.52	2.44
16B	9	35	90	12.1	0.51	2.44
17T	3.5	25	45	11.1	0.41	1.57
17B	4.5	20	45	11.6	0.39	1.57
18T	5	20	90	11.7	0.41	1.79
18B	5.5	25	90	11.3	0.44	1.79
19T	5	15	0	11.2	0.48	1.35
19B	5	15	0	10.8	0.52	1.35
20T	4	15	90	11.7	0.37	NA
20B	3.5	10	80	11.7	0.39	NA
Average	7	25	58	12	0.45	1.88
COV (%)	59	27	65	6	14	24

BC-2X12-SPF (B.C. 2X12 Members)

Board #	Rings/ In.	L.W.	Ring Angle w/ Respect to Load (Degrees)			M.C.	S.G.	M.O.E. X 10 ⁶ psi
			Top	Middle	Bottom			
		%						
1	3	30	45	0	45	9.4	0.49	1.51
2	14	35	60	20	45	9.7	0.43	1.6
3	4	30	30	10	45	11.0	0.38	1.02
4	4	30	20	0	45	10.4	0.43	1.23
5	4	30	70	20	70	9.4	0.38	1.13
6	3	25	20	10	35	10.6	0.43	1.18
7	4	20	60	0	45	10.9	0.37	1.17
8	5	30	30	10	45	10.1	0.47	1.74
9	8	40	40	10	20	10.9	0.52	1.69
10	5.5	25	30	0	30	9.6	0.44	1.45
11	6	35	30	20	30	12.1	0.51	1.82
12	5	25	0	10	10	9.1	0.46	1.29
13	4.5	30	45	0	60	9.8	0.45	1.28
14	7	35	60	10	40	9.5	0.60	2.11
15	5	30	50	10	45	9.8	0.46	2.11
16	9	30	20	10	30	11.0	0.49	1.73
17	4	25	40	0	40	9.5	0.48	1.88
18	5.5	35	30	0	30	10.6	0.46	1.8
19	3.5	35	45	0	45	9.3	0.46	1.45
20	6.5	30	80	80	80	10.3	0.52	1.21
Average	6	30	40	11	42	10.1	0.46	1.52
COV (%)	46	16	48	161	38	8	12	22



BC-2X12-SPF (T.P. 2X4 Members)

Board #	Rings/ In.	L.W.	Ring Angle w/ Respect to Load	M.C.	S.G.	M.O.E.
		%	Degrees	%		X 10 ⁶ psi
1T	8	25	90	14	0.37	1.43
1B	8	25	90	16	0.36	1.43
2T	5.5	20	0	17	0.34	1.15
2B	5	20	0	16	0.33	1.15
3T	8.5	25	0	13	0.36	1.17
3B	7	20	0	13	0.36	1.17
4T	7	25	0	14	0.37	1.29
4B	7.5	25	0	14	0.36	1.29
5T	7	20	0	15	0.36	1.32
5B	7.5	25	0	15	0.38	1.32
6T	7	20	0	15	0.36	1.42
6B	6.5	25	0	15	0.37	1.42
7T	12	25	0	15	0.38	1.48
7B	9	20	0	14	0.39	1.48
8T	6	25	0	14	0.41	1.01
8B	7.5	20	0	15	0.39	1.01
9T	12	30	0	14	0.39	1.48
9B	10	30	0	14	0.42	1.48
10T	21	50	0	15	0.35	0.64
10B	21	45	0	14	0.36	0.64
11T	6	20	0	14	0.32	1.05
11B	5.5	20	0	13	0.33	1.05
12T	10.5	20	0	13	0.38	0.978
12B	10.5	25	0	15	0.39	0.978
13T	7.5	25	0	14	0.36	1.44
13B	7.5	25	0	15	0.35	1.44
14T	8	20	0	14	0.31	1.22
14B	7	15	0	15	0.31	1.22
15T	5	15	0	14	0.37	1.18
15B	5	15	0	15	0.38	1.18
16T	5	10	0	14	0.34	0.956
16B	5	15	0	14	0.33	0.956
17T	8	20	0	15	0.34	1.4
17B	8	20	0	15	0.35	1.4
18T	9	15	0	15	0.33	0.683
18B	11	20	0	15	0.33	0.683
19T	5	20	0	15	0.36	1
19B	5.5	20	0	15	0.36	1
20T	6	20	0	13	0.36	1.1
20B	5.5	20	0	14	0.37	1.1
Average	8	23	5	15	0.36	1.17
COV (%)	44	32	441	6	7	21

BP-SPF (B.P. 2X4 Members) ☒

Board #	Rings/In.	L.W.	Ring Angle w/ Respect to Load	M.C.	S.G.	M.O.E.
		%	Degrees	%		X 10 ⁶ psi
1	7	30	90	13.5	0.36	1.43
2	5	25	0	13.8	0.34	1.15
3	6	25	0	13.0	0.37	1.17
4	7	30	0	13.9	0.37	1.29
5	6.5	35	0	14.0	0.36	1.32
6	6.5	35	0	14.6	0.36	1.42
7	6.5	25	0	14.7	0.38	1.48
8	6.5	25	0	14.6	0.42	1.01
9	10	35	0	15.5	0.41	1.48
10	17	25	0	16.2	0.35	0.64
Average	8	29	9	14	0.37	1.24
COV (%)	45	16	316	7	7	21

ASTM-2X4-DF



Board #	Rings/In.	L.W.	Ring Angle w/ Respect to Load	M.C.	S.G.	M.O.E.
		%	Degrees	%		X 10 ⁶ psi
1	15	40	10	11.7	0.54	2.55
2	4	25	35	10.9	0.40	1.64
3	4.5	30	35	11.4	0.32	1.21
4	3	20	45	11.3	0.40	1.19
5	4.5	25	45	11.5	0.38	1.3
6	9.5	40	0	10.7	0.53	2.04
7	10	25	45	11.5	0.41	1.92
8	9	30	45	12.1	0.51	2.24
9	13	35	45	11.2	0.52	2.72
10	3.5	25	0	12.1	0.39	1.42
11	6.5	35	0	12.1	0.43	2
12	9.5	30	10	12.2	0.46	2.09
13	3.5	25	30	12.8	0.44	1.72
14	14	30	45	11.6	0.52	2.3
15	3.5	25	10	11.5	0.43	2.18
16	10.5	35	10	13.0	0.52	2.44
17	4	25	60	14.9	0.42	1.57
18	5	30	30	13.1	0.44	1.79
19	6	25	45	11.4	0.46	1.35
20	3.5	20	20	12.2	0.38	NA
Average	7	29	28	12.0	0.45	1.88
COV (%)	55	20	67	8	14	25

ASTM-2X4-SPF



Board #	Rings/In.	L.W.	Ring Angle w/ Respect to Load	M.C.	S.G.	M.O.E.
		%	Degrees	%		X 10 ⁶ psi
1	9	35	45	13.0	0.36	1.43
2	5.5	20	45	12.2	0.34	1.15
3	6	25	45	13.8	0.36	1.17
4	7	30	0	13.9	0.38	1.29
5	7	25	45	14.0	0.37	1.32
6	7	20	45	14.6	0.37	1.42
7	8	30	45	15.4	0.38	1.48
8	7	30	45	13.6	0.40	1.01
9	11	35	45	14.3	0.40	1.48
10	20	40	0	13.5	0.37	0.64
Average	9	29	36	14	0.37	1.24
COV (%)	49	23	53	6	5	21

ASTM-2X8-DF



Board #	Rings/In.	L.W.	Ring Angle w/ Respect to Load	M.C.	S.G.	M.O.E.
		%	Degrees	%		X 10 ⁶ psi
1	8	40	0	11.8	0.51	2.11
2	8	30	30	12.7	0.54	1.75
3	4	25	60	11.8	0.44	1.91
4	4	25	30	9.7	0.43	1.3
5	4	25	90	9.9	0.45	1.75
6	5	20	90	10.0	0.41	1.49
7	7.5	30	0	11.5	0.55	1.56
8	3	20	30	11.8	0.39	1.54
9	6.5	35	90	11.0	0.52	1.07
10	4	35	60	11.9	0.50	1.13
11	3	15	10	11.6	0.43	1.29
12	7	35	30	11.0	0.56	2.22
13	6	35	20	9.6	0.49	1.6
14	4	35	70	13.6	0.49	1.88
15	7.5	40	60	12.5	0.52	2
16	3	25	10	10.3	0.36	1.3
17	7	50	45	12.7	0.61	2.3
18	6.5	30	60	10.8	0.53	2.06
19	5	30	0	12.4	0.38	1.52
20	4.5	30	0	12.0	0.41	1.48
Average	5	31	39	11.4	0.48	1.66
COV (%)	33	27	81	10	14	22

ASTM-2X12-DF

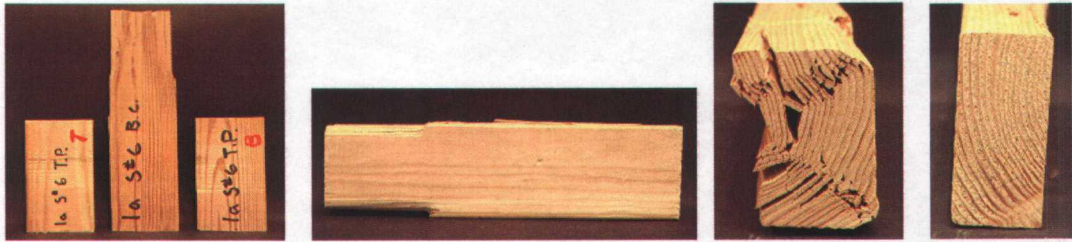


Board #	Rings/In.	L.W.	Ring Angle w/ Respect to Load	M.C.	S.G.	M.O.E.
		%	Degrees	%		X 10 ⁶ psi
1	4.5	30	60	10.6	0.49	1.51
2	16	35	20	11.6	0.46	1.6
3	5	25	60	13.4	0.37	1.02
4	3	20	50	12.5	0.46	1.23
5	4	35	45	11.6	0.46	1.13
6	4.5	15	80	12.9	0.43	1.18
7	4	30	60	13.9	0.33	1.17
8	6.5	35	50	11.5	0.46	1.74
9	5	25	80	13.5	0.47	1.69
10	5.5	35	60	11.3	0.45	1.45
11	4	40	80	12.8	0.53	1.82
12	6	25	0	9.5	0.44	1.29
13	5	60	45	10.8	0.57	1.28
14	6.5	40	45	10.9	0.63	2.11
15	6.5	35	45	12.8	0.50	2.11
16	8	35	70	11.2	0.50	1.73
17	7.5	35	60	12.9	0.44	1.88
18	6	35	60	12.8	0.44	1.8
19	6.5	30	50	11.3	0.47	1.45
20	6.5	35	10	11.7	0.49	1.21
Average	6	33	52	12.0	0.47	1.52
COV (%)	44	28	42	10	14	22

7.6 APPENDIX F: COMPRESSION DAMAGE PICTURES

BC-2X4-DF T#1BC-2X4-DF T#2BC-2X4-DF T#3BC-2X4-DF T#4BC-2X4-DF T#5

BC-2X4-DF T#6



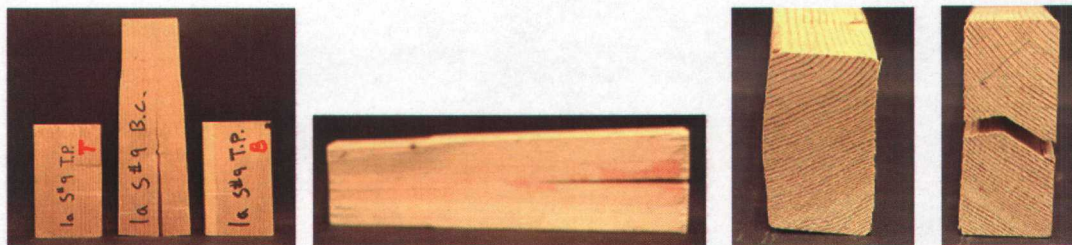
BC-2X4-DF T#7



BC-2X4-DF T#8

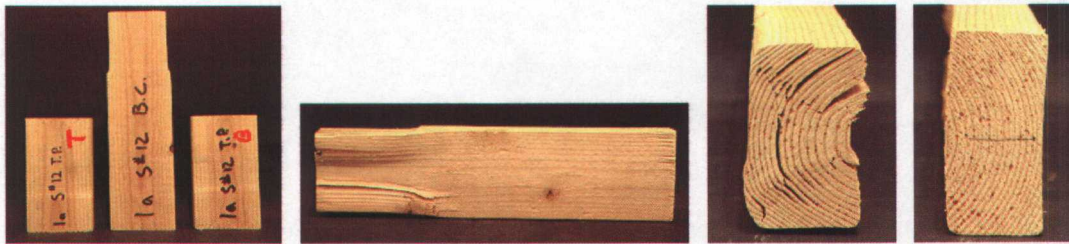
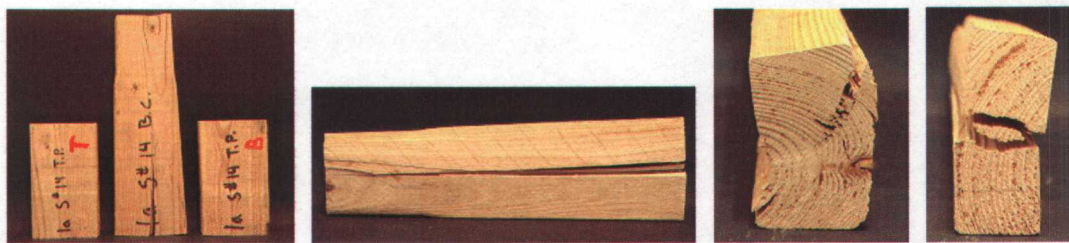


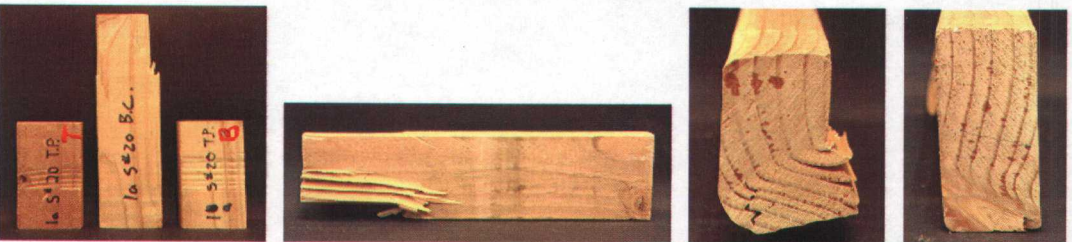
BC-2X4-DF T#9



BC-2X4-DF T#10



BC-2X4-DF T#11BC-2X4-DF T#12BC-2X4-DF T#13BC-2X4-DF T#14BC-2X4-DF T#15

BC-2X4-DF T#16BC-2X4-DF T#17BC-2X4-DF T#18BC-2X4-DF T#19BC-2X4-DF T#20

BC-2X4-SPF T#1



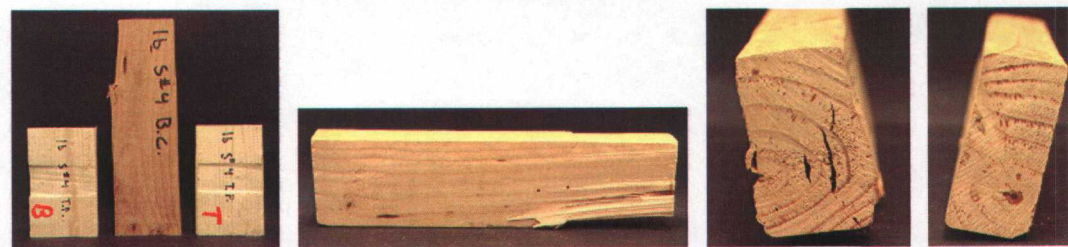
BC-2X4-SPF T#2



BC-2X4-SPF T#3

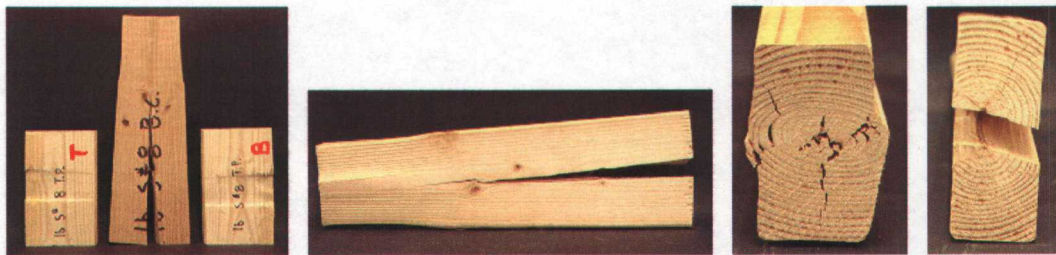


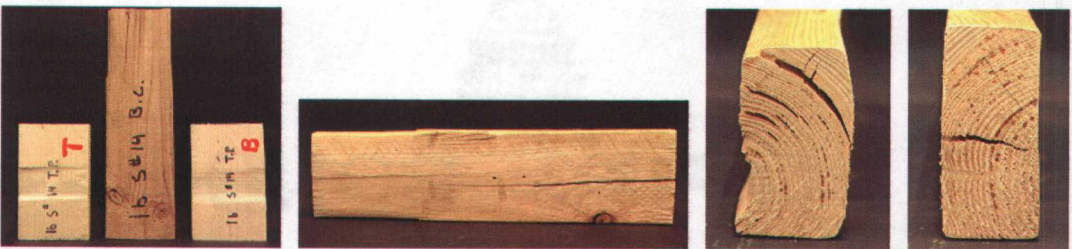
BC-2X4-SPF T#4



BC-2X4-SPF T#5



BC-2X4-SPF T#6BC-2X4-SPF T#7BC-2X4-SPF T#8BC-2X4-SPF T#9BC-2X4-SPF T#10

BC-2X4-SPF T#11BC-2X4-SPF T#12BC-2X4-SPF T#13BC-2X4-SPF T#14BC-2X4-SPF T#15

BC-2X4-SPF T#16



BC-2X4-SPF T#17



BC-2X4-SPF T#18



BC-2X4-SPF T#19



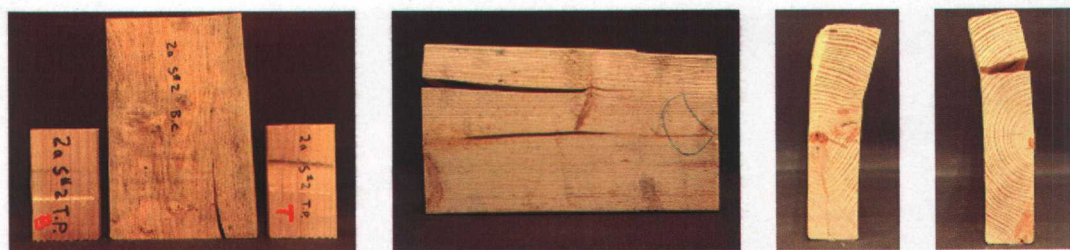
BC-2X4-SPF T#20



BC-2X8-DF T#1



BC-2X8-DF T#2



BC-2X8-DF T#3



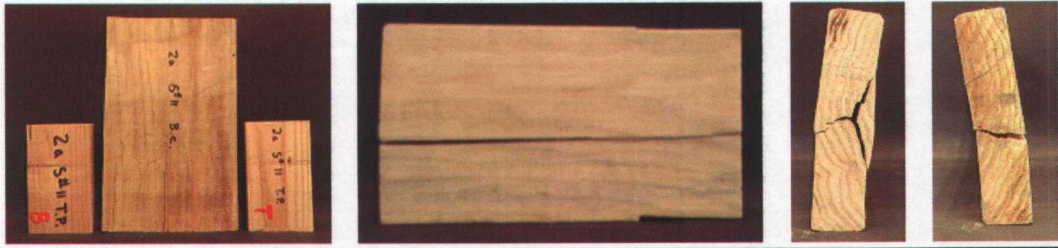
BC-2X8-DF T#4



BC-2X8-DF T#5



BC-2X8-DF T#6BC-2X8-DF T#7BC-2X8-DF T#8BC-2X8-DF T#9BC-2X8-DF T#10

BC-2X8-DF T#11BC-2X8-DF T#12BC-2X8-DF T#13 (Note: Failure post 10% strain)BC-2X8-DF T#14BC-2X8-DF T#15

BC-2X8-DF T#16



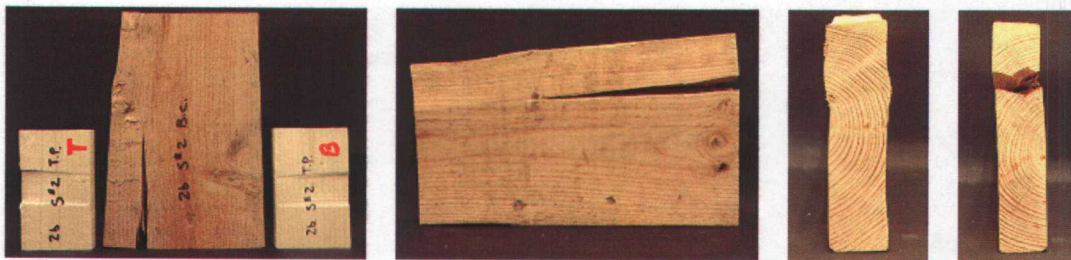
BC-2X8-DF T#17



BC-2X8-SPF T#1



BC-2X8-SPF T#2



BC-2X8-SPF T#3



BC-2X8-SPF T#4



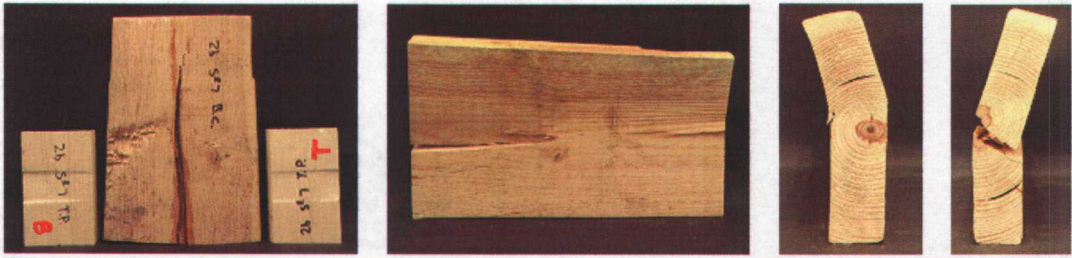
BC-2X8-SPF T#5



BC-2X8-SPF T#6



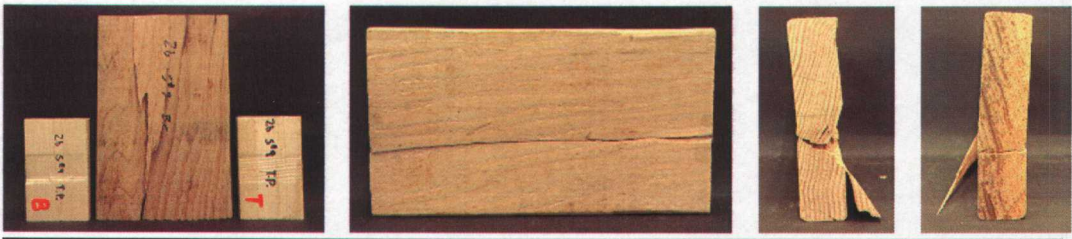
BC-2X8-SPF T#7



BC-2X8-SPF T#8

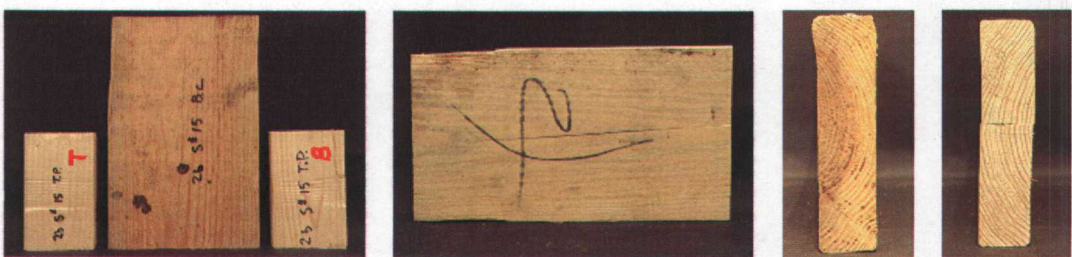


BC-2X8-SPF T#9



BC-2X8-SPF T#10



BC-2X8-SPF T#11BC-2X8-SPF T#12BC-2X8-SPF T#13BC-2X8-SPF T#14BC-2X8-SPF T#15

BC-2X8-SPF T#16



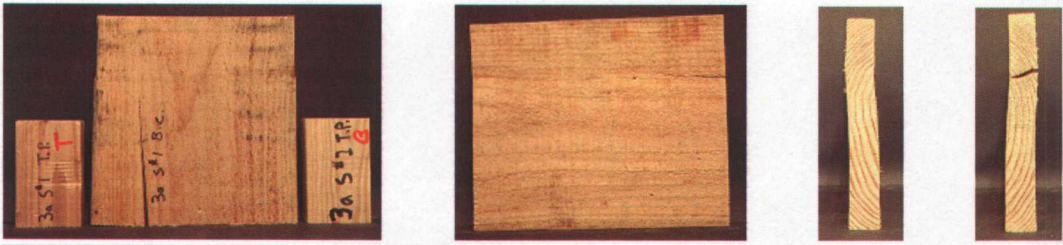
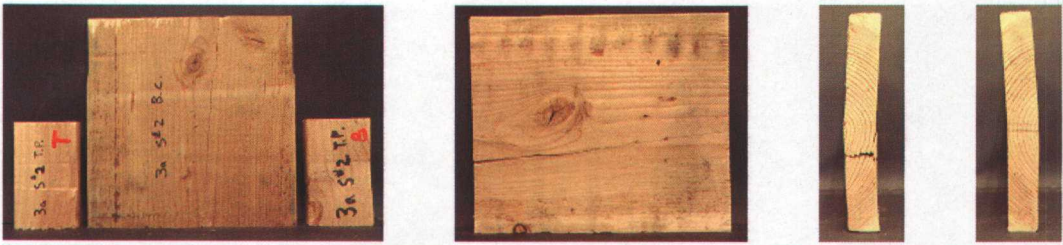
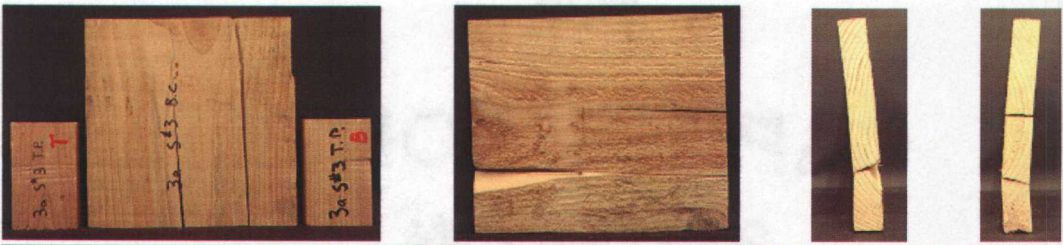
BC-2X8-SPF T#17



BC-2X8-SPF T#18



CARROLL BOND
COTTON

BC-2X12-DF T#1BC-2X12-DF T#2BC-2X12-DF T#3BC-2X12-DF T#4BC-2X12-DF T#5

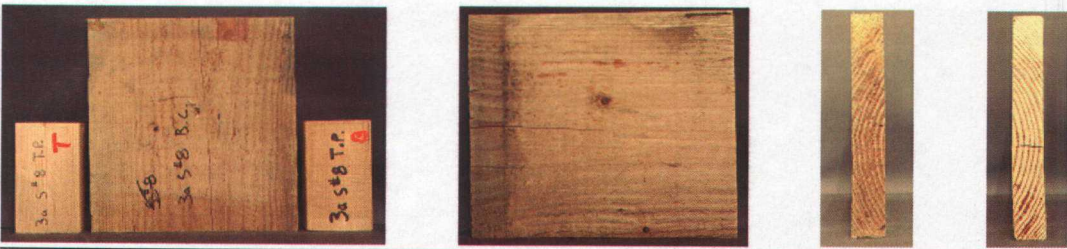
BC-2X12-DF T#6



BC-2X12-DF T#7



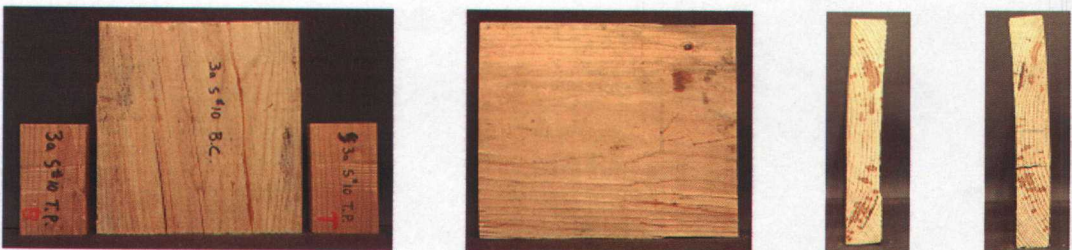
BC-2X12-DF T#8



BC-2X12-DF T#9



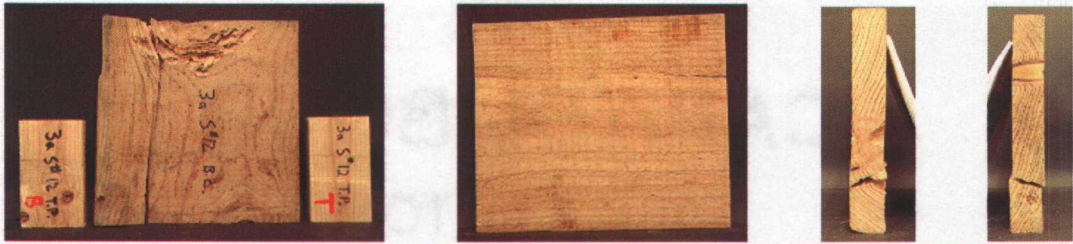
BC-2X12-DF T#10



BC-2X12-DF T#11



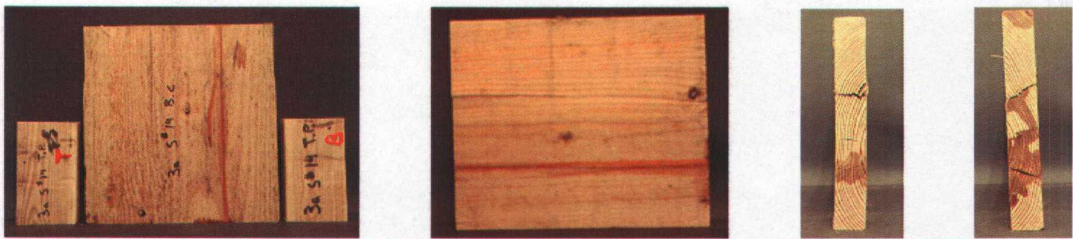
BC-2X12-DF T#12



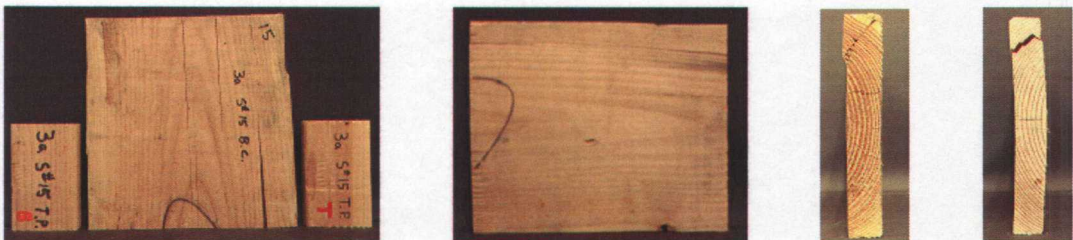
BC-2X12-DF T#13



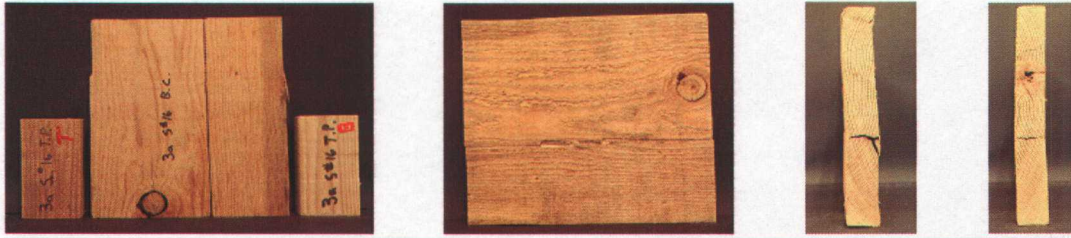
BC-2X12-DF T#14



BC-2X12-DF T#15



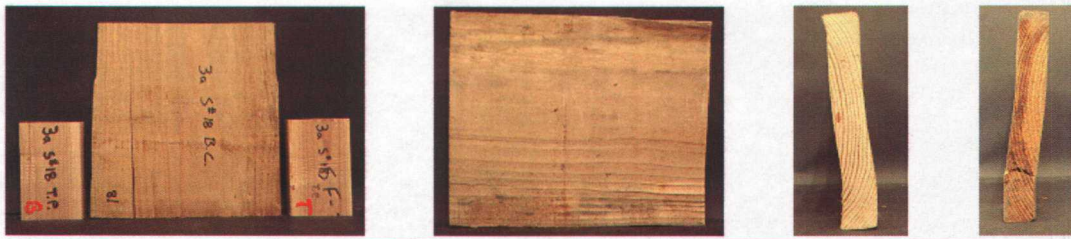
BC-2X12-DF T#16



BC-2X12-DF T#17



BC-2X12-DF T#18

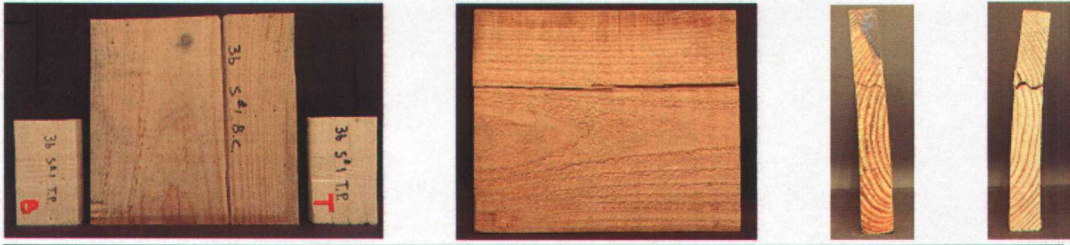
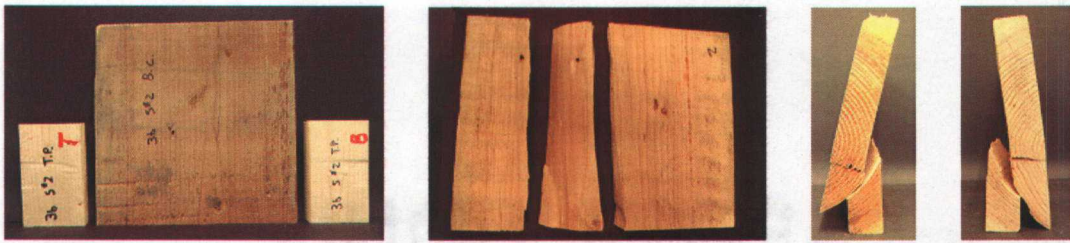
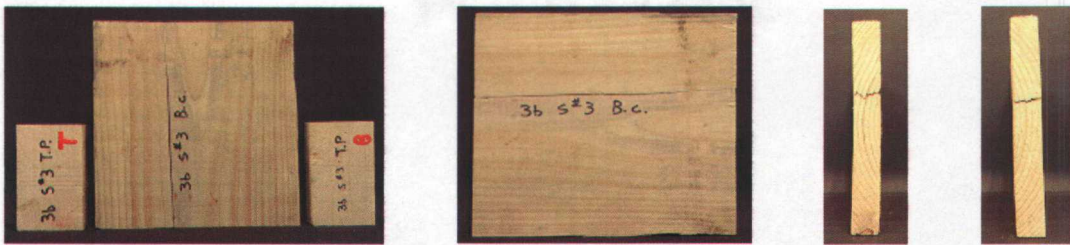
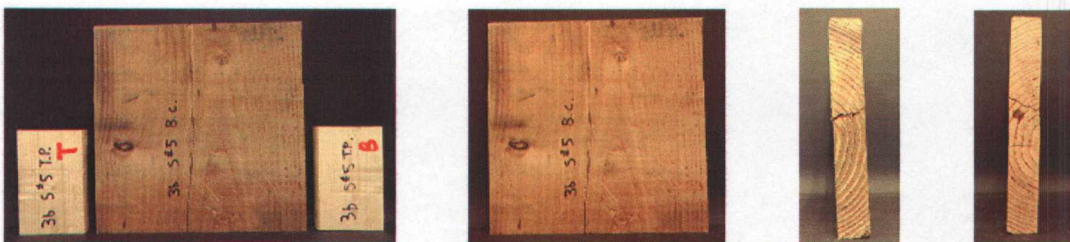


BC-2X12-DF T#19



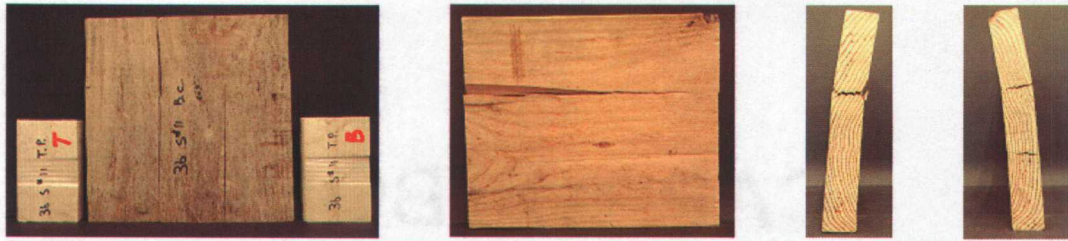
BC-2X12-DF T#20



BC-2X12-SPF T#1BC-2X12-SPF T#2BC-2X12-SPF T#3BC-2X12-SPF T#4BC-2X12-SPF T#5

BC-2X12-SPF T#6BC-2X12-SPF T#7BC-2X12-SPF T#8BC-2X12-SPF T#9BC-2X12-SPF T#10

BC-2X12-SPF T#11



BC-2X12-SPF T#12



BC-2X12-SPF T#13



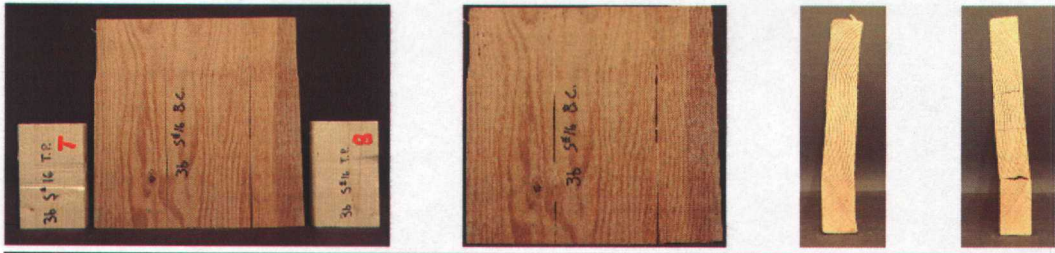
BC-2X12-SPF T#14



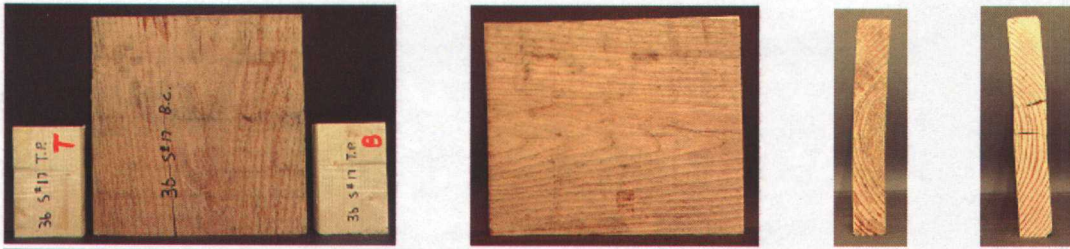
BC-2X12-SPF T#15



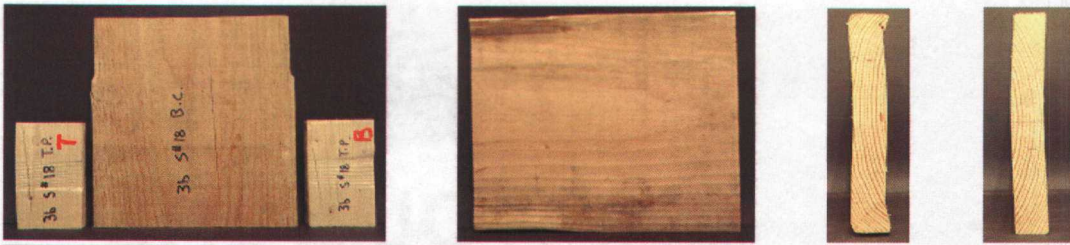
BC-2X12-SPF T#16



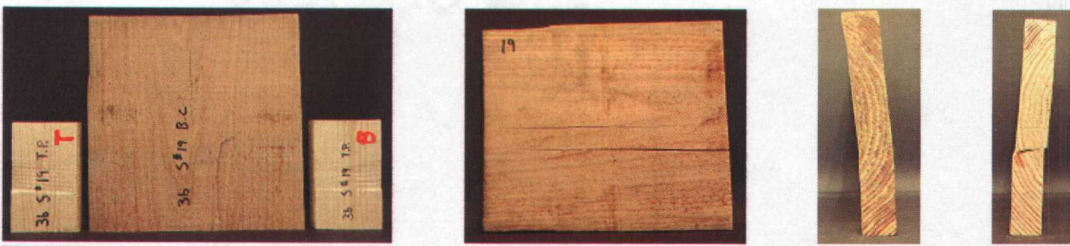
BC-2X12-SPF T#17



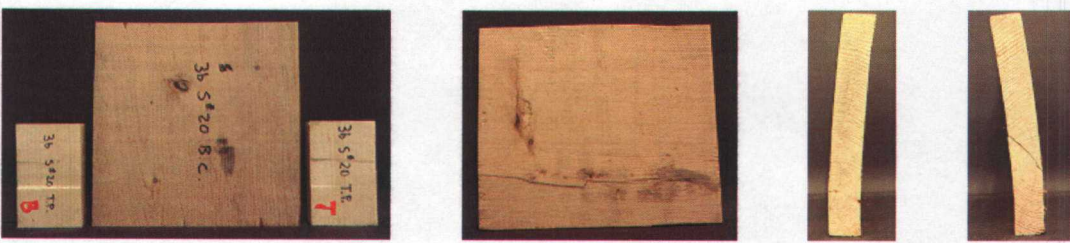
BC-2X12-SPF T#18



BC-2X12-SPF T#19



BC-2X12-SPF T#20



BP-DF T#1&2BP-DF T#3&4BP-DF T#5&6BP-DF T#7&8BP-DF T#9&10BP-DF T#11&12BP-DF T#13&14BP-DF T#15&16

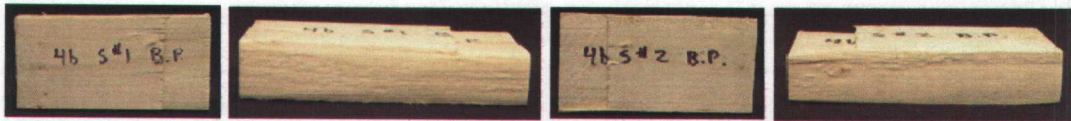
BP-DF T#17&18



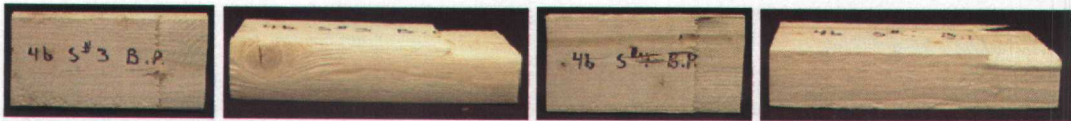
BP-DF T#19&20



BP-SPF T#1&2



BP-SPF T#3&4



BP-SPF T#5&6



BP-SPF T#7&8



BP-SPF T#9&10



7.7 STATISTICAL CODE

****SAS CODE; SPLIT BLOCK MODEL FOR ALL BC ASSEMBLIES****

```

options ps=50 ls=78;
options nodate nonumber nosource2 nomprint pageno=1 compress=yes;
options formchar='|----|+|---+=|-\<>';

proc import out=list
    datafile='Z:\data\AOV20block.xls' /*Adjust pathway to your computer*/
    DBMS=excel replace;
    getnames=yes;
run;

data AOV;
    set list;
RangleBCAvg2 = R_angle_BCAvg*R_angle_BCAvg;
run;

proc mixed data=AOV method=reml;
class BLOCK Config T_P_Material;
model Off_Stress = Config T_P_Material Config*T_P_Material/ ddfm=satterth;
random BLOCK Config*BLOCK T_P_Material*BLOCK;
parms/ nobound;

lsmeans Config/cl pdiff adjust=tukey;
lsmeans T_P_Material/cl pdiff adjust=tukey;
lsmeans Config*T_P_Material/slice=Config cl pdiff adjust=tukey;
lsmeans Config*T_P_Material/slice=T_P_Material cl pdiff adjust=tukey;
run;

proc mixed data=AOV method=reml;
class BLOCK Config T_P_Material;
model Peak_Stress = Config T_P_Material Config*T_P_Material/ ddfm=satterth;
random BLOCK Config*BLOCK T_P_Material*BLOCK;
parms/ nobound;

```

```

lsmeans Config/cl pdiff adjust=tukey;
lsmeans T_P_Material/cl pdiff adjust=tukey;
lsmeans Config*T_P_Material/slice=Config cl pdiff adjust=tukey;
lsmeans Config*T_P_Material/slice=T_P_Material cl pdiff adjust=tukey;
run;

```

```

/* Note the Inconclusive Config*Rangle Interaction */
proc mixed data=AOV method=reml;
class BLOCK Config T_P_Material;
model Off_Stress = Config T_P_Material Config*T_P_Material S_G_TP
          S_G_BC   R_angle_BCAvg   RangleBCAvg2   S_G_TP*S_G_BC
Config*R_angle_BCAvg Config*RangleBCAvg2/ ddfm=satterth;
random BLOCK Config*BLOCK T_P_Material*BLOCK;

parms/ nobound;

```

```

lsmeans Config/cl pdiff adjust=tukey;
lsmeans T_P_Material/cl pdiff adjust=tukey;
lsmeans Config*T_P_Material/slice=Config cl pdiff adjust=tukey;
lsmeans Config*T_P_Material/slice=T_P_Material cl pdiff adjust=tukey;

run;

```

```

proc mixed data=AOV method=reml;
class BLOCK Config T_P_Material;
model Off_Stress = Config T_P_Material Config*T_P_Material S_G_TP
          S_G_BC   R_angle_BCAvg   RangleBCAvg2   S_G_TP*S_G_BC/
ddfm=satterth;
random BLOCK Config*BLOCK T_P_Material*BLOCK;
parms/ nobound;
lsmeans Config/cl pdiff adjust=tukey;
lsmeans T_P_Material/cl pdiff adjust=tukey;
lsmeans Config*T_P_Material/slice=Config cl pdiff adjust=tukey;
lsmeans Config*T_P_Material/slice=T_P_Material cl pdiff adjust=tukey;
run;

```

```

proc mixed data=AOV method=reml;
class BLOCK Config T_P_Material;
model Peak_Stress = Config T_P_Material Config*T_P_Material
          S_G_BC L_W_BC R_angle_BCAvg RangleBCAvg2
Config*T_P_Material/ ddfm=satterth;
random BLOCK Config*BLOCK T_P_Material*BLOCK;
parms/ nobound;

```

```

lsmeans Config/cl pdiff adjust=tukey;
lsmeans T_P_Material/cl pdiff adjust=tukey;
lsmeans Config*T_P_Material/slice=Config cl pdiff adjust=tukey;
lsmeans Config*T_P_Material/slice=T_P_Material cl pdiff adjust=tukey;
run;

```

****SAS CODE; BC-2X4, BC-2X8, and BC-2X12 ASSEMBLY TESTS vs. CORRESPONDING ASTM TESTS****

```

options ps=50 ls=78;
options nodate nonumber nosource2 nomprint pageno=1 compress=yes;
options formchar='|----|+|---+|=|<>';

```

```

proc import out=list
          datafile='Z:\data\Testastm.xls'/*Adjust pathway to your computer*/
          DBMS=excel replace;
          getnames=yes;
run;

```

```

data AOV;
set list;
RingAngle2 = R_angle_*R_angle_;
run;

```

```

data four;
set AOV;
if B_size = '2X4';
run;

```

```
data eight;
set AOV;
if B_size = '2X8';
run;
```

```
data twelve;
set AOV;
if B_size = '2X12';
run;
```

```
/* Two_per_Strain_Str_4*/
proc glm data=four;
class Df_SPF_ASTM Board_Des_Num;
model Two_per_Strain_Str_ = Df_SPF_ASTM Board_Des_Num;
lsmeans Df_SPF_ASTM/cl pdiff adjust=tukey;
run;
```

```
/* Two_per_Strain_Str_8*/
proc glm data=eight;
class Df_SPF_ASTM Board_Des_Num;
model Two_per_Strain_Str_ = Df_SPF_ASTM Board_Des_Num;
lsmeans Df_SPF_ASTM/cl pdiff adjust=tukey;
run;
```

```
/* Two_per_Strain_Str_12*/
proc glm data=twelve;
class Df_SPF_ASTM Board_Des_Num;
model Two_per_Strain_Str_ = Df_SPF_ASTM Board_Des_Num;
lsmeans Df_SPF_ASTM/cl pdiff adjust=tukey;
run;
```

```
/* Zero_four_Defl_Str_*/
proc glm data=four;
class Df_SPF_ASTM Board_Des_Num;
model Zero_four_Defl_Str_ = Df_SPF_ASTM Board_Des_Num;
lsmeans Df_SPF_ASTM/cl pdiff adjust=tukey;
```

```
run;
```

```
/* Zero_four_Defl_Str_ 8*/
```

```
proc glm data=eight;
```

```
class Df_SPF_ASTM Board_Des_Num;
```

```
model Zero_four_Defl_Str_ = Df_SPF_ASTM Board_Des_Num;
```

```
lsmeans Df_SPF_ASTM/cl pdiff adjust=tukey;
```

```
run;
```

```
/* Zero_four_Defl_Str_ 12*/
```

```
proc glm data=twelve;
```

```
class Df_SPF_ASTM Board_Des_Num;
```

```
model Zero_four_Defl_Str_ = Df_SPF_ASTM Board_Des_Num;
```

```
lsmeans Df_SPF_ASTM/cl pdiff adjust=tukey;
```

```
run;
```

```
/* Zero_four_Defl_Off_Str_ 4*/
```

```
proc glm data=four;
```

```
class Df_SPF_ASTM Board_Des_Num;
```

```
model Zero_four_Defl_Off_Str_ = Df_SPF_ASTM Board_Des_Num;
```

```
lsmeans Df_SPF_ASTM/cl pdiff adjust=tukey;
```

```
run;
```

```
/* Zero_four_Defl_Off_Str_ 8*/
```

```
proc glm data=eight;
```

```
class Df_SPF_ASTM Board_Des_Num;
```

```
model Zero_four_Defl_Off_Str_ = Df_SPF_ASTM Board_Des_Num;
```

```
lsmeans Df_SPF_ASTM/cl pdiff adjust=tukey;
```

```
run;
```

```
/* Zero_four_Defl_Off_Str_ 12*/
```

```
proc glm data=twelve;
```

```
class Df_SPF_ASTM Board_Des_Num;
```

```
model Zero_four_Defl_Off_Str_ = Df_SPF_ASTM Board_Des_Num;
```

```
lsmeans Df_SPF_ASTM/cl pdiff adjust=tukey;
```

```
run;
```

```

/* Two_per_Str_Off_4*/
proc glm data=four;
class Df_SPF_ASTM Board_Des_Num;
model Two_per_Str_Off_ = Df_SPF_ASTM Board_Des_Num;
lsmeans Df_SPF_ASTM/cl pdiff adjust=tukey;
run;

```

```

/* Two_per_Str_Off_8*/
proc glm data=eight;
class Df_SPF_ASTM Board_Des_Num;
model Two_per_Str_Off_ = Df_SPF_ASTM Board_Des_Num;
lsmeans Df_SPF_ASTM/cl pdiff adjust=tukey;
run;

```

```

/* Two_per_Str_Off_12*/
proc glm data=twelve;
class Df_SPF_ASTM Board_Des_Num;
model Two_per_Str_Off_ = Df_SPF_ASTM Board_Des_Num;
lsmeans Df_SPF_ASTM/cl pdiff adjust=tukey;
run;

```

```

/**** Covariates with Two_per_Str_Off_ for 8 and 12 only ****/

```

```

/* Two_per_Str_Off_8 + Covariates*/
proc glm data=eight;
class Df_SPF_ASTM Board_Des_Num;
model Two_per_Str_Off_ = Df_SPF_ASTM Board_Des_Num R_angle_RingAngle2;
lsmeans Df_SPF_ASTM/cl pdiff adjust=tukey;
run;

```

```

/* Two_per_Str_Off_12 + Covariates*/
proc glm data=twelve;
class Df_SPF_ASTM Board_Des_Num;
model Two_per_Str_Off_ = Df_SPF_ASTM Board_Des_Num S_G_R_angle_
RingAngle2 ;
lsmeans Df_SPF_ASTM/cl pdiff adjust=tukey;

```

```
run;
```

SAS CODE; BP ASSEMBLIES

```
options ps=50 ls=78;
```

```
options nodate nonumber nosource2 nomprint pageno=1 compress=yes;
```

```
options formchar='|----|+|---+|=|-^<>*';
```

```
proc import out=list
```

```
    datafile='Z:\data\Test4aov.xls' /*Adjust pathway to your computer*/
```

```
    DBMS=excel replace;
```

```
    getnames=yes;
```

```
run;
```

```
data AOV;
```

```
set list;
```

```
RingA_Squared = R_angle*R_angle;
```

```
run;
```

```
data DFvsDFASTM;
```

```
set AOV;
```

```
if (D_fir_SPF_ASTM = "ASTM_DF" or D_fir_SPF_ASTM = "D-fir");
```

```
run;
```

```
data SPFvsSPFASTM;
```

```
set AOV;
```

```
if (D_fir_SPF_ASTM = "ASTM_SPF" or D_fir_SPF_ASTM = "SPF");
```

```
run;
```

```
data SPFvsDF;
```

```
set AOV;
```

```
if (D_fir_SPF_ASTM = "SPF" or D_fir_SPF_ASTM = "D-fir");
```

```
run;
```

```
/* Zero_Four_Defl*/
```

```
proc glm data=DFvsDFASTM;
```

```
class Board_Des_Num D_fir_SPF_ASTM;  
model Zero_Four_Defl =Board_Des_Num D_fir_SPF_ASTM;  
lsmeans D_fir_SPF_ASTM /cl pdiff adjust=tukey;  
run;
```

```
proc glm data=SPFvsSPFASTM;  
class Board_Des_Num D_fir_SPF_ASTM;  
model Zero_Four_Defl =Board_Des_Num D_fir_SPF_ASTM;  
lsmeans D_fir_SPF_ASTM /cl pdiff adjust=tukey;  
run;
```

```
proc glm data=SPFvsDF;  
class D_fir_SPF_ASTM;  
model Zero_Four_Defl = D_fir_SPF_ASTM;  
lsmeans D_fir_SPF_ASTM /cl pdiff adjust=tukey;  
run;
```

```
/*Zero_Four_Defl_Off*/
```

```
proc glm data=DFvsDFASTM;  
class Board_Des_Num D_fir_SPF_ASTM;  
model Zero_Four_Defl_Off =Board_Des_Num D_fir_SPF_ASTM;  
lsmeans D_fir_SPF_ASTM /cl pdiff adjust=tukey;  
run;
```

```
proc glm data=SPFvsSPFASTM;  
class Board_Des_Num D_fir_SPF_ASTM;  
model Zero_Four_Defl_Off =Board_Des_Num D_fir_SPF_ASTM;  
lsmeans D_fir_SPF_ASTM /cl pdiff adjust=tukey;  
run;
```

```
proc glm data=SPFvsDF;  
class D_fir_SPF_ASTM;  
model Zero_Four_Defl_Off = D_fir_SPF_ASTM;  
lsmeans D_fir_SPF_ASTM /cl pdiff adjust=tukey;  
run;
```

```
/* Two_Per_Str*/
```

```
proc glm data=DFvsDFASTM;  
class Board_Des_Num D_fir_SPF_ASTM;  
model Two_Per_Str =Board_Des_Num D_fir_SPF_ASTM;  
lsmeans D_fir_SPF_ASTM /cl pdiff adjust=tukey;  
run;
```

```
proc glm data=SPFvsSPFASTM;  
class Board_Des_Num D_fir_SPF_ASTM;  
model Two_Per_Str =Board_Des_Num D_fir_SPF_ASTM;  
lsmeans D_fir_SPF_ASTM /cl pdiff adjust=tukey;  
run;
```

```
proc glm data=SPFvsDF;  
class D_fir_SPF_ASTM;  
model Two_Per_Str = D_fir_SPF_ASTM;  
lsmeans D_fir_SPF_ASTM /cl pdiff adjust=tukey;  
run;
```

```
/* Two_Per_Str_Off*/
```

```
proc glm data=DFvsDFASTM;  
class Board_Des_Num D_fir_SPF_ASTM;  
model Two_Per_Str_Off =Board_Des_Num D_fir_SPF_ASTM;  
lsmeans D_fir_SPF_ASTM /cl pdiff adjust=tukey;  
run;
```

```
proc glm data=SPFvsSPFASTM;  
class Board_Des_Num D_fir_SPF_ASTM;  
model Two_Per_Str_Off =Board_Des_Num D_fir_SPF_ASTM;  
lsmeans D_fir_SPF_ASTM /cl pdiff adjust=tukey;  
run;
```

```
proc glm data=SPFvsDF;  
class D_fir_SPF_ASTM;
```

```

model Two_Per_Str_Off = D_fir_SPF_ASTM;
lsmeans D_fir_SPF_ASTM /cl pdiff adjust=tukey;
run;

```

```

/*Two_Per_Str_Off + Covariates(Ring Angle, Ring Angle^2)*/

```

```

proc glm data=DFvsDFASTM;
class Board_Des_Num D_fir_SPF_ASTM; /* no sig covariates */
model Two_Per_Str_Off =Board_Des_Num D_fir_SPF_ASTM;
lsmeans D_fir_SPF_ASTM /cl pdiff adjust=tukey;
run;

```

```

proc glm data=SPFvsSPFASTM;
class Board_Des_Num D_fir_SPF_ASTM;
model Two_Per_Str_Off = Board_Des_Num D_fir_SPF_ASTM R_angle
RingA_Squared ;
lsmeans D_fir_SPF_ASTM /cl pdiff adjust=tukey;
run;

```

```

proc glm data=SPFvsDF;
class D_fir_SPF_ASTM;
model Two_Per_Str_Off = D_fir_SPF_ASTM s_g ;
lsmeans D_fir_SPF_ASTM /cl pdiff adjust=tukey;
run;

```

S-PLUS CODE; LOGISTIC REGRESSION MODEL FOR BC-2X8 & BC-2X12 ASSEMBLIES

```

attach(Logisticdata) /*Adjust pathway to your computer*/

```

```

two.eight <- ifelse(Config == "Two.X.Eight",1,0)
spf <- ifelse(T.P.Material == "SPF",1,0)

```

```

two.twelve <- ifelse(Config == "Two.X.Twelve",1,0)
d.f <- ifelse(T.P.Material == "Doug.fir",1,0)

```

```
#####
```

```
#####
```

```
### Fit 20 = former current winner
```

```
fit20<-glm(Failed ~ R.Angle.BC.TB + R.Angle.BC.TB^2+ two.twelve, family=binomial,
  data=Logisticdata)
summary(fit20, cor=F)
```

```
### fit 21 shows 2 x12 vs 2 x 8 is highly significant
```

```
fit21<-glm(Failed ~ two.twelve, family=binomial, data=Logisticdata)
summary(fit21, cor=F)
```

```
half.width <- qnorm(.975) *0.76903
lower <- 4.2813-half.width
upper <- 4.2813+half.width
c(exp(lower),exp(upper))
```

```
#####          Two          Separate          Models          is          Best
#####
```

```
### Current Winner 2x12 does not need a quadratic term
```

```
Failed1 <- Failed[Config == "Two.X.Twelve"]
R.Angle.BC.TB.1 <- R.Angle.BC.TB[Config == "Two.X.Twelve"]
cbind(Failed1,R.Angle.BC.TB.1)
```

```
fit.2.12 <- glm(Failed1 ~ R.Angle.BC.TB.1 + R.Angle.BC.TB.1^2, family=binomial)
summary(fit.2.12, cor=F)
1-pchisq(30.142-28.679, 2)
```

```
### Current Winner 2x8 does not need a quadratic term
```

```
Failed2 <- Failed[Config == "Two.X.Eight"]
R.Angle.BC.TB.2 <- R.Angle.BC.TB[Config == "Two.X.Eight"]
```

```
fit.2.8 <- glm(Failed2 ~ R.Angle.BC.TB.2, family=binomial)
summary(fit.2.8, cor=F)
```